INTELLIGENT CONTROL FOR A NOVEL ASSIST MECHANISM IN FUNCTIONAL ELECTRICAL STIMULATION CYCLING

By
Shwan Chatto Abdulla

A thesis submitted to the University of Sheffield for the degree of
Doctor of Philosophy

Department of Automatic Control and Systems Engineering
The University of Sheffield
Mapping Street
Sheffield, S1 3JD
United Kingdom

July 2014

Acknowledgements

Abstract

This study investigates the feasibility and the benefits of using a novel assist mechanism, represented by a flywheel and electrical clutch, in functional electrical stimulation (FES)-based cycling exercise by stimulating the quadriceps muscle of paralyzed individuals. The flywheel, as energy storage device, engages with the crank via the clutch to absorb the excess kinetic energy in the system and produce brake action. Also, it engages again to discharge the stored kinetic energy to speed up the system and support the legs. The mechanism is used to assist the legs, suppress the fluctuation in cadence, and prolong the exercise by delaying the appearance of muscle fatigue.

To minimize the trials and experiments of different control approaches that might be costly in time and harsh for the disabled, a humanoid and a bicycle model equipped with the new assist mechanism is built using Visual Nastran 4D dynamic simulation platform. Also, in the early stages of the research, a simple linear quadriceps muscle model is incorporated with the humanoid model to simulate the behaviour of a paralysed muscle in response to FES signal. Since the utilized muscle model lacks muscle fatigue information, a force-drop indicator is derived from clinically recorded data set to be used for assessment purposes between FES-cycling using muscle effort only and FES-cycling assisted by the new proposed mechanism.

FES-cycling by stimulating the quadriceps muscle of both legs is implemented using proportional-integral-derivative (PID) and fuzzy logic (FL) controllers to follow a predefined knee joint trajectory of a specific speed. The controllers are used to regulate the stimulation intensity of FES signal on the muscle to perform smooth and coordinated pedalling movement. Also, the control of the assist mechanism is achieved using two intelligent control approaches. The first depends on the angular velocity of the knee joints, while the second relies on the angular velocity of the crank. The

derived force drop indicator shows that the new mechanism delays the fatigue by approximately 14%-17% as compared with FES-cycling without assistance.

To improve the cycling cadence, FLC is used to control the stimulation intensity on the muscle, i.e. physiological based nonlinear quadriceps muscle model, in a cadence control approach in an attempt to obtain 35rpm cycling cadence. Controlling the cycling cadence by stimulating the quadriceps only, without using any assist mechanism, is difficult to achieve and leads to premature termination of the exercise due to successive muscle stimulation by FES. The flywheel and electrical clutch mechanism is used in a cadence control approach to provide the necessary assistance. The engagement of the flywheel by the clutch is controlled using FLC approach and depends on the angular velocities of both the crank and the flywheel. It is shown that FES-cycling with the aid of the flywheel mechanism produces superior results in terms of reducing the stimulation intensity by approximately 20% as compared with that without assist mechanism in a cadence control approach.

In an attempt to improve the outcome of the exercise, i.e. maximum power output, minimum muscle energy expenditure and minimum cadence error, investigations are performed on choosing the best design parameters such as flywheel size, gear ratio between the flywheel and the crank, and crank position with respect to hip joint. Also, the genetic algorithm optimization technique is used to obtain the optimal parameters' values of the design with the objective of minimizing the error in cadence. Furthermore, in an attempt to obtain a satisfactory solution to the problem of two conflicting objectives, i.e. minimum cadence error and maximum efficiency, multi-objective genetic algorithm (MOGA) is utilized to produce a set of non-dominated optimal solutions. An optimal solution, as a good compromise between the two objectives, is selected and tested. The proposed control approach together with the new assist mechanism achieve robust, efficient and prolonged FES-cycling exercise by stimulating the quadriceps muscle for disabled individuals.

Table of Contents

List of Figures

xviii

List of Tables

Chapter 1: Introduction

1.1 Introduction

Individuals with spinal cord injury (SCI) are subject to serious health challenges and poor quality of life. The lack and disability in voluntary movement control, due to damage in the spinal nerve, prevent them from moving their body parts and practice the basic activities in life such as walking, standing and running. Being laid or sitting on a wheelchair for a long time leads to serious physiological and psychological health degradation due to lack of active movement. To improve their health condition and quality of life, rehabilitation exercise becomes an essential requirement.

It has been reported that in the UK, around 1200 persons suffer from SCI each year. Also, the total number of individuals suffer from paralysis living in the UK is estimated to exceed 40,000 (Apparelyzed, 2013) while in the U.S. the annual incidence of SCI is approximated to 40 cases per million of the population which can be estimated to 12000 new cases each year. The total number of individuals with SCI living in the U.S. is approximated to be 238,000 to 332,000 persons in 2013 (NSCISC, 2013). The caring cost of people with SCI exceeds £500 million per year only in the UK. Approximately 21% of the people with SCI are sent to hospitals, nursing homes or caring settings rather than their own private homes after being discharged from SCI centres. 20% of them leave the centres suffering from clinical depression (Everyeighthours, 2014).

The statistics reported in (NSCISC, 2013) show that SCI affects primarily young adults and 80.7% of the cases reported occurred among males. Since 2010, the most common causes of the SCI are shown as motor vehicle accidents (36.5%), falling accidents (28.5%), violence (14.3%), sports (9.2%) and other reasons (11.4%).

1.2 Spinal Cord Injury

The spinal cord is the largest nerve in the nervous system in the human body. The spinal cord consists of several spinal nerve fibres that transmit messages between the centre (i.e. the brain) and different parts of the body. Those messages may tell a body part (i.e. a peripheral) to move.

For its extraordinary importance, the spinal cord is protected and surrounded by bones called the backbones or the vertebrae. The vertebrae are arranged on the top of each other constructing what is called the spinal column or the vertebrae column. The spinal cord passes through the middle of the spinal column which is considered as the main support to the body.

The length of the spinal cord is about 0.457 meters. The cord extends from the base of the brain and down to the waist. The nerve fibers that the spinal cord is constructed from are called the upper motor neurons (UMNs). While the nerve fibers that branch from the spinal cord to the body are called the lower motor neurons (LMNs) (NSCIA, 2012).

As shown in Figure 1.1, the spinal column is divided into four main portions. The top section is the cervical area. It consists of eight cervical nerves and seven cervical vertebrae. Moving down the back, the next portion is the thoracic area. It covers the chest area and consists of twelve thoracic vertebrae. The lower back portion is the lumbar area and has five lumbar vertebrae. The bottom portion is the sacral area and has five sacral vertebrae. The bones in the sacral area are fused all together into one bone.

The extent of the paralysis depends on the level of the affected area. The closer the injury is to the brain, the more effect it has on the movement or feeling of the body. More feeling or movement control of the body is present with the lower level of injury. For example, a person with L-1 level of injury would show more feeling and movement than another with a T-6 level of injury (NSCIA, 2012).
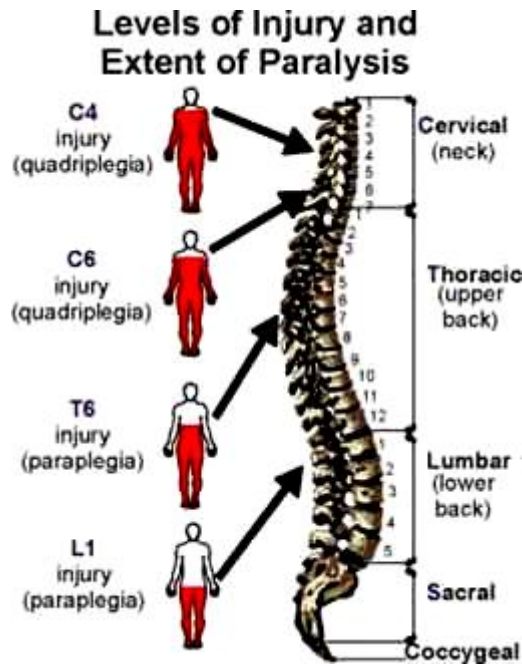
Figure 1.1: Levels of spinal cord injury. The red colour indicates the extent of paralysis (NSCIA, 2012)

Damage to the spinal cord can be caused by a traumatic accident or by a disease to the spinal column. After the injury, all the nerves above the level of injury remain intact and send messages from brain to the peripherals as usual, while the nerves below the level of injury become unable to receive signals from the brain due to the injury.

In general, SCI can be classified into two categories: complete injury and incomplete injury. In the complete injury type, the damage affects the whole area and no signal can pass through the ruined area. This results in a complete absence of sensation in the genital region. In such cases, the recovery becomes extremely difficult. In the incomplete injury type, feeling or sensation to the genital region still occurs which implies that part of the spinal cord is affected in the injury and hence the recovery or improvement in such cases is much easier.

Individuals with SCI suffer from one of the problems, namely obesity, pain, urinary tract infection and pressure sores, due to lack of movement (Medtronic, 2013). To overcome the physiological and psychological problems that individuals with SCI usually suffer from, and to improve their life quality, rehabilitation and continuous

exercise become a must. One of the most important exercises for paraplegics and quadriplegics is to use functional electrical stimulation (FES).

1.3 Functional electrical stimulation

Functional electrical stimulation (FES), also known as functional neuromuscular stimulation (FNS), is a technique of supplying a train of electrical stimuli to trigger nerves of paralysed muscles, due to SCI or brain injury or stroke, to cause muscle contraction and produce movement.

A FES-based system consists of a stimulator, electrodes, leads, and manual or automatic control unit, as shown in Figure 1.2. The stimulator has single or several outputs (channels) that are usually utilized in sequence or in parallel to obtain the required motion (SCI-therapies, 2009). Figure 1.2 explains the principle of controlling the knee joint angle by stimulating the quadriceps. The knee joint angle is measured and fed back to the controller, which in turn generates a suitable stimulation pattern to achieve the tracking of a reference trajectory. Stimulation can either be applied directly to the peripheral motor nerves or, if the reflex arcs in the lower spinal cord are still intact, to the sensory nerves to provide an indirect stimulation of motor nerves (Fachgebiet Regelungssysteme, 2009). The electrodes can be either surface electrodes placed over the skin, or percutaneous electrodes, placed close to motor nerve with the help of a needle, or completely implanted electrodes placed under the skin by surgical operation. Stimulation with surface electrodes is easier, cheaper, non-invasive, and has no potential of infection as compared with other types (Chen et al., 2004).

Over the last decades, several FES-based devices have been developed and used for therapeutic and function restoration purposes. An example of the most popular FES-based devices is the pacemaker, as a heart pulse regulator, which is now utilized by more than a million people every year (Medtronic, 2013). Also, FES has been utilized to provide movement in the lower extremities for people with complete and

incomplete spinal cord injuries in an attempt to restore locomotion through different exercises such as walking, standing and cycling.
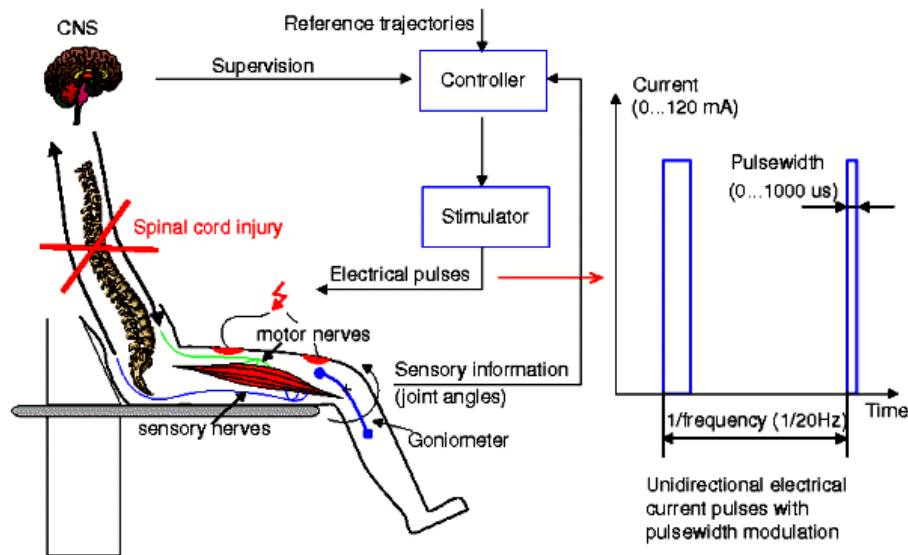
Figure 1.2: FES system to control leg movement. CNS refers to the central nervous system (Fachgebiet Regelungssysteme, 2009)

1.4 FES-assisted cycling

FES-based cycling is a type of exercise that employs FES signals to stimulate leg muscles of paralyzed people in a specific sequence to perform pedalling motion. The amount of legs' joint torque required for the disabled to perform cycling is maintained by a computer through controlling the stimulation intensity (pulse width; pulse frequency; pulse amplitude) on the leg muscles. FES cycling exercise is considered as easy-to-implement, attractive, and comfortable for individuals with paraplegia as compared to FES-based walking and standing activities.

FES-cycling is more beneficial for a disabled person than weight lifting, although it provides smaller increase in muscle size, the cardiac output of paralyzed individuals during weight lifting induced by FES produces 7 litres/min while the cardiac output has been shown to rise to 15 litres/min during FES-cycling exercise (Petrofsky et al., 1983; Petrofsky and Smith, 1988). Also, other studies have shown that continuous FES-cycling exercise for paralyzed people increases the cardiovascular

fitness, muscle size, blood circulation in lower limbs, in addition to reverse muscle atrophy and prevention of bone loss (Davis et al., 2008; Fornusek and Davis, 2004; Griffin et al., 2009; Hooker et al., 1995; Mutton et al., 1997; Petrofsky and Smith, 1992).

1.5 FES-assisted cycling ergometers

Researchers have developed several stationary and mobile FES cycling ergometers with different designs and specifications, in an attempt to provide more stable, easy-to-use and comfortable devices for the disabled with prolonged training session for both in-door and out-door exercise. One of the first designs was produced by (Petrofsky et al., 1983) who modified a standard Huffy three-wheel bicycle to be used for exercise and locomotion of paraplegics and quadriplegics. The bicycle had its own stimulator as well as batteries so as it could be used for hours before recharging was necessary. The bicycle was equipped with a sensor, a 360° potentiometer linked through a chain driver to sprocket on the pedal, to read pedal position during cycling. The sensor's signal was fed to a small digital computer through an A/D converter. A portable, Z80 microprocessor-based system was used to control the stimulation of the quadriceps and gluteus maximus muscles of both legs. To provide more comfort and postural control, the bicycle's seat was modified to a high-back seat. A hand lever connected with a rotary potentiometer to provide throttle type brake was used to control the speed of the bicycle. The designed tricycle relied on the force generated by the muscles to move; therefore, at the beginning of the exercise the tricycle was pushed by hands to prevent imposing high loads on the musculoskeletal muscles. The disadvantage of this design was that the wheelbase of the design made the tricycle unstable during turns. Also, the absence of a precise muscle fatigue indicator made the paralysed persons unaware of the extent of the fatigue in their muscles, which resulted in termination of the out-door exercise and inability to return home.

To solve the stability problem, Pons et al. (1989) designed a device called paracycle composed of four wheels to be used by paraplegics as either a stationary or mobile exercise device for locomotion. The device was equipped with a mechanism to adjust seat position, in supine recumbent posture, to provide more comfort and stability for different subjects, in addition to direction control with right forearm through steering lever. Speed control was achieved by left arm through a lever to control the stimulation intensity, resistive and mechanical braking. The device was equipped with electrical motor and gearing of 18 gears to provide assistance during cycling. Instead of continuous-turn potentiometers, used by (Petrofsky et al., 1983), which are prone to wear out, in this work an optical shaft encoder was used to measure the crank angle. During cycling trials, good stability of the legs was noticed, but due to device wirings, locomotion of up to 5m distance was achieved. Also, Petrofsky and Smith (1992) developed their previous work by modifying a commercially available tricycle used for two people sitting beside each other and cycle at the same time. The side-by-side design made the wheelbase wider and more stable. The tricycle was also equipped with a high-back bucket-type seat to provide better back support. In addition to aluminium stabiliser bars used to prevent the paralysed legs from moving in and out. The tricycle had a position sensor located on the pedal to allow calculating the required stimulation according to the position of the pedal and the stimulated muscle. A throttle with a potentiometer was used as a break. The potentiometer's signal was fed to a computer and the intensity of stimulation was increased or decreased accordingly.

Gföhler et al. (1998) developed a tricycle for paraplegics to ride the vehicle and exercise without assistance. The tricycle relied on a hydraulic mechanism to adjust the saddle height that enabled the disabled to ride the tricycle alone and adjust the saddle's height to a position similar to that of normal cycling. The proposed tricycle solves the problem of stability especially when riding around bends for its ability to incline in parallel with both of the rear wheels and the tricycle frame. The cycling power is assumed to be provided by applying FES signals on the quadriceps, hamstrings and

gluteus muscles of both legs. An auxiliary motor is utilized to provide assistance when necessary. A throttle is used on the handlebar to adjust the driving power by controlling the stimulation intensity and the motor at the same time. The crank angular velocity, crank position and pedalling force are measured by a ganiometer and a force measurement pedal and accordingly the controller adjusts muscle stimulation and the speed of the motor. The heavy weight of the tricycle (28kg) that resulted from the hydraulic components and the motor, made it difficult for a paraplegic to generate enough driving torque to propel the vehicle without the assistance of the motor, in addition to the number of cables used for stimulating multiple muscles that caused mechanical wiring problems.

In order to provide better exercise by utilizing both the lower limbs and the upper body of a paraplegic, Chen et al. (2004) developed a hybrid FES cycling ergometer for home training that makes use of an arm-crank to assist the disabled initialize the cycling and warm up before starting the electrical stimulation to legs, as shown in Figure 1.3. The system utilizes a wireless communication to upload different training programs and online monitoring the performance of the user. Also the system benefits from a hysteresis brake that is utilized to provide different resisting levels for various training protocols. Both the quadriceps and the hamstring muscles were stimulated. The drawbacks of this system were that the ergometer had limitations in height adjustment that the legs and arms might collide during hybrid cycling with taller persons, while for shorter persons the pedals might be too distant. Also, it was suggested to use a fixed-engaged flywheel to prevent jerking during cycling exercise and overcome the dead points problem. Further, as a stationary ergometer, Fornusek et al. (2004) developed an isokinetic FES cycling device for home training equipped with a motor. The motor was used to maintain fixed cycling cadence, while stimulation patterns were calculated in advance. The design was equipped with a speed control circuit to maintain a required pedalling cadence by driving or braking the motor. The motor was used to obtain an isokinetic exercise over a wide range of speeds, 5-60 rpm,

to promote both cardiorespiratory fitness and muscular strength. A calibration equation was derived between the motor current and the torque applied to the axle. The current of the motor reflected the torque required to oppose the FES-evoked muscle movement of a subject or to assist the pedalling to pass the dead points. Although a speed control circuit was used, the results showed that the cadence was not smooth enough, i.e. fluctuated, during muscle stimulation period.
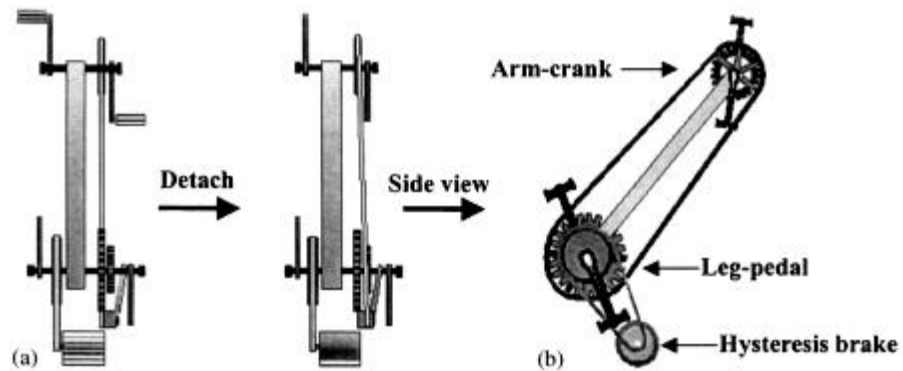
Figure 1.3: Internal mechanical structure of the hybrid cycling system (a) the front view (b) the side view of the system (Chen et al., 2004)

Takahashi et al. (2004) developed a mobile vehicle based on a wheelchair for daily FES cycling exercise as well as locomotion. The cycling chair consisted of two relatively big front wheels, connected through a mechanical chain to the pedals, as well as two small rear wheels for steering purposes. A steering angle is controlled through a steering stick by the left hand, while the stimulation intensity is controlled through a joystick located on the right hand side as shown in Figure 1.4. The pedals were equipped with special mechanical torque diode that allows the transmission of the torque from the input to the output regardless of the direction of pedalling. A shaft encoder on the crank is also used to measure the crank angle during cycling. The system controller was implemented using an onboard micro computer (Hitachi SH-2 + Altera FPGA).
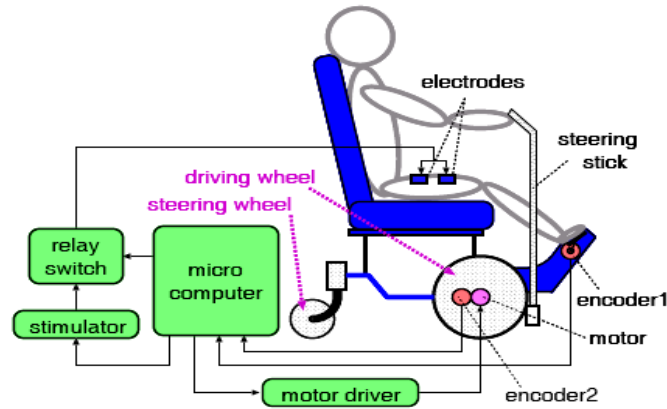
Figure 1.4: The developed cycling chair (Takahashi et al., 2004)

In addition to surface electrodes, implanted electrodes have also been used in FES cycling. Perkins et al. (2002), for the first time utilized implanted electrodes to perform mobile and stationary FES cycling by modifying a commercially available recumbent tricycle for a female complete T9 paraplegic with lumbo-sacral anterior root stimulator (LARSI), as shown in Figure 1.5. The designed controller divided the crank into 16 stimulation phases through 7-bit shaft encoder. A lookup table was used to decide between the 12 roots and the intensity of stimulation according to crank position. A 250ms phase advance shift was utilised to compensate for the delay in muscle response. The patient was able to cycle for 1.2km with speeds between 25-85 rpm maintaining smooth cycling.

Figure 1.5: The developed tricycle with implanted electrodes
(Perkins et al., 2002)

1.6 FES-assisted cycling control strategies

For the importance of FES induced cycling exercise in improving the health condition of disabled people, researchers have focused on improving the performance of FES cycling system by mainly improving its control system.

Usually, in FES cycling systems, the lower limb muscles are stimulated with electrical current pulses to excite the nerve and cause muscle contraction, which in turn leads to joint torque that causes leg movement. Major problems that limit the success of the current FES systems is the nonlinear behaviour of muscles and the rapid appearance of muscle fatigue that terminate the exercise. Most of the FES control systems are open-loop, where the output of the controller depends on an input from the user through push buttons to allow the delivery of fixed stimulation patterns to the muscles (Abbas and Triolo, 1997). Several problems are associated with fixed-pattern open-loop systems. As several parameters differ from person to person, such as muscle response to FES, skin sensitivity and muscle's training condition etc, the stimulation parameters applied in open-loop systems are specific for single user and may not produce the same performance with other persons. Further, the open-loop approach cannot account for unforeseen conditions such as muscle spasm and mechanical disturbance. For these reasons, researchers have focused on developing feedback control approaches (Abbas and Chizeck, 1991; Bajzek and Jaeger, 1987; Chizeck et al., 1988; Lan et al., 1991). The feedback control action depends on the information received from the sensors to decide whether to increase or decrease muscle stimulation and thus can account for the problems encountered in open-loop systems. However, several problems arise in systems utilizing feedback control such as the delay in muscle response and rapid muscle fatigue. Furthermore, the success of the feedback controller depends on the measured variables and quality of signals. For these reasons, researchers have developed both feedback and adaptive control strategies to overcome the above mentioned restrictions (Abbas and Chizeck, 1995; Ann et al., 1997; Chen et al., 1997; Massoud, 2007).

To dynamically adapt for changes and differences in musculoskeletal properties (i.e. segment mass, segment length and joint stiffness) and to resist external disturbances during cycling, Abbas and Chizeck (1995) designed a neural network based control system to control the cyclic leg movement in functional neuromuscular stimulation system through on-line adaptation to stimulation parameters. The neural network consisted of two stages utilizing both feed-forward and PD feedback control techniques. The first stage, pattern generator (PG), is used to generate periodic signals. The second stage, pattern shaper (PS), is utilized to filter the signal received from the PG and provide the muscle with appropriate activation signal. The joint angle is compared with the desired angle to generate an error signal which is used to activate the feedback controller and the adaptation. A new learning algorithm, called time-averaged learning, was developed to provide online rapid learning to changes in musculoskeletal properties. The proposed approach was implemented on a planar one-segment musculoskeletal model in simulation environment. The simulation results showed the ability of the approach to account for changes in musculoskeletal system by adapting the control parameters online. The drawback of the controller was that the developed learning algorithm was not fast enough to perform online learning, causing a clear angle tracking error at first stages.

To improve the efficacy of FES cycling systems and to avoid the complexity of exact modelling of cycling ergometers and muscles activated by FES, Chen et al. (1997) proposed a model-free fuzzy logic approach to control FES induced cycling movements for subjects with paraplegia. A symmetric approach to derive stimulation patterns is produced based on gravitational force on lower limbs. By analysing the cycling movement geometrically, five-bar linkage, consisting of thigh, shank, and crank, was assumed and a relation between hip angle and gravitational force was concluded. From that relation, the required stimulation patterns were determined taking into account the delay in muscle response and the passive stretch in the hip joint. The stimulation patterns were derived to stimulate two muscle groups, the

quadriceps and the hamstring. The author grouped the quadriceps and the hamstring muscles as a single force generator. The controller used consisted of two inputs, error in speed and the derivative of error, and one output to modulate the stimulation intensity. The fuzzified input and output membership functions were represented by seven asymmetric triangle-shaped functions. The rule base used was a standard seven by seven rules table. The defuzzification method utilized was chosen as the centre of area for its better performance in steady-state response. A comparison between the proposed fuzzy approach and PD controller showed superior performance of fuzzy controller in terms of adaptation for different speeds. Further, the proposed fuzzy approach has flexible structure and does not require system parameters` identification. The results showed acceptable tracking in different speeds, although jerky output appeared from time to time due to uncoordinated movement of the limbs. They suggested further investigation especially for different seat configurations and cycling under different loads. For this reason, Ann et al. (1997) developed an adaptive fuzzy logic control (AFLC) system for on-line tuning of cycling system parameters. The main objective of the work was to design a controller for training paralyzed people at different cycling speeds and loads. Fuzzy gain scheduling approach was utilised. The controller consisted of two parts: fuzzy PI and fuzzy PD controllers. The PI part was to map the control input, the cycling speed, and the stimulation current. While the gain scheduling fuzzy PD controller used was to adapt the gain of stimulation current by monitoring the stimulation current and cycling speed at the same time. The introduced controller was shown to be able to increase the stimulation current, when muscle fatigue occurs and the cycling load increases, to maintain a desired speed. Although the results were shown to be satisfactory, further investigation was suggested due to occurrence of adaptation errors especially when the desired cadence dropped from high to low ranges.

To automatically generate and adjust stimulation patterns and account for muscle recruitment's nonlinearity and muscle dynamics during FES cycling, Riess and Abbas

(2000) investigated the effectiveness of using adaptive feed-forward control technique for cycling with FES. To test the controller under isotonic conditions, they took into account muscle length-tension and force-velocity properties in addition to the dynamics of lower limbs. The controller was based on neural network to build pattern generator (PG) and pattern shaper (PS) units. The pattern generator (PG) unit was used to generate a periodic stable signal of fixed frequency as that of the output. The pattern shaper (PS) was implemented as a single layer neural network with each neuron output of a shape of cosine wave activated by the signal of the pattern generator (PG) unit. The PS unit filters and adapts the signal received from the pattern generator (PG) unit to meet a stimulation pattern to accordingly activate the muscle and govern a cyclical motion of a specific speed. The adaptation is achieved by changing the weights of each neuron of the PS through the learning algorithm used. Although the proposed technique was tested on the quadriceps of a single leg and was shown to have superior tracking results as compared with PD feedback approach, the author suggested further investigation for the approach over longer cycling sessions and testing its ability to alter the stimulation intensities when greater muscle fatigue is induced.

Similarly, as an attempt to eliminate the time-consuming trial-and-error calculations required for determining the stimulation parameters prior to FES cycling session, Kim et al. (2008) investigated a control strategy to automatically generate stimulation parameters for different muscles in FES cycling to suit different subjects. The control strategy depended on feedback information of the lower extremities to generate quasi-joint torque by imitating the biological neuronal system. The neuronal system used was composed of two controllers, a high level and a low level controller. The higher level controller was used to determine the quasi-joint torque from a sensory feedback system while the lower level controller used static optimization technique to optimize the desirable muscle (hamstring and vasti) force with different intensities taking into consideration minimizing muscle fatigue as a cost function. A muscle delay compensator of 200ms is used to compensate for the delay in muscle response to FES

through surface electrodes. The sensory feedback system used constructed from conventional PD control, to control the knee joint torque for joint movement away from the current posture, and an inverse dynamics function, to calculate the joint torque with respect to zero acceleration, zero angular velocity and current joint angle, to compensate for the gravity and maintain the current posture. Since the PD parameters depend on the posture, the cycling movement is divided into eight phases and the PD parameters were optimized for each phase using genetic algorithm. Although the proposed simulated approach is shown to be successful and robust to muscle fatigue, modelling error and external disturbances, further investigation is suggested to minimize the burden on the muscle before utilizing the approach clinically. Also, Li et al. (2010) developed a control system to automatically calculate the stimulation intensity and the proper muscle group to provide FES cycling exercise with the ability of compensation for time-variant properties such as muscle fatigue. The proposed approach is based on artificial neural network of two layers. The outer layer is responsible for controlling FES cycling model dynamics and the generation of the desired torque, while the inner layer is responsible for controlling different muscles to generate torque to follow and track the previously generated desired torque. The distribution of FES stimulation intensities is achieved by least square optimization technique with the objective of minimizing FES input energy and consequently reducing muscle fatigue. The FES cycling system, implemented in simulation environment, consisted of four sections; dynamics and kinematics of musculoskeletal with crank model, desired torque generator, muscle activation, and a control system for multi channel FES generation and distribution. In this work, radial basis function (RBF) network was used to approximate the modelling parameters (e.g. inertia, gravity, friction vector) of human body. Multilayer perceptrons (MLP) was used to approximate the maximum crank moment generated by each muscle and trained offline by extreme learning machine (ELM) algorithm. The simulation showed positive results in compensation for muscle fatigue during FES cycling.

Hunt et al. (2004) investigated feedback control strategies to perform FES cycling with the assistance of a motor using a recumbent tricycle. The work was focused on developing a control strategy that simultaneously controls both cycling cadence and leg power output (subject's work rate). The control strategy consisted of two closed-loops, as shown in Figure 1.6, one loop was used to automatically vary the motor's input to maintain the required cycling cadence, and the other loop was to automatically vary the stimulation intensity to maintain the leg power close to an arbitrary reference value. Thus the leg power output can be controlled to arbitrary values ranging from zero and up to values obtained by maximum stimulation intensity. Separately for both loops, with the aid of paraplegic subjects, open-loop dynamics were identified, by applying input signals and recording the resulting output, and system identification approaches were used to estimate a linear dynamic transfer function, using least squares method, that describes the behaviour of the system. Pole assignment approach was used to design model-based controllers of both loops. Different cycling cadence, loads and disturbance were tested, and satisfactory tracking results were obtained. The proposed control strategy was effective in extending the achievable work rate, and was found as a promising technique to improve the overall performance in mobile FES cycling.
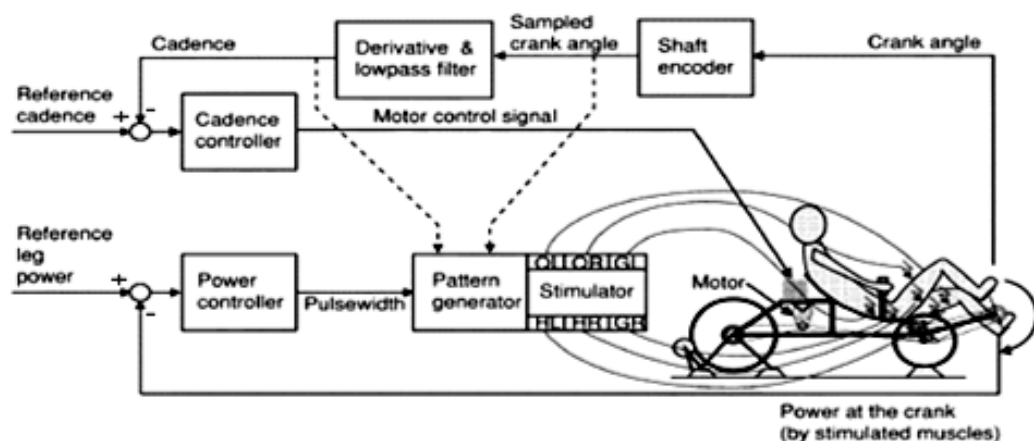
Figure 1.6: Integrated feedback controller (Hunt et al., 2004)

Takahashi et al (2004) aimed to control the force distribution of the legs and the assistance of a motor using a wheelchair-based cycling device. They compared two types of controllers, PD and physical work estimator, and tested them on a quadric paresis subject. Both controllers aimed to govern a desired cycling speed. The PD controller was used to minimize the assistance of the motor used and allow maximum utilization of leg force to propel the vehicle in order to increase the overall energy efficiency of the system. When the error between the desired and the actual velocity is small, no significant drop in the voltage appears around the saturation block which prevents successive muscle stimulation. When the error is large, voltage drop appears around the saturation block which excites the motor to produce rotational torque to assist the leg. The torque generated by the motor is added to the torque generated by the leg through mechanical torque diode. The physical work estimator-based controller is used to enhance both the efficiency and the optimality of power assistance. The physical work-based controller estimates the required physical work to govern a desired speed, according to a pre-defined criterion the controller distributes the work between the stimulator and the motor. The estimation performed was an off-line estimation and took into account the maximum leg force, system's weight and friction. From the results, it is clear that the cycling suffered from jerking with both controllers, even though the physical work-based controller's performance was better than that of PD controller in terms of desired speed tracking.

Similar to the work of Hunt et al. (2004), Hongyuan et al. (2008) proposed an automatic power control method to improve the performance of the lower limb during FES cycling. The author estimated the dynamic models of the response from muscle stimulation intensity to power. System identification approach was used to identify the system model and derive a relationship between pulse width and power output. A linear third order transfer function was obtained and used in the design of a state feedback controller. The cycling speed was supposed to be fixed to 30rpm, and three muscle groups were stimulated (gluteus, hamstrings, quadriceps). Dynamic stimulation

patterns were used to allow different subjects to train on the same device, and the stimulation patterns were forwarded by 18º to compensate for muscle's response delay (0.1s). The controller was able to track arbitrary signals measured from healthy people, while failed to track high frequency signals. Also, Massoud (2007) introduced a feedback control method based on FLC approaches to achieve FES cycling for paraplegics by stimulating the quadriceps muscle group only with the aid of a spring. Although the control approach was shown to be successful, the use of a spring to provide flexion action and replace legs' flexor muscles can be considered as a disadvantage on the overall training session as the spring takes its energy from the leg during the pushing phase and imposes additional load on the quadriceps and consequently fatigues the muscle.

In addition to classical and adaptive control approaches, robust control technique has also been used in FES cycling. Farhoud and Erfanian (2010, 2014) proposed a control method based on second-order sliding mode technique to control leg power during FES cycling. The proposed robust control was utilized to account for nonlinearity and time-variant properties of the musculoskeletal systems stimulated by FES signals. Although classical sliding mode technique is effective in dealing with nonlinearities, uncertainties and external disturbances, the authors utilized higher order sliding mode technique with super-twisting algorithm to avoid chattering, i.e. high frequency oscillation in the input, which usually appears with first-order sliding mode. The results of the proposed technique show good tracking for both leg power and cycling cadence, but the results show continuous muscle stimulation to govern the tracking which can cause rapid muscle fatigue and termination of the training session.

1.7 Physiology of human muscle

The muscle system is responsible for providing motor power for all movements of body parts. There are three types of muscle in the body; skeletal, smooth and cardiac. Smooth muscles are responsible for unconscious body activities such as the movement of food through the digestive system. Cardiac muscles are also involuntary but responsible for heart contraction to pump blood to the body. On the other hand, skeletal muscles, stimulated by the central nervous system and subject to conscious control, are responsible for all voluntary movements such as walking and maintaining posture. This research reviews only skeletal muscles of lower limbs, such as the quadriceps, to provide training and functional movement by FES for disabled individuals.

Skeletal muscles are attached to bones by tendons at the end of the muscle. Each muscle is composed of long cylindrical cells called muscle fibres run from one tendon to another. Groups of fibres are bundled together and wrapped by a connective tissue making subunits of the muscle called fascicles. Fibre's length can be measured in centimetres with 10 to 100μm diameter. Each muscle fibre contains a large number, hundreds to thousands, of long cylinders of muscle protein called myofibrils which in turn are composed of a series of contractile elements known as sarcomeres lined up end-to-end (Marieb and Hoehn, 2006). The sarcomeres of a myofibril are the force generating units of muscle. The sarcomere is composed of two types of myofilaments; thick and thin filaments, as shown in Figure. 1.7.
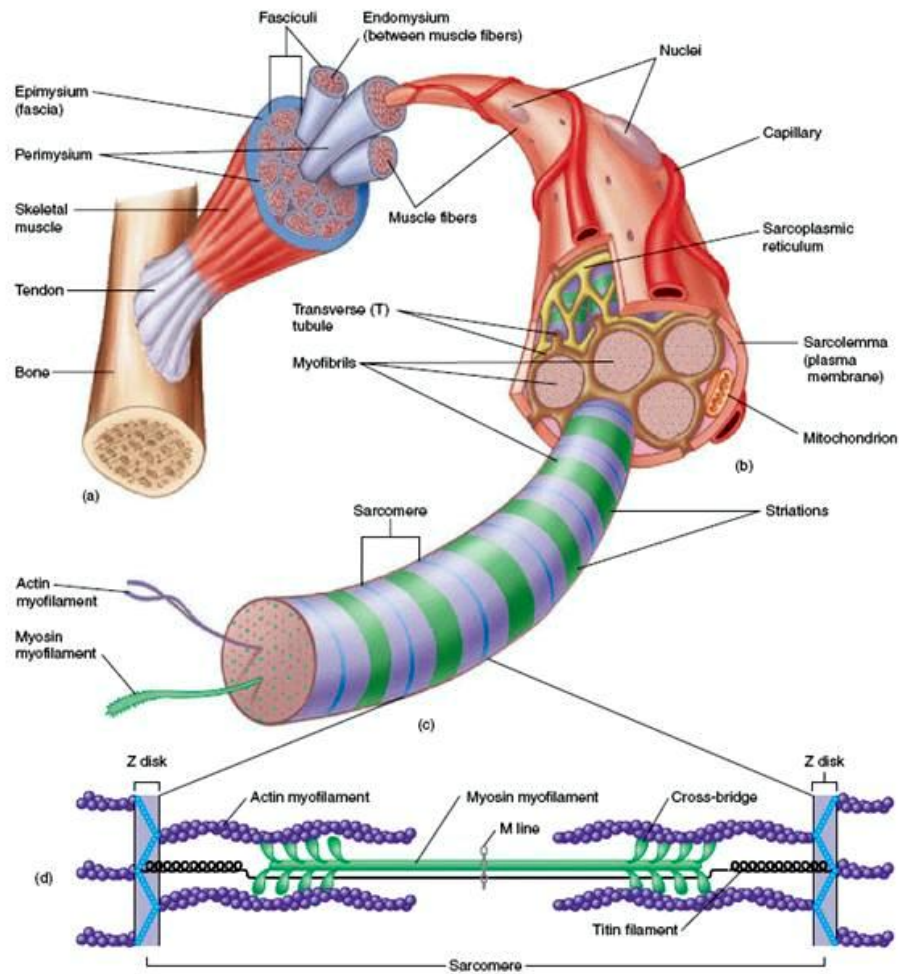
Figure 1.7: Structure of skeletal muscle (Gross Anatomy, 2010)

Muscle cell, i.e. fibre, membrane is called sarcolemma which forms a physical barrier against the external environment and is responsible for passing the impulses, sent from the central nervous system, along the membrane to generate contraction. Under the sarcolemma, there are other components that surround the myofibrils such as the mitochondria, sarcoplasmic reticulum (SR) and transverse-tubules (T-tubules). The SR forms a network around the myofibril that stores and releases calcium ions (Ca^{2+}) necessary for muscle contraction. The T-tubules surround the myofibrils and conduct the impulses from the surface of the cell, i.e. sarcolemma, to the SR.

In each sarcomere, each thick filament is typically surrounded by six thin filaments. The think filaments are located in the centre of the sarcomere, while the thin filaments slide over the thick filament from each end towards the centre of the

sarcomere. The thick filaments are composed of Myosin protein with thick heads usually called cross bridge. The cross bridge has binding sites for both Actin protein and Adenosine Tri-Phosphate (ATP) molecules that transfers chemical energy within cells. The thin filaments composed of chain of Actin proteins and surrounded by Troponin, which have binding sites of Ca^{2+}, and Tropomyosin proteins.

When the muscle is relaxed, the Tropomyosin lies between the Myosin and Actin preventing their contact. When Ca^{2+} is released from the SR and fills the site, due to impulse, it causes changes in the shape and position of the Troponin. Since the Troponin is attached with the Tropomyosin, the shift of the Troponin causes movement of the Tropomyosin and consequently the attachment of the Myosin heads with the Actin. This attachment leads to the swivel of the cross bridge, sliding of the thin filament, breakage of ATP, attached to the Myosin heads, into adenosine diphosphate (ADP) and inorganic phosphate (Pi). When the ATP binds again with the cross bridge it causes the separation of the cross bridge from the Actin, and the cross bridge attaches with another Actin molecule. The slide of the thin filament towards the centre of the sarcomere causes the sarcomere, hence the fibrils and fibres, to shrink causing muscle contraction. As the ATP concentration in the muscle reduces, the Myosin heads remain bound to the Actin and can no longer swivel. The drop of ATP levels in a muscle results in muscle fatigue (Ritchison, 2001).

1.7.1 Motor units

The nervous system communicates with skeletal muscles through neuromuscular junctions. Although each muscle fibre has only one neuromuscular junction, the axon of the motor neuron divides into branches and form junctions with several fibres. If a motor neuron axon is activated in the spinal cord, all the fibres connected to it will synchronously contract. Therefore a single axon with all the fibres it innervates is collectively known as the motor unit, as shown in Figure 1.8. A single muscle may consist of hundreds of motor units. A single motor unit may innervate 3-6 fibres in the

muscles that perform fine control such as muscles that control the movement of fingers and eyes. Other motor units may innervate up to 600 fibres as in leg muscles.

The fibres of each motor unit are of the same type. Slow motor units consist of type I, slow and fatigue resistant, fibres. Moderate motor units compose of type IIA, fast and fatigue resistant, fibres. While fast motor units innervate type IIB, fast and fatigable, fibres. Although the composition of the motor unit is homogenous, i.e. composed of the same fibre type, a given muscle may be composed of different types and sizes of motor units.
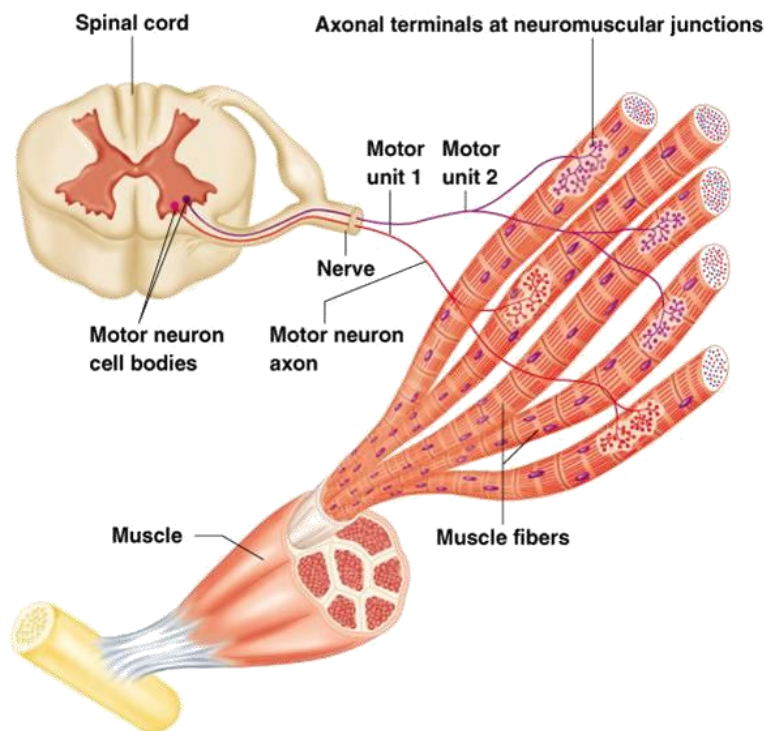
Figure 1.8: Neuron axon with all fibres it innervates forming a motor unit (Marieb and Hoehn, 2006)

The force generated by a muscle is controlled by the brain using two principles; the size and firing rate. The smaller motor units, of few fibres and a low activation threshold, are recruited first. As more force is required, bigger motor units, of more fibres and higher activation threshold, are recruited. Usually small motor units are composed of slow twitch fibres while big motor units consist of fast twitch muscle

fibres. The second criterion is the firing rate of the stimulus. Within each motor unit there is a range of firing frequencies. Slow units operate at lower frequencies than fast units. Within the frequency range of a given motor unit, the force generated can be increased with the increase in frequency of the action potential. If a muscle fibre receives an action potential before relaxing from the previous contraction, force summation will occur (Exercise Physiology, 2014).

In any activity or exercise, to maintain the required force, a sufficient number of motor units are recruited. Initially, the required force may be obtained by activating few or none of fast units. However, as the slow units fail to produce the required force due to fatigue, faster units are recruited for more force production. This additional recruitment of fast fatigable motor units leads to increased lactate production and consequently the acceleration of fatigue towards the end of long or severe bouts. However, with continuous exercise, some units are firing while others recover, and this leads to a built in recovery period and fatigue resistance (Exercise Physiology, 2014).

During exercising the disabled by FES the same motor units are innervated and the reverse recruitment order of motor neurons may take place. This leads to premature termination of the exercise due to fatigue and consequently limits the benefits of the exercise.

1.8 Muscle model

Researchers have focused on studying and modelling the behaviour of human muscles for use in simulation environments. One of the well-known and frequently employed muscle models is that developed by Hill (1938).

The Hill muscle model, Figure 1.9, describes the behaviour of a muscle using three main elements, the series or elastic (Es), the contractile (Ec) and the parallel element (Ep). The series element represents the elasticity in the myofilaments, while the contractile element represents the active muscle force generated from muscle's

energy stores. The parallel element is added to interpret the passive resistance, i.e. viscosity, of the tissues that surround the contractile element. The contractile element, is modelled as the product of three experimentally measured factors namely the force-length, force-velocity and the activation dynamics.
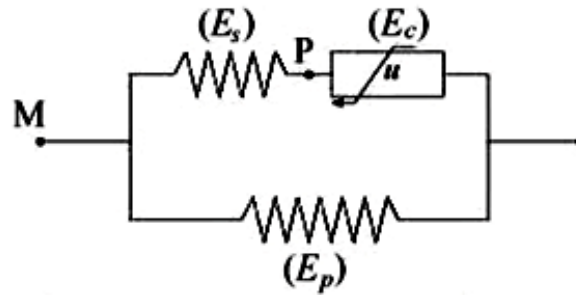
Figure 1.9: Hill-type muscle model

Since the development of Hill's muscle model, several attempts have been made to increase the accuracy of the model by adding further information to the model. For example, by adding the effect of the tendon and accounting for the pennation angle of muscle fibre, Zajac et al. (1986) introduced a more accurate model, as shown in Figure 1.10, than that of Hill.
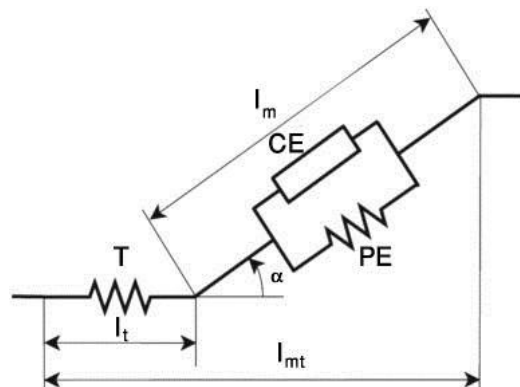
Figure 1.10: Zajac-type muscle model

Other researchers (Makssoud et al., 2004; Riener et al., 1996) introduced more complex but more accurate muscle models by interpreting the physiologically-based behaviour of the muscle such as calcium dynamics, muscle fatigue and the cross-bridge phenomena. The muscle model proposed by Riener et al. (1996) has three main parts, the activation, the contraction, and the body segmental dynamics. The activation

24

dynamics part represents the activation required by the muscle to produce force. It is represented by a first order function of both signal's pulse width and frequency. Also, it includes calcium dynamics and fitness function to account for the effect of fatigue in the muscle. The contraction dynamics part, based on Hill model, is used to describe the properties responsible for generating muscle force such as activation, force-length and force-velocity relations. The body segmental dynamics were described by taking into account the equation of motion and the properties of passive muscle. Ferrarin and Pedotti (2000) produced a simplified model that describes the behaviour of the quadriceps muscle stimulated by FES signal. The knee movement after stimulating the quadriceps muscle and the produced muscle torque was recorded. Autoregressive with exogenous inputs (ARX) model structure was used to estimate a single pole transfer function that describes the relationship between electrical stimulus and the generated active muscle torque.

Another muscle model proposed by Makssoud et al. (2004) consisted of two sections, the activation part and the mechanical part. The activation part depends on pulse width and the frequency of the stimulation signal, while the mechanical part addressed the mechanical behaviour of the muscle. Although this model is based on physiological interpretations, it lacks description of calcium dynamics and muscle fatigue. Also, Jailani (2010) developed a muscle model by making use of a data set obtained clinically through the application of FES signals to the quadriceps and hamstring of a paraplegic and record of the resultant leg force. The author used Adaptive neuro fuzzy inference system (ANFIS) technique to derive quadriceps and hamstring muscle models.

1.9   Functional electrical stimulators and stimulated muscles

Functional electrical stimulation to paralyzed muscles can be performed by using surface, percutaneous or implanted electrodes. Researchers have used either amplitude,

i.e. voltage or current, or pulse width controlled stimulators to stimulate different combinations of muscle groups in lower extremities to perform FES cycling training.

Using surface electrodes, Petrofsky et al. (1983) used a portable sequential pulse generator of four channels controlled by Z80 microprocessor to stimulate the muscles. Sequential stimulation of the muscles was used to reduce muscle fatigue and allow better movement control. The stimulator utilized was to generate signals of 50Hz frequency, 300 µsec fixed pulse width with voltage controlled output of 0-300 volt signals of trapezoidal shape to prevent jerking due to sudden contraction. They stimulated the quadriceps and the gluteus maximus muscles of both legs to perform cycling exercise. While in another work, (Petrofsky and Smith, 1992), they used a Motorola single-chip microprocessor (68705R3)-based current-controlled stimulator of twelve channels providing biphasic square waveforms with 30Hz frequency to stimulate the quadriceps, hamstring and gluteus maximus muscle groups of both legs. Takahashi et al. (2004) used an onboard computer-controlled stimulator to stimulate leg muscles using voltage controlled stimulation signals of fixed 100Hz frequency and fixed 250µs pulse width. Pons et al. (1989) used current controlled stimulator of 25Hz frequency, biphasic waveforms, 150V at maximum pulse width of 400µs and 90-100mA current. Trapezoidal shape signals were used to stimulate the quadriceps, hamstrings and the gastrocnemius muscles. Chen et al. (1997) utilized a monophasic type stimulation to stimulate both the quadriceps and the hamstring muscles with FES signals of fixed 20Hz frequency, fixed 300µs pulse width and variable stimulation intensity of maximum 120mA current.

Using pulse width modulation, Hunt et al. (2004) used a portable multichannel stimulator operated at constant frequency of 20Hz. The stimulator current, 10mA – 120mA, was first adjusted for each channel to an appropriate value before the start of each experiment, to get the optimal muscle response, then fixed and used. The pulse width was kept variable, 0-800µs, to adjust the stimulation intensity during FES cycling. The quadriceps, hamstrings and the gluteus muscles were used to perform the

cycling. Also, Farhoud and Erfanian (2010) used pulse width modulation ranging from 0 to 700µs through a computer-controlled closed-loop FES system to stimulate the quadriceps and the hamstring muscle groups with bipolar stimulation pulses of constant amplitude and 25Hz frequency. Later, they developed their work using pulse width and pulse amplitude modulation (Farhoud and Erfanian, 2014).

Perkins et al. (2002) was the only one to the author's knowledge who utilized implanted lumbo-sacral anterior root stimulator (LARSI) to perform FES propelled cycling for a female of complete T9 injury. The stimulator was of fixed 3.2mA current, 20Hz frequency, and variable, 2-990µs, pulse width.

1.10 Assisting mechanisms

People with SCI usually have weaker muscles, as compared with healthy persons, and suffer from rapid muscle fatigue, during FES-based training, and that leads to rapid termination of the training session. Further, due to having very weak muscles, some disabled persons cannot perform any FES exercise without assistive means. For these reasons, researchers have tried different assisting mechanisms to achieve prolonged training sessions. Pons et al. (1989) utilized an electrical motor to provide passive cycling of low speed as well as assisting and retarding the cycling achieved by active FES exercise on the legs. The initial drive of the vehicle was provided by the motor to prevent high loads on the muscles. Also, the motor was used to ensure that pedalling speed was over 25 rpm to prevent termination of the session. Gearing of 18 gears was also equipped to allow weak muscles propel the vehicle.

Gföhler et al (1998) installed an auxiliary motor on the front wheel to assist the cycling, in case of insufficient muscle torque, and provide braking in case of exceeding the desired speed. The motor was necessary to give the first movement and overcome the initial inertia, assist the driver to cycle over gradients, drive the disabled back in case of muscle fatigue and assist paraplegics with weak muscles to drive the tricycle.

Hunt et al. (2004) simultaneously controlled both cycling cadence and leg power output, i.e. subject's work-rate, with the aid of a motor. Takahashi et al (2004) used an electrical motor to continuously provide assisting torque to the leg. Furthermore, Perkins et al. (2002) utilized a manual gear to slowdown the speed in case of running outside the safe speed range, in addition to an auxiliary motor fitted in the tricycle for the patient to be able to return home in case of muscle fatigue.

Petrofsky and Smith (1992) recruited a non-paralysed healthy person, using a modified tricycle of two side-by-side seats, to provide pedalling assistance for a paraplegic during FES to propel the vehicle, pass the cycling dead spots and also to provide assistance to pass steep hills and in case of muscle fatigue. Chen et al. (2004) utilized an arm-crank to assist the legs and provide hybrid exercise. Table 1.1 shows brief information about the different assisting mechanisms and the stimulated muscle groups used by researchers to perform FES cycling training.

Table 1.1: A classification of researches according to the utilized assisting mechanism and the stimulated muscle group. (Q=Quadriceps, H=Hamstring, G=Gluteus maximus, I=iliacus, TA=Tibials anterior, GS=Gastrocnemius, P= Peroneal nerve)

Author	Muscles							Assisting device		
	Q	H	G	I	TA	GS	P	Motor	Flywheel	Spring
Petrofsky et al., (1983)	X		X							
Petrofsky et al., (1984)	X			X					X	
Pons et al., (1989)	X		X		X			X		
Petrofsky and Smith, (1992)	X	X	X							
Glaser et al., (1996)	X	X	X		X	X			X	
Chen et al., (1997)	X	X							X	
Gföhler et al., (1998)	X	X	X					X		
Angeli et al., (1999)	X	X	X				X	X		
Takahashi et al., (2004)	X	X	X					X		
Fornusek et al., (2004)	X	X	X					X		
Massoud et al., (2007)	X									X
Farhoud and Erfanian (2014)	X	X						X		

1.11 Motivation of the research

Controlling the movement of paralyzed limbs with FES using open-loop control strategy is particularly difficult. As several parameters differ from person to person, such as muscle response to FES, skin sensitivity and muscle's training condition, the stimulation parameters applied in open-loop systems are specific for single user and may not produce the same performance with other persons (Abbas and Triolo, 1997; Berkelmans, 2008). The procedures of determining the stimulation parameters are time consuming; trials lasted for 20-45 minutes to find the optimal parameters for the leg, by stimulating quadriceps only, to follow a desired trajectory (McNeal et al., 1989). Moreover, the open-loop approach cannot account for unforeseen conditions such as muscle spasm and mechanical disturbances. For these reasons researchers have focused on utilizing closed-loop control strategies to overcome these problems (Farhoud and Erfanian, 2014; Kim et al., 2008; Takahashi, 2004).

To reduce the possible mechanical problems that might occur during FES-cycling due to several electrode wirings and in an attempt to provide more comfortable exercise by reducing the pre-cycling preparations required for locating the electrodes at their optimal locations over the skin to get optimal muscle response, Massoud (2007) produced stimulation patterns, to perform coordinated FES-assisted cycling movement, based on stimulating single muscle group, the quadriceps, of each leg.

The flywheel, as an energy storage device, has been widely used in many commercial FES cycling ergometers. It has been used to provide smoothness to the cycling and help pass the cycling dead spots for individuals able to pedal under loads (Fornusek et al., 2004). Usually, disabled people encounter difficulties to pedal the crank of the ergometer due to weak leg muscles (Peng et al., 2011). A fix-geared flywheel imposes extra load on the crank which in turn makes it harder for individuals of weak muscles to generate sufficient force and overcome the inertia to drive the flywheel without external assistance (Fornusek et al., 2004). Moreover, the use of a fix-geared flywheel is usually accompanied with a braking mechanism to govern the

required speed. As a result, the excessive energy in the system dissipates due to the brake.

A hybrid kinetic energy recovery mechanism consisting of a flywheel, clutch and a continuously variable transmission (CVT) was designed for use in formula 1 motor sports in 2009 for the purpose of fuel consumption (Cross and Brockbank, 2009). The flywheel is used to store the kinetic energy in the vehicle during braking, and later reuse the same stored energy to accelerate the vehicle. The test results showed the ability of the system to save up to 21% of the driving energy of the vehicle.

To overcome the afore mentioned limitations in using fixed-geared flywheel in FES-cycling and delay the appearance of muscle fatigue, a flywheel and electrical clutch assist mechanism can be utilized to absorb the excessive energy in the system and reuse it to assist the leg when necessary. Consequently, reducing the stimulation intensity on the muscle and prolonging the exercise.

Although increasing the stimulation intensity is required when exercising against loads for short periods to increase the muscle bulk, which is out of the scope of the current project, reducing the stimulation intensity of FES, to delay the appearance of muscle fatigue, and prolonging the period of cycling exercise is necessary to obtain cardiovascular related benefits for SCI individuals (Idso, 2004).

1.12 Aims and objectives of the research

The aim of the research is to develop a portable and efficient FES-assisted cycling ergometer to exercise individuals with spinal cord injury by stimulating single muscle group only, the quadriceps, and achieve performance enhancement through the use of a novel assisting mechanism to assist the legs, provide smooth cycling and extend the period of the exercise.

The main objectives of the research are summarized as:

I.   To develop a bicycle exercise ergometer and a humanoid model with intelligent control strategies to obtain coordinated FES driven cycling by stimulating the quadriceps muscle group of both legs.

II.   To further develop the exercise ergometer by incorporating a novel assisting mechanism, represented by a flywheel and electrical clutch, and utilize it for the first time in FES-cycling with intelligent control strategies to decrease the stimulation intensity, delay muscle fatigue, prolong and smoothen the exercise.

III.   To optimize the design parameters to obtain enhanced cycling performance and minimize muscle fatigue using evolutionary algorithms.

1.13 Thesis outline

Chapter 1: This chapter introduces brief information about spinal cord injury, the physiology of human skeletal muscle and the use of functional electrical stimulation for rehabilitation purposes. Moreover, the importance and the benefits of FES-assisted cycling exercise, as compared with other types of exercises by FES, are outlined in this chapter. A detailed literature review is outlined about FES-cycling ergometers, assist mechanisms, control approaches and the developed muscle models. Also, the types of stimulators used and the different combinations of muscles stimulated during FES-cycling are mentioned. Finally, the objectives of the research, the contributions and the list of publications arising from this work are outlined.

Chapter 2: This chapter explains in detail the modelling of a humanoid-bicycle using Visual Nastran 4D (vN4D) dynamic simulation software. The integration between vN4D and Matlab/Simulink software is briefly introduced. Also, information about the utilized linear muscle model, to mimic the behaviour of quadriceps muscle group stimulated by FES signal, is presented. Further, it describes in detail the development

of force-drop indicator model, from clinically recorded data, to be used for assessment purposes in subsequent chapters.

Chapter 3: This chapter presents the closed-loop control of FES-cycling based on the knee angle of each leg. It describes the closed-loop control of FES-cycling by regulating the stimulation intensity on the quadriceps muscle group using PD and fuzzy logic control. Also, it introduces the closed-loop control of FES-cycling by stimulating the quadriceps with the aid of a flywheel and electrical clutch assist mechanism. Boolean and fuzzy logic based closed-loop control approaches are introduced to build the decision making of the engagement/disengagement of the flywheel, with the crank of the bicycle, by the electrical clutch to provide the required assistance. From fatigue point of view, an assessment between FES-cycling with and without the assist mechanism is introduced using the derived force-drop indicator.

Chapter 4: This chapter investigates the ability to obtain the desired cycling cadence by stimulating the quadriceps in FES-cycling. Also, a physiological based dynamic nonlinear muscle model of the quadriceps is used to obtain more realistic results. Fuzzy logic based closed-loop control of FES-cycling, based on the desired cadence, is introduced. Also, a closed-loop cadence control with the aid of a flywheel and electrical clutch mechanism is introduced. A comparison between the two approaches, from cadence control and stimulation intensity points of view, is made.

Chapter 5: This chapter describes the effect of different gear ratios, between the flywheel and the crank, on the performance of FES-cycling. Fifty eight different gear ratios are set up to evaluate the effect of the gear ratio on the cycling performance from cadence and efficiency points of view. The results obtained from fifty eight gear ratios are discussed. Also, to enhance the performance further, the effect of different crank

positions with respect to the hip joints is studied. Twenty five different positions of the crank are set up and the results studied to find out the best crank position. The best crank position with seventeen gear ratios is further tested. The results are analysed and the best gear ratio is specified and selected for use with the best crank position for performance enhancement.

Chapter 6: This chapter describes the parameter optimization of FES-cycling using evolutionary algorithms. Genetic algorithm (GA) is used to optimize five design parameters, fuzzy logic control and flywheel angular velocity scaling factor, to obtain minimum cadence error. To reduce the cadence error further, GA is used to optimize eleven parameters to include the stimulation phases and flywheel related parameters. Moreover, multi-objective genetic algorithm optimization technique is used to optimize eleven design parameters for performance enhancement of the FES-cycling. The optimal solution is selected, tested and system performance assessed.

Chapter 7: This chapter concludes the work and recommendations are presented for possible further development of the work in the future.

1.14 Contributions

Dynamic modelling of FES-cycling with flywheel and clutch mechanism: The cycling ergometer, flywheel and electrical clutch assist mechanism and the humanoid are modelled using Visual Nastran 4D (vN4D) dynamic simulation software. The use of vN4D allows the model to be simulated in a virtual environment with the ability of real-time measurement and parameter adjustments of each part of the design. This enables on-line visualization of the system behaviour and simultaneous evaluation of the performance. To the author's knowledge, the flywheel and electrical clutch

mechanism with different gear ratios have not been previously modelled and used in FES-cycling.

Modelling of force-drop indicator: In this study, a force-drop indicator is developed for assessment purposes between two control approaches from fatigue point of view. The indicator is derived from clinically recorded data using curve fitting techniques. The data is recorded during an isometric test of the quadriceps muscle of a paraplegic participant. The indicator combines the pulse width of the signal and number of the stimulus with the resultant muscle force. To the author's knowledge, the development of such indicator has not been reported.

Control of FES-cycling with flywheel mechanism: In this study, control of FES-cycling by stimulating the quadriceps of each leg is presented using PID and fuzzy logic control. The integration of the flywheel and electrical clutch assist mechanism in a closed-loop control approach leads to decrease in the stimulation required to govern a desired cycling cadence. The engagement of the flywheel is implemented using Boolean and fuzzy logic approaches. To the author's knowledge, the closed-loop control of FES-cycling by stimulating the quadriceps with the aid of the flywheel and electrical clutch mechanism is a novel and new work.

Control of assist mechanism using two closed-loop approaches: The control of the assist mechanism is implemented using two approaches. The first approach is based on the angular velocity of the leg. The second approach is based on the angular velocity of the crank. Both approaches depend on the angular velocity of the flywheel to decide on the proper engagement/disengagement of the flywheel with the crank to provide the necessary assistance. Both of the approaches are novel and have not been reported.

Optimal design of FES-cycling with flywheel mechanism using evolutionary algorithm: Two evolutionary algorithms are used to optimise the design parameters of FES-cycling exercise assisted by a flywheel and electrical clutch mechanism. Genetic algorithm is used to optimise eleven design parameters, including fuzzy logic control's parameters; stimulation phases; flywheel weight and engagement mechanism's scaling factor, to minimize the error in cadence. Also, multi-objective genetic algorithm is used to optimise these parameters, based on two objectives (minimize the cadence error and maximize the efficiency), simultaneously. The use of evolutionary algorithms to optimize FES-cycling with flywheel mechanism has not been reported and is considered as a contribution.

1.15 Publications

The list of publications arising from this research work to date is shown below:

Journal papers:

Abdulla, S. and Tokhi, O. (2014) "Functional electrical stimulation assisted cycling exercise optimized by multi-objective genetic algorithm", *Integrated Computer-Aided Engineering (ICAE)* (Submitted).

Abdulla, S., Sayidmarie, O. and Tokhi, O. (2014) "Functional electrical stimulation-based cycling assisted by flywheel and electrical clutch mechanism: A feasibility simulation study", *Robotics and Autonomous Systems, 62*, pp.188-199.

Conference papers:

Abdulla, **S.,** Sayidmarie, O., Gharooni, S. and Tokhi, O. (2012) "Modelling and control of a novel FES driven assisted cycling mechanism", *the 17'th International*

Conference on Methods and Models in Automation and Robotics, Miedzyzdroje, Poland, 27-30 August 2012, pp.464-469.

Abdulla, S. and Tokhi, O. (2012) "Fuzzy logic based FES driven cycling by stimulating single muscle group", *the 1`st International Conference on NeuroRehabilitation*, Toledo, Spain, 14-16 November 2012, pp.173-182.

Abdulla, S. and Tokhi, O. (2014) "A novel closed-loop control approach for a flywheel and electrical clutch assist mechanism in FES cycling", *International Conference on Advances in Control Engineering*, Istanbul, Turkey, 5-7 September 2014, pp.51-55.

Abdulla, S. and Tokhi, O. (2014) "Comparative assessment of two fuzzy logic based control approaches for a flywheel and electrical clutch assist mechanism in FES cycling", *the 19'th International Conference on Methods and Models in Automation and Robotics*, Miedzyzdroje, Poland, 2-5 September 2014. (Accepted)

Abdulla, S. and Tokhi, O. (2014) "Optimization of indoor FES-cycling exercise assisted by a flywheel mechanism using genetic algorithm", *IEEE Multi-Conference on Systems and Control,* 8-10 October 2014, Nice, France. (Accepted)

Oral presentations:

Abdulla, S. and Tokhi, O. (2013) "Functional electrical stimulation-based cycling exercise for paraplegics using flywheel and electrical clutch mechanism", *PhD. Presentation Showcase, United Kingdom Automatic Control Council (UKACC)*, 31st October 2013, IMechE, London, United Kingdom.

Chapter 2: Modelling of cycling ergometer with humanoid, muscle and force drop indicator

2.1 Introduction

To study, analyze and control any system in real life, computer modelling and simulation of the system is necessary where practical measurements are not possible. It has been possible to obtain complex measurements, such as muscle tonus and energy consumption, during different human motion activities, such as rowing and walking, using simulation models (Iwami et al., 2009).

The accuracy of the utilized model affects the correctness of the obtained results. Mathematical representation of musculoskeletal dynamics is highly complex and accompanies several simplifications and assumptions. A precise model of a thorough system requires complex mathematics and correct definition of several parameters, which may lead to convolute, difficult to implement equations and/or an unacceptable solution time (Pennestri et al., 2007). The emergence of the dynamic 3D simulation software was an important facility to simulate the behaviour of complex dynamic systems with high accuracy and reduced time. This work, utilizes Visual Nastran 4D (vN4D) software to build a dynamic model, i.e. humanoid and cycling ergometer, used for FES-cycling motion analysis and control studies in a dynamic simulation environment. The vN4D software is selected for its ability to combine motion, animation and finite element analysis (FEA) in a single software and easily incorporated with Matlab/Simulink platform.

This chapter provides detailed information about the developed humanoid-bicycle model. Also, information about the utilized muscle model, to mimic the behaviour of the quadriceps muscle group stimulated by FES signal, is presented. Further, it produces details about the derived force-drop indicator to be used for assessment purposes in subsequent chapters.

2.2 Visual Nastran software

Visual Nastran 4D (vN4D) is an engineering software environment used by designers and engineers to develop robust three dimensional (3D) designs for a wide range of applications. This software combines motion and FEA into a single integrated modeling system. It produces physics-based animations with the ability to make analyses of temperature, stress, dynamic performance and collision responses of each part in the system. It supports most computer aided-design (CAD) systems through the use of industry standard file format. With Visual Nastran, users can simulate the dynamic of the whole problem as a single part, rather than studying the problem in small parts, leading to more accurate dynamic motion and FEA results.

The vN4D comprises four main parts; *draw it*, *move it*, *break it* and *control it*. The *draw it* tool is associated with the integration of CAD files of different extensions with the virtually three dimensional CAD system, as well as photo-realistic rendering, shadowing and movie creation of the simulated system. The *move it* tool is associated with sophisticated motion analysis and animation. It provides the ability to measure different matters, such as force; velocity; acceleration and position, for each individual segment in the design. The *break it* tool is responsible for combining the motion with the FEA. It provides static and dynamic stress analyses with automatic calculations of loads and stresses throughout the assembly. It automatically clusters mesh elements around greatest stress providing accurate results in less time (Wang, 2001). The *Control it* tool is responsible for providing the integration between vN4D with Matlab/Simulink and other programs such as Visual Basic and Excel.

The vN4D software combines CAD, motion and FEA with control technologies in a single integrated environment. Different CAD files, such as Solid Works® and Inventors®, can be imported by the user into the software, perform dynamic motion simulation and FEA analyses. The vN4D mechanical model is easily linked with Matlab/Simulink, hence control approaches can be easily tested in a dynamic environment through a set of meters or sensors provided for each segment of the 3D

model developed in the vN4D software. For its accuracy and ease of use with Matlab/Simulink environment, vN4D is used in this work as the design tool to develop a dynamic model, represented with a humanoid and cycling ergometer, to be incorporated with Matlab/Simulink software for control purposes.

2.3 Humanoid model

A humanoid model, to simulate a disabled person, is necessary in this work to perform different trials and tests of different control approaches in a simulation platform. This is essential to minimize the trials and experiments that might be costly in time and harsh for the disabled person. To be able to build a mechanical humanoid model and simulate the normal motion of a human, and the reactions of each body segment to external forces in real life, body segment parameters, such as the mass; length and width of each segment, are required.

The accurate determination of human body segment parameters has been a challenge for a long time in biomechanics. Precise body segment parameters are required for proper body motion analysis and for the design of other applications such as cockpit, pressure suit, crash-test dummies and orthosis (Hong and Bartlett, 2008).

The quality of the humanoid model depends on the accuracy of the data used to build the model. The dimensions of human body segments vary with age, racial origin and gender. An estimate of body segments' length as a portion of total body height has been introduced by Drillis et al. (1964) and then by Winter (1990). The introduced segment proportions are considered as a good estimation in the absence of a more accurate data recorded directly from the individual (Winter, 2010).

In this work, the humanoid model is developed, with the aid of vN4D software, using the standard anthropometric human dimensions introduced by Winter (1990) as shown in Figure 2.1. The length and the mass of each body segment are expressed as fraction of the overall body height and weight respectively.
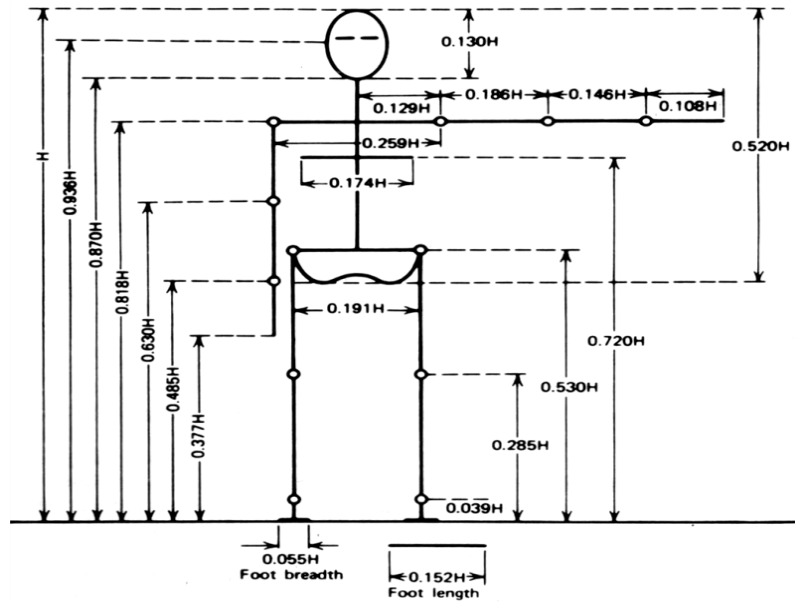
Figure 2.1: Standard anthropometric humanoid dimensions (Winter, 1990)

The humanoid developed in this work is based on a human body of 1.80m height (H) and 70kg in weight (M). The length and mass of each segment of the developed humanoid model are shown in Table 2.1 and Table 2.2 respectively.

Table 2.1: Body segment length of the developed humanoid model

Segment	Segment length, fraction of height[H]	Humanoid model length[m]
Head	0.130H	0.234
Neck	0.052H	0.0936
Trunk	0.288H	0.5184
Upper arm	0.186H	0.3348
Lower arm (Forearm)	0.146H	0.2628
Hand	0.108H	0.1944
Pelvis and Thigh	0.245H	0.441
Shank	0.246H	0.4428
Foot height	0.039H	0.0702
Foot breadth	0.055H	0.099
Foot length	0.152H	0.2736

Table 2.2: Body segment weight of the developed humanoid model

Segment	Segment mass, fraction of mass[M]	Humanoid model mass [Kg]
Head and Neck	0.081M	5.67
Trunk	0.497M	34.79
Upper arm	0.028M	1.96
Lower arm (Forearm)	0.016M	1.12
Hand	0.006M	0.42
Pelvis and Thigh	0.100M	7
Shank	0.0465M	3.255
Foot	0.0145M	1.015

The centre of mass and the density of each segment were obtained from the same anthropometric data. The centre of mass was essential to determine the shape of each segment, while the density of each segment was used to obtain the volume and consequently the segment's width. Table 2.3 shows the location of centre of mass, density and volume of each segment of the developed humanoid model.

Table 2.3: Body segment's centre of mass, density and volume of the humanoid model

Segment (S)	Location of centre of mass, segment length (Proximal)	Location of centre of mass, segment length (Distal)	Density (Kg/l)	Volume (m³)
Head and Neck	1.000S	-	1.11	0.0051
Trunk	0.500S	0.500S	1.03	0.0337
Upper arm	0.436S	0.564S	1.07	0.0018
Lower arm (Forearm)	0.430S	0.570S	1.13	0.0009
Hand	0.506S	0.494S	1.16	0.0003
Pelvis and Thigh	0.433S	0.567S	1.05	0.0066
Shank	0.433S	0.567S	1.09	0.0029
Foot	0.500S	0.500S	1.10	0.0009

Each body segment is connected with joints provided by vN4D software as constraints. The head and neck joints were considered as rigid joints as they have no significant effect on the performance of FES cycling training. Also, the ankle joint that connects the foot with the shank is considered as a rigid joint to represent the ankle-foot orthosis (AFO) used in FES cycling for safety purposes and to allow full

transmission of leg's torque into the crank of the bicycle. The shoulder, elbow and wrist joints are represented by freely revolute joints. While the knee and hip joints of right and left legs are represented by revolute motors in order to be controlled by the torque from quadriceps muscle group of each leg. Table 2.4 shows the type of each joint, axis of rotation, control parameter and degree of freedom for each segment.

Table 2.4: Properties of the developed humanoid joints

Segment	Type of Joint	Axis of rotation (X,Y)	Control parameter	Degree of freedom
Head	Rigid	N/A	N/A	0
Neck	Rigid	N/A	N/A	0
Shoulder	Revolute	X	N/A	1
Elbow	Revolute	X	N/A	1
Wrist	Revolute	Y	N/A	1
Hip	Revolute motor	X	Torque	1
Knee	Revolute motor	X	Torque	1
Ankle	Rigid	N/A	N/A	0

The humanoid model developed using vN4D software, with the aid of the standard anthropometric dimensions, can be seen in Figure 2.2. The humanoid model will be used together with the bicycle model and the new proposed assist mechanism represented by a flywheel and electrical clutch.
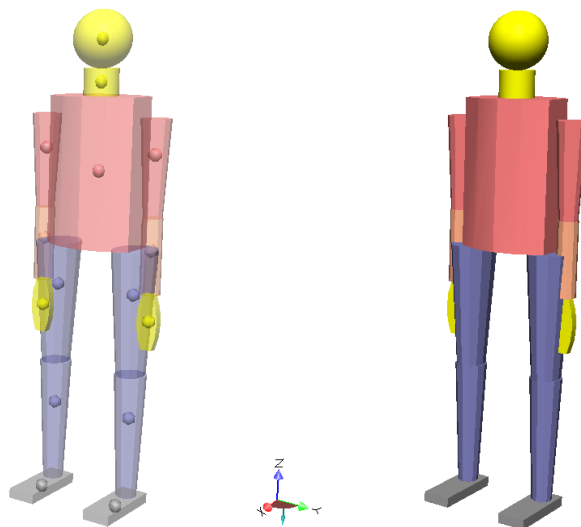
Figure 2.2: The developed humanoid model with and without segmental centres of mass

2.4 Stationary cycling ergometer model

The bicycle model was also developed using vN4D software. The dimensions of the bicycle were considered as (pedal: 0.13 x 0.08 x 0.02m; crank arm: 0.01 x 0.14 x 0.02m; crank (shaft): 0.01 x 0.15m). The material of the crank arm and the crank (shaft) was considered as steel in vN4D software. The specifications of the designed bicycle model were obtained from a real cycling ergometer available in the laboratory at the department of Automatic Control and Systems Engineering, The University of Sheffield. To simulate a more realistic system and obtain more reasonable results, a standard ball bearings friction with rotational coefficient (0.0015) and effective radius (0.01m) was added to the model. The developed bicycle model is shown in Figure 2.3.
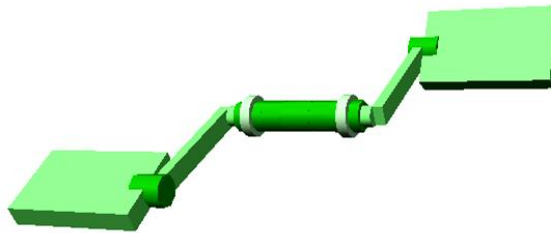
Figure 2.3: The developed bicycle model

As an assisting mechanism, a flywheel and an electrical clutch, was added to the bicycle model using the vN4D software. The flywheel dimensions used are (Radius: 0.2m, height: 0.01m, weight: 3.48kg). To simulate the behaviour of an electrical clutch that is responsible for engaging/disengaging the flywheel with/from the crank (shaft), a rigid constraint with on/off operating condition, between the flywheel and the crank (shaft) was implemented in vN4D software. The engagement and disengagement of the flywheel is to be controlled through an on/off control input via Simulink/Matlab software. The developed humanoid-bicycle model with the flywheel and electrical clutch mechanism is shown in Figure 2.4.
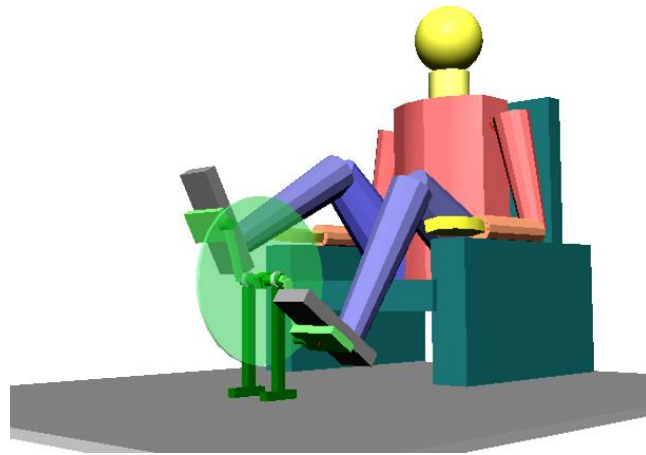
Figure 2.4: The developed humanoid-bicycle model with flywheel and electrical clutch mechanism

2.5 Visual Nastran linked with Matlab/Simulink

The humanoid-bicycle model developed in vN4D software is to be used for investigating different FES-cycling control approaches in subsequent chapters. The control approaches will be implemented in Matlab/Simulink platform. One of the most important advantages of vN4D software is its ease of use with Matlab/Simulink software. A block representing vN4D model, available in the library of the software, can be inserted into the Matlab/Simulink environment and linked with other available blocks of the proposed control block diagram.

Another advantage of vN4D is its ability to receive control input signals from Matlab/Simulink to control joint variables; such as torque, force, rotational velocity and acceleration, as well as the ability to provide different sensor information, i.e. meters, such as position, velocity, acceleration and linear momentum, etc, for each segment in the design as an output to Matlab/Simulink. The information sent from the meters can be used as a feedback signal in control design or for system behaviour analysis.

Figure 2.5 shows a general block diagram of a vN4D model linked with a muscle model in Matlab/Simulink environment. The muscle model receives FES signal and

generates torque sent to the knee joint in the humanoid-bicycle model to produce leg movement.
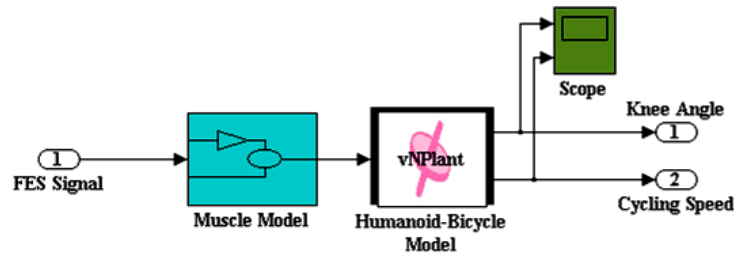
Figure 2.5: Block diagram of a vN4D model linked with a muscle model in Matlab/Simulink

2.6 Muscle model

The human musculoskeletal muscles, that are responsible for producing voluntary movement, have been widely described in the literature (Ferrarin and Pedotti, 2000; Hill, 1938; Huxley, 1957; Makssoud et al., 2004; Zajac et al., 1986; Zajac, 1989). Since the development of Hill's muscle model several attempts have been made to increase the accuracy of the model by adding further information, such as adding the tendon effect (Zajac, 1989; Zajac et al., 1986) or interpreting the physiological behaviour of the muscle (Riener and Fuhr, 1998; Riener and Quintern, 1997; Riener et al., 1996). Although muscle models based on the physiological behaviour of the muscle are assumed to be more accurate than others, several parameters need to be optimized to obtain acceptable performance, which increases the implementation complexity. For this reason, in the early stages of this work, it is preferred to use the model featured in (Ferrarin and Pedotti, 2000), which is simple to implement and accurate enough as it has been derived from data obtained experimentally, from paraplegics and healthy subjects, using system identification approaches.

2.6.1 Muscle model developed by Ferrarin

A model of knee extensor muscle, the quadriceps, that relates the electrical parameters, i.e. pulse width and frequency, of FES signal to the resultant dynamic knee joint torque has been developed by Ferrarin and Pedotti (2000). To derive the model, the lower limb was modelled as two rigid segments represented by the thigh and shank-foot combination as shown in Figure 2.6. The ankle movement was not taken into consideration and the ankle was fixed to 90° to represent the ankle-foot orthosis (AFO) usually used to restore gait and prevent injuries. This reduced the number of degrees of freedom and prevented the gastrocnomious, i.e. bilateral, muscle to affect the passive properties of the knee joint due to ankle movement. The thigh was supposed to be fixed on a supporting table and only the dynamics of the shank-foot part were considered.
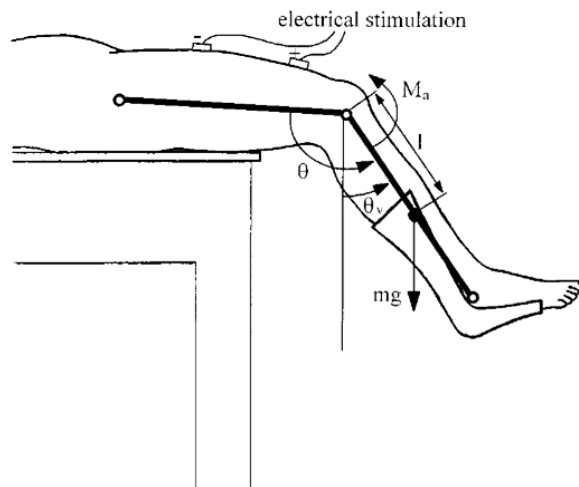
Figure 2.6: Lower limb with surface stimulation to the quadriceps. θ is the knee joint angle, θ_v is the vertical inclination of the shank, M_a is the active joint torque, l is the distance between the shank-foot center of mass and knee joint center, mg is the gravitational force (Ferrarin and Pedotti, 2000)

The dynamic equilibrium of the moments acting on the knee joint in the sagittal plane was first described, as:

$$M_i = M_g + M_s + M_d + M_a \tag{2.1}$$

where M_i is the torque due to inertial component, M_g the torque due to gravity, M_s the passive torque due to stiffness or elasticity, M_d the passive damping torque due to viscosity, M_a the active torque resulting from quadriceps stimulation.

This can be expressed as a non-linear second-order differential equation as:

$$J \,.\, \ddot{\theta}_v = -m \,.\, g \,.\, l \,.\, \sin(\theta_v) + M_s - B \,.\, \dot{\theta} + M_a \tag{2.2}$$

where J is the moment of inertia of shank-foot combination about the knee joint, $\dot{\theta}$ knee joint angular velocity, θ_v shank angle (between shank and vertical direction in sagittal plane), $\ddot{\theta}_v$ shank angular acceleration, m mass of shank-foot combination, g gravitational acceleration, l distance between knee and centre of mass of shank-foot combination, B viscous coefficient.

The torque due to knee joint stiffness, M_s, is calculated using an exponential term to take into account the nonlinear component in the elasticity of the knee joint, as:

$$M_s = -\lambda \,.\, e^{-E.\theta}(\theta - \theta_r) \tag{2.3}$$

where λ and E are coefficients of exponential terms, while θ_r represents the resting elastic knee angle at which the elastic component of the knee torque equals to zero.

To estimate the unknown viscous-elastic parameters of the knee joint, passive pendulum test was performed to a group of healthy and disabled participants. The test was carried out with the subject lying in a semi-supine, the thigh was fixed on a table, and the knee was hanged on the edge of the table to allow free swing movement. The shank of a participant was then raised by the examiner, until the leg muscles were relaxed, after that the shank was left to swing freely. The movement of the freely swinging leg was recorded until it reached to its final resting position. The recorded

data was used to estimate the unknown viscous-elastic parameters with the aid of least square optimization algorithm to minimize the error between the two sides of:

$$J \cdot \ddot{\theta}_v = -m \cdot g \cdot l \cdot \sin(\theta_v) + M_s - B \cdot \dot{\theta} \qquad \textbf{(2.4)}$$

After obtaining the passive parameters, trials were performed to record leg movement induced by FES signals on the quadriceps to derive the active knee joint torque. Stimulation trains of predetermined amplitude, 60-80mA, were applied to the muscle with different frequencies; 20, 25, 33 and 50Hz, and pulse width, 0-220μs, to characterise muscle recruitment. The kinematic data, resulted during the stimulation of the quadriceps, was recorded and used to calculate the active knee torque using equation (2.2).

Autoregressive with exogenous inputs (ARX) model structure, with the aid of a least square method to minimize the error between the data and the model, was used to estimate a single-pole transfer function that describes the relationship between the pulse width of the electrical stimuli on the leg as an input, and the resultant active knee joint torque, as:

$$H(s) = \frac{G}{1 + s\tau} \qquad \textbf{(2.5)}$$

where, τ is the time constant and G is the static gain.

In the current work, an average value of the knee joint`s viscous coefficient for paraplegic subjects (0.287 N.m.s./rad) is added to the knee joint of the humanoid model (Ferrarin and Pedotti, 2000). Also the static gain (0.04 Nm/μs), for 33Hz frequency, and time constant (0.45 sec) values were chosen as provided by Ferrarin and Pedotti (2000).

2.7 Muscle fatigue

In healthy people, where the link between the central nervous system and the muscle is intact, the smaller and more fatigue resistant motor units, i.e. of slow twitch fibers, are activated before the large, fast twitch and more fatigable motor units. Although the large motor units have higher threshold than that of smaller ones, they are usually superficial and closer to the skin. Therefore, when using surface electrodes to stimulate the muscle, the large fibers are activated first which is the main reason of increased muscle fatigue. An additional cause is the use of synchronous stimulation mode that leads to simultaneous activation of all muscle fibers which in turn speeds up the appearance of muscle fatigue (Giat et al., 1993).

There are several factors that affect the fatigue resistance of paralyzed muscles stimulated by FES. These include the training history, stimulation parameters and stimulation protocols. It has been reported that long training helps in transformation of fast twitch fibers into slow twitch, hence increase the fatigue resistance of the muscle (Giat et al., 1993). Also, it has been shown that the use of intermittent stimulation with high frequency, 100Hz, reduces muscle fatigue as compared with intermittent stimulation of 20Hz frequency (Matsunaga et al., 1999). Furthermore, the use of optimal N-let, i.e. a set of N closely stimulation pulses, pulse train is shown to delay the appearance of muscle fatigue by 36% as compared with standard singlet stimulation (Karu et al., 1995). In addition, a recent study showed that the use of sequential activation, with 90° phase shift between successive electrodes, of different groups of motor units using spatially distributed sequential stimulation (SDSS), as compared with single electrode stimulation (SES), delays the fatigue time by 280% (Nguyen et al., 2011).

The force generated from paralyzed muscle, when stimulated by FES, decays with time due to fatigue. To precisely predict and analytically describe the force generated from stimulated paralyzed muscle by FES; several attempts have been made to model the phenomenon of muscle fatigue, based on analytical or physiological

information. Rabischong and Chavet (1997) produced a nonlinear fatigue equation of four coefficients to fit data, recorded during quadriceps fatigue test, and extracted fatigue indices showing the amount and rate of decrease in the resultant torque. Giat et al. (1993, 1996) built a musculotendon model with fatigue profiles obtained by monitoring the metabolic state of the stimulated muscle. They found that the metabolic parameters, such as pH, undergo significant changes during fatigue and recovery phases. These changes were related to the depletion of energy during extensive muscular activation that leads to muscle fatigue. It was assumed that the metabolic parameters, especially the pH value, reflect the force producing capability of the muscle induced by FES. The effect of muscle fatigue was modelled through the use of curve fitting technique to obtain the decay of pH with time as well as the decay of muscle force with the corresponding pH level during prolonged stimulation by FES. The model was able to produce a good fit for isometric contraction, but lacks the ability to predict force responses with different frequencies as it didn't include stimulation frequency and patterns as inputs.

Other studies, based on physiological observations, modelled the fatigue of the resultant muscle force through the introduction of muscle fitness as a function of stimulation pulse width and frequency (Riener and Fuhr, 1998; Riener et al., 1996). Ding et al. (2000) produced a fatigue model of four parameters, coupled with isometric force generation, able to predict muscle fatigue in isometric contractions induced by different stimulation patterns.

In this work, due to the use of a linear muscle model proposed by Ferrarin and Pedotti (2000) that lacks the effect of muscle fatigue, a need for a fatigue indicator was raised to assess the benefits of two different control approaches in FES cycling, described in chapter three. The indicator needed was the one with the ability to combine the pulse width and the number of stimulus with the resultant muscle force. As the literature lacked such an indicator, it was developed in this work.

2.8   Force drop indicator

As the muscle model used, in the early stages of this work, is linear and has no fatigue indicator, a muscle force drop indicator was needed to assess the performance of the control techniques applied and the effect of the utilized assisting mechanism on FES training session from muscle fatigue point of view.

In order to obtain results close to those usually obtained during real FES training sessions for paraplegics, experimentally-obtained data was used to derive the force drop monitor.

2.8.1   Experimental procedure

The experiment, an isometric test, was carried out with the aid of a paraplegic subject of incomplete spinal cord lesion T2-T3. The subject was seated in semi-supine position (45º-60º) with the thigh fixed to the seat (80º-90º knee angle), with thigh supporters, to allow free leg movement. In addition to Velcro straps that were used to support and stabilize the trunk, waist and the thigh during the experiment to prevent any external influence on the quadriceps response to FES signal.

Muscle stimulation was performed using RehaStim Pro 8 channels (Hasomed GmbH, Germany) stimulator, which received its commands from Matlab software through USB connection. Electrical stimulus was delivered to the quadriceps through two Multistick gel surface electrodes (Pals platinum, Axelgaard, USA, size: 50mm x 90mm). The cathode (-) was placed over the motor point of the rectus femoris (proximal to trunk) while the anode (+) was placed above the patella (distal to trunk). To find out the optimal location of the cathode, i.e. to obtain the highest muscle contraction, the electrode was moved around the skin over the motor point using the same stimulation signal for all trials, with the knee almost fully extended. To record the muscle force resulting from FES signals, a force transducer (PCE-FM200, PCE group company, Deutschland) was used. The force transducer was placed about 4cm

proximal to the lateral malleolus, against the anterior aspect of the leg (Perumal et al., 2002) through a padded cuff equipped with a hook, as shown in Figure 2.7. The force transducer was fixed in housing for measuring the isometric contraction forces resulting from stimulating the quadriceps. The force transducer was connected to a computer through an RS-232 port to simultaneously record muscle force resulting from FES signals. The isometric fatigue test has previously been used to test muscle performance, before and after load, in non-isometric, i.e. isotonic and isokinetic, cycling exercise (Sinacore et al., 1994; Verbitsky et al., 1997).
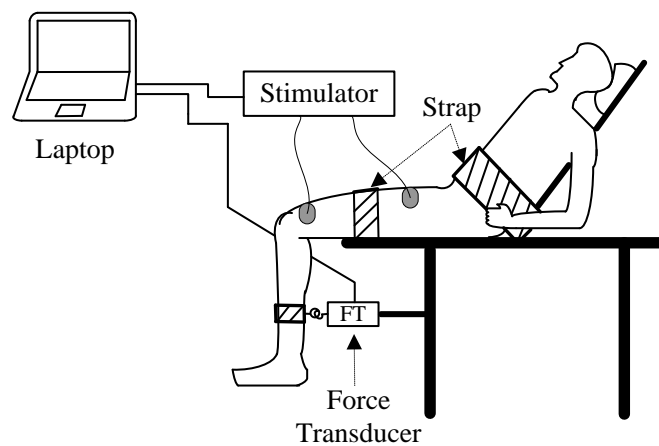
Figure 2.7: Experimental set-up to record quadriceps isometric contraction force in response to FES signal

The test was performed by applying one stimulus per ten seconds (3 sec on and 7 sec off), with different pulse width (200μs to 400μs) while keeping other parameters fixed (current 40mA, frequency 30Hz).

2.8.2 Experimental results and curve fitting

The maximum muscle force recorded during the isometric test for different pulse widths can be seen in Figure 2.8.
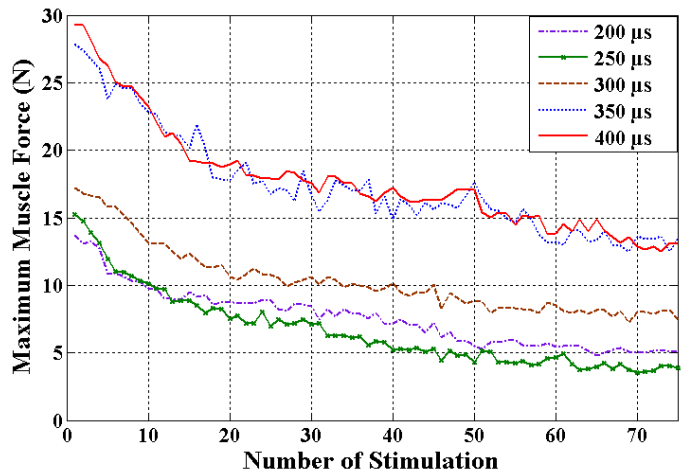
Figure 2.8: Peak muscle force for 75 stimulations of different pulse widths

To derive the force drop monitor, first of all, each line of the data obtained in Figure 2.8 is normalized, i.e. subtracting the maximum force value, resulted by a specific pulse width, from each force point obtained from that pulse width and then dividing the result with the same maximum force value. This operation calculates the rate of force drop in the muscle stimulated with a specific pulse width. After normalization, the resultant data together with the number of stimulus and pulse width are utilized, with the aid of curve fitting toolbox, to derive the monitor as shown in Figure 2.9.
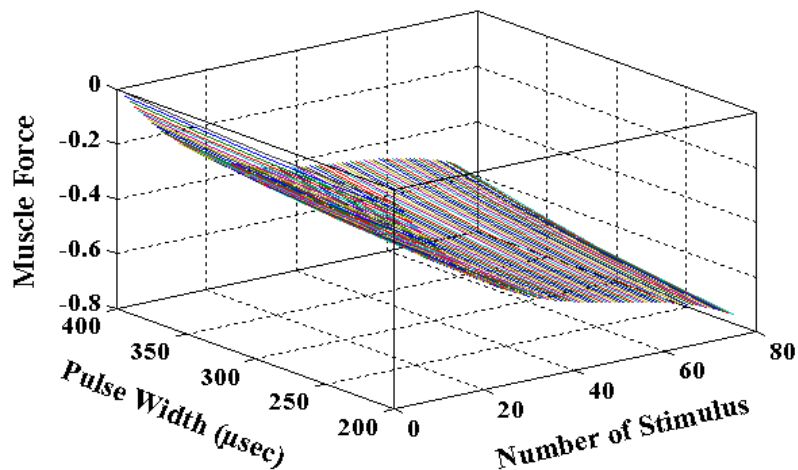
Figure 2.9: The derived force-drop monitor

For a more accurate model and reducing the root mean square error to as minimum as possible (0.0651), 3rd order linear model, polynomial fitting is implemented with 9 coefficients; the resultant relationship combines the pulse width (Y) and the number of stimulus (X) with the resulted muscle force (F) as shown in:

$$F(x, y) = P_{00} + P_{10}X + P_{01}Y + P_{20}X^2 + P_{11}XY + P_{02}Y^2$$
$$+ P_{30}X^3 + P_{21}X^2Y + P_{12}XY^2 \qquad \textbf{(2.6)}$$

The coefficients (with 95% confidence bounds) of equation (2.6) are shown in Table 2.5. The statistics shown in Table 2.6 are used to assess the goodness of the fit.

Table 2.5: The derived force-drop indicator's coefficients

Coefficient	Value
P_{00}	0.01435
P_{10}	-0.02739
P_{01}	-0.0004771
P_{20}	0.0004631
P_{11}	2.976e-006
P_{02}	1.176e-006
P_{30}	-3.052e-006
P_{21}	-2.456e-008
P_{12}	1.291e-008

Table 2.6: Statistics of the derived force-drop indicator

Statistic	Value
Sum of Squares Due to Error (SSE)	1.552
R-Squared Error	0.8531
Adjusted R-Squared	0.8499
Root Mean Square Error (RMSE)	0.06512

The sum of squares due to error (SSE), also known as sum of squared residuals, is a measure of the inconsistency between the observed data and the data estimated by the model. Closer value to zero of the SSE indicates the ability of the model to predict the real data more efficiently with less error. The R-square statistic describes the percentage of total variation in a data set that is described by the model. The R-Square value ranges between 0 and 1 where a value closer to one indicates a greater proportion of variance is accounted for by the model. For example, an R-square value of 0.8058 means that the fit explains 80.58% of the total variation in the data about the average. The adjusted R-square is used to compare between the powers of two derived models having different number of coefficients. The adjusted R-square is always smaller than the R-square value. The root mean square error, also known as the standard error of the fit, is a measure of the difference between the values estimated by a model and the observed values. It is considered as a good measure of the accuracy of the fit and the closer the value to zero, the more accurate the fit.

From the statistics obtained in Table 2.6, the derived force-drop monitor is assessed as acceptable as it has the ability to cover 85.31% of the total variation of the data from the average, i.e. R-square equals to 0.8531, with small SSE and RMSE values.

Equation (2.6) will be used in chapter three to assess the performance of control techniques applied and the benefits of the proposed cycling assist mechanism from fatigue point of view.

2.9 Summary

This chapter has described the development of a humanoid and cycling ergometer model. The humanoid has been developed using standard anthropometric dimensions by which the length and weight of each segment in the body is determined as a proportion of the total body's height and weight. The humanoid model has been built

using Visual Nastran 4D (vN4D) dynamic simulation software. Each segment of the body is connected with each other using different joints or constraints. Also, a stationary bicycle model, of dimensions taken from real ergometer, has been built using the same software. An assist mechanism, a flywheel with an on/off constraint to simulate the operation of an electrical clutch between the flywheel and the bicycle's crank, has been added to the bicycle model.

A linear muscle model, derived by Ferrarin and Pedotti (2000), that mimics the behaviour of the quadriceps muscle stimulated by FES, has also been presented in this chapter. This muscle model, implemented in Matlab/Simulink software, has been incorporated into the humanoid-bicycle model to represent the final plant to be controlled.

Since the muscle model used lacks a fatigue index that combines the pulse width and the number of stimulus with the resultant muscle force, a force-drop indicator derived from clinically recorded data using curve fitting technique has been introduced in this chapter. This indicator will be used for assessment purposes between different control approaches explained in chapter three.

Chapter 3: Automatic control of FES-cycling based on predefined trajectory

3.1 Introduction

Control of functional electrical stimulation to restore functional movements of the lower extremities can be approached by defining trajectories or set points for certain variables of the system (Veltink et al., 1992). The design of a suitable control approach, to provide smooth and coordinated FES-cycling for disabled individuals by stimulating single muscle group, the quadriceps, requires understanding the natural pedalling movement. Although performing FES-cycling by stimulating the quadriceps only, i.e. extensor muscle, is an attractive exercise for disabled individuals, the control of pedalling movement using one directional actuator is a challenge.

In this chapter, a linear muscle model to mimic the behaviour of the quadriceps stimulated by FES is used. To obtain the best performance, two different controllers, PID and FLC, are tested. A novel assist mechanism, represented by a flywheel and electrical clutch, is used to assist the legs in FES-cycling exercise. The control of the assist mechanism is achieved using two different closed-loop approaches. The first depends on the angular velocity of the knee joint, while the second is based on the angular velocity of the crank. From fatigue point of view, a comparison between the FES-cycling exercise with and without the newly proposed assist mechanism is presented.

3.2 Predefined knee trajectory

In this section, the pedalling movement in FES-cycling exercise for disabled individuals is controlled by tracking predefined knee trajectory movement. The predefined knee trajectories of both legs are used as reference input signals. The controlled torque is applied to the knee joints, i.e. motor joints, to provide coordinated

pedalling movement of the required speed. One of the cycling speeds widely used in rehabilitation centres (Chen et al., 1997; Massoud, 2007) is 35 rpm, i.e. one complete cycle for approximately every 1.71 seconds. To be able to record the knee trajectory of 35 rpm cycling speed, a motor with angular velocity of 35 rpm is used to rotate the crank of the bicycle in vN4D software. The knee trajectory for the mentioned speed is recorded using a position sensor, i.e. goniometer, located on the knee level of both legs in the humanoid-bicycle model. The recorded knee trajectories for both legs can be seen in Figure 3.1.
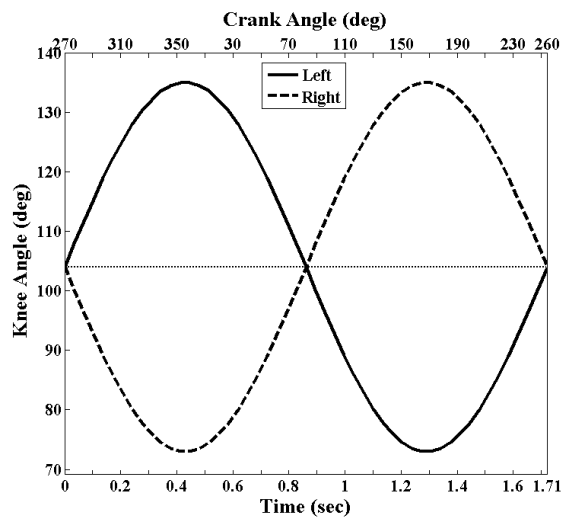
Figure 3.1: Knee angle trajectory of right and left legs recorded for
35 rpm cycling speed

Pedalling mechanism has two dead points, i.e. around 0° and 180° of the crank in case the hip joint is at the same horizontal position of the crank, at which significant torque is difficult to be produced by the legs to rotate the crank, i.e. the point of transition between extension moment and flexion moment (Chen et al., 1997). However, healthy individuals can overcome these points by means of a complicated interplay of muscle actions difficult to generate by FES due to involvement of deep muscles that are difficult to stimulate by surface electrodes (Rasmussen el al., 2004). An illustration of the cycling dead spots can be seen in Figure 3.2.
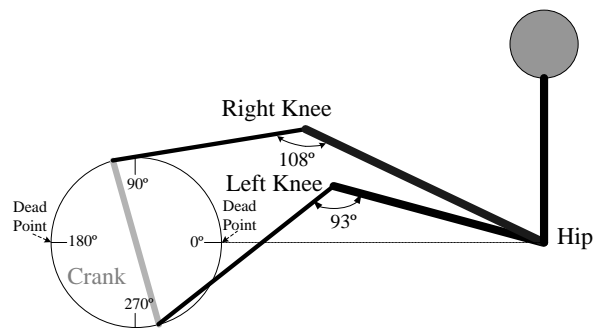
Figure 3.2: Illustration of the cycling dead points

In FES-cycling, researchers have stimulated a flexor muscle, i.e. the hamstring, around the dead spots to provide leg flexion action and overcome the rapid changes in speed due to the dead spots (Chen et al., 1997; Gföhler and Lugnar, 2004). However, Massoud (2007) showed the ability to perform FES-cycling by stimulating single extensor muscle, the quadriceps. Massoud divided each pedalling cycle into three phases based on the crank angle. The three phases proposed by Massoud, shown in Figure 3.3, are as follows:

- Push phase: in this phase, the quadriceps muscle is stimulated to provide knee extension and speed up the cycling. During this phase, the parallel leg is at rest phase.

- Resist phase: in this phase, the quadriceps is stimulated to extend the leg and provide resistance to the motion if required. This phase takes place while the parallel leg is at rest phase.

- Rest phase: in this phase, the quadriceps muscle is left to rest without stimulation.
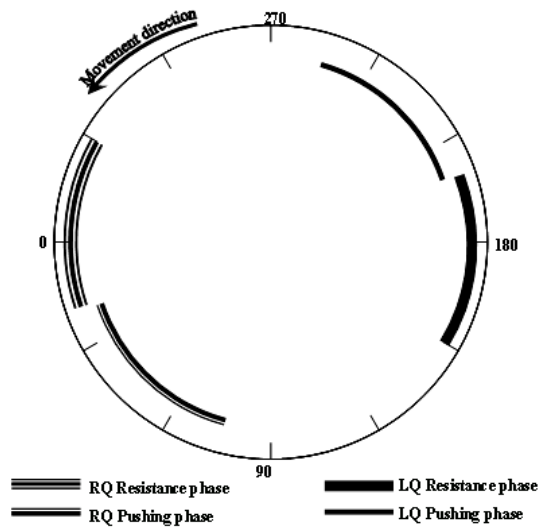
Figure 3.3: Cycling phases by stimulating the quadriceps muscle
defined according to crank angle (Massoud, 2007)

In this work, the control approach is based on the knee angle as a reference signal. The activation period of each phase and the synchronization between the two legs are achieved based on the crank angle. The three stimulation phases of the quadriceps are defined according to the knee trajectory as shown in Figure 3.4.
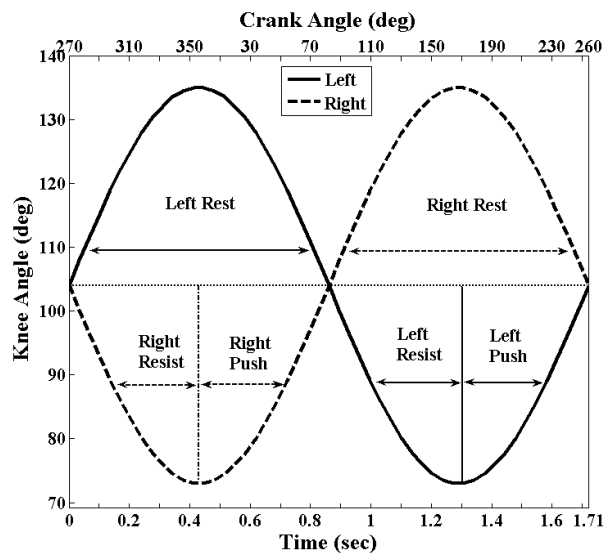
Figure 3.4: Cycling phases by stimulating the quadriceps muscle
based on knee joint angle

3.3 PID control of FES-cycling

This section describes the use of PID controllers to control the FES-cycling by stimulating the quadriceps muscle of each leg. PID control is widely used to control industrial systems. It can be adjusted by different manual and automatic tuning methods (Ogata, 2002). Many non-linear processes can be controlled using PID especially when the mathematical model of the plant is not known, providing that control parameters are well tuned (Vukic and Kuljaca, 2002). Information about PID controllers can be found in Appendix A. The action of a PID controller is expressed as:

$$u(t) = K_p \, e(t) + K_i \int e(t) dt + K_d \left(\frac{de}{dt} \right) \qquad \textbf{(3.1)}$$

Pedalling movement in FES-cycling is controlled by PID controllers to track a predefined knee trajectory. The PID is used to regulate the stimulation intensity, i.e. pulse width, on the quadriceps muscle and govern the required leg movement. A quadriceps muscle model, derived in (Ferrarin and Pedotti, 2000) and described in chapter two, is used in this chapter taking into account that the stimulation frequency is 33Hz, stimulation amplitude is 80mA, and the sampling time used is 200Hz. The resultant muscle torque is applied to the knee joint of the humanoid model to drive the legs in FES-cycling exercise.

3.3.1 Implementation of PID control of FES-cycling

The torque generated by a muscle, as a response to FES signal, can be controlled by varying the pulse width of the stimulus in a closed-loop control approach. Knee trajectory of 35 rpm speed was recorded and used as a reference. The actual knee angle, using a position sensor in the humanoid-bicycle model, is measured. The knee angle is used as feedback and compared with the knee angle reference to form the error signal.

The error signal is used as an input to the PID controllers to regulate the stimulation pulse width on the muscle, generate the required muscle torque and consequently control leg pedaling movement to follow the reference accordingly. By stimulating the quadriceps, only extension, i.e. pushing, torque can be generated. To control the cycling movement to follow a desired trajectory of a specific speed, it is required to provide an opposite torque to resist the movement in case the leg speed exceeds the required cadence. This torque can only be provided by stimulating the quadriceps of the opposite leg at specific positions of the crank, i.e. Resist phase. Four PID controllers are used, two for each leg. One controller is used to control the stimulation during Push phase and the other is used to control the stimulation during Resist phase. The reason of using two controllers is that the stimulation required during Push phase may differ from that required during Resist phase. Inspired from Figure 3.3, the stimulation phases are specified using logic gates as shown in Figure 3.5. The stimulation phases for the right and left legs are the same but with 180° phase shift. The control block diagram can be seen in Figure 3.6. The PID controllers parameter values were obtained heuristically as PID1 and PID4: Kp=3.6, Ki=0, Kd=2.1, PID2 and PID3: Kp=4, Ki=0, Kd=1.8. Due to the delay in muscle response, the integral part of the controller has not been used to avoid worsening the performance due to the windup problem. Also, to prevent over stimulation to the muscle and the negative signal of the controller, as the quadriceps is a one directional actuator, a saturation block is added to the input of muscle model block.
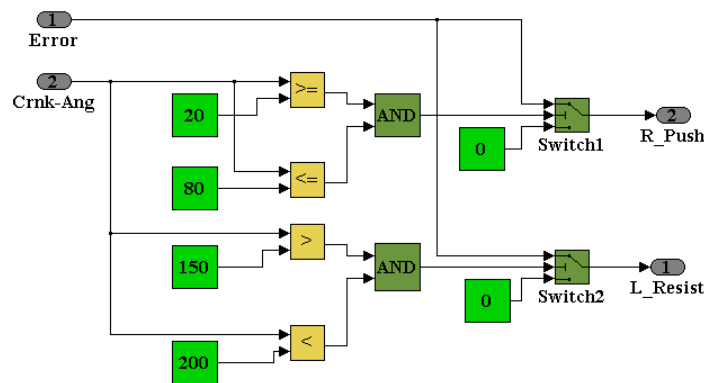
Figure 3.5: Push and resist phases of right leg
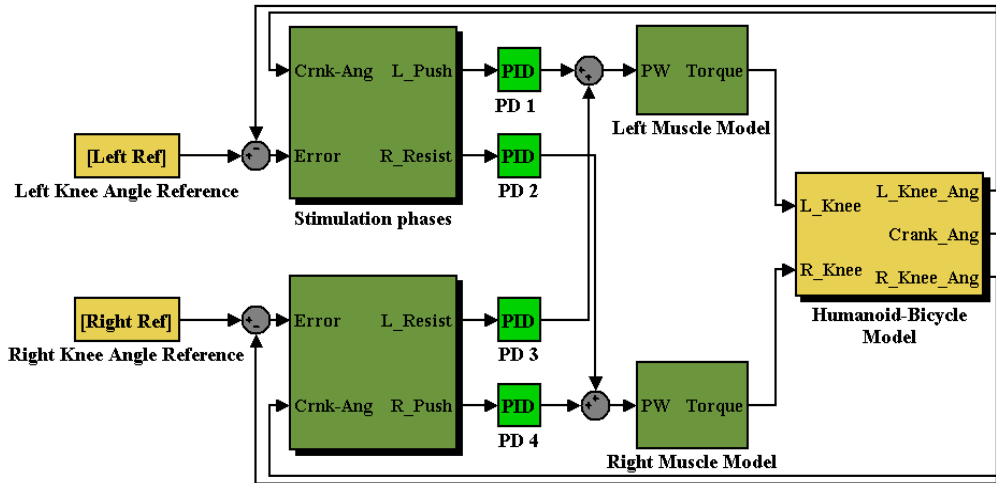
Figure 3.6: The control block diagram using PID controllers

3.3.1.1 Results

It can be seen from Figures 3.7 and 3.8 that the tracking error is high at the beginning. However, the controllers were successful in tracking the desired trajectory in subsequent cycles. The mean square tracking error was 0.024 radians. Also, it can be seen from Figures 3.9-3.12 that the muscle of each leg was stimulated twice per cycle, once to speed up the movement, i.e. Push phase, the other to retard the movement, i.e. Resist phase, to obtain the desired speed.
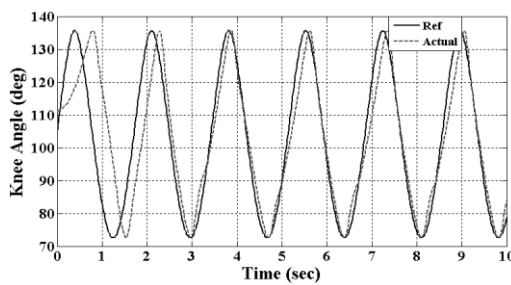
Figure 3.7: Right leg tracking the reference
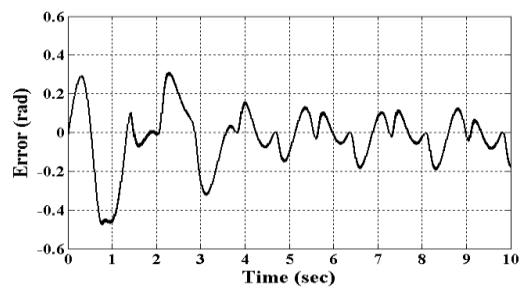
Figure 3.8: Right leg tracking error
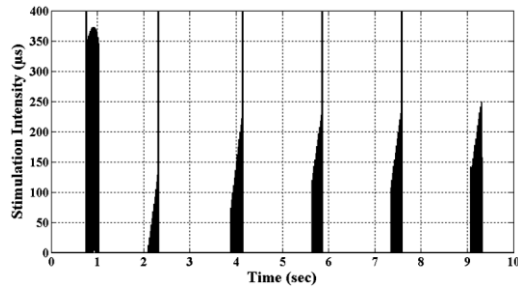
Figure 3.9: Stimulation intensity at Left-Push phase
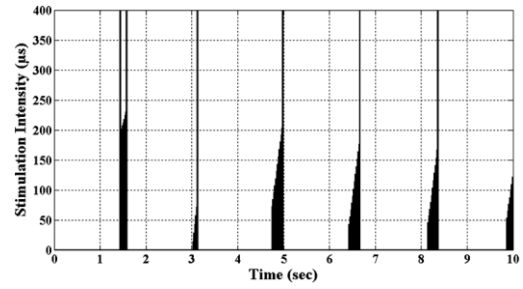
Figure 3.10: Stimulation intensity at Right-Push phase
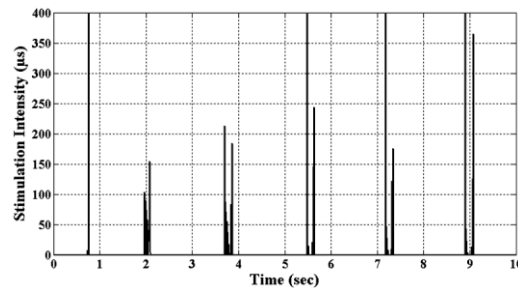
Figure 3.11: Stimulation intensity at Left-Resist phase
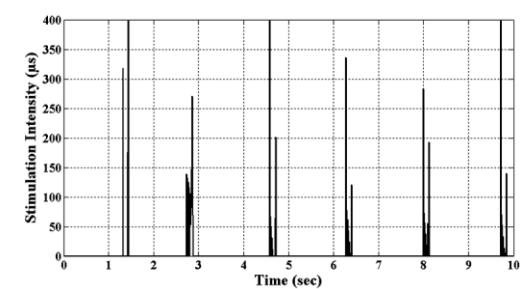
Figure 3.12: Stimulation intensity at Right-Resist phase

Although the control strategy was successful, it is obvious from Figures 3.9-3.12 that the controllers produced simultaneous sharp stimulus on the muscle. This leads to undesired simultaneous muscle contraction which may lead to spasm. To improve the tracking performance and smoothen the stimulation intensity on the muscles, another type of controller, such as fuzzy logic control (FLC), will be tested.

3.4 Fuzzy logic control of FES-cycling

A degree of fuzziness exists in the behavior of motor systems and muscles in human. The fuzziness is due to the lack of a precise mathematical description of their behavior. The number of muscles and joints involved in an activity makes the musculoskeletal system highly complex and nonlinear.

Fuzzy logic control (FLC) is well known for its effectiveness in controlling complex and nonlinear systems. FLC is a model-free mechanism based on linguistics rather than on mathematics. Moreover, FLC is very functional especially with complex

systems difficult to model mathematically, controlled by human operators, ambiguous or vague.

3.4.1 Implementation of fuzzy logic control of FES-cycling

In this work fuzzy logic is implemented to control and achieve FES cycling by stimulating the quadriceps muscle only. The closed-loop control structure used is shown in Figure 3.13. The controllers are utilized to change the pulse width of the stimulus applied to the muscle to adjust the amount of the generated muscle force required to track a predefined leg trajectory of 35 rpm speed. The crank angle is used to specify the cycling phases i.e. Push; Resist and Rest, for each leg, previously explained in section 3.2.
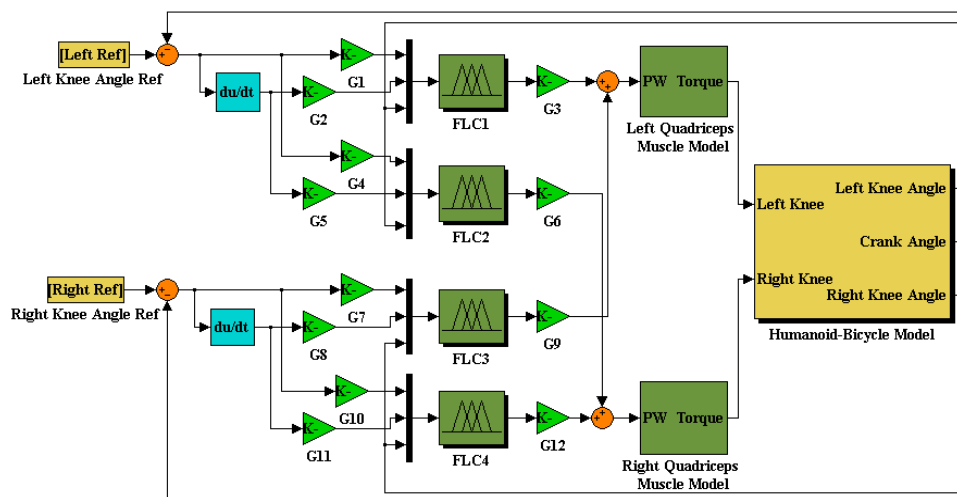
Figure 3.13: The control structure using fuzzy logic controllers

Since the amounts of push and resist, required to maintain a desired speed, are not equal, two different FLC controllers are used for each leg. Right and left knee angle reference of 35 rpm cycling speed is used to compare with the actual knee trajectory signal taken from a position sensor located in the humanoid-bicycle model. The difference, i.e. error, between these signals and the derivative, i.e. rate of change of error, are used by the fuzzy controller of each leg to accordingly adjust the pulse width of the stimulus.

Each FLC has three inputs and one output. The first two inputs, the error and the rate of change of error, are normalized by input scaling factors (G1, G2, G4, G5, etc.), while the third input is the crank angle which is measured by a position sensor in the humanoid-bicycle model. The two normalized FLC inputs (error and rate of change of error) are fuzzified using fuzzy set of five equally distributed, with 50% overlapping, Gaussian membership functions. While the third FLC input, the crank angle which is used to achieve the synchronization among the four controllers by dividing it into phases, is fuzzified using fuzzy set of four variables (RR, RP, LR and LP) that are defined using trapezoidal membership functions to ensure minimum overlapping among the defined phases. The fuzzy output, results from the fired fuzzy rules of the FLC, changes to crisp values using the center of area defuzzification method. The output is defuzzified using five equally distributed Gaussian membership functions. The fuzzy input/output membership functions of each controller are depicted in Figures 3.14 and 3.15.

(a)　　　　　　　　　　　　　　(b)

(c)
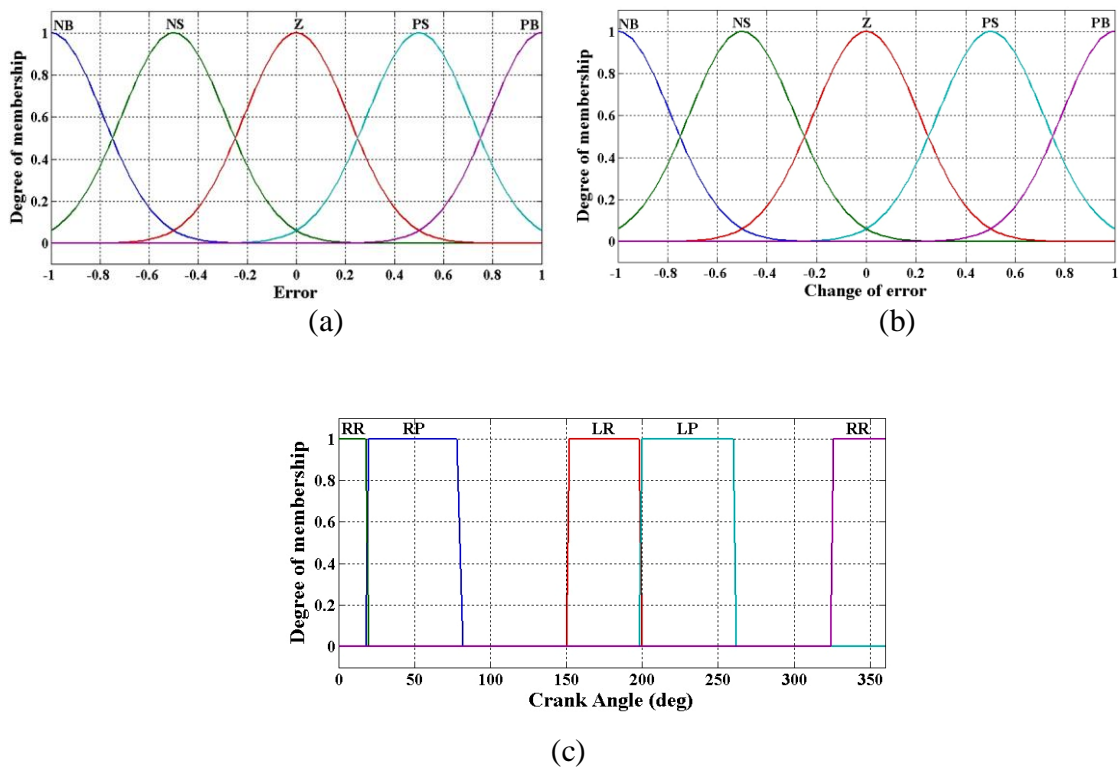
Figure 3.14: FLC`s input membership functions, the third input (c) shows the phases (RR= right resist, RP= right push, LR= left resist, LP= left push)
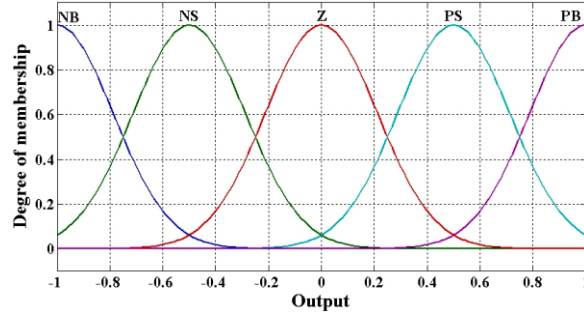
Figure 3.15: Controller's output membership functions

The standard twenty five fuzzy rules are used for each controller, as shown in Table 3.1, in addition to the third input which allows the activation of each controller during its own phase. Since the quadriceps is the only muscle group stimulated in this work, which can produce extension torque only, i.e. cannot produce negative or flexion torque, the negative action of the controller is prevented using a saturation block added to the input of muscle model block.

Table 3.1: Fuzzy rule base

Δe / e	NB	NS	Z	PS	PB
NB	NB	NB	NB	NS	Z
NS	NB	NB	NS	Z	PS
Z	NB	NS	Z	PS	PB
PS	NS	Z	PS	PB	PB
PZ	Z	PS	PB	PB	PB

The input and output scaling factors of each controller are obtained heuristically. The values of the scaling factors used are: G1=G10= 0.008, G2=G11= 0.0032, G4=G7= 0.016, G5=G8= 0.0034, G3=G6=G9=G12= 900.

3.4.1.1 Results

It is obvious from Figure 3.16 that the proposed control strategy was successful in achieving coordinated leg pedaling movement with acceptable tracking performance. The mean square tracking error is 0.024 radians. At the beginning of the cycling the

tracking error is high, as in Figure 3.17. The reason behind this is that the starting position of the leg was chosen to be at 110º of the crank angle, at which the leg muscle is not stimulated due to being at resting phase as previously shown in Figure 3.14 (c), in order to benefit from the gravitational force on the leg to start the movement and overcome the inertia. Despite the initial large error, the controllers were successful in minimizing the error in successive cycles. However, the cycling cadence was not steady, i.e. cadence error was extremely high as shown in Figure 3.18. This is due to the effect of the cycling dead points that caused rapid changes in the angular velocity of the crank.
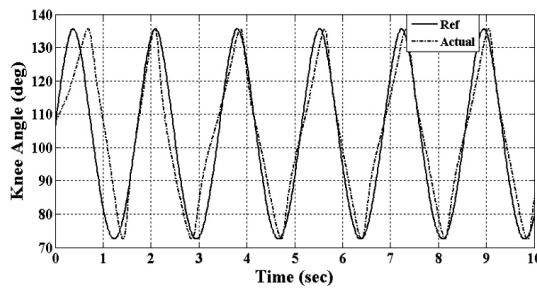
Figure 3.16: Right leg tracking the reference
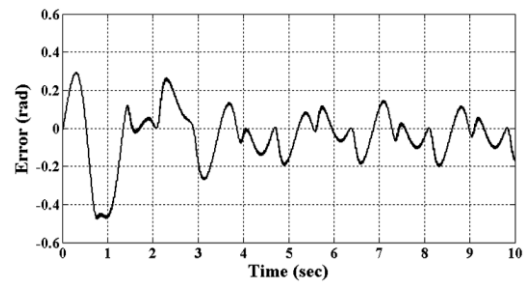
Figure 3.17: Right leg tracking error
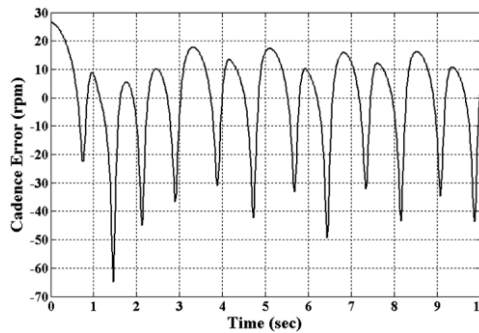
Figure 3.18: Error in crank angular velocity

The muscle torque of each leg and the pulse width regulated by the FLC unit of each phase can be seen in Figures 3.19–3.24. It is clear that the torques produced by both legs were not equal, which implies that one of the legs has received more stimulation than the other. This is due to the fact that the input/output scaling factors of the controllers, as well as the firing angles of the defined phases, were chosen

heuristically and will need fine tuning for both legs to receive equal amount of exercise and to equally contribute to the cyclic pedalling motion. Moreover, it is clear that the quadriceps muscle of each leg was stimulated twice per cycle, one to speed up, i.e. push, and the other to retard, i.e. resist, the movement. Due to the tracking delay at the beginning of the cycling, resulting from the free-fall of the right leg, the stimulation intensity during pushing phase of the left leg was relatively high, as in Figure 3.21. As the resist action took place in successive cycles, as in Figure 3.23 and Figure 3.24, the tracking error was reduced and hence the stimulation intensity.
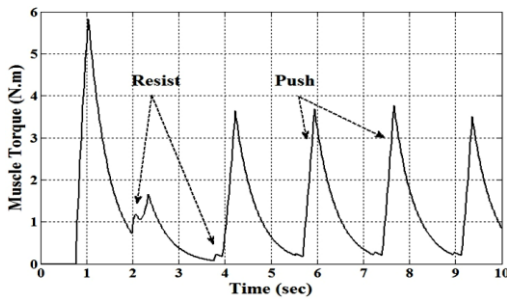
Figure 3.19: Muscle torque of left leg
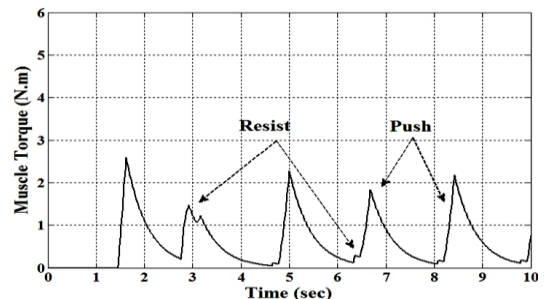
Figure 3.20: Muscle torque of right leg
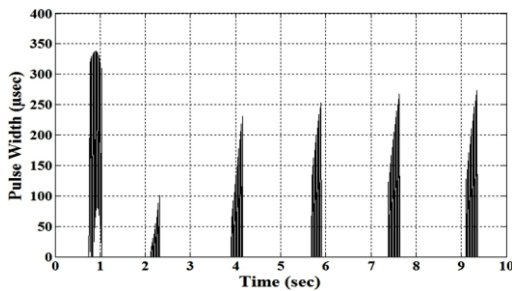
Figure 3.21: Pulse width in Left-Push phase
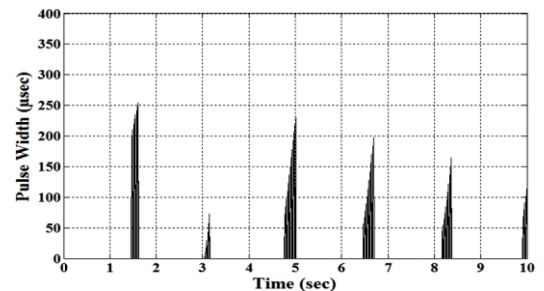
Figure 3.22: Pulse width in Right-Push phase
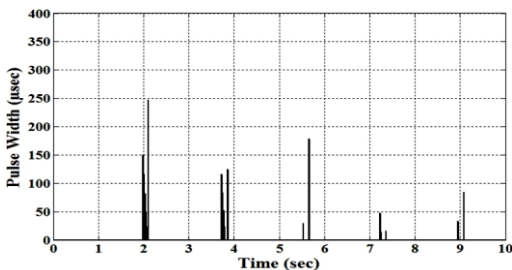
Figure 3.23: Pulse width in Left-Resist phase
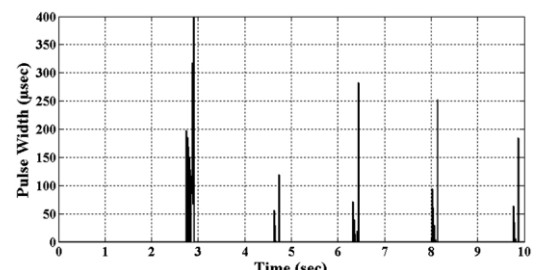
Figure 3.24: Pulse width in Right-Resist phase

69

As a comparison between the PID, in section 3.3.1, and FLC, it is noted that both approaches produced similar tracking performance. However, the stimulation intensity on the muscle was smoother, i.e. less sharp, using the introduced FLC approach. For this reason and for the ability of the FLC to cope with nonlinear and complex systems, FLC has been used in subsequent stages of this work.

Although the control approaches showed good tracking for a predefined knee trajectory, crank cadence suffered severe fluctuation and the effect of the dead spots, causing rapid changes in the speed, was dominated. Moreover, to be able to track a predefined trajectory, the quadriceps muscle was stimulated twice per cycle. It is worth mentioning that successive stimulation to the muscle leads to muscle fatigue and terminates the exercise rapidly.

3.5   Control of FES-cycling assisted by flywheel mechanism

In this section, FES-cycling by stimulating the quadriceps muscle of each leg assisted by a flywheel and electrical clutch mechanism is introduced. The flywheel as energy storage device can be used to absorb the excessive energy in the system, store it as kinetic energy, and provide the required damping. Also, loaded with kinetic energy, it can be used to speed up the system and assist the legs.

As presented in previous sections, the control of a predefined pedalling trajectory can be performed by stimulating the quadriceps of each leg twice per cycle. To prevent successive stimulation of the quadriceps an energy storage device can be used to replace the stimulation required for Resist phase (Massoud, 2007). In this work, a flywheel and electrical clutch mechanism is used to replace the stimulation in Resist phase and provide the required assistance to the legs in FES-cycling exercise. The electrical clutch, to engage a disk cylinder flywheel with the crank of the bicycle, is simulated using an on/off constraint in vN4D software. The clutch is activated and deactivated by a control signal sent from a controller in Simulink/Matlab environment.

3.5.1 Implementation of fuzzy logic control of FES-cycling assisted by flywheel mechanism

In this section, the aim is to track a predefined trajectory and perform FES cycling by stimulating single muscle group, the quadriceps of each leg, with the aid of a flywheel and electrical clutch assist mechanism. A closed loop control can be used to control the stimulation intensity on the muscle by altering the pulse width of the stimulus. The controller changes the pulse width according to the error signal between the required reference and the actual feedback signal. By controlling the amount of the stimulation, the resultant muscle torque, and hence the leg movement, can be controlled to maintain the desired cycling speed. The knee angular position of both legs, for a speed of 35rpm, is recorded and used as a reference signal. Two fuzzy controllers (FLC), one for each leg, are used to control the stimulation intensity, i.e. pulse width of the stimulus, on the muscle. The control block diagram is shown in Figure 3.25.
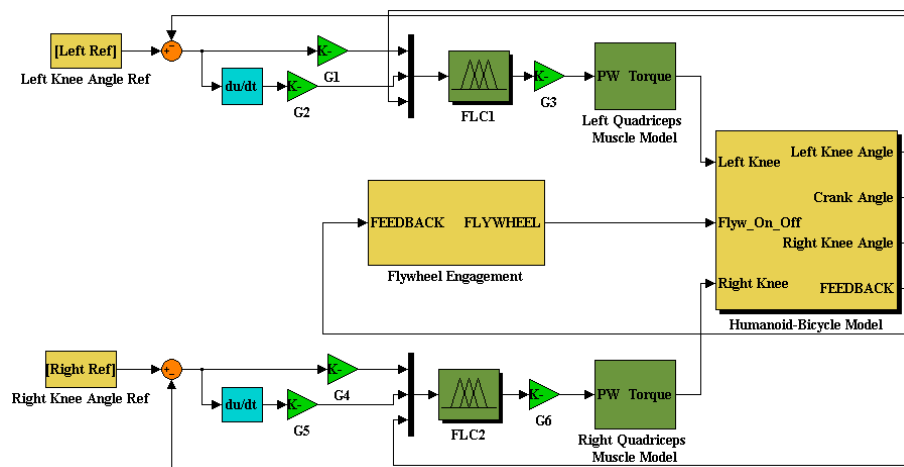
Figure 3.25: The closed-loop control block diagram

Each FLC, Mamdani type, has three inputs and one output. The first two inputs represent the error and the change of error, while the third input represents the bicycle's crank angle. The output resulted from the FLC represents the pulse width of the stimulus. The crank angle input is used to specify the periods at which the controller is active or inactive, i.e. to synchronize between the two controllers. The

first two inputs are normalized by scaling factors before fuzzification. The normalized inputs are fuzzified by a fuzzy set of five equally distributed Gaussian membership functions with 50% overlap. The third FLC input, the crank angle which is divided into two phases; Push Right (PR) and Push Left (PL) phase, is fuzzified using two trapezoidal membership functions. The fuzzy output, resulting from the fired fuzzy rules, is changed to crisp value using the centre of area defuzzification method. The output is then scaled by a scaling factor. The FLC input and output membership functions can be seen in Figures 3.26-3.27. The values of input and output scaling factors (G1=G4= 0.008, G2=G5= 0.0032, G3=G6= 900) were obtained heuristically. A standard twenty five PD-like fuzzy rules are used for each controller. The right leg controller is only active in PR, i.e. Push-Right, phase while the left leg controller is active only in PL, i.e. Push-Left, phase, as in Figure 3.26 (c).

(a)

(b)

(c)
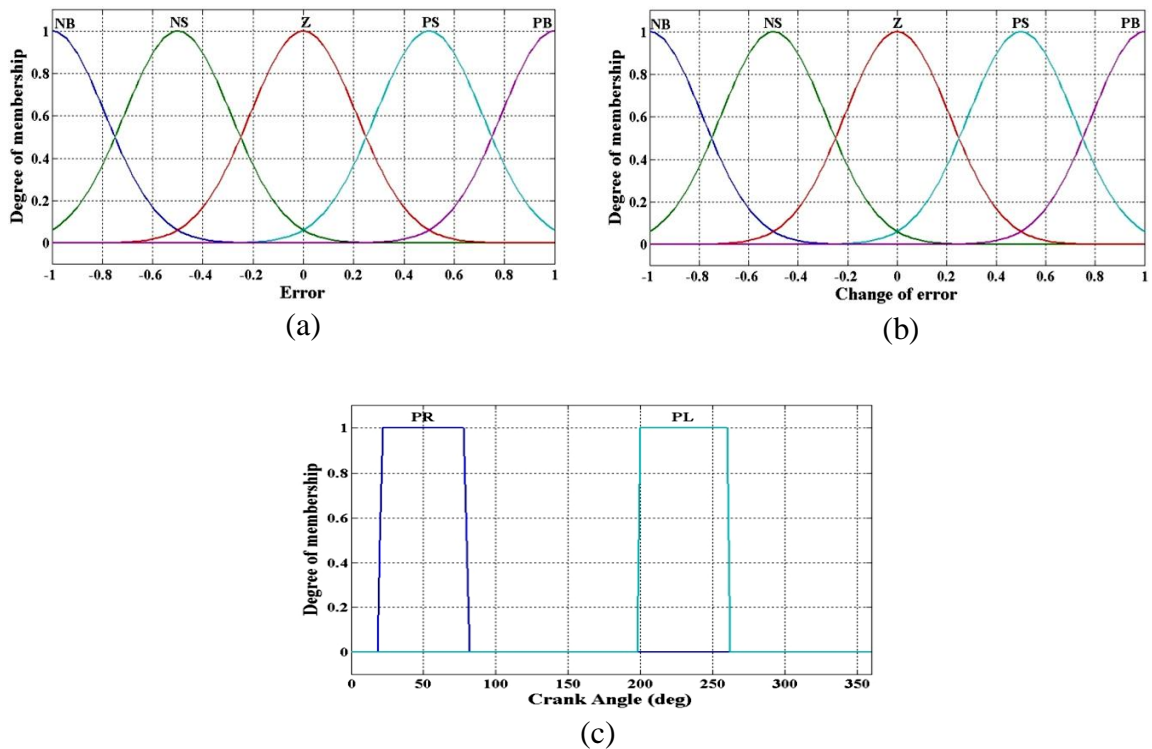
Figure 3.26: FLC's input membership functions, the third input (c) shows the phases (PR= right push, PL= left push)
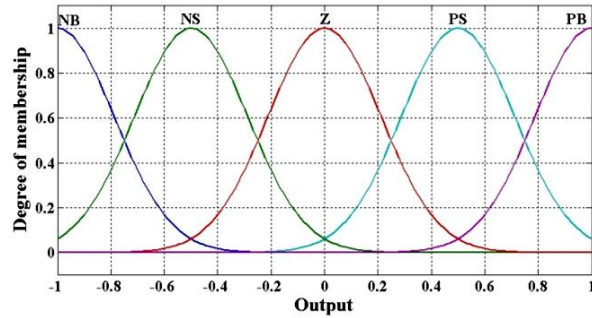
Figure 3.27: FLC's output membership functions

3.5.1.1 Control of flywheel engagement mechanism

The flywheel, as an energy storage device, is used to absorb and release energy from/to the crank of the bicycle when necessary in a feedback control approach. The flywheel engages with the crank to absorb the excessive energy, store it as kinetic energy, and reduce the speed. Also, loaded with kinetic energy, the flywheel engages again to release its energy into the crank, speed up the system and assist the legs. The engagement and disengagement of the flywheel is achieved through the use of an electrical clutch. The decision of the engagement/disengagement of the flywheel is performed in a closed-loop control approach to obtain the necessary assessment. The engagement process is controlled using two different approaches: the first depends on the angular velocity of the knee joints, while the other relies on the angular velocity of the crank.

3.5.1.1.1 Flywheel engagement based on knee joint angular velocity (Scenario I)

In this scenario, the decision of flywheel engagement is made according to the angular velocity of the knee joint compared with the angular velocity of the flywheel. The knee joint angle feedback signal of both legs, obtained from a position sensor in the humanoid-bicycle model, is used. A derivative of this signal is used to obtain the knee angular velocity value. The flywheel engagement decision, in addition to knee and flywheel angular velocities, depends on the tracking error and the position of the crank. If the tracking error is negative, i.e. excessive energy available, and if the flywheel's

angular velocity is less than that of the leg, i.e. the flywheel is ready to absorb energy, the flywheel engages to resist the movement. If the tracking error is positive, i.e. assist is required, and if the flywheel's angular velocity is higher than that of the leg, i.e. the flywheel is ready to assist, the flywheel engages to speed up the movement. Since the tracking error of the right leg is the opposite of that of the left, two flywheel engagement blocks are used in this scenario, one with each leg, and the crank angle is used to differentiate between them. A fuzzy logic controller, Sugeno type, of four inputs and one output, is utilized as shown in Figure 3.28.
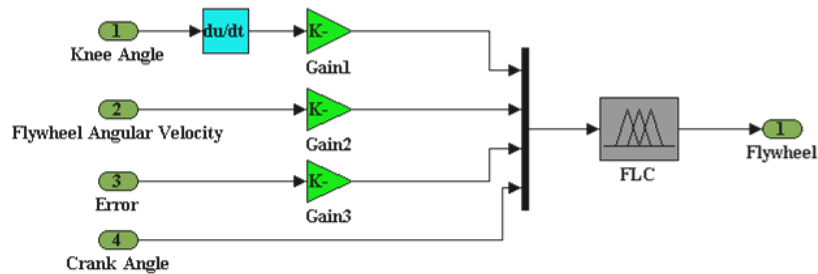
Figure 3.28: Flywheel engagement mechanism

The inputs represent the knee angular velocity, the flywheel angular velocity, the tracking error and the crank angle. The output is either zero or one, using a threshold, to activate/deactivate the clutch responsible for the engagement/disengagement of the flywheel. The first two normalized inputs are fuzzified by a fuzzy set of four variables described by equally distributed Gaussian membership functions, with 50% overlap, namely; Low, Med, Fast and V.Fast as shown in Figures 3.29 and 3.30. The third and fourth inputs, i.e. tracking error and crank angle, are fuzzified by a fuzzy set of two variables described by equally distributed PI-shaped membership functions with 50% overlapping, namely Neg, Pos and Right, Left respectively as shown in Figures 3.31 and 3.32. The fired rules are defuzzified using the weighted average defuzzification method. Table 3.2 shows the sixteen, the rest are "off", fuzzy rules used for the flywheel engagement mechanism.
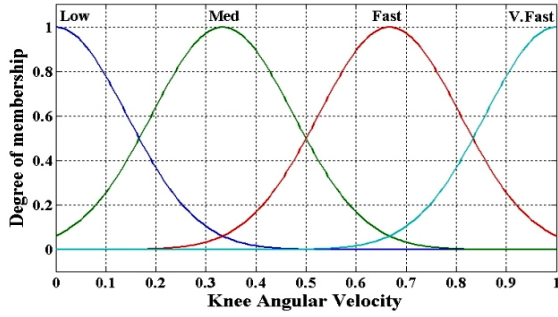
Figure 3.29: First input membership functions of flywheel engagement FLC
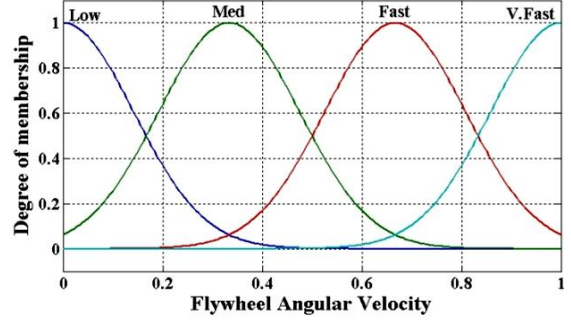
Figure 3.30: Second input membership functions of flywheel engagement FLC
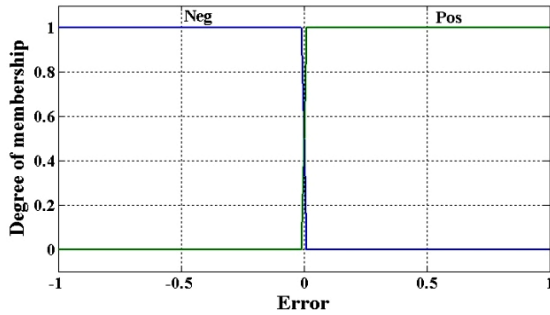
Figure 3.31: Third input membership functions of flywheel engagement FLC
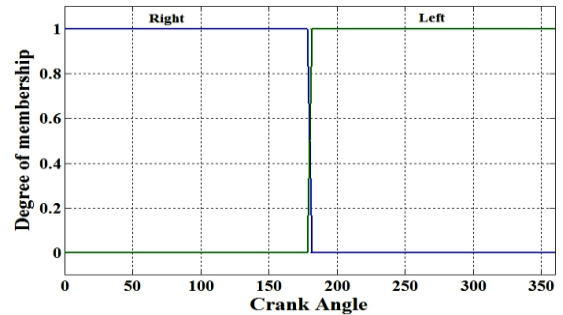
Figure 3.32: Fourth input membership functions of flywheel engagement FLC

Table 3.2: Fuzzy rule base (Scenario I)

Flywheel Ang Vel / Knee Ang Vel	Low	Med	Fast	V.Fast
Low	Off	On if Err=Pos	On if Err=Pos	On if Err=Pos
Med	On if Err=Neg	Off	On if Err=Pos	On if Err=Pos
Fast	On if Err=Neg	On if Err=Neg	Off	On if Err=Pos
V.Fast	On if Err=Neg	On if Err=Neg	On if Err=Neg	Off

3.5.1.1.1.1 Results (Scenario I)

The tracking performance of this scenario, as shown in Figures 3.33 and 3.34, is acceptable. The mean square error of the tracking is 0.027 radians. The flywheel engagement mechanism was activated after 2 seconds, Figure 3.35, while the right leg was left to rotate under the effect of the gravity, without stimulation by FES, to make use of the rotational momentum caused by the gravitational force on the legs to initiate the cycling in order to prevent the extra effort required by the muscles to overcome the

inertia of the bicycle. Despite the big error due to the delay of the legs, the controllers were effective in reducing the tracking error in successive cycles. It can be noticed from Figures 3.36 and 3.37 that the flywheel absorbed and released energy, i.e. produced resist and assist action, when necessary and was successful in reducing the fluctuation in the angular velocity of the crank appearing in section 3.4.1. Although this approach produced good tracking performance with relatively low flywheel engagement frequency (1.75 Hz), the crank cadence suffered significant jerking, i.e. abrupt change in speed, which might cause undesired leg spasm during the exercise. Also, from a hardware implementation point of view, the disadvantage of this scenario is that it requires two engagement decision blocks, one for each leg, each of which depends on the corresponding knee joint angle that can be measured using two position sensors, i.e. goniometer. The use of two goniometers is considered as a disadvantage because of the mechanical errors that may take place due to wirings in cycling exercise.
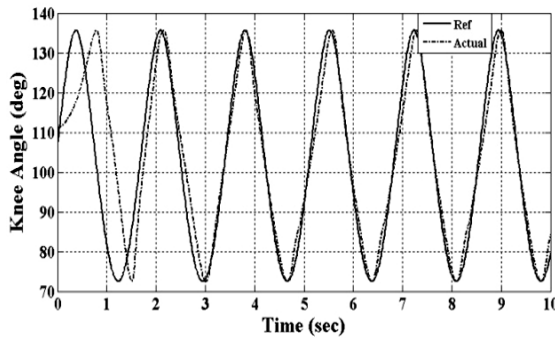
Figure 3.33: Right leg tracking performance (Scenario I)
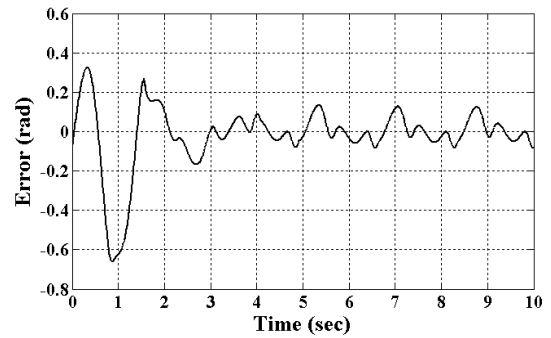
Figure 3.34: Tracking error (Scenario I)
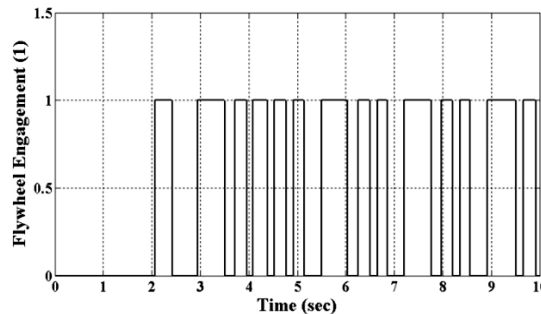
Figure 3.35: Flywheel engagement periods (Scenario I)
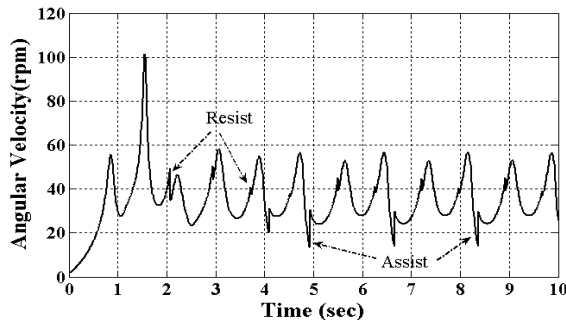
Figure 3.36: Angular velocity of the crank (Scenario I)
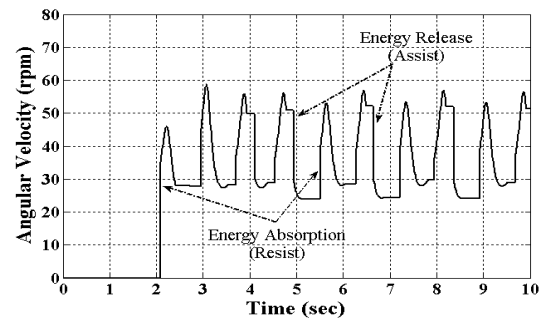
Figure 3.37: Angular velocity of the flywheel (Scenario I)

3.5.1.1.2 *Flywheel engagement based on crank angular velocity (Scenario II)*

In this scenario, the engagement process of the flywheel with the crank was controlled according to two factors; the first is whether the angular velocity of the crank is higher or lower than the desired cadence, and the second is whether the angular velocity of the flywheel is less or greater than that of the crank. If the crank`s speed is higher than the required speed, i.e. the tracking error is negative, and the flywheel`s speed is less than the speed of the crank, i.e. the flywheel has the ability to resist the movement, the clutch will engage the flywheel with the crank to absorb the surplus in the energy and store it as kinetic energy, and produce damping effect on the movement. If the crank`s speed is less than the required speed, i.e. the tracking error is positive, and the flywheel`s speed is higher than that of the crank, i.e. the flywheel has the ability to assist the leg, the flywheel will be engaged to assist and speed-up the cycling by discharging its kinetic energy into the system. The engagement decision process of the flywheel, via an electrical clutch, is implemented using Boolean logic as shown in Figure 3.38. The angular velocity of the flywheel is measured by a velocity meter in the humanoid-bicycle model provided by vN4D software. While the derivative of the crank angle, provided by the same software, is used to measure the angular velocity of the crank.
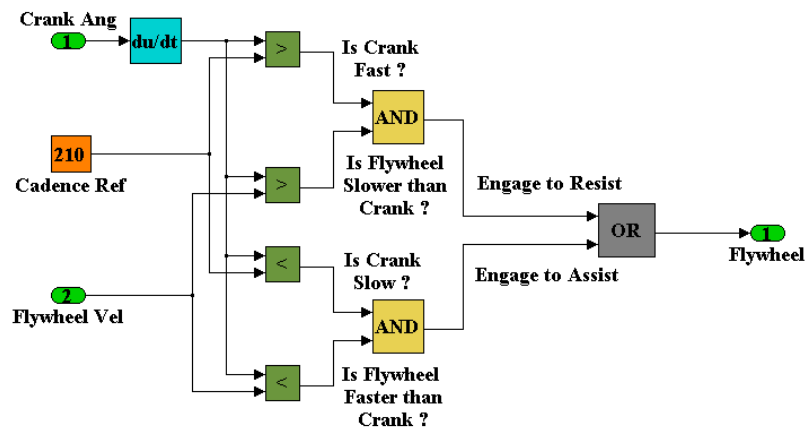
Figure 3.38: The flywheel engagement decision making (Scenario II)

3.5.1.1.2.1 Results (Scenario II)

The right leg tracking performance, tracking error and the flywheel`s engagement periods can be seen in Figures 3.39-3.42. Although the control strategy produced acceptable tracking performance and coordinated pedalling movement, it is obvious from Figure 3.39 that there was a slight delay in the tracking at the first cycle. This is due to the fact that the flywheel assist mechanism was activated after two seconds from the start to benefit from the rotational momentum caused by the gravitational force on the leg. The controllers and the flywheel mechanism were successful in following the reference in subsequent cycles. The mean square of tracking error obtained in this scenario was 0.028 radians, as shown in Figure 3.40. The engagement periods of the flywheel, for both resist and assist actions, can be seen in Figures 3.41 and 3.48. Using this engagement decision making approach, the engagement frequency of the flywheel was 12Hz. From Figures 3.43 and 3.44 it is obvious that the flywheel retarded the movement by absorbing the crank`s energy and then speeded-up the movement by releasing the stored kinetic energy into the crank.
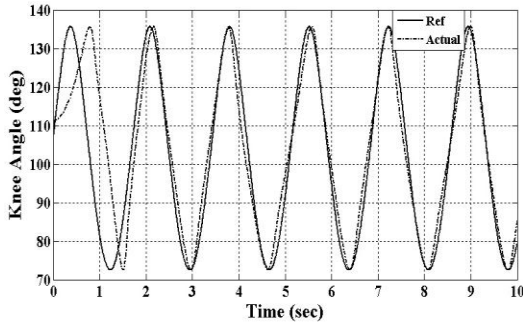
Figure 3.39: Right leg tracking the reference
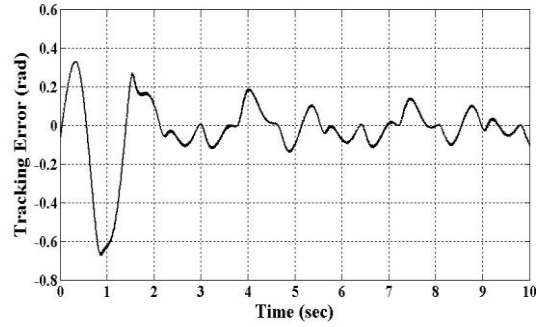
Figure 3.40: Right leg tracking error
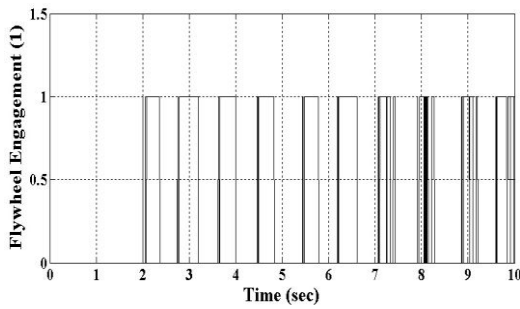
Figure 3.41: Flywheel engagement
(Resist periods)
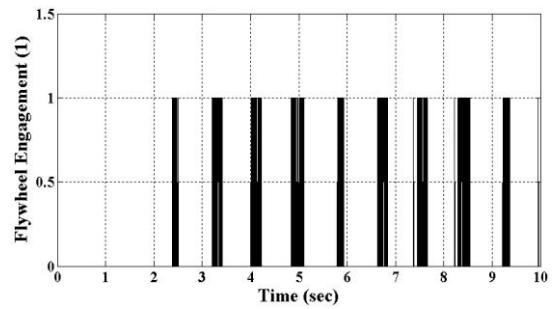
Figure 3.42: Flywheel engagement
(Assist periods)
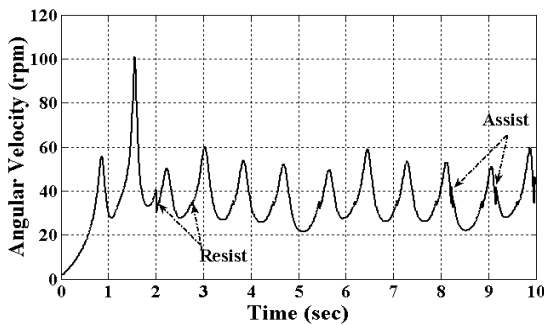
Figure 3.43: Crank angular velocity
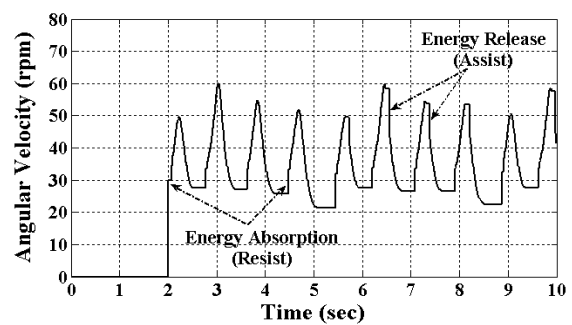
Figure 3.44: Flywheel angular velocity

As a comparison with scenario I, this method is superior in terms of producing smoother cadence, i.e. less jerking, as in Figure 3.36 and Figure 3.43. However, the engagement frequency of the flywheel was much higher, 12Hz, which implies that it requires a highly sensitive and robust electrical clutch to obtain satisfactory performance.

In an attempt to reduce the sensitivity of the engagement due to the use of Boolean logic, the decision making of the engagement mechanism was also built using fuzzy logic control; this is described in chapter four. The use of FLC reduced the

engagement frequency to 6.5 Hz. For the promising results obtained from this approach, this method will be used in subsequent chapters.

As a comparison of this scenario with FES-cycling without assist mechanism, proposed by Massoud (2007) and explained in the beginning of this chapter, it can be noticed that the flywheel reduced the fluctuation in the crank angular velocity, by suppressing the rapid changes in the angular velocity at the dead points, and produced smoother and closer to the desired cadence, as in Figure 3.43 and Figure 3.18. Also, it is clear from Figure 3.45 and Figure 3.46 that the muscles were stimulated only once per cycle during pushing phase and there were no successive stimulations as appeared in section 3.4.1. However, from Figure 3.47 and Figure 3.48 it can be seen that the stimulation intensity is slightly increased as compared with that in section 3.4.1.1, as in Figures 3.21-3.24. The reason behind this increase in the stimulation intensity is that the flywheel has slightly slowed down the speed, as in Figure 3.18 and Figure 3.43, in the system and imposed a slight load on the crank. Thus, the controllers, in turn, slightly increased the stimulation intensity on the legs to speed up the movement. However, since the flywheel replaces the stimulation in the Resist phase, in this case the muscle is stimulated only once per cycle, during the pushing phase, and hence this reduces muscle stimulation period, in comparison with that in section 3.4.1, and consequently allows more time for the muscle to rest before the next stimulus is due. It is clear from Figures 3.45-3.48 that the right and left leg muscles produced different torque levels due to the receipt of unequal amount of stimulation. This is believed to be the result of either the heuristic tuning of controller parameters or a slight imbalance between the right and left sides of the bicycle model.
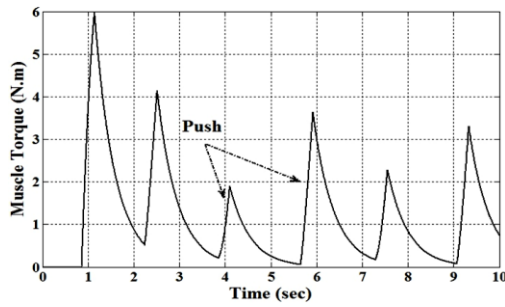
Figure 3.45: Left muscle torque
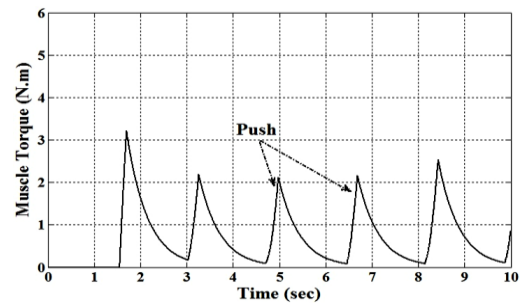
Figure 3.46: Right muscle torque
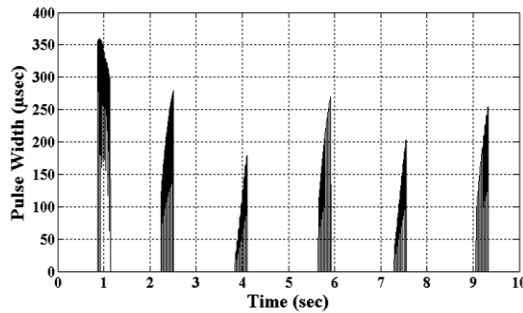
Figure 3.47: Pulse width of left muscle
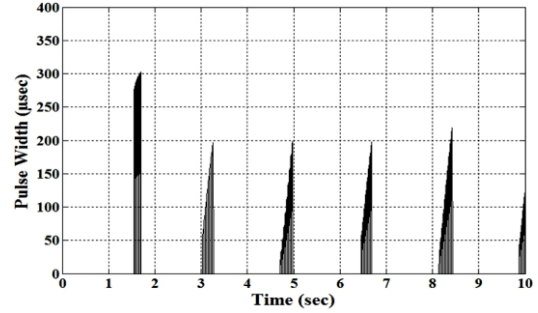
Figure 3.48: Pulse width of right muscle

From fatigue point of view, as it is difficult to compare between the increased/decreased pulse width in both approaches, i.e. with and without assist mechanism, as in Figures 3.21-3.24 and Figures 3.47-3.48, the need for a force drop indicator, derived and described in chapter two, was raised.

Equation (2.6) is used to assess the performance of both approaches, i.e. with and without assist mechanism, and assess the benefits of the proposed assist mechanism from fatigue point of view. After applying the derived indicator in both scenarios, as in Figure 3.49, it is obvious that the force drop using the flywheel mechanism, denoted as scenario II in Figure 3.49, was slower and delayed by approximately 14-17% as compared with that without assist mechanism, as in Figure 3.50. It can be concluded that the new assist mechanism is promoting prolonged FES-cycling session by delaying the appearance of muscle fatigue.
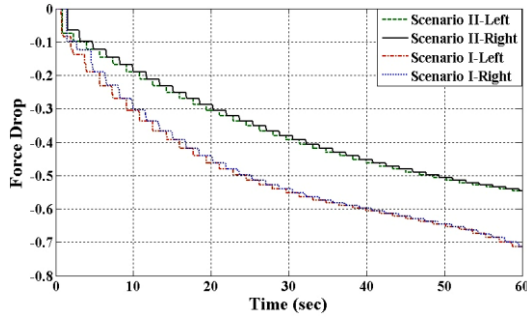
Figure 3.49: Force drop in right and left leg muscles. Scenario I (lower two lines), indicate cycling without assist mechanism. Scenario II (upper two lines), indicate cycling with assist mechanism
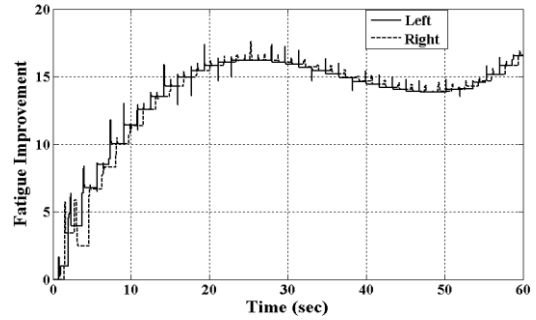
Figure 3.50: Fatigue improvement percentage of FES-cycling using the assist mechanism over that without assist mechanism

3.6 Summary

FES-cycling by stimulating the quadriceps muscle of both legs is implemented using PID and FLC controllers. The controllers were used to regulate the stimulation intensity, i.e. pulse width, of FES signal on the muscle. To perform smooth and coordinated FES-cycling by stimulating the quadriceps only, the muscle should be stimulated twice per cycle, push phase and resist phase, to follow a desired trajectory. A comparison of the results showed that both the PID and FLC in the proposed control approach produced acceptable and close tracking performance with no significant differences. However, the introduced FLC approach produced smoother stimulation intensity on the muscle than that with PID. Also, the ability of the FLC to cope with nonlinear and complex systems made the decision on using FLC in subsequent stages more reasonable.

A new assist mechanism for FES-cycling is presented. The introduced mechanism, represented by a flywheel and an electrical clutch, is utilized in FES-cycling application for the first time. The flywheel, as an energy storage device, together with an electrical clutch can be used to absorb the excess energy in the system, store it as kinetic energy and reuse the same energy to assist the legs.

The control of the assist mechanism is achieved using two different closed-loop approaches. The first approach depends on the angular velocity of the knee joints, while the second relies on the angular velocity of the crank. Both approaches showed successful performance, however, both have cons and pros. The first approach is superior in terms of reduced engagement frequency, 1.75Hz, which implies that moderately-sensitive clutch is enough to obtain satisfactory performance. However, this scenario produces undesired jerking in the cadence. The second approach is superior in terms of smoother cycling cadence. However, it requires highly sensitive electrical clutch, 12Hz, to achieve the purpose.

The flywheel mechanism has been utilized to assist the legs in FES-cycling exercise. With the new proposed mechanism, the muscle is stimulated once per cycle and the cycling dead spots, 0° and 180° of the crank, were passed smoothly and the fluctuation in cadence is suppressed due to the use of the flywheel. Results showed that the stimulation intensity has slightly increased with the new mechanism, even though the derived force drop indicator showed that the new mechanism delayed the fatigue by approximately 14-17% as compared with FES-cycling without assistance. As a result, it can be concluded that the new mechanism is promoting prolonged FES-cycling session and extended work rate for both legs.

Both of the introduced FES-cycling control approaches, with and without assist mechanism, show good leg tracking performance. Although the use of the flywheel has suppressed the fluctuation in the cadence significantly, the error in cadence is still large. To improve the cycling cadence, a cadence control approach will be implemented in subsequent chapters to obtain cycling cadence as close to the desired as possible by stimulating single muscle. Also, to be able to measure the efficiency of the exercise and obtain results closer to reality, i.e. dynamically consider muscle force-length, force-velocity and fatigue properties, the linear muscle model used in this chapter will be replaced by a physiological based, nonlinear and dynamic muscle model.

Chapter 4:   Automatic control of FES-cycling based on desired cadence

4.1 Introduction

Cadence control in FES-cycling is important for studies investigating the therapeutic and medical evolutions and monitoring the training effects at a specific speed (Hunt et al., 2001). To control the cadence in FES-cycling exercise, researchers have investigated different control approaches with the aid of different assist mechanisms and by stimulating different leg muscles. Chen et al. (1997), avoiding the complexity of exact modeling of musculoskeletal system, utilized model-free FLC to control the cycling speed by stimulating the hamstring and quadriceps muscle group using a fix-geared flywheel. Chen et al. (2004) used the same control approach in (Chen et al., 1997) to control the cadence with the aid of an arm-crank. Hunt et al. (2004) designed a controller, using system identification approaches, to control the cycling cadence and leg power simultaneously with the aid of a motor and stimulating three leg muscles, the quadriceps, hamstring and the gluteus maximus. The proposed control approach provided feedback control of both the leg power, by adjusting the stimulation intensity on the muscles, and cycling cadence via electrical motor control. Farhoud and Erfanian (2014) used higher-order sliding mode and FLC, with the aid of a motor, to control both the cadence and leg power in FES-cycling by stimulating the hamstring and quadriceps muscles.

Designing the stimulation patterns in FES-cycling depends on which muscles are stimulated (Chen et al., 1997). Although the final stimulation patterns of best results bore little relation to that of normal subjects, Petrofsky et al. (1983), then followed by Pons et al. (1989), determined the stimulation patterns of the quadriceps and the gluteal muscles by making use of the electromyography (EMG) signals of healthy subjects. By analyzing the gravitational potential of lower limbs in cycling movement, Chen et al., (1997) produced stimulation patterns based on stimulating the quadriceps

and hamstring muscles. Hunt et al., (2004) designed stimulation patterns to perform FES-cycling using three muscles; quadriceps, hamstring and gluteus maximus, by stimulating each muscle individually and determining the best crank position at which the muscle produces significant torque. Making use of the approach in (Chen et al., 1997), Massoud (2007) designed stimulation patterns for FES-cycling by stimulating the quadriceps only. In an attempt to eliminate the effort required to determine the stimulation patterns of the vasti and hamstring muscles, Kim et al. (2008) produces a pattern-free control approach for FES-cycling by making use of feedback information of the lower extremities to generate the necessary joint torque. However, using this method, the crank cadence suffered severe fluctuation, approximately 2-3 [rad/s].

In an attempt to improve the cycling cadence obtained in the previous chapter, in this chapter, making use of the stimulation patterns produced by Massoud (2007), a cadence control approach in FES-cycling by stimulating the quadriceps only is introduced using FLC. Also, in this chapter, a physiological based quadriceps muscle model is used to simulate the behavior of a real fatigable non-linear dynamic muscle in FES-cycling exercise. Further, an energy expenditure model of skeletal muscles, to be used in subsequent chapters, is presented. In addition, a cadence control approach in FES-cycling by stimulating the quadriceps with the aid of the flywheel and electrical clutch mechanism is introduced. Due to the use of the flywheel mechanism, new stimulation patterns are used. The assist mechanism is controlled in a closed-loop approach using FLC to provide assistance and resistance when necessary during the exercise. A comparison between FES-cycling with and without assist mechanism is presented and discussed.

4.2 Physiological based muscle model

Riener and Fuhr, (1998) developed a physiological based muscle model that comprises of three main parts; muscle activation, muscle contraction and body segmental dynamics. Muscle activation describes the excitation needed by the muscle to produce force. It is described as a function of pulse width and frequency of the stimulus, and takes the effect of muscle fatigue into consideration through the introduction of fitness function, as well as a linear second order calcium dynamics. Muscle contraction is described as a force generating property, based on a generic Hill type muscle (Riener et al., 1996, 1997), that takes into account the force-length and force-velocity properties. The body segmental dynamics are described considering the active and passive moments of the joints the muscle spans. The passive elastic properties of a muscle are described by double exponential equations to account for the effect of the adjacent joints the muscle spans, while the passive viscous property is described by a linear damping function.

4.2.1 Muscle activation

Muscle activation is described by four main parts; recruitment characteristics, frequency characteristics, calcium dynamics and muscle fatigue, as shown in Figure 4.1.
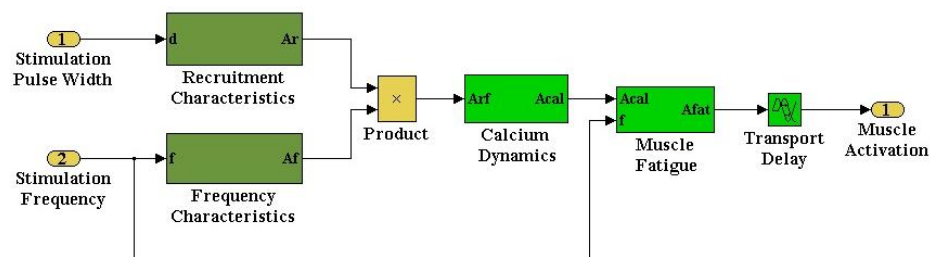
Figure 4.1: Muscle activation model

The recruitment characteristics part describes the normalized portion, i.e. percentage, of muscle's motor units recruited and considered, based on the recruitment

curve shown in Figure 4.2, as a function of pulse width, d, of the stimulus. The recruitment level, a_r, is described as:

$$a_r(d) = c_1\{(d - d_{thr})\arctan[k_{thr}(d - d_{thr})] - (d - d_{sat})\arctan[k_{sat}(d - d_{sat})]\} + c_2 \qquad \textbf{(4.1)}$$

where d_{thr} and d_{sat} represent the threshold and saturation pulse width respectively. c_1 and c_2 are constants used to keep the recruitment curve limited between 0 and 1. The shape of the curve at the region between the threshold and saturation can be modified by the values k_{thr} and k_{sat} respectively.
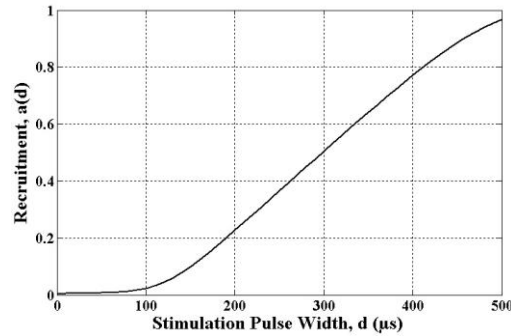
Figure 4.2: Motor units' recruitment curve with respect to pulse width

The frequency characteristics unit describes, as a function of stimulation frequency, f, the normalized amount of activation, $a_f(f)$, in a single motor unit. This function is introduced to capture the force-frequency characteristics of artificially stimulated muscle, as:

$$a_f(f) = \frac{(\alpha f)^2}{1 + (\alpha f)^2} \qquad \textbf{(4.2)}$$

where α is a shape factor.

The calcium dynamics unit describes the phenomena of releasing calcium ions in the sarcoplasmic reticulum. It has been modeled by two first order transfer functions,

with time constant τ_{ca}, in series. The input, a_{rf}, of the calcium dynamics unit is represented by the product of the recruitment level, a_r, and the amount of activation, a_f. The calcium dynamics, a_{cal}, is described as:

$$a_{cal}(s) = \left(\frac{1}{\tau_{ca}s+1}\right)\left(\frac{1}{\tau_{ca}s+1}\right)a_{rf}(s) = \frac{1}{\tau_{ca}^2 s^2 + 2\tau_{ca}s+1}a_{rf}(s) \qquad (4.3)$$

Muscle fatigue and recovery is described by the introduction of fitness function, fit, taking into consideration that the fatigue increases with the increase of stimulation frequency, f, as:

$$\frac{dfit}{dt} = \frac{(fit_{min} - fit)a\lambda(f)}{T_{fat}} + \frac{(1-fit)(1-a\lambda(f))}{T_{rec}} \qquad (4.4)$$

$$\lambda(f) = 1 - \beta + \beta\left(\frac{f}{100}\right)^2 \quad for \quad f < 100\,Hz \qquad (4.5)$$

where fit_{min} represents the minimum fitness, while T_{fat} and T_{rec} represent the time constants for fatigue and recovery respectively. The term $\lambda(f)$ is a function of stimulation frequency, to account for the dependency of muscle fatigue on the stimulation frequency, and β is a shape factor. The activation of fatiguing muscle is expressed as:

$$a_{fat}(t) = a_{cal}(t)\,fit(t) \qquad (4.6)$$

The last part of muscle activation unit, represented by the time delay T_{del}, is introduced to account for finite conduction velocities in the membrane system and the delays from the involved chemical reactions.

4.2.2 Muscle contraction

The muscle contraction dynamics model accounts for the force-length, f_{fl}, and force-velocity, f_{fv}, properties of the muscle and scales the muscle activation by the maximum isometric muscle force, F_{max}, in order to obtain the absolute muscle force, as shown in Figure 4.3. The active muscle force of a muscle group is obtained by multiplying the absolute muscle force with the moment arm of the joints the muscle spans.
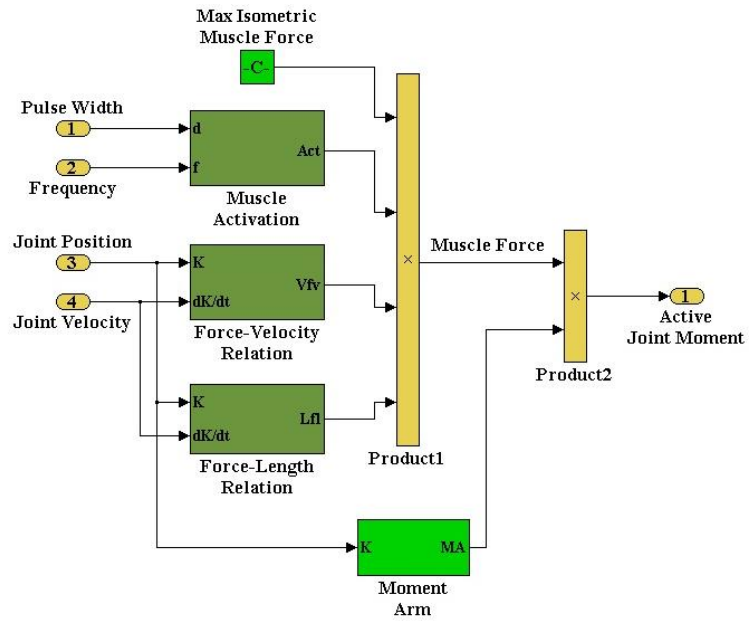
Figure 4.3: Muscle contraction model with moment arm to generate active joint moment

The force-length relation is expressed as:

$$f_{fl} = \exp\left[-\left(\frac{\bar{l}-1}{\varepsilon}\right)^2\right] \qquad \textbf{(4.7)}$$

where $\bar{l}$ represents the normalized muscle length with respect to the optimal muscle length, l_{opt}, and ε is a shape factor. The length of a muscle, l_i, of a group, i, is calculated as:

$$l_i = C_i + \sum_j \int_{\varphi_j} ma_{ij}(\varphi_j) \, d\varphi_j \qquad\qquad \textbf{(4.8)}$$

where ma_{ij} is the moment arm of muscle group, i, around joint, j, and φ_j represents the position of the joint the muscle spans, while C_i represents the integration constant resulting from integrating the moment arm functions. The force-velocity relation is expressed as:

$$f_{fv} = 0.54 \arctan(5.69\,\bar{v} + 0.51) + 0.745 \qquad\qquad \textbf{(4.9)}$$

where $\bar{v} = v / |v_m|$ is the normalized muscle velocity with respect to maximum muscle contraction velocity, v_m, and $v = dl/dt$, $v < 0$ for muscle contraction.

The velocity, v_i, of a muscle group, i, is calculated as:

$$v_i = \sum_j \dot{\varphi}_j \, ma_{ij}(\varphi_j) \qquad\qquad \textbf{(4.10)}$$

where ma_{ij} is the moment arm of muscle group, i, around joint, j, while φ_j and $\dot{\varphi}_j$ represent the position and angular velocity of the joints the muscle spans respectively.

4.2.3 Body segmental dynamics

Body segmental dynamics model takes into account the active and passive joint moments. The total moments of a joint are expressed as the sum of active moment (muscle force multiplied by moment arm), passive elastic moment and passive viscous moment. The moment arms of the rectus femoris and vasti about knee and hip joints, provided by Riener and Fuhr, (1998), are expressed as:

90

$$ma_{rf\_H} = 0.025\varphi_H^2 + 0.41\varphi_H - 0.040 \qquad \textbf{(4.11)}$$

$$ma_{rf\_K} = -0.058\exp(-2.0\varphi_K^2)\sin\varphi_K - 0.0284 \qquad \textbf{(4.12)}$$

$$ma_{vs\_K} = -0.070\exp(-2.0\varphi_K^2)\sin\varphi_K - 0.0250 \qquad \textbf{(4.13)}$$

where ma_{fr_H} is the moment arm of the rectus femoris muscle about the hip joint, ma_{rf_K} is the moment arm of the rectus femoris muscle about the knee joint, ma_{vs_K} is the moment arm of the vasti muscle about the knee joint, φ_H and φ_K are the positions of hip and knee joints respectively.

The passive elastic moment equations used in this work, introduced by Edrich et al. (2000), are expressed as double exponential equations that account for the influence of the adjacent joint angle, as:

$$M_{elast} = \exp\left(e_1 + e_2\varphi_{dist} + e_3\varphi + e_4\varphi_{prox}\right) - \exp\left(e_5 + e_6\varphi_{dist} + e_7\varphi + e_8\varphi_{prox}\right) + e_9 + M_K \quad \textbf{(4.14)}$$

where M_{elast} is the elastic joint moment, φ is the angle, in degrees, of the joint being investigated, φ_{prox} is the angle of the proximal joint, φ_{dist} is the angle of the distal joint, M_K is equal to $\exp(e_{10} + e_{11}\varphi)$ and is added only when calculating the knee joint moment. $e_1 - e_{11}$ are parameters determined by fitting the simulated curves to the averaged measured curves. The parameters for both hip and knee joints for paraplegics, (Edrich et al., 2000), are shown in Table 4.1.

Table 4.1: Passive elastic moment's model coefficients

Parameter	Knee joint	Hip joint
e_1	2.2	1.9
e_2	-0.017	0
e_3	-0.05	-0.09
e_4	0	0
e_5	-6.4	0.95
e_6	0	0
e_7	0.067	0.024
e_8	-0.009	0
e_9	0	14
e_{10}	1.2	-
e_{11}	-0.2	-

The passive viscous moment of joint, j, is described by Riener and Fuhr (1998) as a linear relation between the angular velocity $\dot{\varphi}_j$ and the damping coefficient k_j. The passive viscous moments of the knee and hip joints are expressed as:

$$M_{vis} = k_j \dot{\varphi}_j \qquad \qquad \textbf{(4.15)}$$

where k_j, the damping coefficient , equal to 1.0 for knee joint and 2.0 for hip joint.

4.3 Muscle energy expenditure

Muscle energy expenditure can be predicted from thermal and mechanical energy liberation during contractions of stimulated muscle. A phenomenological model of skeletal muscle energy expenditure was developed and evaluated by Umberger et al. (2003) to be used with Hill-type muscle model in simulation platform. The model parameters used where based largely on mammalian muscle data with preference given, were possible, to human data. The total rate of muscle energy expenditure can be described as:

$$\dot{E} = \dot{h}_A + \dot{h}_M + \dot{h}_{SL} + \dot{w}_{CE} \qquad\qquad (4.16)$$

where $\dot{E}$ is the total energy expenditure [Watt/Kg], $\dot{h}_A$ is the activation heat rate, $\dot{h}_M$ is the maintenance heat rate, $\dot{h}_{SL}$ is the shortening and lengthening heat rate and $\dot{w}_{CE}$ is the mechanical work rate.

4.3.1 Activation and maintenance heat rate

The heat rate of activation and maintenance ($\dot{h}_{AM}$) measured in [Watt/Kg] can be expressed together as:

$$\dot{h}_{AM} = \dot{h}_A + \dot{h}_M = 1.28\, x\,\% FT + 25 \qquad\qquad (4.17)$$

where FT is the fast twitch muscle fiber type, ST is the slow twitch muscle fiber type, and the $\%FT$ is the percentage of fast twitch muscle fibers. In human muscle, 40% of $\dot{h}_{AM}$ represents the activation process ($\dot{h}_A$) and 60% of $\dot{h}_{AM}$ represents the maintenance ($\dot{h}_M$) heat rate.

4.3.2 Shortening and lengthening heat rate

During shortening of contractile element (CE), the heat production above the activation and maintenance heat rate ($\dot{h}_{AM}$) has been modeled as the production of the shortening coefficient (α_S) and the contraction velocity ($\tilde{V}_{CE}$). The shortening heat coefficients for ST and FT fibers are formulated as:

$$\alpha_{S(ST)} = \frac{100}{\tilde{V}_{CE(MAX-ST)}} \qquad\qquad (4.18)$$

$$\alpha_{S(FT)} = \frac{153}{\tilde{V}_{CE(MAX-FT)}} \tag{4.19}$$

where $\tilde{V}_{CE(MAX-ST)}$ and $\tilde{V}_{CE(MAX-FT)}$ are the maximal shortening velocity of ST and FT fibers.

The $\tilde{V}_{CE(MAX-FT)}$ is defined by the Hill-coefficients A_{REL} and B_{REL} and is assumed to be 2.5 times greater than $\tilde{V}_{CE(MAX-ST)}$, as:

$$\tilde{V}_{CE(MAX-FT)} = \frac{B_{REL}}{A_{REL}} \tag{4.20}$$

$$\tilde{V}_{CE(MAX-ST)} = \frac{\tilde{V}_{CE(MAX-FT)}}{2.5} \tag{4.21}$$

The shortening heat rate (when $\tilde{V}_{CE} \leq 0$) is given as:

$$\dot{h}_{SL} = -\alpha_{S(ST)}\tilde{V}_{CE}(1 - \%FT/100) - \alpha_{S(FT)}\tilde{V}_{CE}(\%FT/100) \tag{4.22}$$

where $\tilde{V}_{CE} = \dfrac{V_{CE}}{L_{CE(OPT)}}$ and $\alpha_{S(ST)}\tilde{V}_{CE}$ cannot exceed 100 W/Kg.

The lengthening heat rate (when $\tilde{V}_{CE} > 0$) is described as:

$$\dot{h}_{SL} = \alpha_L \tilde{V}_{CE} \tag{4.23}$$

where $\alpha_L = 4\alpha_{S(ST)}$

4.3.3 Mechanical work rate

The mechanical work rate [Watt/Kg] is described as:

$$\dot{W}_{CE} = -\frac{F_{CE}V_{CE}}{m} \tag{4.24}$$

where m is the mass of the muscle involved, F_{CE} is the force of the muscle and V_{CE} is the contraction velocity of the muscle.

Muscle mass [Kg] is related to the cross sectional area of the muscle as:

$$m = PCSA \; \rho \, L_{CE(OPT)} \tag{4.25}$$

where m is the mass [Kg], $PCSA$ is the physiological cross sectional area of the muscle [m^2], $L_{CE(OPT)}$ is the optimal length [m], and ρ is the muscle density [Kg/m3].

4.3.4 Scaling factors

Scaling factors are used to account for the length and activation dependence of both $\dot{h}_{AM}$ and $\dot{h}_{SL}$, and the dependence of total heat rate on the metabolic working conditions (aerobic and anaerobic). To account for the length dependence, both quantities, $\dot{h}_{AM}$ and $\dot{h}_{SL}$, are scaled by the normalized isometric force-length (F_{ISO}) relation when $L_{CE} > L_{CE(OPT)}$. From (Nagano 2001) F_{ISO} is described as:

$$F_{ISO} = C \left(\frac{L_{CE}}{L_{CE(OPT)}} \right)^2 - 2C \left(\frac{L_{CE}}{L_{CE(OPT)}} \right) + C + 1 \tag{4.26}$$

$$C = -\frac{1}{width^2} \tag{4.27}$$

where $width$ is the maximum length range of force production relative to $L_{CE(OPT)}$.

To account for the activation dependence, scaling factors for $\dot{h}_{AM}$ and $\dot{h}_{SL}$ are defined as:

$$A_{AM} = A^{0.6} \tag{4.28}$$

$$A_S = A^{2.0} \tag{4.29}$$

where A is a scaling factor defined as the muscle activation.

The value of $\dot{h}_{SL}$ is scaled by A_S when $\tilde{V}_{CE} \leq 0$ (shortening) while scaled by A when $\tilde{V}_{CE} > 0$ due to lack of data for lengthening velocities.

To account for metabolic working conditions (aerobic and anaerobic), a scaling factor S is defined, where $S = 1$ for anaerobic and $S = 1.5$ for aerobic conditions. The total energy liberation (W/Kg) for a muscle of mass (m) is described as:

if $L_{CE} \leq L_{CE(OPT)}$ (4.30)

$$\dot{E} = \dot{h}_{AM} \ A_{AM} \ S \ +$$

$$\begin{cases} [-\alpha_{S(ST)} \ \tilde{V}_{CE}(1 - \%FT/100) - \alpha_{S(FT)} \tilde{V}_{CE}(\%FT/100)] A_S \ S & \text{if } \tilde{V}_{CE} \leq 0 \\ \alpha_L \ \tilde{V}_{CE} \ A \ S & \text{if } \tilde{V}_{CE} > 0 \end{cases}$$

$$- (F_{CE} \ V_{CE})/m$$

if $L_{CE} > L_{CE(OPT)}$

$$\dot{E} = (0.4\dot{h}_{AM} + 0.6\dot{h}_{AM} \ F_{ISO}) A_{AM} \ S \ +$$

$$\begin{cases} [-\alpha_{S(ST)} \ \tilde{V}_{CE}(1 - \%FT/100) - \alpha_{S(FT)} \tilde{V}_{CE}(\%FT/100)] \ F_{ISO} \ A_S \ S & \text{if } \tilde{V}_{CE} \leq 0 \\ \alpha_L \ \tilde{V}_{CE} \ F_{ISO} \ A \ S & \text{if } \tilde{V}_{CE} > 0 \end{cases}$$

$$- (F_{CE} \ V_{CE})/m$$

The total energy rate is not allowed to fall under 1.0 [Watt/Kg] to account for the resting energy rate of human skeletal muscle. The parameters used in this study to build the energy expenditure model are shown in Table 4.2. It is important to mention that the muscle energy expenditure model will be used in subsequent chapters for the purpose of calculating the efficiency of FES-cycling exercise in different scenarios.

Table 4.2: Parameters used to build the energy expenditure model

Parameter	Rectus Femoris	Vasti	Reference
%FT	65	50	Umberger 2003
A_{REL}	0.36	0.3	Umberger 2003
B_{REL}	4.32	3.6	Umberger 2003
width	1.443	0.627	Nagano 2001
ρ	1059.7 Kg/m3	1059.7 Kg/m3	Umberger 2003
$L_{CE(OPT)}$	0.084 m	0.087 m	Nagano 2005
PCSA	10.92 cm^2	18.53 cm^2	Wang 2004
m	0.0995 Kg	0.1688 Kg	Umberger 2003

4.4 The quadriceps muscle model

In this work, the quadriceps muscle group, rectus femoris and three vasti muscles, is used to provide knee extension when stimulated by FES signal. The quadriceps muscle group, i.e. Rectus femoris and vasti, is modeled basing on the physiological muscle model proposed by Riener and Fuhr, (1998). The quadriceps muscle is modeled in Matlab/Simulink as shown in Figure 4.4. The parameters used to build the model, provided by Riener and Fuhr, (1998), are listed in Table 4.3.
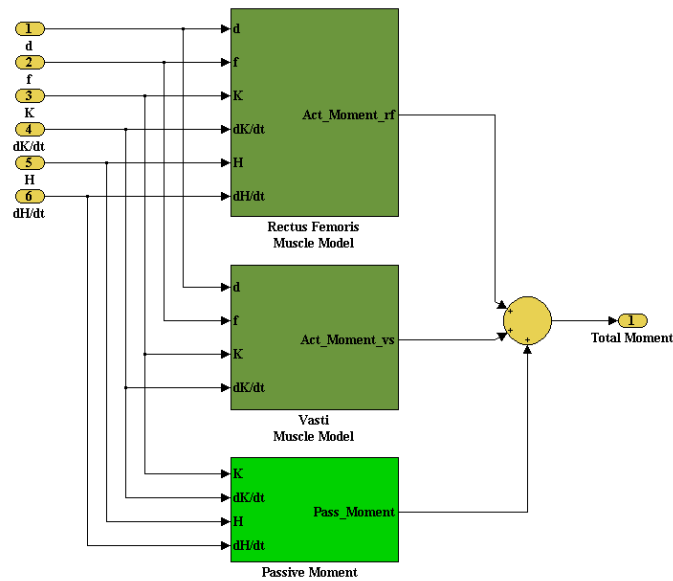
Figure 4.4: Quadriceps muscle model

Table 4.3: Parameters used for quadriceps model

Parameter	Rectus femoris	Vasti
c_1	0.00091	0.00091
c_2	0.4731	0.4731
d_{thr}	122	122
d_{sat}	487	487
k_{thr}	122	122
k_{sat}	487	487
α	0.1	0.1
f	33	33
τ_{ca}	0.03	0.04
fit_{min}	0	0
T_{fat}	18	18
T_{rec}	30	30
β	0.6	0.6
T_{del}	0.025	0.025
l_{opt}	0.086	0.086
ε	0.4	0.45
c_i	0.11	0.04
v_m	0.51	0.48
F_{Max}	450	2340

The quadriceps muscle model is tested with a free swinging leg of the humanoid model built using Visual Nastran (vN4D) software. The swinging leg is initially positioned at 85º knee angle and allowed to swing freely. A stimulation pulse width of 220µs and 33Hz frequency is applied to the muscle model, in Matlab/Simulink environment, as shown in Figure 4.5. The resulted knee active torque and the actual knee trajectory due to stimulation can be seen in Figures 4.6 and 4.7. Due to nonlinear behavior of the muscle, the torque is fluctuated at the beginning of stimulation but settled within two seconds. Also, it is clear from Figures 4.6 and 4.7 that the knee torque has dropped gradually and led to decrease in the knee angle, after 3rd second. This is due to the effect of muscle fatigue resulting from continuous stimulation to the muscle. Further, as a comparison with linear muscle model proposed by Ferrarin, used in previous chapters, it can be seen from Figure 4.8 that the active torques of both

muscle models are close in magnitude. However, the response of the model proposed by Riener is nonlinear and faster than Ferrarin's muscle model. The quadriceps muscle model, developed according to the work of Riener and Fuhr (1998), will be used in this and consequent chapters.
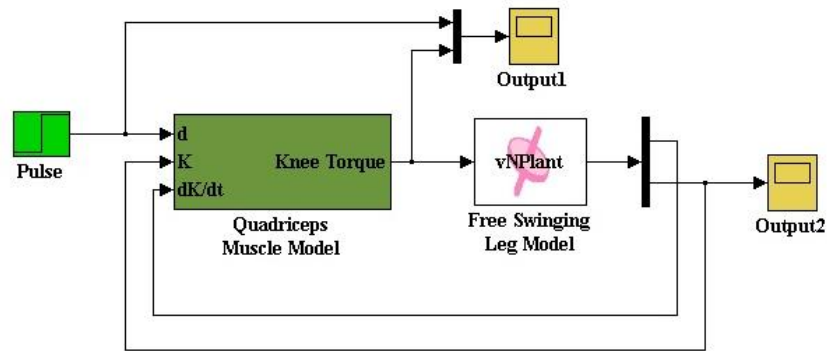
Figure 4.5: Test of the quadriceps model using free swinging leg
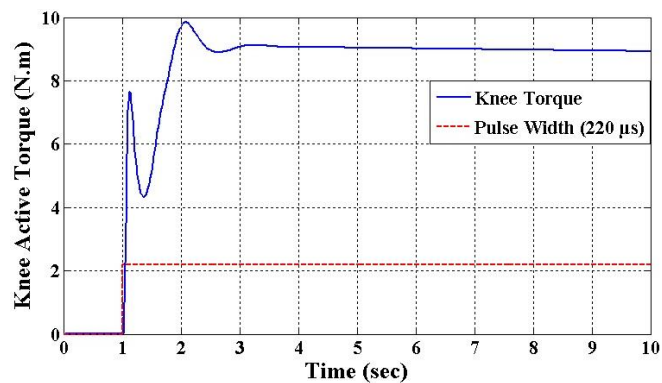
Figure 4.6: Knee torque obtained from stimulating the quadriceps model
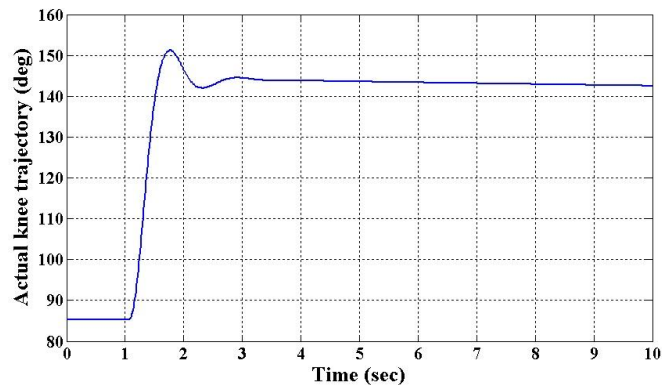
Figure 4.7: Knee trajectory obtained from stimulating the quadriceps model
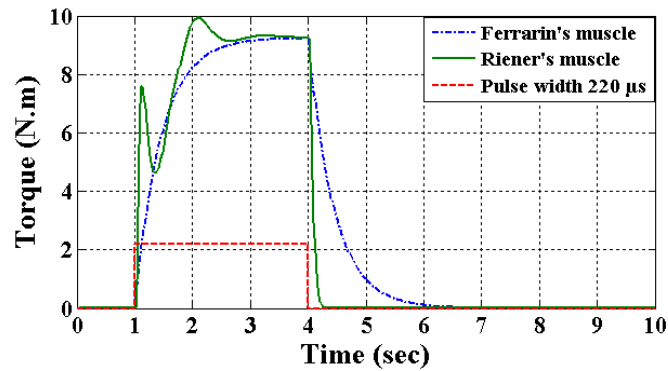
Figure 4.8: Comparison between linear (Ferrarin's) and nonlinear (Riener's) muscle models

4.5 The control strategy

The main objective is to achieve FES-cycling exercise for disabled individuals at a required cadence, i.e. cycling speed, by stimulating single muscle group, the quadriceps, of each leg. Closed-loop control approaches can be utilized in FES-cycling to regulate the amount of the signal applied to the muscle and control the magnitude of the force generated by the muscle, hence maintain the required leg movement. Also, the stimulation intensity of the signal can be controlled by altering either the frequency or the pulse width of the signal or both at the same time. In this work, the frequency of the stimulation signal is fixed to 33Hz, as in (Ferrarin and Pedotti, 2000), and the pulse width is kept variable to be adjusted by the controller. A cycling cadence reference of 35 rpm is used in this work as it is widely used in rehabilitation centres (Chen et al., 1997). A feedback signal of the actual cycling cadence, obtained from a sensor located in the bicycle model, is compared with the desired cadence reference and the resultant error signal is supplied to the controller to alter the stimulation pulse width accordingly. The main challenge here is to maintain the required cycling cadence by stimulating single muscle, one-directional actuator, represented by the quadriceps of each leg.

4.5.1 FES-cycling without assist mechanism (Scenario I)

Stimulating the quadriceps muscle group leads to knee extension and is essential in cycling to produce forward movement. Also, the quadriceps muscle can be stimulated,

at some positions, to extend the knee and retard the cyclic motion (Massoud, 2007). In an attempt to govern the cycling speed, the crank position is divided into three phases; Push, Resist and Rest phases for each leg, as explained in chapter three. The Push phase is the period at which the quadriceps is stimulated to speed up the movement, and the Resist phase is the period at which the quadriceps is stimulated to retard the movement if required. While the Rest phase is the period at which the muscle is left without stimulation in order to rest before the next stimulus is due.

Since the amount of Push and Resist required may differ, two fuzzy-logic controllers (FLC) are used, to separately regulate the stimulation intensity during Push and Resist phases, for each leg, as shown in Figure 4.9. The stimulation phases blocks, constructed using logic gates according to the crank angle, are used to allow each controller pass its signal only during its own phase. A saturation block is used, at the output of each FLC, together with a reference pulse constant to fine tune and regulate the minimum and maximum output value of each FLC.
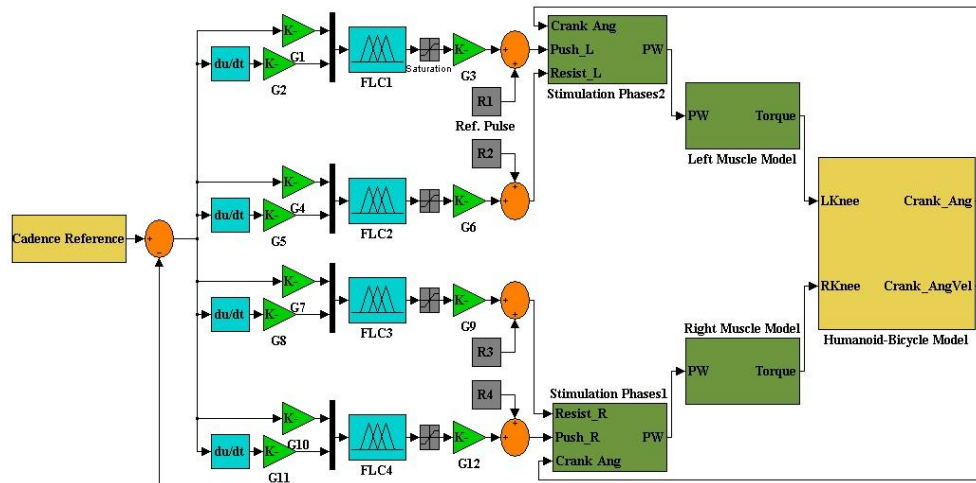
Figure 4.9: The control block diagram used in Scenario I

Each FLC, Mamdani type, has two inputs and one output. The FLC inputs represent the error and change of error, while the output forms the pulse width of the stimulus applied to the muscle. The two inputs are normalized by scaling factors before fuzzification. The normalized inputs are fuzzified by a fuzzy set of five equally distributed Gaussian membership functions with 50% overlap. The fuzzy output,

resulting from the fired fuzzy rules, is converted to crisp value using the centre of area defuzzification method. The output, after a saturation block, is then scaled by a scaling factor. The fuzzy input and output membership functions can be seen in Figures 4.10 and 4.11. A standard PD-like fuzzy rule base is used as shown in Table 4.4.
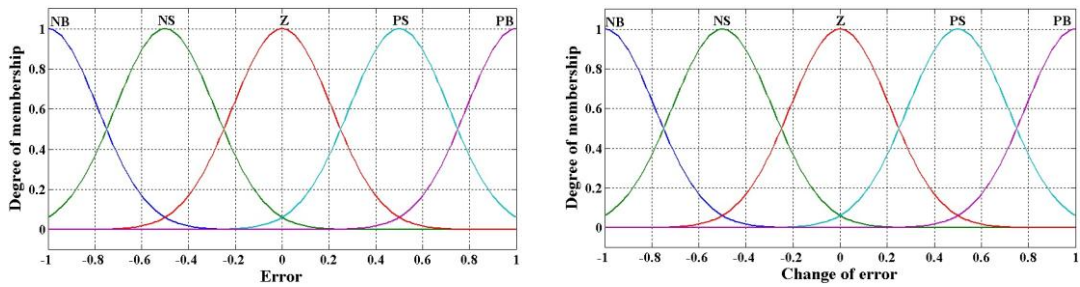
Figure 4.10: Controller`s input membership functions
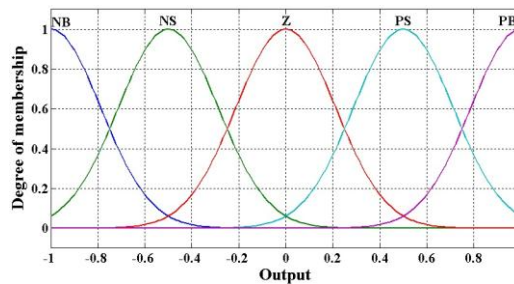
Figure 4.11: Controller`s output membership functions

Table 4.4: Fuzzy rules base used for FLC

Δe \ e	NB	NS	Z	PS	PB
NB	NB	NB	NB	NS	Z
NS	NB	NB	NS	Z	PS
Z	NB	NS	Z	PS	PB
PS	NS	Z	PS	PB	PB
PB	Z	PS	PB	PB	PB

4.5.1.1 Results

The angular velocity of the crank, cadence error and the stimulation intensity of both legs, obtained for minimum tracking error, can be seen in Figures 4.12-4.15. It is clear from Figures 4.12 and 4.13 that the resultant angular velocity of the crank has fluctuated, by approximately ±10 rpm, around the desired reference with a mean

square error in cadence equal to 0.63 rad/s. This is due to the fact that the effect of the cycling dead spots, around 0° and 180° of crank angle, has caused rapid changes in the angular velocity. Also, the resistance, produced by the legs during Resist phase, was not sufficient to prevent the effect of the dead spots. Due to stimulating the muscle twice per cycle, during Push and Resist phases, the average stimulation intensity on both legs is relatively high, 223μs, as in Figures 4.14 and 4.15, which leads to rapid muscle fatigue and premature termination of the exercise.
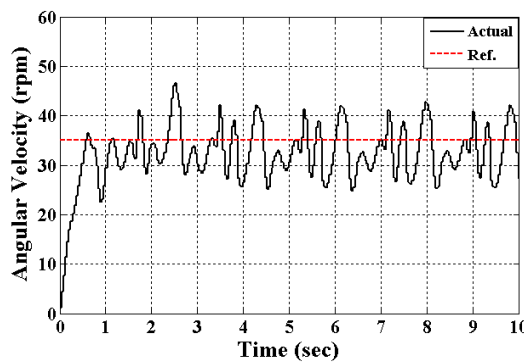
Figure 4.12: The angular velocity of the crank (Scenario I)
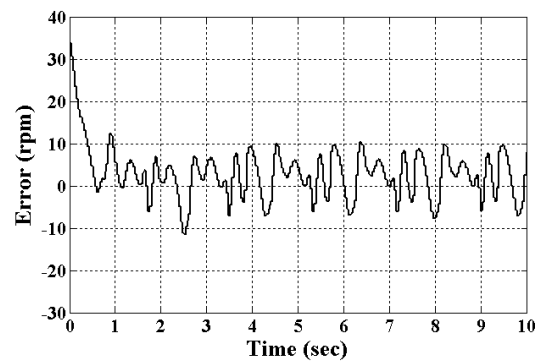
Figure 4.13: Cadence error (Scenario I)
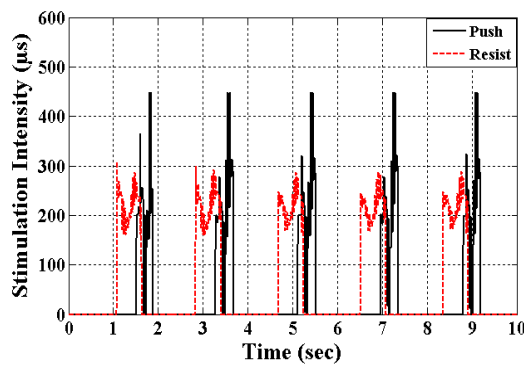
Figure 4.14: The stimulation intensity of the right leg (Scenario I)
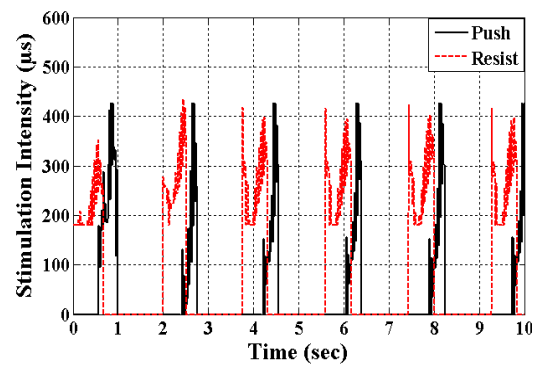
Figure 4.15: The stimulation intensity of the left leg (Scenario I)

4.5.2 FES-cycling with assist mechanism (Scenario II)

In this scenario, it is aimed to prevent the drawbacks that appeared in Scenario I, and obtain improved cadence with minimized stimulation intensity to prolong the exercise. A flywheel and electrical clutch mechanism, introduced in the previous chapter, is to

be used in this scenario for cadence control to provide assistance and resistance when required. The flywheel, as an energy storage device, engages with the crank to absorb the excessive energy in the system, store it as kinetic energy, and retard the movement. Also, loaded with kinetic energy, the flywheel engages with the crank, discharge its energy into the system, and speeds up the movement. The engagement and disengagement of the flywheel is achieved by an electrical clutch. The control block diagram of this scenario can be seen in Figure 4.16. The stimulation patterns, specified according to the crank angle, used in this scenario are shown in Figure 4.17. It is clear that the flywheel engagement mechanism has replaced the Resist phase, appeared in Scenario I, and the muscle will be stimulated only once per cycle during the Push phase.
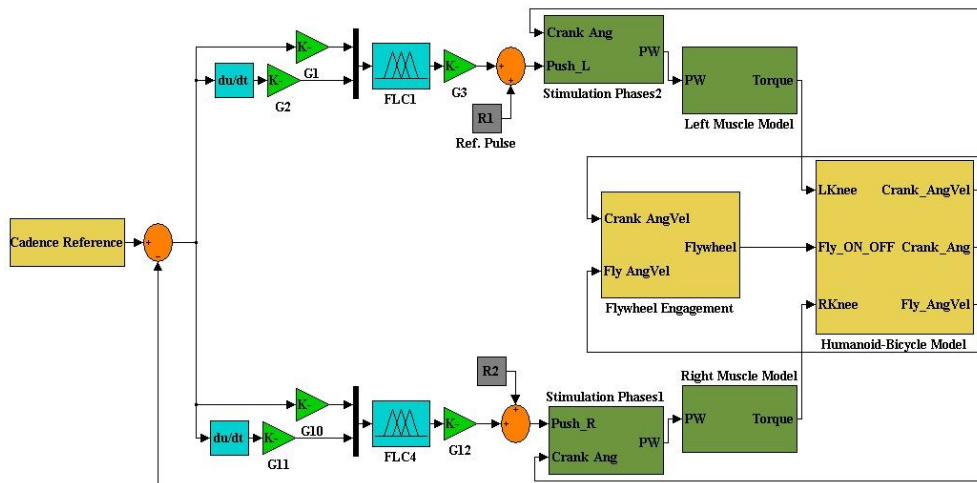
Figure 4.16: The control block diagram used in this scenario
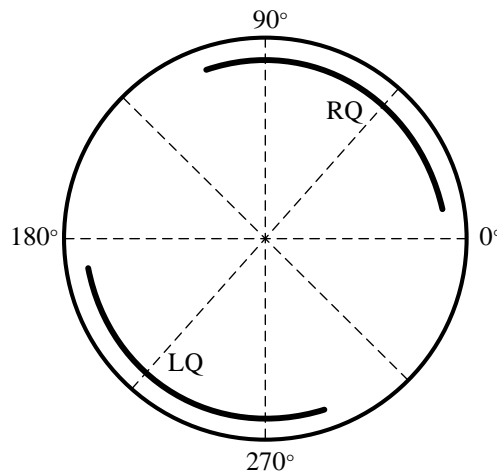
Figure 4.17: The stimulation patterns used with flywheel engagement mechanism

The flywheel engagement mechanism used in this scenario depends on the angular velocity of both the crank and the flywheel. When the angular velocity of the crank exceeds the desired speed, i.e. excessive energy in the system, and also if the angular velocity of the flywheel is lower than that of the crank, i.e. the flywheel has the potential to resist the movement, engagement of the flywheel with the crank takes place, by the clutch, to slow down the motion. On the other hand, when the angular speed of the crank is lower than the desired speed, i.e. assistance is required, and at the same time if the angular speed of the flywheel is higher than that of the crank, i.e. the flywheel has the potential to assist, the engagement should take place to assist and speed up the movement. The flywheel engagement decision process is implemented using fuzzy logic, Sugeno type, controller of two inputs and one output, as in Figure 4.18. The reason for using FLC, instead of Boolean logic, is that the decision mechanism using fuzzy logic produces a range of crisp values between 0 and 1 at the output, rather than either 0 or 1 using Boolean logic, which can be utilized, using a threshold, to reduce the engagement frequency of the flywheel with close performance.
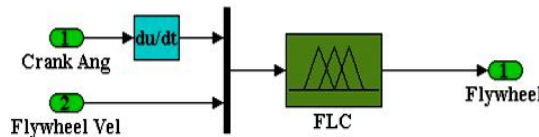
Figure 4.18: Flywheel engagement mechanism

The two FLC inputs are fuzzified by a fuzzy set of four variables, namely; VerySlow, Slow, Fast and VeryFast, defined by modified Gaussian membership functions, as shown in Figure 4.19. The output resulting from the fired fuzzy rules is changed to crisp value, between zero and one, by the weighted average defuzzification method. The output is converted to either zero or one, to activate/deactivate the clutch, with the aid of a threshold. The sixteen fuzzy rules base used in this scenario is shown in Table 4.5.
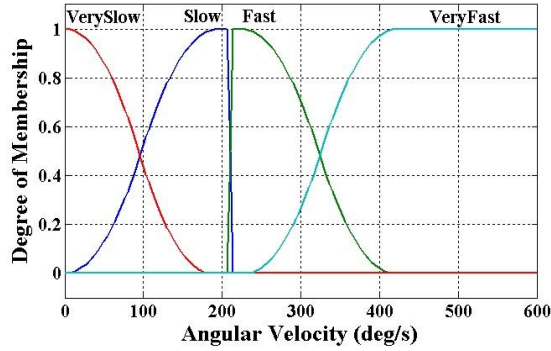
Figure 4.19: Inputs membership functions of the flywheel engagement mechanism

Table 4.5: Fuzzy rules used for the flywheel engagement mechanism

Crank Vel / Fly Vel	Very Slow	Slow	Fast	Very Fast
Very Slow	Off	Off	On	On
Slow	On	Off	On	On
Fast	On	On	Off	On
Very Fast	On	On	Off	Off

4.5.2.1 Results

The results of this scenario can be seen in Figures 4.20-4.22. It can be noticed from Figures 4.20 and 4.21 that initially the tracking error was large. However, the flywheel mechanism was successful in suppressing the fluctuation in the cadence and reducing the error by absorbing/supplying energy from/to the crank when necessary, as shown in Figure 4.22. The large tracking error appearing at the beginning is due to the fact that the flywheel mechanism is activated after the first two seconds, although it can be activated earlier, in order to recognize the effect of the flywheel mechanism, before and after activation, on the cycling cadence. The mean square error in cadence obtained from this scenario, after the activation of the mechanism, was 0.38 rad/s, while the engagement frequency of the flywheel was 6.25 Hz, as in Figure 4.23.

Also, it is obvious from Figures 4.24 and 4.25 that the stimulation intensity on both legs was reduced by almost 20% as compared with that in Scenario I. The average stimulation intensity on both legs in this scenario was approximately 178μs while in scenario I was 223μs per cycle. This is due to the fact that the stimulation in Resist

phase, that appeared in Scenario I, is replaced by the resistance produced by the flywheel mechanism and the muscle is stimulated only once per cycle. This leads to delay in the appearance of muscle fatigue and hence prolongs the exercise.
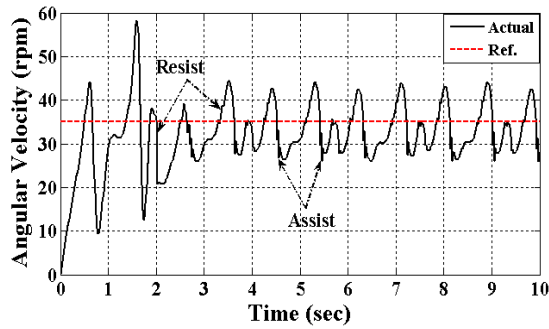
Figure 4.20: Angular velocity of the crank (Scenario II)
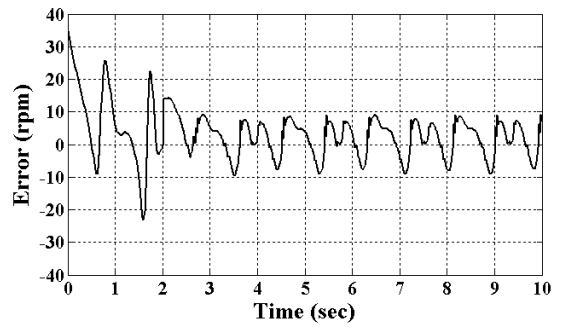
Figure 4.21: Error in crank cadence (Scenario II)
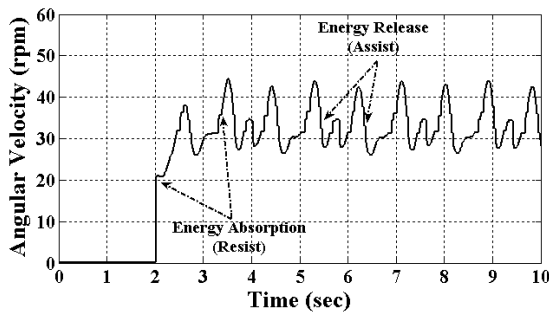
Figure 4.22: Angular velocity of the flywheel (Scenario II)
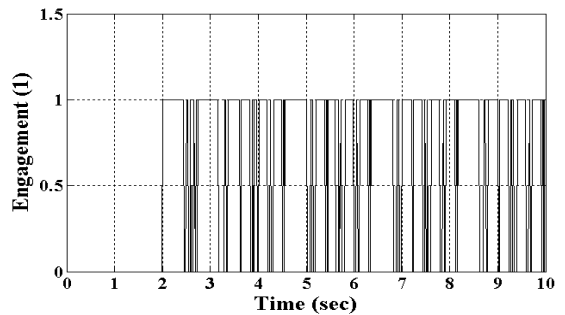
Figure 4.23: Flywheel engagement periods (Scenario II)
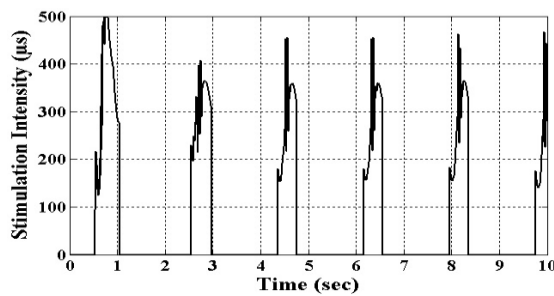
Figure 4.24: Stimulation intensity of left leg (Scenario II)
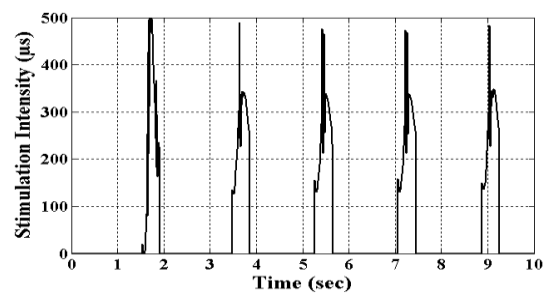
Figure 4.25: Stimulation intensity of right leg (Scenario II)

The results of this scenario are encouraging; however, the error in cadence is still high. The performance can be enhanced by improving the assistance and resistance

provided by the flywheel mechanism. This can be obtained by optimizing the gear ratio between the flywheel and the crank. Also, further improvement can be achieved through optimizing the crank position of the bicycle with respect to hip joint, the controller parameters as well as the stimulation patterns. This is explored in chapter five.

4.6 Summary

A quadriceps muscle model, on the basis of a nonlinear physiological based muscle model, has been built and tested. The muscle model comprises of three main parts; muscle activation, muscle contraction and body segmental dynamics. It takes into consideration the effect of muscle fatigue through the use of muscle fitness function as well as the force-length and force-velocity properties. Also, a phenomenological model of skeletal muscle energy expenditure proposed by Umberger et al. (2003) is introduced to be used, in subsequent chapters, to estimate the energy expended by the quadriceps in different FES-cycling scenarios.

FLC has been used to control the stimulation intensity on the quadriceps, in a cadence control approach, in an attempt to obtain 35rpm cycling cadence. Controlling the cycling cadence by stimulating the quadriceps only, without using any assist mechanism, is difficult to achieve due to the effect of the dead spots that cause rapid changes in the angular velocity of the crank. In addition to large cadence error, using the approach proposed by Massoud (2007) leads to premature termination of the exercise due to successive and increased stimulation on the muscle.

The flywheel and electrical clutch mechanism has been used in a cadence control approach to provide the necessary assistance and resistance. The engagement of the flywheel by the clutch, controlled using FLC approach, depends on the angular velocities of both the crank and the flywheel. The results show that FES-cycling with the aid of the flywheel mechanism produced superior results in terms of reducing the

stimulation intensity (178μs) by approximately 20% as compared with that without assist mechanism (223μs). It can be concluded that the new assist mechanism promotes prolonged FES-cycling exercise.

Although the cadence obtained using the flywheel mechanism is close to the desired, the results can be further improved by improving the assistance and resistance of the flywheel mechanism. This can be achieved by optimizing the gear ratio between the flywheel and the crank. Also, optimizing the crank position, controllers' parameters as well as the stimulation periods is expected to further improve the performance. The optimization process will be achieved in subsequent chapters.

Chapter 5: Flywheel mechanism and crank position optimization

5.1 Introduction

Optimizing the parameters of the design can significantly improve the outcome of the exercise and enable SCI individuals to exercise efficiently. Improving the performance of the exercise depends on the pedalling target such as steady cadence cycling or longer pedalling time (Massoud, 2007). Steady cadence cycling is important for studies investigating the therapeutic benefits in specific cycling speed (Hunt et al., 2001). Also, exercising by FES-cycling for a long time, minimum 30 minutes, is essential to obtain cardiovascular related benefits in SCI individuals (Idso, 2004). However, stimulating the muscle for long periods may lead to premature termination of the exercise due to muscle fatigue. Increasing the efficiency of the exercise, by maximizing the output power and minimizing the energy expenditure of the muscle, at a specific cadence is necessary to prolong the exercise session and achieve the desired benefits.

Several ways can be used to improve the FES-cycling performance, such as changing the stimulation parameters, the seat position, optimizing the stimulation patterns, the pedalling rate and the mechanical design of the ergometer (Massoud, 2007). Schutte et al. (1993) proposed two strategies to improve the FES-cycling performance; one strategy is to increase the number of SCI who can pedal by decreasing the stimulation intensity on the muscle and the other to increase the cardiovascular exercise achieved. Increasing the number of SCI who can pedal can be achieved by individualizing the seat configuration and the stimulation patterns to minimize the strength required for pedalling and the stimulation intensity on the muscle. On the other hand, increasing the cardiovascular exercise can be obtained through increasing the stimulation period, optimizing the target cadence, moving the seat closer to the crank and tilting the entire ergometer (Schutte et al., 1993). Gföhler

and Lugnar, (2000) improved the performance through optimizing the stimulation patterns using electrically stimulated muscle. The stimulation patterns obtained were based on maximizing the average drive power on the crank with minimum muscle force.

The use of assist mechanisms to improve the performance in FES activities is also reported in the literature (Gharooni et al., 2007; Hussain, 2009; Massoud, 2012). By optimizing the crank position and the parameters of a spring orthosis, Massoud (2007) enhanced the FES-cycling performance and obtained the optimal stimulation patterns for minimum cadence error, maximum power and minimum muscle stimulation.

The flywheel, as energy storage element, has been widely used in commercial FES-cycling ergometers, such as ERGYS, to assist the leg, smoothen the pedalling movement and reduce the effect of rapid changes in speed that occur at the dead spots. The flywheel parameters, such as size, weight and velocity, affect the amount of kinetic energy the flywheel absorbs and releases (Östergård, 2011). Increasing the size of the flywheel augments its ability to store more kinetic energy. However, the size of the flywheel is always limited by several factors such as size and cost of the design. For this reason, the use of a suitable gear ratio between the crank and the flywheel is necessary to obtain mechanical advantages, increase the flywheel speed, and enhance the performance of the flywheel mechanism.

In normal cycling, the gear ratio plays an effective role in changing the crank inertial load of the bicycle (Fregly et al., 2000). To maintain a specific pedalling rate and work rate, the cyclists usually use high gear ratios, between the crank and the rear wheel, during uphill cycling and low gear ratios during horizontal cycling (Hansen et al., 2002). In FES-cycling, the use of gears between the crank and the wheel is reported to change the inertial load of the bicycle to reduce the required driving force and enable the disabled of weak muscles to pedal (Pons et al., 1989) and also to provide braking effect when the pedalling speed exceeds the desired limit (Perkins et

al., 2002). Gearing, in form of different rim sizes, is also used to provide mechanical advantages for disabled individuals in hand propelled manual wheelchairs for both racing and rehabilitation purposes (Van Der Woude et al., 2006).

Altering the gear ratio between the flywheel and the crank leads to change the effective inertia of the flywheel, i.e. equivalent to use different flywheels of different inertia. To the author's knowledge, an investigation on the effect of different gear ratios on the performance of the newly proposed assist mechanism and its impact on the overall FES-cycling performance has not been reported. In the previous chapters, the use of the flywheel assist mechanism was shown to reduce the stimulation intensity on the quadriceps in FES-cycling exercise. However, the cadence error was still high. In this chapter, to improve the FES-cycling performance by minimizing the cadence error and maximizing the efficiency, i.e. minimum energy expenditure and maximum output power, different design parameters are tested. These parameters include the gear ratio between the flywheel and the crank, and the crank position with respect to hip joint.

5.2   Cycling power output

Cycling power is an indicator used by the cyclists to provide them with instantaneous feedback about their output and to measure their performance. Most cycling ergometers are equipped with strain gages to measure the torque applied by the rider and calculate the cycling power by multiplying the torque with the angular velocity of the crank. Certain newer devices use handlebar-mounted apparatus to measure the opposing forces, such as gravity; inertia; rolling and wind resistance, together with the velocity to calculate the rider's work rate, or cycling power output (Cyclingpower, 2014).

The work, measured in Joule, is the result of force acting on an object causing a displacement, in the direction of motion, and in some cases hindering the motion. The

power, measured in Watt or Joule per second, is equivalent to the amount of energy consumed per time. Since the energy transfer can be used to do work, the power is also expressed as the rate at which the work is performed (Semat and Katz, 1958), as:

$$P = \frac{dW}{dt} = T.\omega \qquad \qquad \textbf{(5.1)}$$

where P is the power [w], T is the torque [N.m], which can be calculated from the measured pedalling force F [N] multiplied by the crank arm length L [m], and ω is the angular velocity [rad/sec] of the crank.

Several researchers have used the above equation to calculate the cycling output power (Gföhler and Lugnar, 2000; Hunt et al., 2004; Hunt et al., 2012; stone, 2005); In this work, since Visual Nastran (vN4D) software only provides the bending torque at joint's level, rather than the driving torque that causes the movement, the driving torque at the crank is calculated by:

$$T = I.\alpha \qquad \qquad \textbf{(5.2)}$$

where I is the moment of inertia [kg. m^2] and α is the acceleration [rad/sec^2] of the crank.

Practically, the inertia of a cycling ergometer, equipped with a fixed flywheel, is calculated by accelerating the flywheel at constant rate by different resistive loads. The angular acceleration is proportional to the measured resistive torque of the flywheel. The moment of inertia is calculated as the mean of the proportional constant value resulting from dividing the resistive torque of the flywheel by the resultant angular acceleration at different loads (Hibi, 1996). However, in this study, a different approach is used due to the use of Visual Nastran (vN4D) simulation software as in (Massoud, 2007). A constant resistive torque (0.04 N.m) is applied to the crank and the gravity effect is removed. At the start of each movement, the velocities of each part of

the bicycle and the humanoid are set to zero. Since the inertia of the bicycle and the humanoid changes at different crank angles, the movement is allowed for one crank angle each time and the resultant crank acceleration (α) is recorded. The inertia (*I*) of the bicycle and the humanoid is calculated, as in Appendix B, for each crank angle using:

$$I = \frac{0.04}{\alpha} \tag{5.3}$$

To measure and study the effect of continuously engaging/disengaging flywheel with the crank on the cycling performance, the instantaneous power of the flywheel is calculated during the engagement periods. The kinetic energy and the inertia of a solid disk flywheel are given as:

$$E_k = \frac{1}{2}I\omega^2 \tag{5.4}$$

$$I_f = \frac{1}{2}mr^2 \tag{5.5}$$

where, E_k is the rotational kinetic energy [J], I_f is the inertia of the flywheel about the rotating axis [kg.m²], ω is the angular velocity of the flywheel [rad/s], m is the mass of the flywheel [kg], r is the radius of the flywheel [m].

As the work is a form of energy transfer (Giambattista, 2004), the power of the flywheel can be calculated as the derivative of flywheel's kinetic energy (E_k), with respect to time, as:

$$P_f = \frac{dW}{dt} = \frac{dE_k}{dt} = I_f.\alpha_f.\omega_f \tag{5.6}$$

where, P_f is the flywheel power [w], I_f is the inertia of the flywheel about the rotating axis [kg.m²], α_f is the angular acceleration of the flywheel [rad/s²] and ω_f is the angular velocity of the flywheel [rad/s]. The angular velocity and angular acceleration of the flywheel are obtained by two sensors at the bicycle model in vN4D software

The instantaneous power output for paraplegics, in FES-cycling exercise, is reported around 5-10W (Raymond et al., 2002; Theisen et al., 2002), while the power output for healthy people performing voluntary cycling exercise is approximately 43W (Raymond et al., 2002). The potential benefits of training by functional electrical stimulation for individuals with spinal cord injury (SCI) are limited due to the low obtainable power output that leads to low efficiency (Duffel, 2009).

5.3 Cycling efficiency

The mechanical, also known as metabolic (Hunt et al., 2012), efficiency of human performing submaximal exercise can be defined as the mechanical output work divided by the metabolic energy expenditure during the exercise (Whipp and Wasserman 1969). The performed mechanical work is the external work resulting from the application of force by the muscles through a distance (Ferrario, 2006). In case of cycling exercise, the work performed by lower limbs is usually calculated by multiplying the torque at the crank with the angular velocity of the crank (Hunt et al., 2012). The calculation of energy expenditure during the exercise depends on the rate of pulmonary oxygen uptake (VO2) (Ferrario, 2006; Stainbsy et al., 1980). Four widely accepted methods for calculating the efficiency of the exercise have been reported in the literature (Ferrario, 2006; Gaesser and Brooks, 1975; Hunt et al., 2012). The different efficiency calculation methods are characterised according to the base-line chosen to correct the loss of energy in the system. However, any of the definitions can be used as long as there is awareness of the limitations in the measurements (Massoud, 2007; Ferrario, 2006). These definitions are:

$$Gross\,Efficiency \;=\; \frac{Work\,accomplished}{Energy\exp ended}\,x100 \;=\; \frac{P^{out}}{P^{in}}\,x100 \qquad\qquad \textbf{(5.7)}$$

$$Net\,Efficiency \;=\; \frac{Work\,accomplished}{Energy\exp ended\,above\,that}\,x100 \;=\; \frac{P^{out}}{P^{in}-P^{r}}\,x100 \qquad \textbf{(5.8)}$$
$$at\,rest$$

$$Work\,Efficiency \;=\; \frac{Work\,accomplished}{Energy\exp ended\,above\,that}\,x100 \;=\; \frac{P^{out}}{P^{in}-P^{0}}\,x100 \qquad \textbf{(5.9)}$$
$$in\,cycling\,without\,a\,load$$

$$Delta\,Efficiency \;=\; \frac{Delta\,work\,accomplished}{Delta\,energy\exp ended}\,x100 \;=\; \frac{\varDelta P^{out}}{\varDelta P^{in}}\,x100 \qquad \textbf{(5.10)}$$

where P^{out} is the power output [W], P^{in} is the metabolic power [W], P^{r} is the resting metabolic power and P^{0} is the metabolic power at unloaded exercise. The Gross efficiency takes into consideration the entire energy expended by the subject to perform the exercise. The Net efficiency excludes the energy required by the body at steady-state resting condition from the entire energy. The Work efficiency excludes the energy required to move the legs during unloaded cycling, i.e. no external resistance is applied. The Delta efficiency is the ratio between increments in the output power to the corresponding increments in the rate of energy expenditure due to the increase in oxygen uptake (VO2).

In this work, the efficiency definition utilized is the Gross efficiency. Also, to estimate the energy expenditure in FES-cycling exercise and calculate the efficiency of the exercise in simulation platform, the energy expenditure model proposed by Umberger et al. (2003), described in detail in chapter four, is used.

A research reported in (Glaser, 1989) shows that the efficiency of FES-cycling for people with spinal cord injury is lower than in voluntary cycling for healthy individuals. Twenty disabled (9 quadraplegics and 11 paraplegics) and twenty healthy

individuals participated in this study. It shows that the efficiency in FES-cycling of disabled people (2-14%) is approximately one-half of that in voluntary cycling of healthy subjects (4-34%). Similar results were obtained by (Raymond et al, 2002) in one of their researches. A group of six paraplegics, performed FES induced cycling exercise, with six healthy individuals performing voluntary cycling, using the same ergometer. The maximum output power sustained by able subjects was 42.8W while for the SCI subjects was 9.2W. For close metabolic expenditure, i.e. the oxygen uptake was 0.74 l/min and 0.75 l/min for able and SCI respectively, the net efficiency estimated from the exercise was 22% for healthy individuals and 5% for the disabled. Also, Theisen et al. (2002) reported that the efficiency of the exercise can significantly vary in prolonged, constant stimulation FES-cycling exercise. In a 40 minutes long isokinetic cycling exercise, the gross efficiency of five SCI participants increased from $3.3\pm1.1\%$ after the first 6 minutes to $4.7\pm1.2\%$ after 19.5 minutes and $4.2\pm1.5\%$ at the end of the exercise.

Further, the net efficiency of healthy individuals performing FES-cycling, after anaesthesia, is reported as in (Kjaer et al., 1994) to drop to 7% as compared to voluntary exercise, 22%, of the same group at a work rate consumed the same, 1.9 l/min, oxygen uptake. This shows that even with subjects of healthy muscles, the FES-cycling exercise is less efficient, by a factor of 3, than voluntary exercise. These results suggest that the main reason behind the low FES-cycling efficiency is the recruitment properties of the electrically stimulated muscle (Ferrario, 2006).

5.4   The gear ratios between the crank and the flywheel

In this part of the work, it is aimed to improve the cycling performance and reduce the cadence error through the use of a suitable gear ratio (R) between the flywheel and the crank of the bicycle. In the proposed assist mechanism, i.e. flywheel and electrical clutch, the gear ratio between the flywheel and the crank plays a significant role in specifying the amount of resist and assist produced by the mechanism during the

exercise. This is due to the fact that changing the gear ratio will change the effective/referred inertia of the flywheel. For this reason, to specify the best gear ratio for the exercise, 58 different gear ratios are tested. The gear ratio is specified through a gear constraint placed between the crank (shaft) of the bicycle and the flywheel in Visual Nastran (vN4D) software. A flywheel of 0.2m radius and 5Kg weight was used. Some gear ratios tested are greater than one, at which the gear of the flywheel is larger than the gear of the crank, and others are smaller than one. The inertia of the flywheel was calculated according to equation (5.5). The effective/referred inertia of the flywheel with respect to the input using different gear ratios, derived in Appendix A, is calculated as:

$$J_{flywheel\ effective} = \frac{J_{flywheel}}{hR^2} \quad\quad\quad (5.11)$$

where $J_{flywheel}$ is the inertia of the flywheel, h is the efficiency factor of the gearbox, R is the gear ratio. The results obtained in this work are based on the assumption of using a frictionless gearbox with efficiency factor (h) equal to 1.

5.4.1 The control approach

The control approach used in this part is the cadence control with assist mechanism. Two fuzzy controllers, one for each leg, are used to regulate the stimulation intensity of FES signal on the legs. The error, i.e. the difference between the actual and the desired cadence, and the change of error are used as inputs of the controllers. The output of each controller, after multiplied by a scaling factor, is added to a constant of a reference pulse width value. The periods of stimulation, i.e. the stimulation phases, for each leg are specified by logic gates as explained in chapter four.

The flywheel engagement mechanism is implemented through a closed-loop approach that takes into consideration the actual angular velocities of the crank and the flywheel as well as the desired reference cadence. When the angular velocity of the flywheel is smaller than that of the crank implies that the flywheel has the potential to resist the movement in case the angular velocity of the crank is greater than the desired velocity. Hence in this case, the mechanism engages the flywheel to resist and slows down the motion. Also, if the angular velocity of the flywheel is greater than that of the crank, it implies that the flywheel has the potential to assist and speed up the cycling movement in case the angular velocity of the crank is smaller than the desired cadence. In this case, the mechanism engages the flywheel to speed up the movement and assist the legs. The engagement mechanism is implemented using Boolean logic as explained in detail in chapter three.

5.4.2 The effect of gear ratio on the cycling performance

To determine the effect of different gear ratios on the cycling performance, the performance of sample gear ratios, greater and less than one, between the flywheel and the crank is studied and the performance is analysed.

5.4.2.1 Two-to-one gear ratio (R=2)

In this scenario, the gear ratio is set to two-to-one, i.e. $R = 2$, between the crank and the flywheel. The results of the simulation can be seen in Figures 5.1-5.4. It can be noticed from Figure 5.6 that the error in the cadence, approximately ± 18 rpm, was very high. Also, the angular velocity of the flywheel, Figure 5.2, was under 30 rpm. The reason behind this is that at this gear ratio if the crank rotates two complete cycles, the flywheel will rotate only one complete cycle. For this reason, the flywheel will absorb little amount of energy from the crank during the Resist phase, Figure 5.4, that leads to relatively small resistance by the flywheel to the motion, i.e. small effective inertia of

the flywheel with respect to the input, and consequently slow unable-to-assist flywheel, as in Figures 5.2 and 5.3.
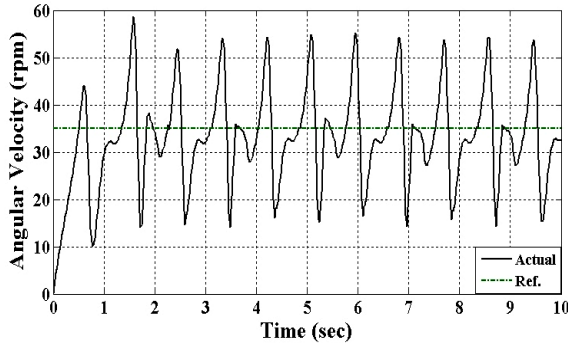
Figure 5.1: The angular velocity of the crank
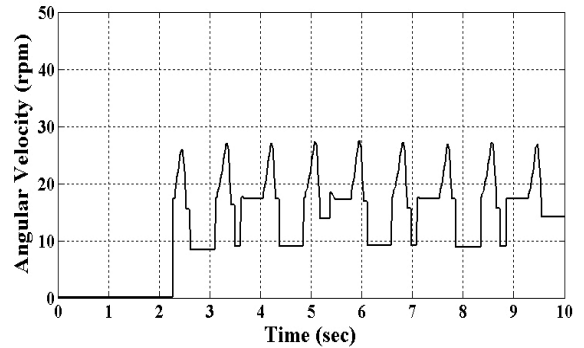
Figure 5.2: The angular velocity of the flywheel
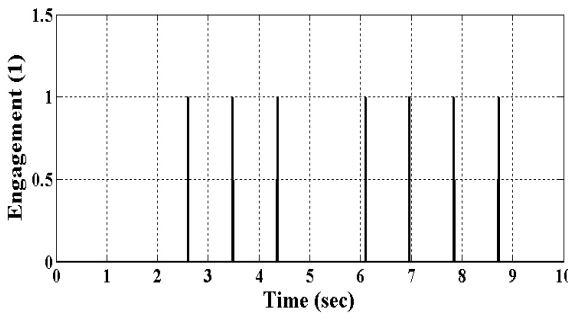
Figure 5.3: Flywheel engagement during assist phase
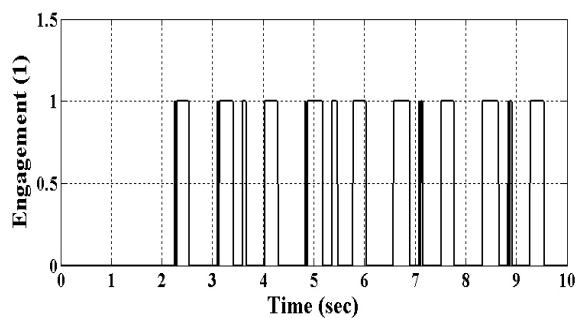
Figure 5.4: Flywheel engagement during resist phase

5.4.2.2 Two-to-one gear ratio with flywheel angular velocity scaling factor

In this scenario, similar to section 5.4.2.1, a two-to-one gear ratio, i.e. *R*=2, between the crank and the flywheel is used. The only difference is that a scaling factor is used to scale the angular velocity of the flywheel at the input level of the engagement mechanism. In section 5.4.2.1, the angular velocity of the flywheel was low due to the gear ratio used that led to very short assist periods and insufficient resist. Since the decision of the engagement mechanism depends on the angular velocity of the flywheel and the crank, a scaling factor is used to multiply the flywheel's angular velocity by two, i.e. the same as the value of the gear ratio, at the input level of the decision mechanism. The results of this scenario can be seen in Figures 5.5-5.8. It is clear from Figure 5.6 that the angular velocity of the flywheel was doubled due to the

120

scaling factor (FAVSF). Due to this scaling factor that makes the actual angular velocity of the flywheel, at the decision level of the engagement mechanism, seems close to the angular velocity of the crank, the mechanism was able to engage/disengage the flywheel continuously during the assist and resist phases, as in Figures 5.7 and 5.13. However, the cadence error remained very high. This is due to the fact that the energy absorbed by the flywheel during the resist phase was very small using this gear ratio. Hence, although the decision of the engagement/disengagement was improved by the use of FAVSF, the effect of the flywheel on the crank, in both assist and resist phases, was very small, i.e. small effective inertia of the flywheel. Finally, it can be concluded that two-to-one gear ratio, with and without FAVSF, has a slight effect on the cycling performance from cadence improvement point of view.
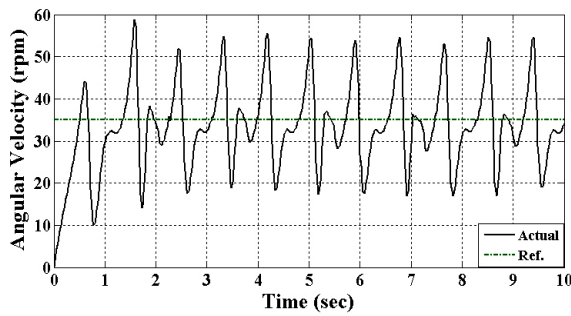
Figure 5.5: The angular velocity of the crank
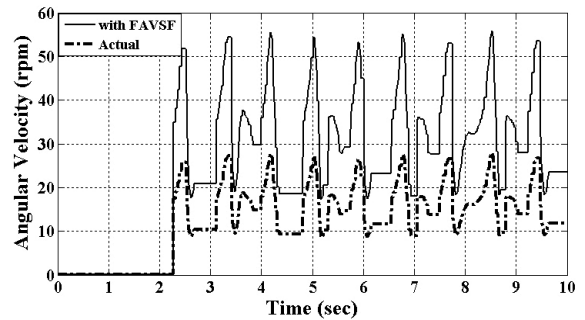
Figure 5.6: The angular velocity of the flywheel with and without FAVSF
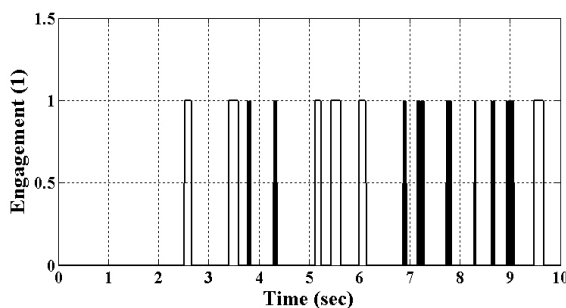
Figure 5.7: Flywheel engagement during assist phase
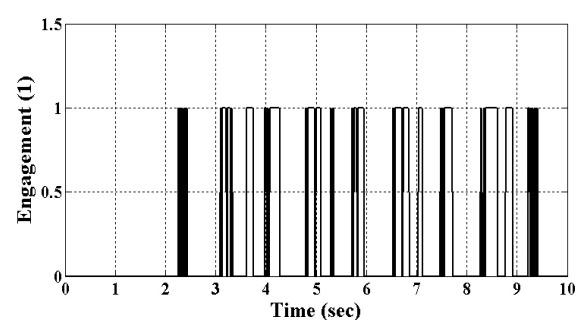
Figure 5.8: Flywheel engagement during resist phase

5.4.2.3 One-to-two gear ratio (R=0.5)

In this scenario, the gear ratio is set to one-to-two, i.e. $R= 0.5$, between the crank and the flywheel. With this gear ratio, if the crank rotates one complete cycle, the flywheel

121

will rotate two complete cycles, i.e. the flywheel will rotate twice the speed of the crank. The simulation results obtained can be seen in Figures 5.9-5.12. It is clear from Figure 5.9 that the error in cadence, approximately -5 to +15 rpm, decreased as compared with previous scenarios. Also, it can be noticed that the flywheel's angular velocity was continuously high, as in Figure 5.10, and the flywheel engagement mechanism engaged the flywheel to assist the motion continuously after the first resist action took place, Figures 5.11 and 5.12. The reason behind this is that using this gear ratio the effective inertia of the flywheel becomes large that leads to high resistance to the motion at the first engagement. As the flywheel rotates twice the speed of the crank, the actual speed of the flywheel becomes high. Since the flywheel's engagement mechanism, which is activated after 2 seconds, depends on the angular velocity of the flywheel and the crank, the mechanism engages the flywheel to resist the motion, as in Figure 5.12, only at the start of the mechanism as the actual flywheel's speed is less than that of the crank. At the moment of this resist action, the speed of the crank is dropped significantly, as shown in Figure 5.9 and Figure 5.12, while the speed of the flywheel has increased to twice of that of the crank, as in Figure 5.10. Since the speed of the flywheel is higher than that of the crank, the mechanism realizes that the flywheel has the potential to assist and will engage the flywheel to assist the cycling as the speed of the crank drops below the desired speed. This explains the reason behind the successive assistance of the mechanism, as in Figure 5.11.

Finally, the one-to-two gear ratio (R=0.5) was able to assist the cycling and has the potential to resist, i.e. retard, the motion due to the resultant high effective inertia of the flywheel. However, with this configuration, it fails to produce the required resist action. For this reason, a flywheel angular velocity scaling factor (FAVSF) will be tested in the next section.
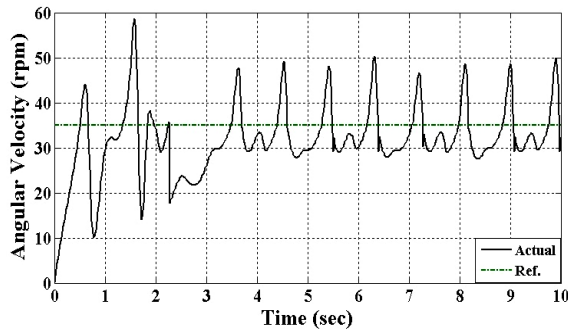
Figure 5.9: The angular velocity of the crank
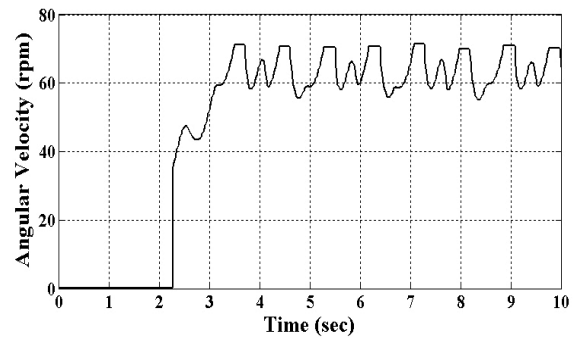
Figure 5.10: The angular velocity of the flywheel
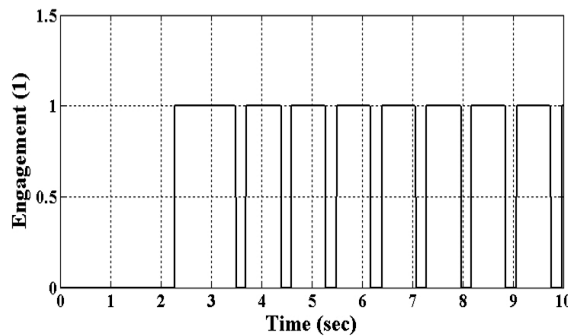
Figure 5.11: Flywheel engagement during assist phase
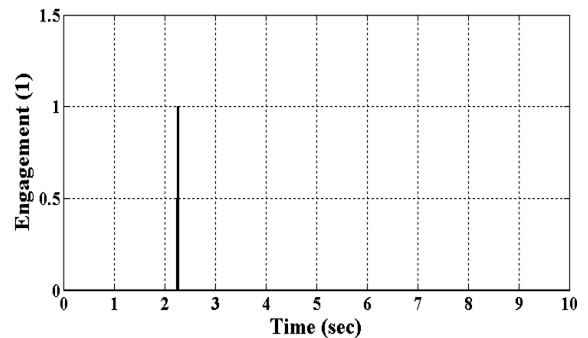
Figure 5.12: Flywheel engagement during resist phase

5.4.2.4 One-to-two gear ratio with flywheel angular velocity scaling factor

In this scenario, the same gear ratio used previously in section 5.4.2.3 is used with the addition of the FAVSF to scale the angular velocity of the flywheel at the input level of the engagement mechanism. As previously mentioned, using this gear ratio leads to rotate the flywheel twice the speed of the crank. For this reason the FAVSF is set to 0.5, i.e. the same as the gear ratio, to scale down the speed of the flywheel at the decision making level. This allows the engagement of the flywheel, when resist is required, to absorb energy from the crank and retard the motion. The simulation results obtained of this scenario can be seen in Figures 5.13-5.16. It can be noticed in Figure 5.13 that the error in cadence is improved, approximately ±5 rpm after the first 4 seconds, as compared with that without FAVSF. The reason behind this improvement is that by using the FAVSF the effective flywheel speed with respect to the input of the

123

gearbox was taken in consideration and compared with that of the crank which led to correct and effective assistance and resistance actions by the mechanism as in Figure 5.15 and Figure 5.16.

Finally, it can be concluded that the use of a one-to-two gear ratio with a FAVSF, of a value equal to the gear ratio, is more effective in reducing the cadence error than the previous scenarios. Also, this might imply that other Small-to-Big gear ratios between the crank and the flywheel with FAVSF, equal to the gear ratio, may lead to better results than those obtained in this section. For this reason, further investigations, with different gear ratios and FAVSF, are required to obtain the optimal performance.
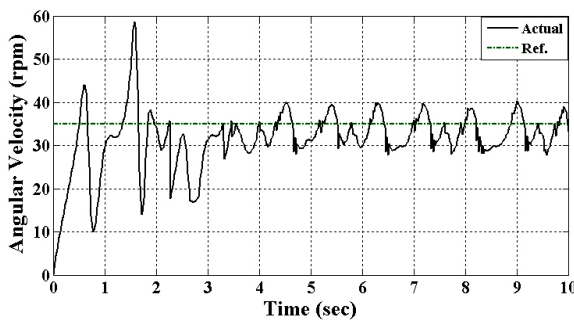
Figure 5.13: The angular velocity of the crank
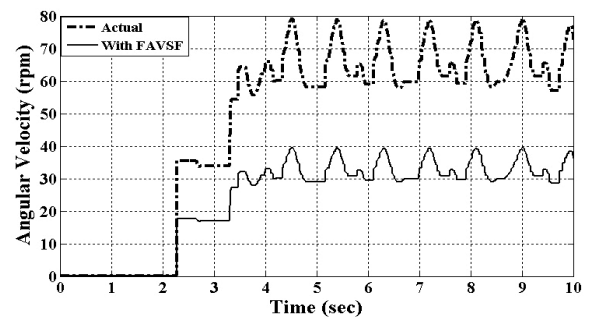
Figure 5.14: The angular velocity of the flywheel with and without FAVSF
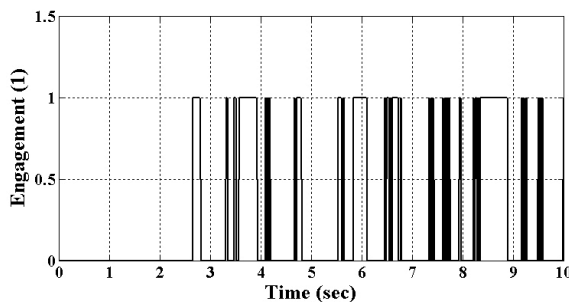
Figure 5.15: Flywheel engagement during assist phase
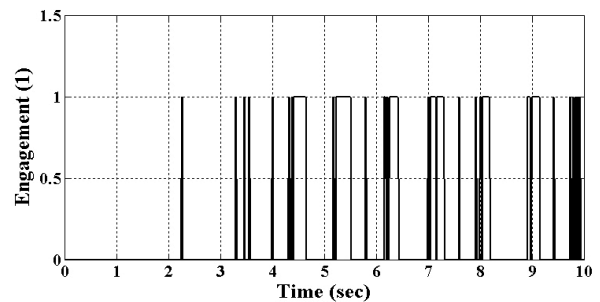
Figure 5.16: Flywheel engagement during resist phase

5.4.3 Different gear ratios with flywheel angular velocity scaling factor

In order to be able to specify the optimal gear ratio and the best flywheel angular velocity scaling factor (FAVSF) for the design different 58 gear ratios, ranging from 0.33 to 3, between the flywheel and the crank are tested. For a disk flywheel of 5Kg

weight and 0.2m radius, the effective inertia of the flywheel, using gear ratios greater than one, is smaller than 0.1 [Kg.m^2], while with gear ratios smaller than one the effective inertia of the flywheel is greater than 0.1 [Kg.m^2].

The test is performed with the use of a FAVSF at the input level of the engagement mechanism, to scale down the actual angular velocity of the flywheel with gear ratios smaller than one and scale up the actual angular velocity of the flywheel with gear ratios greater than one. The value of the FAVSF used is equal to the value of the employed gear ratio. The results of this test can be seen in Figures 5.17-5.20. All the results obtained are recorded for a period of 10 seconds for each gear ratio.

It is clear from Figure 5.17 that the highest error in cadence appeared at the lowest effective flywheel inertia, 0.011[Kg.m^2], i.e. gear ratio equal to three. Also, it is clear that the error decreases as the effective inertia increases, i.e. with the decrease of the gear ratio, and then starts to increase again after effective inertia equal to 0.625 [Kg.m^2], i.e. gear ratio equal to 0.4. The minimum percentage error obtained was 0.1542 at effective flywheel inertia equal to 0.506 [Kg.m^2], i.e. at gear ratio 0.44. This shows an improvement, approximately 11%, in the overall cadence error as compared with that, 0.1742, of the same test performed without FAVSF.
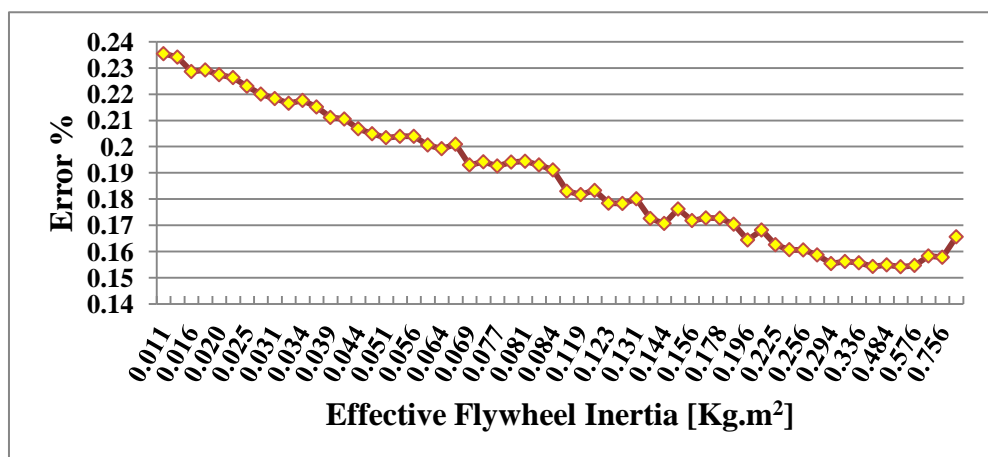
Figure 5.17: Error percentage in cadence at different effective flywheel inertia with FAVSF

From Figure 5.18, it is clear that the average cycling efficiency ranged between 6.1% and 9.5%. Also, it can be noticed that the cycling efficiency decreased with the increase in the effective flywheel inertia, i.e. decrease in the gear ratio. This is due to the fact that the cycling power has slightly dropped due to the increase in the resistance to motion with the decrease of the gear ratio.
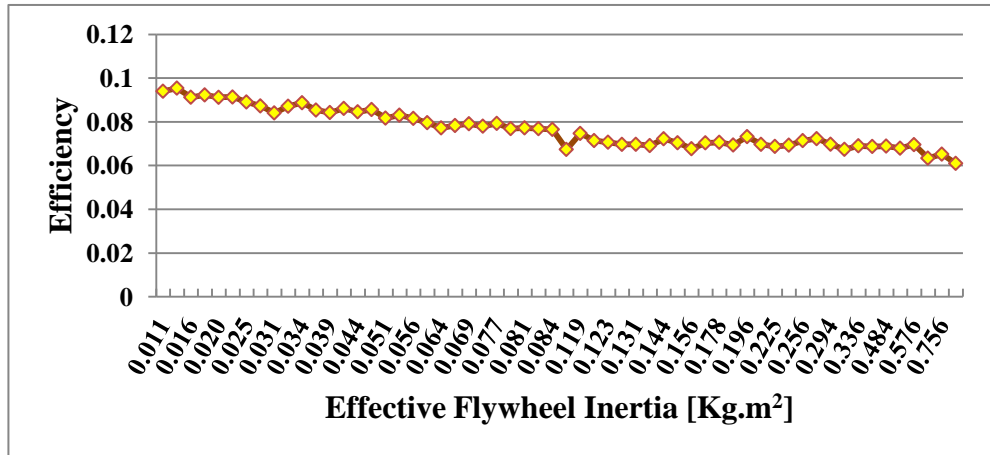
Figure 5.18: Cycling efficiency at different effective flywheel inertia with FAVSF

Figure 5.19 shows the engagement frequency of the flywheel. The engagement frequency is relatively high with all inertia values, ranged between 5.5Hz and 9Hz. This is due to the fact that the engagement mechanism has worked properly with all gear ratios by continuously engaging/disengaging the flywheel when assist and resist actions are required. However, this is considered as a disadvantage from hardware implementation point of view as this performance requires a highly sensitive, durable electrical clutch to cope with considerably highly frequent engagements.
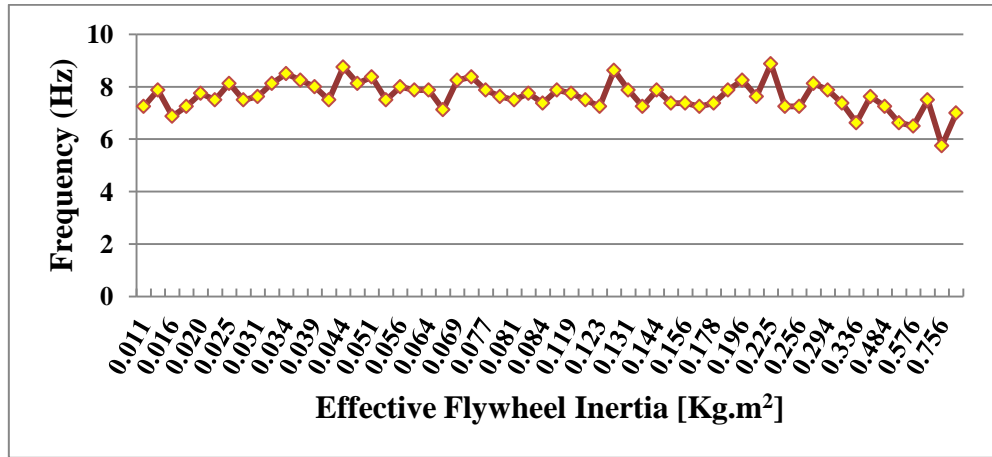
Figure 5.19: Flywheel engagement frequency at different effective flywheel inertia with FAVSF

The average power of the flywheel, measured during flywheel's engagement periods only, was negative especially at high flywheel inertia values i.e. gear ratios smaller than one, as shown in Figure 5.20. This implies that the flywheel mechanism, on average, has played an assistive, rather than resistive, role to the motion.
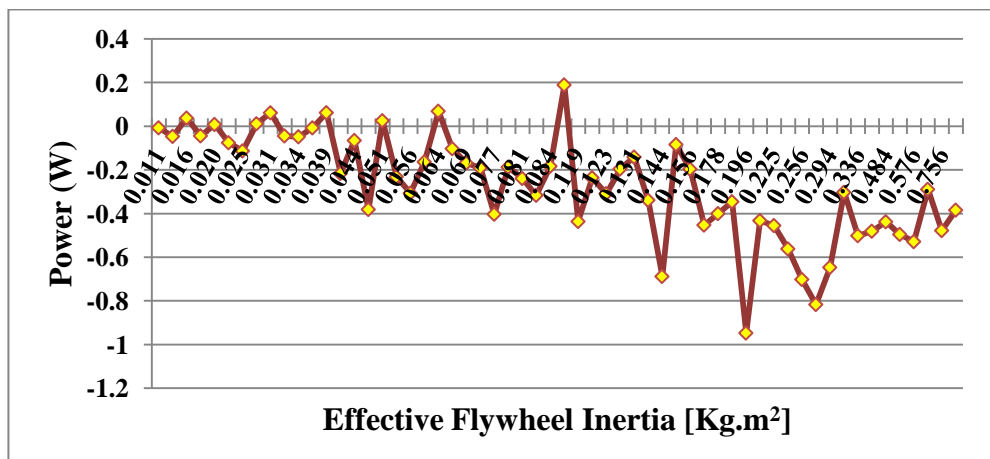
Figure 5.20: Average power of the flywheel at different effective flywheel inertia with FAVSF

Finally, it can be concluded that using the FAVSF is important to decrease the overall cadence error; however, the flywheel engagement frequency is high. Although, the minimum error percentage obtained was 0.1542, at gear ratio and FAVSF, equal to 0.44, i.e. effective flywheel inertia equal to 0.506 [Kg.m^2], changing the crank position

127

may improve the results further. Also, using fuzzy logic approach to control the flywheel engagement process, as explained previously in chapter four, is an attractive option to be considered to decrease the engagement frequency of the flywheel mechanism.

5.5   Optimizing the crank position of the bicycle

In this part of the work it is aimed to find out the best crank position of the bicycle, without using any assist mechanism, with respect to the hip joint of the individual to obtain the best cycling performance in terms of minimum cadence error with minimum stimulation intensity on the muscle without using any assist mechanism.

To achieve these objectives, 25 positions are tested and analyzed. These positions represented by 5 different horizontal positions with 5 different vertical positions for each horizontal position. The horizontal positions are ranged from 0.6m to 0.8m, i.e. the distance between the centre of the crank and the hip joint, with 0.05m increment. While, the vertical positions of each horizontal position are ranged from -0.1m to 0.1m with 0.05m increments. An illustration can be seen in Figure 5.21. The positions are represented as a matrix of black dot points.
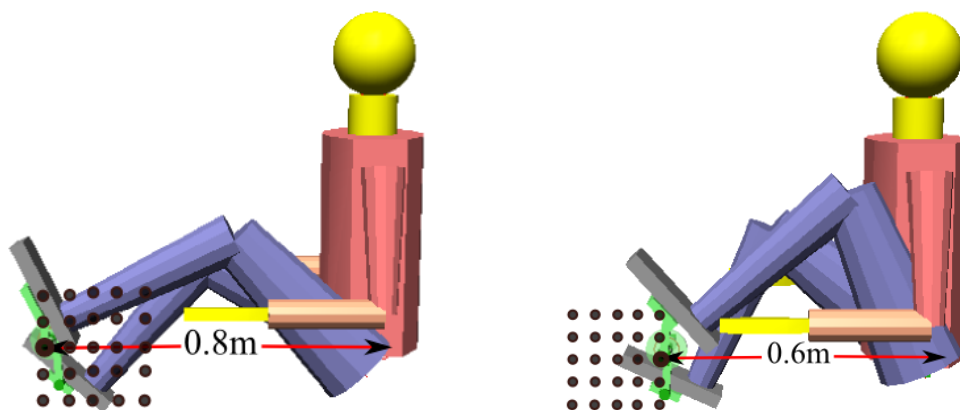
Figure 5.21: Illustration of the 25 positions tested to obtain the best performance

Since the software used to model the humanoid and bicycle model, i.e. vN4D software, does not allow any modifications of the design dimensions to take place dynamically, each position is tested separately. The results of the 25 positions are recorded and the overall performance is analysed.

5.5.1 The control approach

In this part of the research, since one of the objectives is to minimize the error in the cadence, cadence control method is used. Four fuzzy logic controllers (FLC), two for each leg, are used to regulate the stimulation intensity on the quadriceps muscle. Since it is aimed to achieve the cycling exercise by stimulating the quadriceps only, extension action can be obtained from stimulating this muscle. For this reason, in order to govern the speed of the cycling, the quadriceps muscle is stimulated twice per cycle; once to speeding up the movement, and other in opposite and retarding the movement when necessary.

As the amount of assist may differ from the amount of resist required, two different FLC are used for each leg. Each controller has two inputs, the error and the change of error. The error represents the difference between the reference, 35rpm, and the actual cadence. The reference is chosen to be 35 rpm as this speed is the minimum speed in rehabilitation centres and widely used in rehabilitation centres. The boundaries of FLC's output are limited by a saturation block to specify the maximum and minimum negative and positive action of each controller. The output of each FLC is multiplied by a scaling factor then added to a constant value that represents a predefined reference pulse width. The resultant value is applied to the muscle as a stimulation pulse width. The stimulation phases, for both resist and push phases, required for each leg are obtained heuristically according to the crank angle. Detailed information about this control method can be found in chapter four. It is important to mention that the cycling at position 0.8m is unachievable for the currently used bicycle dimensions. This is due to the fact that 0.8m crank position becomes far from the hip

that makes the individual unable to pedal when using a 0.14m crank arm length (the one used in this design).

5.5.1.1 Results

The main objective of the tuning performed was to minimize the overall cadence error for each position. Figure 5.22 shows the best percentage error obtained at each position. It can be noticed that the percentage error in cadence at position 0.6m was high. This is due to the fact that at this position the pedalling movement is difficult to control because the thigh is too close to the trunk that makes one of the legs, which is closer to the trunk, resist the movement of the other. On the other hand, it can be seen that at position 0.75m the error in cadence is also large. This is due to the fact that at this far position from the hip the thigh is almost extended and the quadriceps muscle cannot produce significant torque during resist phase. For this reason, at 0.75m position the effect of the dead spots dominates and leads to large cadence error.

At positions 0.65m and 0.7m the error was almost the same for all vertical positions. This is due to the fact that these positions are moderate in distance from the hip that makes the control of pedalling movement much easier.

Figure 5.23 shows the average cycling efficiency calculated at different crank positions. It is obvious that the efficiency increases with the increase in the distance between the crank and the hip joint. Similar efficiency trend has been obtained in (Massoud, 2007) using different bicycle dimensions.
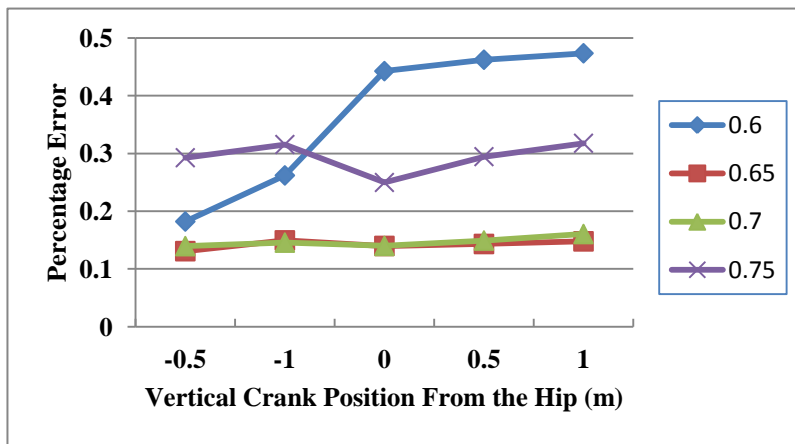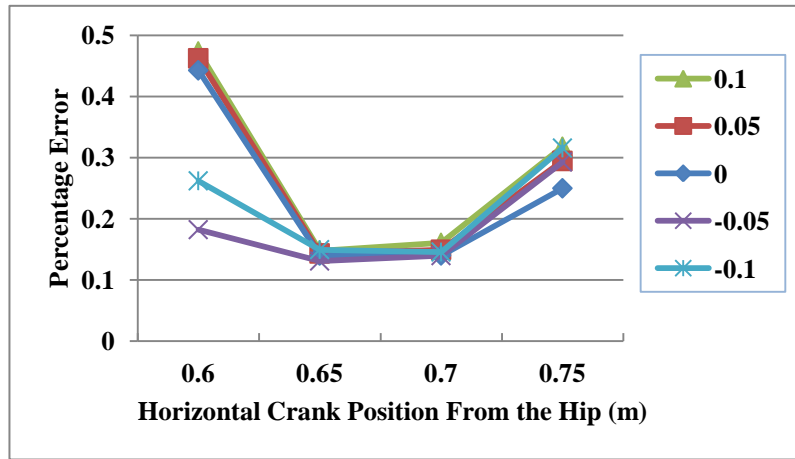
Figure 5.22: Percentage error in cadence at different crank positions
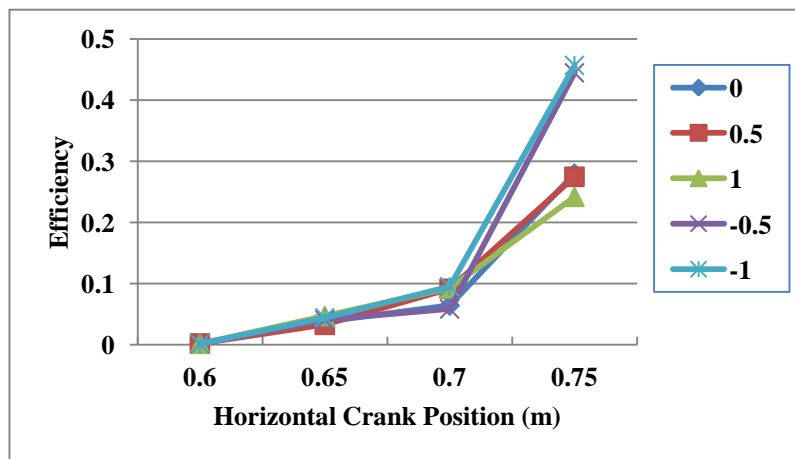
Figure 5.23: Cycling efficiency at different crank positions

Figures 5.24-5.27 show the stimulation phases, i.e. the duration, for both legs at different positions. the stimulation phases were determined heuristically to obtain minimum tracking error with 180° phase shift between the right and left phases. It can

be noticed that the minimum stimulatioin period appeared at position 0.7m with a total of 160° (Right Push:130°, Right Resist: 30°). However, the maximum stimulation period appeared at position 0.75m with a total of 220° (Right Push:120°, Right Resist: 100°) while at position 0.65m the total stimulation period was 190° (Right Push: 120°, Right Resist: 70°) and the same at position 0.6m (Right Push: 130° ,Right Resist: 60°).
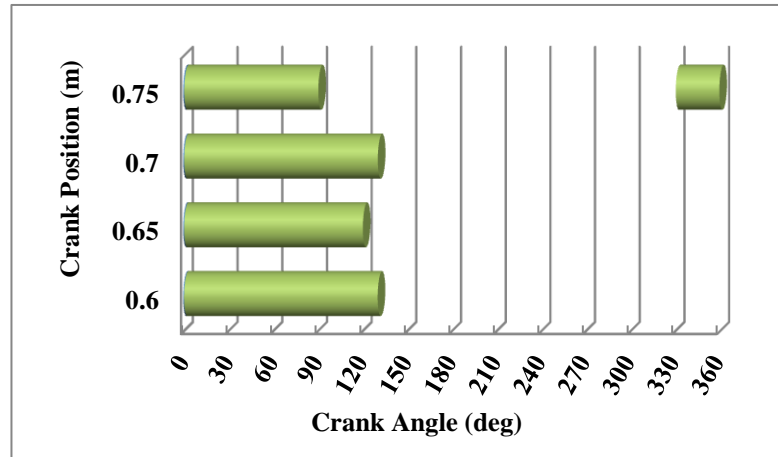
Figure 5.24: Right push phase according to crank angle for each horizontal crank position
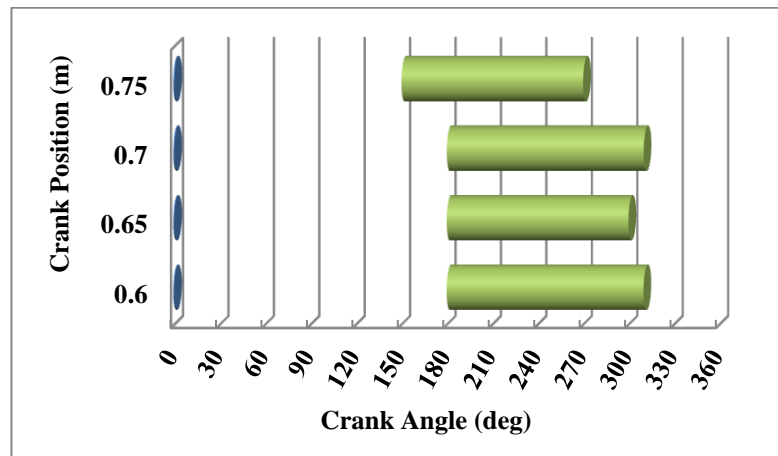
Figure 5.25: Left push phase according to crank angle for each horizontal crank position
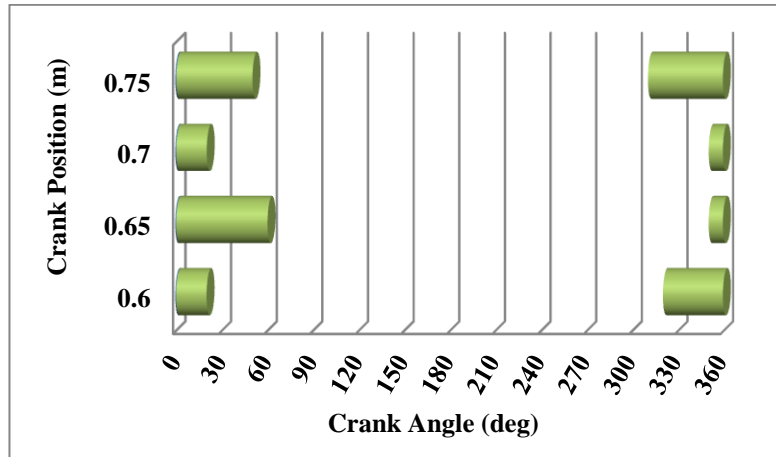
Figure 5.26: Right resist phase according to crank angle for each horizontal crank position
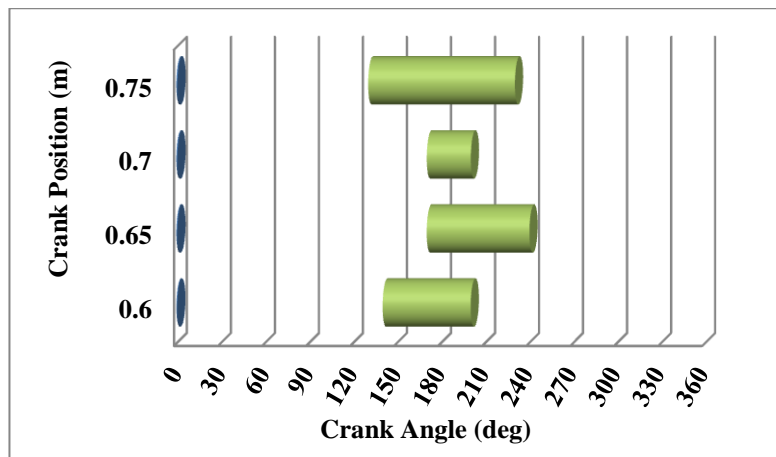
Figure 5.27: Left resist phase according to crank angle for each horizontal crank position

Table 5.1 shows some statistics about each position. It is clear that the minimum percentage error in cadence are bounded at positions (0.65, 0.0), (0.65, -0.5), (0.7, 0.0) and (0.7, -0.5) with minimum value at position (0.65, -0.5). However, the cycling efficiency at position (0.65, -0.5) is less than that at positions (0.7, 0.0) and (0.7, -0.5). Since the average stimulation intensity is lower at position (0.7, 0.0) and the total stimulation period is shorter at position 0.7m than 0.65m, as mentioned previously, it is prefered to consider position (0.7, 0.0) as the best position among the positions mentioned for its relatively acceptable error, stimulation intensity and efficiency.

Table 5.1: Statistics at different crank positions

Horizontal (m)	Vertical (m)	Percentage Error	Efficiency	Average Stimulation (μs)
0.6	1	0.4734	0.0018	241.0284
0.6	0.5	0.4622	0.0023	224.1560
0.6	0	0.4425	0.0025	225.4941
0.6	-0.5	0.1821	0.0014	197.8529
0.6	-1	0.2619	0.0014	179.6580
0.65	1	0.1478	0.0471	165.6449
0.65	0.5	0.1432	0.0328	229.8714
0.65	0	0.1398	0.0375	236.5851
0.65	-0.5	0.1308	0.0408	203.0485
0.65	-1	0.1494	0.0442	203.0972
0.7	1	0.1605	0.0925	210.3131
0.7	0.5	0.1492	0.0916	229.6345
0.7	0	0.1399	0.0644	183.4059
0.7	-0.5	0.1395	0.0587	185.1276
0.7	-1	0.1456	0.0951	188.5722
0.75	1	0.3176	0.2420	287.3869
0.75	0.5	0.2944	0.2748	224.8806
0.75	0	0.2497	0.2798	122.2052
0.75	-0.5	0.2926	0.4448	149.4370
0.75	-1	0.3155	0.4571	167.5415

5.6 Best crank position with different gear ratios

From previous sections, it is concluded that the best crank position to be used is (0.7,0.0) and the use of FAVSF with a proper gear ratio is effective in improving the cycling perfomance with a unique disadvantage represented by the high engagement frequency of the flywheel. In this section, it is aimed to further reduce the cadence error and the engagement frequency by testing 17 gear ratios, i.e. 17 different effective flywheel inertia, at crank position (0.7,0.0) with the use of FAVSF. The value of the FAVSF is equal to the employed gear ratio to obtain proper flywheel engagemet/disengagement when necessary. To reduce the flywheel engagement frequency, fuzzy logic approach for engagement mechanism is utilized in this section.

The closed-loop control approach used in this scenario is the same as that utilized in section 5.4.1. The only difference is the use of a Sugeno-type fuzzy inference-based approach to build the flywheel engagement mechanism. The

engagement mechanism has two inputs; the angular velocity of the flywheel and the angular velocity of the crank. In this section, the actual angular velocity of the flywheel is scaled by FAVSF at the input level of the engagement mechanism. The block diagram of the flywheel engagement mechanism is shown in Figure 5.28.
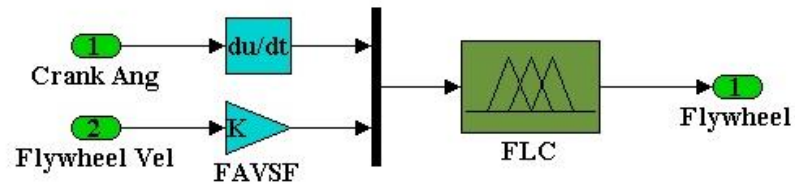
Figure 5.28: The block diagram of the flywheel engagement mechanism showing the use of the FAVSF

Each of the two inputs of the mechanism are fuzzyfied by four variables of modified Gaussian membership functions namely VerySlow, Slow, Fast and VeryFast. The output of the fired rules are converted to crisp values using weighted average method. The output of the mechanism is converted to either zero or one using a threshold. Detailed information about this approach can be found in chapter four.

5.6.1 Results

The results of different effective flywheel inertia, i.e. different gear ratios ranged between 0.33 and 3, recorded for 10 seconds at crank position (0.7,0.0) can be seen in Figures 5.29-5.32. It is clear from Figure 5.29 that the percentage error in cycling cadence dropped below 0.11 at effective inertia between 0.144 and 0.225, i.e. at gear ratios between 0.67 and 0.83, with minimum percentage error of 0.1086 at effective inertia equal to 0.144, i.e. gear ratio 0.67.
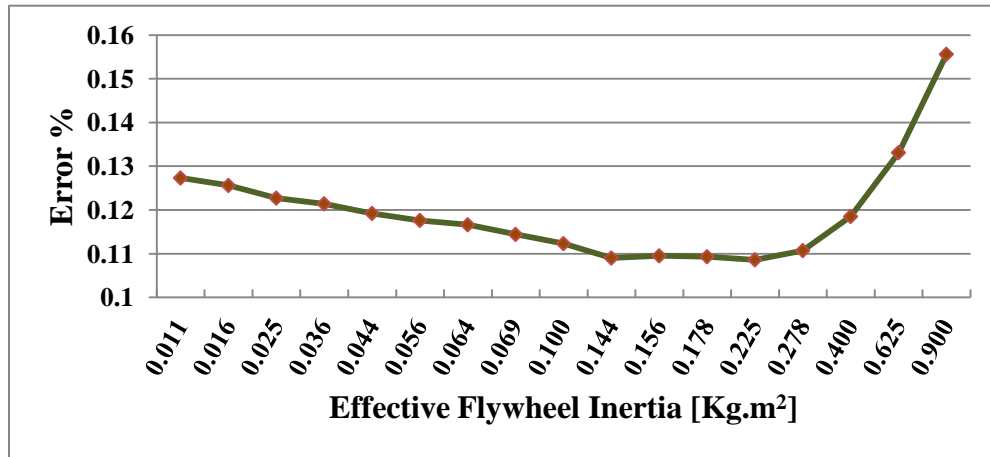
Figure 5.29: Error percentage in cycling cadence at different effective flywheel
inertia using FAVSF and FLC with best crank position

Figure 5.30 shows the average cycling efficiency at different effective flywheel
inertia obtained by different gear ratios. It is clear that the effiiciency at inertia values
greater than 0.1 [Kg.m^2], i.e. at gear ratios smaller than one, was slightly less than that
at effective inertia values smaller than 0.1 [Kg.m^2], i.e. at gear ratios greater than one.
This is due to the increased inertia and the overall resistive-to-motion role of the
flywheel mechanism at gear ratios smaller than one that led to slight decrease in the
cycling power, slight increase in the energy expenditure rate and consequently the drop
in the cycling efficiency.
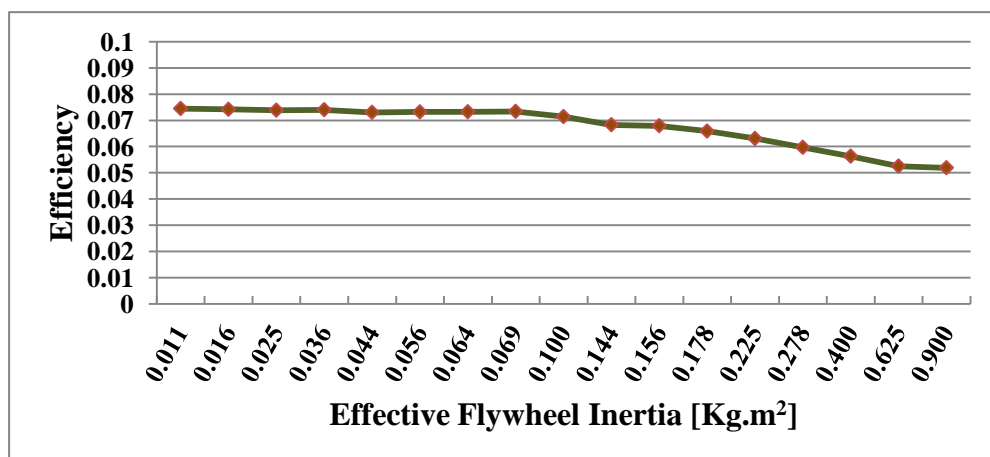
Figure 5.30: Cycling efficiency at different effective flywheel inertia using FAVSF
and FLC with best crank position

The average power of the flywheel in this scenario was positive especially at inertia values greater than 0.1 [Kg.m^2], i.e. at gear ratios smaller than one, as in Figure 5.31. This implies that the flywheel mechanism has absorbed energy from the crank, and imposed a slight load on the crank. However, the approach is effective in reducing the overall error in cadence. The flywheel engagement frequency ranged from 2Hz to 5.5Hz, with frequency greater than 4Hz at effective inertia greater than 0.1 [Kg.m^2], i.e. at gear ratios smaller than one, as can be seen in Figure 5.32. The engagement frequency obtained using the proposed fuzzy logic appraoch was much less than that obtained using boolean logic, 5.5Hz - 9Hz, as explained previously.
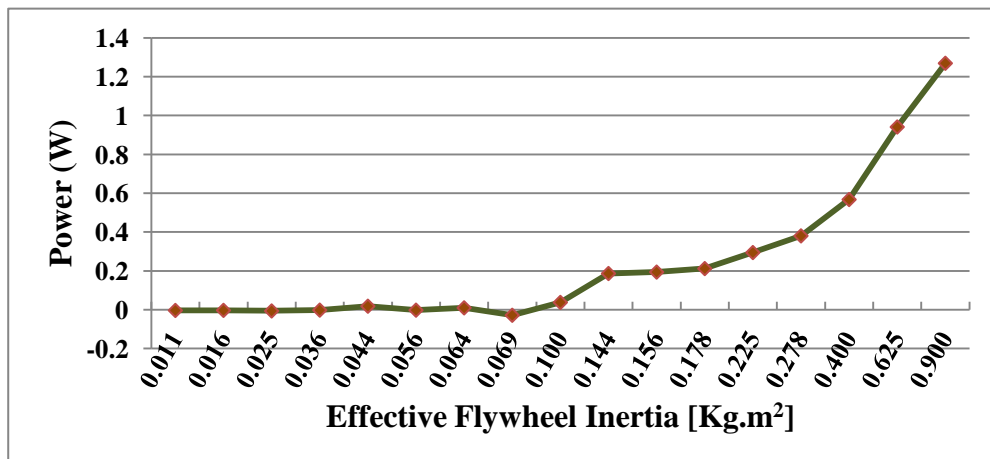
Figure 5.31: Flywheel power at different effective flywheel inertia using FAVSF and FLC with best crank position
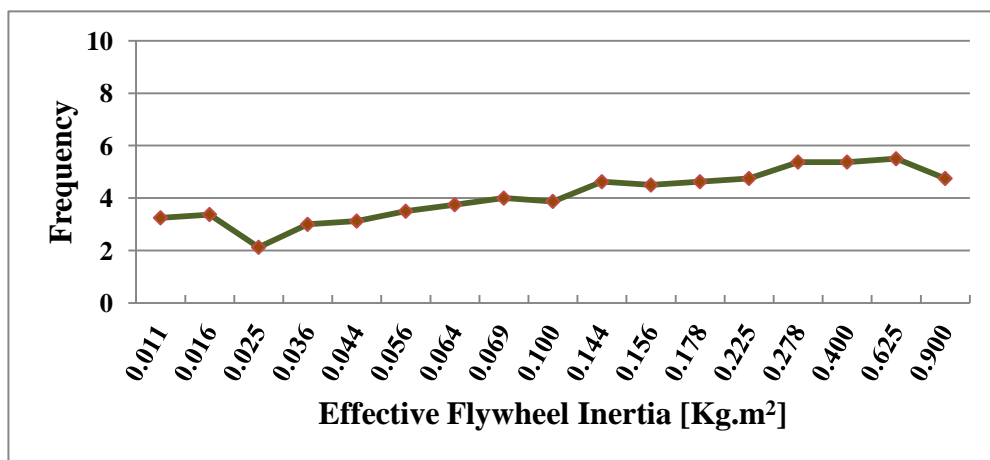
Figure 5.32: Flywheel frequency at different effective flywheel inertia using FAVSF and FLC with best crank position

In this scenario, the minimum percentage error in cadence, 0.1086, was obtained at effective flywheel inertia equal to 0.225 [Kg.m^2], i.e. at gear ratio 0.67, with average stimulation intensity equal to 151.7μsec and cycling efficiency equal to 6.31%. However, at effective inertia 0.144 [Kg.m^2], i.e. at gear ratio 0.83, the percentage error in cadence obtained was 0.1090 with stimulation intensity and efficiency equal to 149.11μsec and 6.83% respectively. For the above statistics it is prefered to consider 0.83 gear ratio as the best gear ratio to be used with the best crank position (0.7, 0.0).

To improve the results further, evolutionary algorithm can be used to optimize the design parameters; controller parameters, flywheel weight, the FAVSF, the start time of the engagement mechanism and the stimulation phases, and obtain more efficient cycling exercise for the disabled. This will be introduced in the next chapter.

5.7   Summary

In this chapter, the effect of different effective flywheel inertia values, using 58 different gear ratios range from 0.33 to 3.0, on the cycling performance from cadence error and cycling efficiency point of view, has been studied. The importance of utilizing the angular velocity scaling factor (FAVSF) to scale the angular velocity of the flywheel, at the decision level of the flywheel engagement mechanism, has been shown. Also, twenty five crank positions are tested to obtain the optimal position for minimum cadence error, minimum stimulation intensity and maximum possible cycling efficiency. The crank position (0.7,0.0) showed a good compromise of the afore mentioned three goals and is selected as the best crank position in FES-cycling exercise.

Further, seventeen different gear ratios, i.e. effective flywheel inertia values, are tested with the seleceted best crank position (0.7,0.0). To decrease the flywheel engagement frequency, fuzzy logic-based engagement mechanism is utilized. The engagement frequency obtained is dropped to 2Hz-5.5Hz as compared with boolean

logic based mechanism, 5.5Hz - 9Hz. Although the minimum percentage error in cadence, 0.1086, is obtained at at effective flywheel inertia equal to 0.225 [Kg.m^2], i.e. gear ratio 0.67, the average stimulation intensity of both legs at this gear ratio is 151.7μsec and the cycling efficiency is 6.31%, while at effective flywheel inertia equal to 0.144 [Kg.m^2], i.e. at gear ratio 0.83, the percentage error in cadence is 0.1090 with average stimulation intensity equal to 149.11μsec and 6.83% efficiency. Therefore, the best gear ratio chosen to be used with the best crank position (0.7,0.0) is 0.83.

To improve the results further and provide as efficient cycling exercise as possible for the disabled, i.e minimize the cadence error and maximize the cycling efficiency, an evolutionary optimization technique can be utilized to obtain the optimal parameters of the design including the controllers' scaling factors, flywheel weight, the activation time of the assist mechanism, the stimulation patterns and the FAVSF. This will be achieved in the next chapter.

Chapter 6: Parameters optimization using evolutionary algorithms

6.1 Introduction

The enhancement of FES-cycling performance through optimizing the crank position and the gear ratio of the flywheel assist mechanism, was discussed in previous chapters. A good choice of these parameters is shown to significantly reduce the cadence error and the stimulation intensity on the muscle and improve the efficiency of the exercise. However, to obtain optimal performance of the design, other design parameters, such as FLC input/output scaling factors; stimulation patterns and the assist mechanism related parameters, need to be optimized. The parameters to be optimized and the objectives to be achieved should be clearly defined to obtain the optimal solution and achieve optimal control of the design (Hussain, 2009). Many researchers have explored the optimization technique to obtain optimal solution of the design in different applications (Davoodi and Andrews, 1999; Huq et al., 2005; Rasmussen et al., 2004).

Parameters optimization of the design depends on a specific objective to be achieved such as minimizing the cadence error, maximizing the exercise time, maximizing the output power or minimizing the stimulation intensity on the muscle. Chen et al. (1997) optimized the stimulation patterns of the quadriceps and the hamstring in FES-cycling exercise with the objective of minimizing the error in cadence. Gföhler and Lugner (2000) investigated the mechanical forces and torques acting on a rider-tricycle system and optimized the stimulation patterns of leg muscles with the objective of maximizing the average drive power and minimizing the active muscle force. Rasmussen et al. (2004) optimized the cycling path of a tri-cycle to eliminate the presence of the dead points by maximizing muscle activation over the cycle. Comolli et al. (2010) developed a cycling ergometer, with two sensors to

measure the torque of each leg separately, and optimized the design with the aim of controlling the movement imbalance due to leg impairment in patients with stroke. Hakansson and Hull (2009) optimized the stimulation patterns of the upper and lower leg muscles to increase muscle endurance in FES-cycling exercise. The optimization is achieved by minimizing the integral of muscle stress as the cost function. The problem of obtaining the optimal stimulation patterns in FES-cycling is a multi-objective optimization problem as the optimal pedalling is obtained by minimizing the muscle fatigue and maximizing the output power at the crank (Massoud, 2007).

Genetic algorithm (GA) is one of the widely used evolutionary algorithms for optimization problems in different applications. Huq et al. (2005) optimized the spring parameters to obtain the optimal design of a spring-brake orthosis for lower body movement using GA. The optimization is achieved with a cost function defined as the mean square error between the desired and the actual knee trajectory. Hussein (2009) used GA to obtain the optimal design parameters of FES-rowing ergometer to minimize the knee trajectory error. Also, they further improved the performance by optimizing the design parameters, including the controller parameters; the spring-orthosis; the inclination angle of the ergometer, using multi-objective GA (MOGA). The MOGA was used to simultaneously minimize the knee trajectory error and the electrical stimulation required by the muscle to perform smooth and prolonged FES-rowing exercise. Further, Massoud (2007) optimized the design parameters, including the controller parameters; stimulation patterns and spring orthosis, using MOGA to minimize the cadence error and maximize the efficiency in FES-cycling exercise.

In this chapter, the optimal design parameters in FES-cycling exercise, with the aid of the flywheel and electrical clutch assist mechanism, are investigated using GA. The minimum mean square error in cadence is defined as the objective function of a single objective optimization process. Also, MOGA is used to improve the performance and obtain the optimal design parameters using two conflicting objectives: to minimize the cadence error and maximize the efficiency of the exercise.

6.2   Single objective optimization of FES-cycling

In this part of the work, the optimal FES-cycling parameters are obtained using a single objective evolutionary algorithm. Genetic algorithm is used to optimize the parameters with the objective of minimizing the error in cadence. In the beginning, the algorithm is used to optimize five parameters only, i.e. the FLC related parameters with the FAVSF. To improve the results further, the number of parameters to be optimized is increased to eleven to include the stimulation patterns and flywheel mechanism related parameters. The performance using the optimized parameters obtained by GA is discussed.

6.2.1 Genetic algorithm

Genetic algorithm, a class of evolutionary algorithms, is a stochastic population-based search method that mimics the process of natural selection and natural genetics (Coley, 1999). After being officially announced by Holland (1975), GA has been used widely in different applications such as robotics, image processing, facial recognition, modelling, control and medicine (Bhanu et al., 1995; Coley, 1999; Lin and Wu, 1999; Ram et al., 1994). Due to its population based nature, GA has the ability to support different solutions simultaneously.

GA is formed by a set of individuals, or population, and a set of operators that can change these individuals. Each individual is a potential solution to the problem. According to the evolutionary theory, the fittest individuals can survive and hence their biological heredity is transferred to the new generation, while weak individuals have small chance to transfer their properties to next generation (Melanie, 1999).

Initially several individuals, or chromosomes, are randomly generated to form an initial population. Each individual of the population is encoded into a set of strings of binary form to be evaluated. From genetic analogy point of view, each individual is similar to a chromosome, and each set of bits in the individual represents a gene in the

chromosome. The individual solutions are then evolved towards better solutions to the problem. The evolution, after initial population, is an iterative process at which the population, in each iteration, is called generation. The fitness of each individual solution is evaluated at each iteration or generation. The fitness value, to determine the goodness of the candidate solution, is usually calculated from the objective function of the problem. According to their calculated fitness, the more fit individuals are selected stochastically for mating and breeding to form the population of the next generation. Each selected individual's characteristics are modified, through randomly recombination and mutation, to form new population. The new individuals, or population of candidate solutions, are then used in the next generation or iteration of the algorithm. The termination of the algorithm usually takes place when the maximum number of generations has been reached or a satisfactory fitness value has been attained by the population. Figure 6.1 shows a flowchart of the GA process.
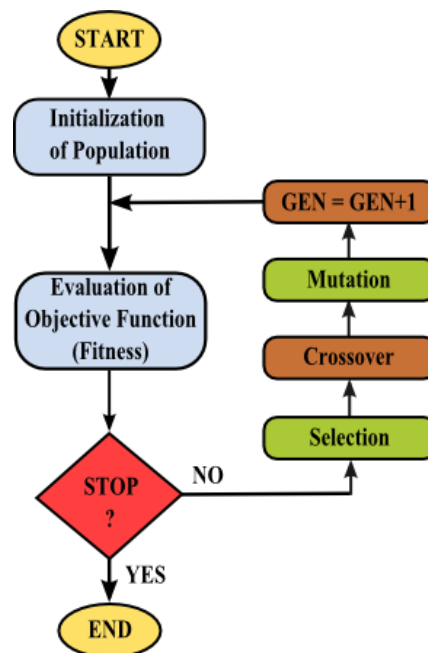
Figure 6.1: Shows a flowchart of genetic algorithm process

6.2.1.1 GA operators

After the first initialization of the population, GA continues to modify and improve the individuals at each generation through the use of its operators; selection, crossover and mutation.

Selection operator

A portion of the population is selected to breed new generation, during each successive generation. The selection process takes place, after fitness assignment for each individual, to determine which individuals to be selected for mating and how many offspring to be produced. The fittest is more likely to survive and produce offspring for next generation to fruit continuously better approximation to a solution. (Chipperfield and Fleming, 1995).

Crossover operator

Crossover, or recombination, produces new individuals, or offspring, by combining the information of the parents in a mating process. The crossover operator swaps part of two selected chromosomes' genetic information to generate new chromosomes. This process is analogous to sexual operation in nature (Ribeiro Filho et al., 1994). As shown in Figure 6.2 after the crossover point has been chosen randomly, the two parents P1 and P2 swap part of their information to produce the offspring strings O1 and O2.
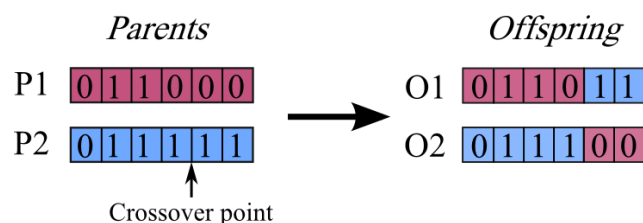
Figure 6.2: Illustrates the Crossover operation in genetic algorithm

Mutation operator

Each offspring undergoes mutation, a process of randomly changing a bit, or number of bits, of offspring strings, as shown in Figure 6.3. Since the modification is not based on previous genetic structure, mutation helps in generating new structure that is useful for exploring other parts of the search space of the problem. Also, the new structure in the population, resulting from mutation process, helps the algorithm to escape from the traps of local minima (Konak et al., 2006; Ribeiro Filho et al., 1994).
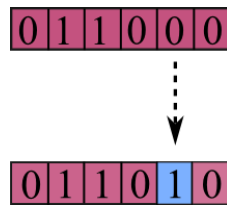
Figure 6.3: Illustrates the mutation operation in genetic algorithm

6.2.2 Optimizing FES-cycling parameters using genetic algorithm

In this section, it is aimed to use GA to improve the cycling performance. This can be done by optimizing the utilized controllers' parameters as well as other design parameters of the cycling ergometer for minimum cadence error.

6.2.2.1 FES-cycling model

The FES-cycling model, previously described in chapter two, is used for the optimization process. The model comprises a humanoid and a bicycle model built in Visual Nastran vN4D dynamic simulation software. Also, a physiological based quadriceps muscle model is incorporated using Simulink/Matlab environment. Further, a bevel gear constraint, with 0.83 gear ratio, is used between the flywheel and the crank of the bicycle. Moreover, the bicycle, i.e. centre of the crank, is positioned at

0.7m, horizontally far from the hip, and at the same vertical position of the hip, since this position was selected in chapter five as the best cycling position.

6.2.2.2 Fuzzy logic control strategy

Pedalling movement of the humanoid model is controlled to track a predefined cadence reference of 35rpm speed. To control the stimulation intensity of FES-signal on both legs, two fuzzy logic controllers are used. Each FLC has two inputs and one output. The actual crank cadence, measured by a sensor located in the bicycle model, is compared with the reference cadence to obtain the error. The error and the change of error, scaled by two input scaling factors G1 and G2, represent the two inputs of the FLC while the output of the FLC is scaled by an output scaling factor G3. The output of each controller is added to a constant value, R1, to form the final value of the stimulation intensity supplied to the quadriceps of each muscle. The control block diagram used is shown in Figure 6.4.
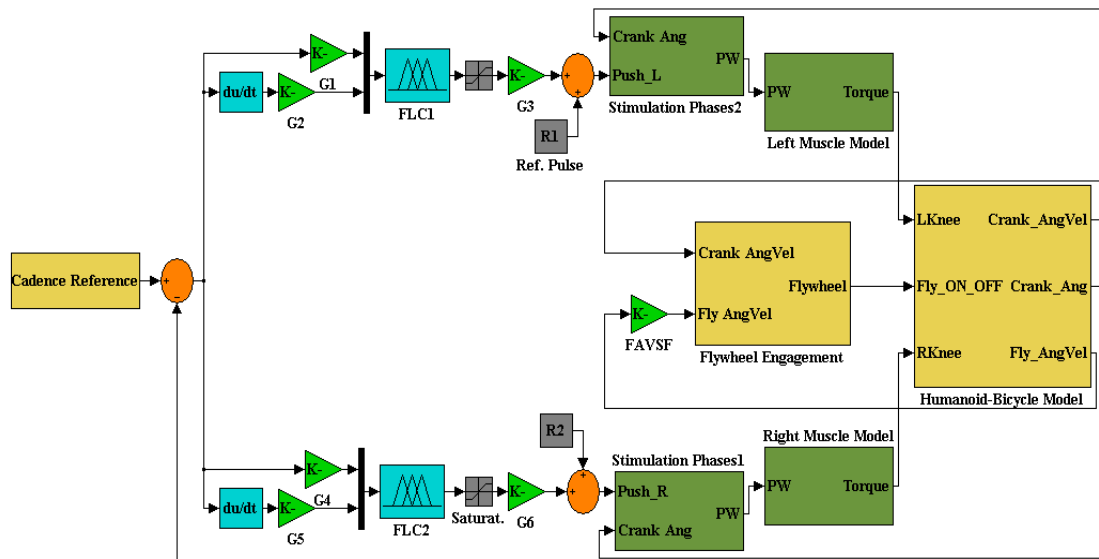
Figure 6.4: The control block diagram used in this scenario

The flywheel and electrical clutch mechanism is used to enhance the FES-cycling performance. The flywheel mechanism is controlled using FLC approach to reduce the flywheel engagement frequency. The block diagram of the FLC-based

engagement mechanism and the two input membership functions are shown in Figure 6.5 and Figure 6.6 respectively. The output of the flywheel engagement mechanism is either one or zero, using a threshold, to activate/deactivate the flywheel by the clutch. Further details about the FLC-based flywheel engagement mechanism can be found in chapter four.
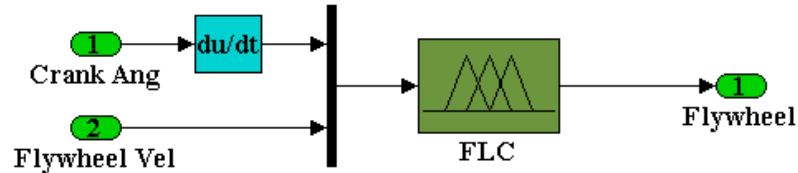
Figure 6.5: Block diagram of the FLC-based flywheel engagement mechanism
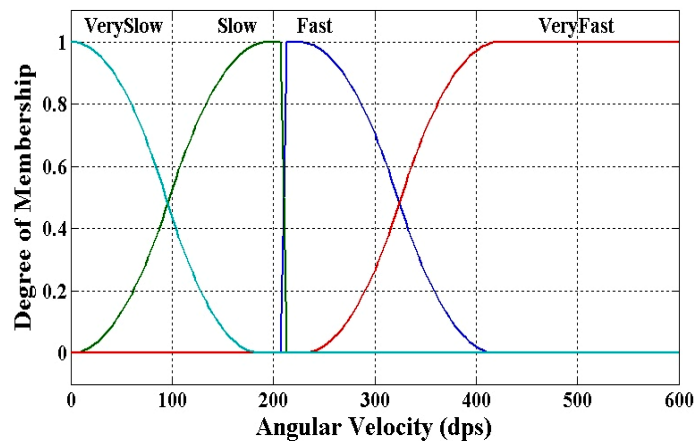
Figure 6.6: FLC inputs membership functions of the flywheel engagement mechanism

The flywheel angular velocity is scaled by the flywheel angular velocity scaling factor (FAVSF) at the input level of the flywheel engagement mechanism, to enable the mechanism to engage/disengage the flywheel when required and obtain the necessary assistance/resistance from the flywheel, as illustrated in detail in chapter five. The gear ratio between the flywheel and the crank is set to 0.83 as this was selected as the best gear ratio obtained in chapter five for best performance.

The input/output scaling factors of each FLC, the predefined pulse width constant and the FAVSF were tuned heuristically in previous chapters to obtain best

performance. In this section, it is aimed to further improve the performance by optimizing the five parameters using GA.

6.2.2.3 Optimizing FES-cycling control parameters with FAVSF

In this section, single-objective GA is utilized to automatically tune the input and output scaling factors of the FLCs as well as the FAVSF. Initially, the algorithm is initialized with 40 individuals or chromosomes. The length of each chromosome is set to 100 binary bits, i.e. five variables of 20 bits long strings, with each variable coded in Gray coding, and concatenated to form the final chromosome. Three of the variables represent the two inputs, K1 and K2, and one output, K3, scaling factors. The other two variables, K4 and K5, represent the pulse width constant and the angular velocity scaling factor, FAVSF, respectively. The ranges of these variables were obtained by manual tuning in previous chapters. The ranges specified for each parameter are 0.0005 to 0.05 for K1, 0.0005 to 0.05 for K2, 100 to 250 for K3, 100 to 300 for K4 and 0.1 to 0.99 for K5. The crossover and the mutation operators were set to 80% and 0.01 respectively.

The objective function used in the optimization process is to minimize the mean squared error in the cycling cadence. The objective function is given as:

$$ObjectiveFunction = \min \left\{ \frac{\sum_{i=1}^{N} (y_{ref} - y_{act})^2}{N} \right\} \tag{6.1}$$

where y_{ref} is the cadence reference, y_{act} is the actual angular velocity of the crank, and N is the total number of samples.

6.2.2.3.1 Results

The optimization algorithm is run for 60 iterations. The GA convergence curve is shown in Figure 6.7. It can be noted that the algorithm is converged at the 23'rd iteration to a value of 3.124 which is close to the final value, 3.123, at the 60'th iteration. The best values obtained for the five parameters after 60 iterations are 0.01 for K1, 0.0249 for K2, 248.6529 for K3, 182.4279 for K4 and 0.8541 for K5. Using the parameters mentioned, the cycling RMS error value becomes 2.73 rpm, the average stimulation on both legs is 147.56µs and the cycling efficiency is 5.5%. Figure 6.8 shows cadence error using the parameters' values obtained at the 60th iteration. To reduce the cadence error further, additional parameters need to be optimized.
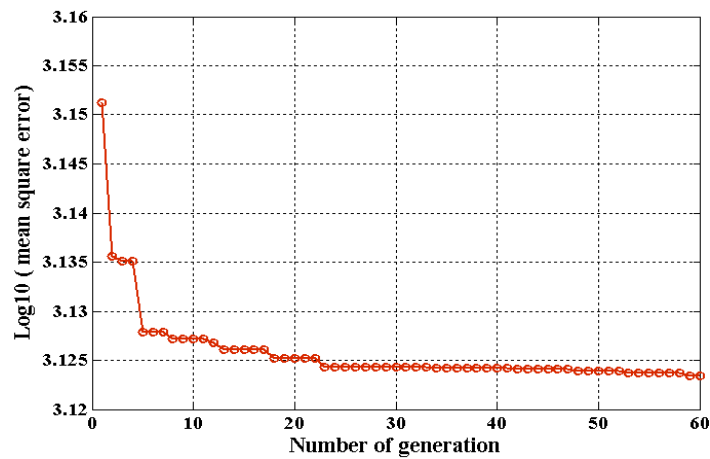
Figure 6.7: GA convergence curve obtained for 60 iterations optimizing five parameters for minimum cadence error
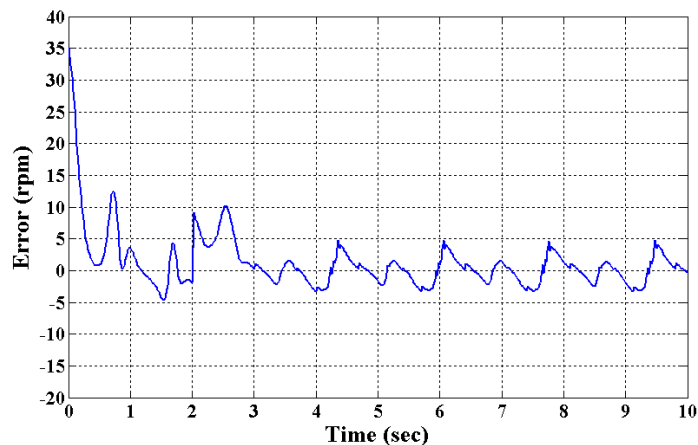
Figure 6.8: Cadence error using the five parameters optimized by GA

149

6.2.2.4 Optimizing FES-cycling parameters including stimulation phases

In this study, it is aimed to improve the performance and further minimize the cycling cadence error by optimizing eleven parameters at the same time using GA. The parameters to be tuned are represented by the two input scaling factors (K1 and K2), the output scaling factor (K3) of the FLC, the constant pulse width value (K4), the FAVSF (K5), the minimum value of the saturation block applied to the output of the FLC at the pushing phase (K6), the maximum value of the saturation block applied to the output of the FLC at the pushing phase (K7), the crank angle value that represents the start of the pushing phase (K8), the crank angle value that represents the end of the pushing phase (K9), the weight of the flywheel (K10) and the activation time of the flywheel engagement mechanism (K11). The ranges of these variables are obtained by manual tuning as in previous chapters. The ranges specified for each parameter are [0.0005 to 0.05] for K1, [0.0005 to 0.05] for K2, [100 to 250] for K3, [100 to 300] for K4, [0.1 to 0.99] for K5, [-1 to 0] for K6, [0 to 1] for K7, [0 to 60] for K8, [70 to 150] for K9, [3 to 6] for K10 and [1 to 3] for K11.

The algorithm is initialized with 40 individuals or chromosomes. Each of the eleven variables is encoded by 20 binary strings, using Gray coding, and concatenated to form the final chromosome. The crossover and the mutation operators were set to 80% and 0.01 respectively.

The objective function used in the optimization process is to minimize the mean squared error in the cycling cadence. The objective function is given in equation (6.1).

6.2.2.4.1 Results

The GA convergence curve for 100 iterations is shown in Figure 6.9. It can be noted that the algorithm converged at the 65th iteration to a value of 3.065 which is close to the final value, 3.062, at the 100th iteration. The best values obtained for the eleven parameters after 100 iterations are 0.0398 for K1, 0.0333 for K2, 241.0270 for K3,

206.5446 for K4, 0.8719 for K5, -0.2373 for K6, 0.8233 for K7, 1.8113 for K8, 131.8657 for K9, 4.9907 for K10, 1.7208 for K11. Using the parameters mentioned, the cycling RMS error value became 2.27 rpm, the average stimulation on both legs was 138.02μs, the cycling efficiency was 5.02%, and the flywheel engagement frequency was 3.75Hz. Figure 6.10 shows cadence error using the parameters values obtained at the 100th iteration.
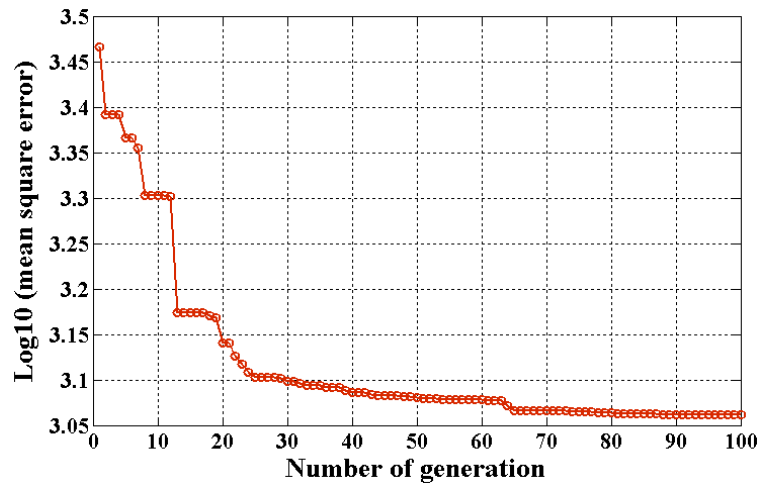
Figure 6.9: GA convergence curve obtained for 100 iterations optimizing eleven parameters
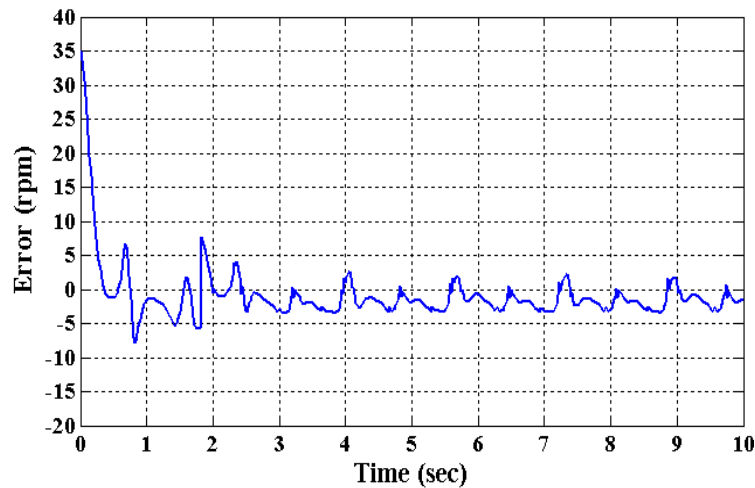
Figure 6.10: Cadence error using the optimal parameter values obtained by GA after 100 iterations

It can be noted that GA was able to minimize the cadence error significantly, however the cycling efficiency dropped. Since the cadence error and the cycling efficiency are two conflicting objectives, single-objective GA is unable to optimize

both of the objectives simultaneously, as improving one of the objectives will degrade the other. For this reason, mutli-objective GA will be used to find a reasonable solution as a trade-off between the cadence error and the cycling efficiency.

6.3   Multi-objective optimization

Multi-objective optimization, also called multicriteria optimization or Pareto optimization, is a field of multiple criteria decision making that deals with problems comprising more than one objective function to be optimized at the same time. Multi-objective optimization has been used in different fields of engineering, finance and logistics (Ombuki et al., 2006; Radu and Besanger, 2006; Tapia and Coello, 2007) at which trade-offs, between two or more conflicting solutions, take place to obtain optimal decisions. Maximizing the performance and minimizing the fuel consumption of a vehicle, maximizing the size of a property and minimizing the cost are examples of two objectives optimization problems.

In multi-objective optimization problems, there is no single solution that can optimize each objective simultaneously. This is due to the fact that the objectives are conflicting and possibly uncountable set of optimal solutions exists. For this reason, a reasonable solution to a multi-objective optimization problem is to examine a set of solutions, each of which satisfies an objective at an acceptable level without being dominated by other solutions (Konak et al., 2006).

A solution is called Pareto optimal or non-dominated solution if the value of an objective function cannot be improved without worsening the value of other objective functions. In other words, a Pareto optimal set is the set of solutions that are non-dominated with respect to each other. When moving from one Pareto solution to another, there is always a certain amount of sacrifice in one or more objectives to achieve a certain amount of gain in the others (Konak et al., 2006). All non-dominated Pareto solutions are considered as good solutions if there is no subjective preference

information. The aim is to find a set of Pareto optimal solutions, evaluate the trade-offs in meeting different objectives, or finding a single solution that meets the preferences of a decision maker.

6.3.1 Multi-objective genetic algorithm

Multi-objective genetic algorithm (MOGA) was first developed by Fonseca and Fleming (1993). MOGA, a modified version of the generic single-objective GA, is a population based stochastic searching method that provides a set of non-dominated solutions, known as Pareto set, as a trade-off between more than one conflicting objectives. The ability of MOGA to search different regions, in parallel, in the search space makes it capable of exploring different sets of non-dominated solutions for difficult problems with a single run. MOGA differs from the standard GA by the way the fitness of each individual is assigned. Other parts, operators, of the algorithm such as selection, crossover and mutation are the same as those in GA. Figure 6.11 shows a flowchart of working principle of the employed MOGA.
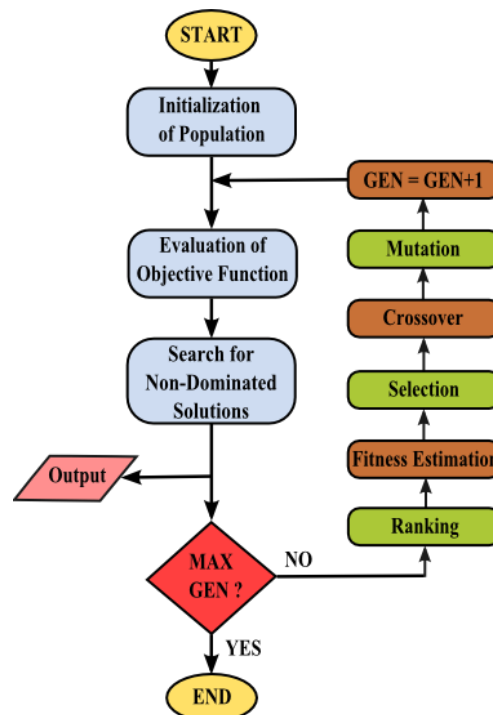
Figure 6.11: Flowchart of multi-objective genetic algorithm (MOGA) process

6.3.1.1 Initialization, evaluation and ranking

Initially, randomly selected individuals of possible solutions, i.e. population, is generated within a specific range. Each individual is evaluated using the objective functions of the problem. In case of a two objective minimization problem, individuals that fall close to the origin or axes of a 2D objective space are better than those that fall away from the origin. Some individuals that fall on the outer edge and close to the origin such as E; A; G and F, as shown in Figure 6.12, having one objective better than the other are non-dominated solutions and form the Pareto optimal set because no other solution provides better value of one objective without degrading the value of the other objective. On the other hand, other individuals that fall behind the outer edge, i.e. away from the origin, such as B, C and D, are called dominated solutions as there are individuals that provide better values of both solutions.

An individual X_i at generation n, dominated by P_i^n individuals, is ranked according to the following (Fonseca and Fleming, 1993):

$$Rank\,(X_i,n) = 1 + P_i^n \tag{6.2}$$

In other words, an individual is ranked according to its degree of dominance, i.e. the number of individuals of better values than those in terms of both objectives, plus one. Since individuals on the Pareto set are non-dominated; they are assigned a rank of one, the highest.
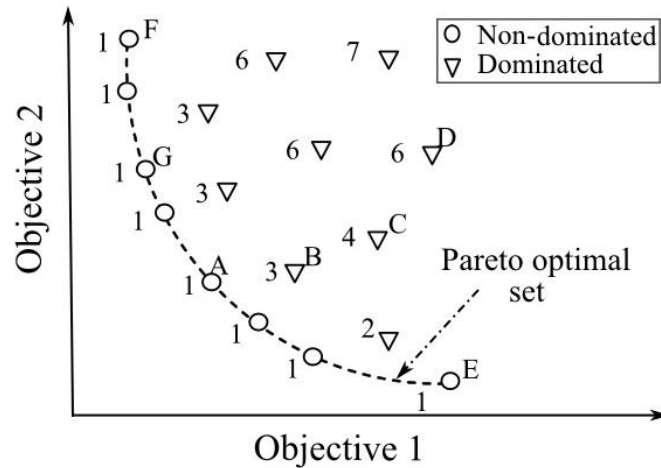
Figure 6.12: Dominated and non-dominated solutions with rank values

6.3.1.2 Fitness assignment

After ranking is performed, each individual is assigned a fitness value based on the given ranking. The assigned fitness denotes the number of offspring an individual is expected to produce through selection. The fitness assignment according to (Fonseca and Fleming, 1993) is achieved as follows:

I.   All the population is sorted according to individuals' ranks.

II. Fitness assignment is performed using a linear, or exponential, function. The function is chosen so as to assign fitness values between N (for the highest ranked individuals) and zero (for the lowest ranked individuals).

III. The fitness, assigned to each individual of the same rank, is then averaged. This allows the individuals of the same rank to obtain the same fitness value and allow all the individuals to be sampled at the same rate while keeping the global population fitness constant.

The next step is to perform other GA operators, Selection; Crossover and Mutation, to form the next generation.

6.3.2 FES-cycling using MOGA

In the previous section, GA was used to optimize the FES-cycling performance by minimizing the cycling cadence error. Although the cycling error was minimized, the cycling efficiency dropped to 5.02%. The cycling efficiency is an important measure of the effectiveness of the FES-cycling exercise. It is important to achieve high FES-cycling efficiency to guarantee that most muscle energy produced by stimulating the muscle is transformed to useful motion (Massoud, 2007).

Successful FES-cycling is achieved by steady-state speed with high cycling efficiency. Since the cadence error and the cycling efficiency are two conflicting objectives, single-objective GA is unable to optimize the design for both objectives simultaneously. For this reason, multi-objective genetic algorithm (MOGA) is used to optimize the design parameters for minimum cadence error and maximum cycling efficiency.

6.3.2.1 Optimizing FES-cycling parameters including stimulation phases using MOGA

In this section, it is aimed to use MOGA to optimize the design parameters for minimum cadence error and maximum efficiency at the same time. The parameters to be tuned are represented by the two input scaling factors (K1 and K2), the output scaling factor (K3) of the FLC, the constant pulse width value (K4), the FAVSF (K5), the minimum value of the saturation block applied to the output of the FLC at the pushing phase (K6), the maximum value of the saturation block applied to the output of the FLC at the pushing phase (K7), the crank angle value that represents the start of the pushing phase (K8), the crank angle value that represents the end of the pushing phase (K9), the weight of the flywheel (K10) and the activation time of the flywheel engagement mechanism (K11). The ranges of these variables were obtained by manual tuning in previous chapters. The ranges specified for each parameter are [0.0005 to

0.05] for K1, [0.0005 to 0.05] for K2, [100 to 250] for K3, [100 to 300] for K4, [0.1 to 0.99] for K5, [-1 to 0] for K6, [0 to 1] for K7, [0 to 60] for K8, [70 to 150] for K9, [3 to 6] for K10 and [1 to 3] for K11.

The algorithm was initialized with 40 individuals or chromosomes and run for 100 iterations. Each of the eleven variables were encoded by 20 binary strings, using Gray coding, and concatenated to form the final chromosome. The crossover and the mutation operators were set to 80% and 0.01 respectively.

The two objective functions used in the optimization process are i) to minimize the percentage error in cadence and ii) to maximize the efficiency in FES-cycling. The equations of both objectives are given as:

$$ObjectiveFunction.1 = \min\left\{ \frac{\sum_{i=1}^{N}(y_{ref} - y_{act})^2}{N.y_{ref}} \right\} \tag{6.3}$$

$$ObjectiveFunction.2 = \min\{Muscle\ Power\ /\ Output\ Power\}$$

$$= \min\{1/\ Efficiency\} \tag{6.4}$$

where y_{ref} is the cadence reference, y_{act} is the actual angular velocity of the crank, and N is the total number of samples, while the calculation of muscle power and output power is as explained in chapters four and five respectively.

6.3.2.1.1 Results

The non-dominated solutions obtained from MOGA after 100 iterations can be seen in Figure 6.13. It can be noticed that the MOGA produced a wide range of non-dominated solutions as a trade-off between the two objectives. From Figure 6.13 it can be seen that solutions of high efficiency values were accompanied with high percentage error in cadence. In order to obtain smooth cadence and keep the error in

cadence as minimum as possible, with acceptable cycling efficiency, one of the solutions, shown in Figure 6.13, was selected as the optimal solution. The optimized design parameters at the optimal solution can be seen in Table 6.1. Using the optimal solution, the percentage error in cadence recorded for 10 seconds, was 9.9%, RMSE was 3.24 rpm, the average stimulation intensity on both legs was 136.34µs and the efficiency was 8.17%.
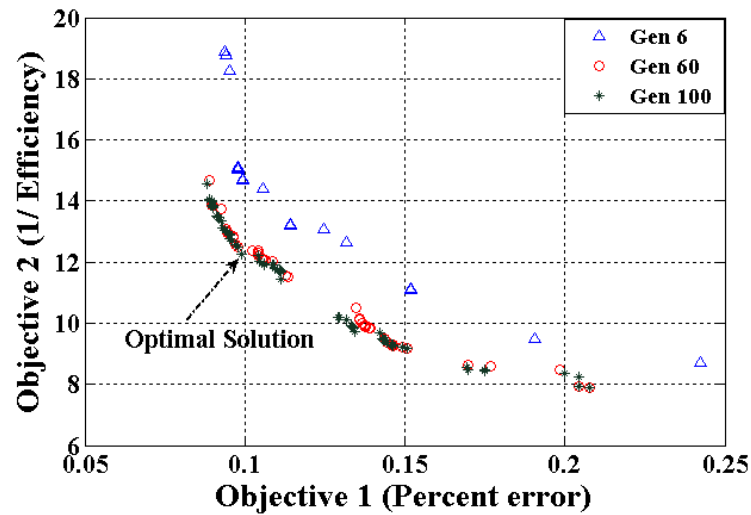
Figure 6.13: Non-dominated solutions obtained using MOGA

Table 6.1: The design parameters obtained at the selected optimal solution

Parameter	K1	K2	K3	K4	K5	K6	K7	K8	K9	K10	K11
Value	0.0139	0.0166	246.2690	212.0339	0.3201	-0.6684	0.6917	9.8227	122.2180	3.5287	1.6429

The design parameters obtained at the selected optimal solution are used and tested for 1200 seconds. For a 35rpm reference, the actual cadence ranged between 30-40 rpm for the whole duration of the exercise after the activation of the engagement mechanism took place in 1.64 second, Figure 6.14. This implies that the control approach together with the flywheel assist mechanism was successful in exercising and assisting the legs, with bounded cadence error, for a long period without suffering from muscle fatigue problem. Also, for comparison purposes, the muscle fitness was recorded with and without using the flywheel assist mechanism as shown in Figure

6.15. It can be noticed that with the assist mechanism the drop in muscle fitness was less than that without assistance. This shows the importance of the flywheel mechanism in reducing the stimulation intensity on the muscle, assisting the legs and prolonging the exercise.
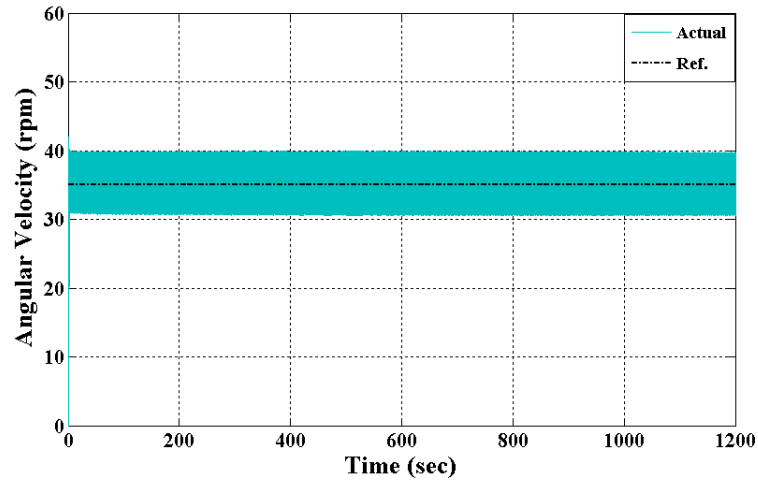
Figure 6.14: Crank angular velocity recorded for 1200 seconds
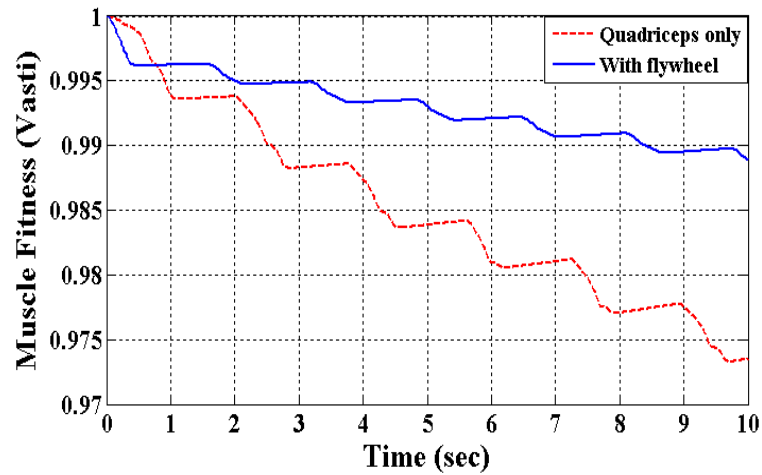
Figure 6.15: Muscle fitness with and without flywheel mechanism

To test the robustness of the control approach to muscle fatigue problem, the time fatigue constant T_{fat} of the quadriceps was dropped from 18 to 4 seconds. The exaggerated time-constant, 4 seconds, has been previously used in the literature (Kim et al., 2008) for the same purpose. It can be noticed from Figure 6.16 and Figure 6.17 that the cadence encountered a slight change but remained bounded within 30-40rpm.

This shows the effectiveness of the control approach to cope with possible changes in muscle fitness during the exercise.
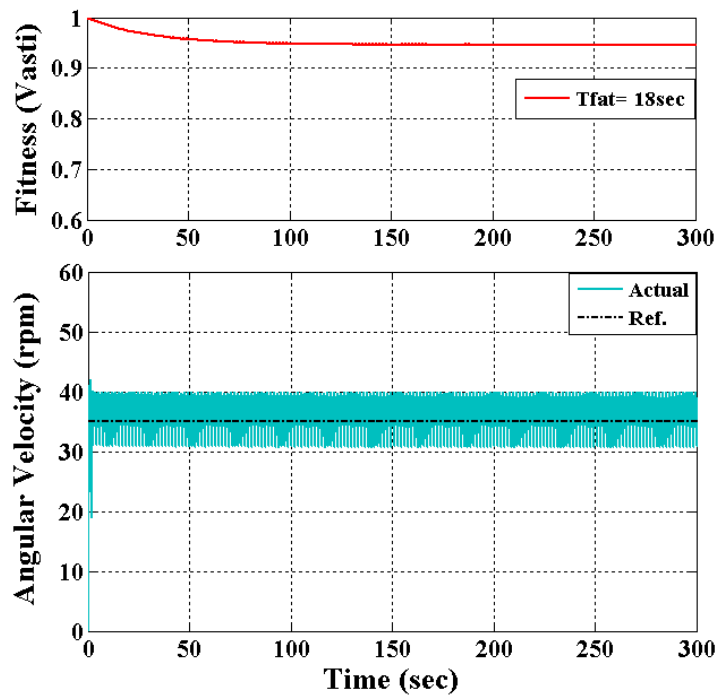
Figure 6.16: Crank angular velocity recorded at time fatigue
constant equal to 18 second
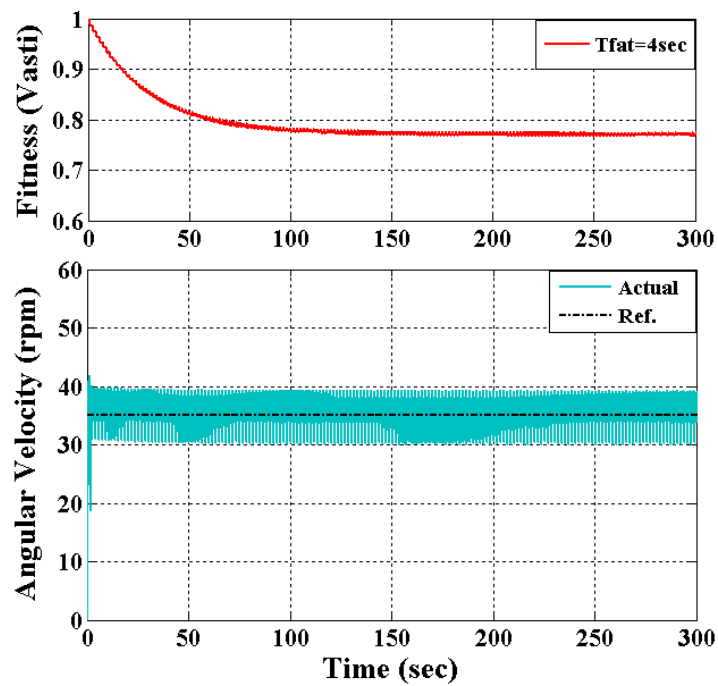
Figure 6.17: Crank angular velocity recorded at time fatigue
constant equal to 4 second

For assessment purposes, the cycling cadence obtained in this work was compared with that obtained by (Chen et al., 2004) as both studies used fuzzy logic control approach; however in (Chen et al., 2004) two muscles, the quadriceps and the hamstring, have been stimulated with assistance provided by an arm crank. It can be noticed from Figure 6.18(b), that the cadence obtained by (Chen et al., 2004), for a reference of 50rpm, fluctuated for more than ±10 rpm, while in this work, by stimulating single muscle, the quadriceps, with a flywheel and clutch mechanism, Figure 6.18(a), the cadence error, for a reference of 35 rpm, ranged between ±5 rpm.

(a)

(b)
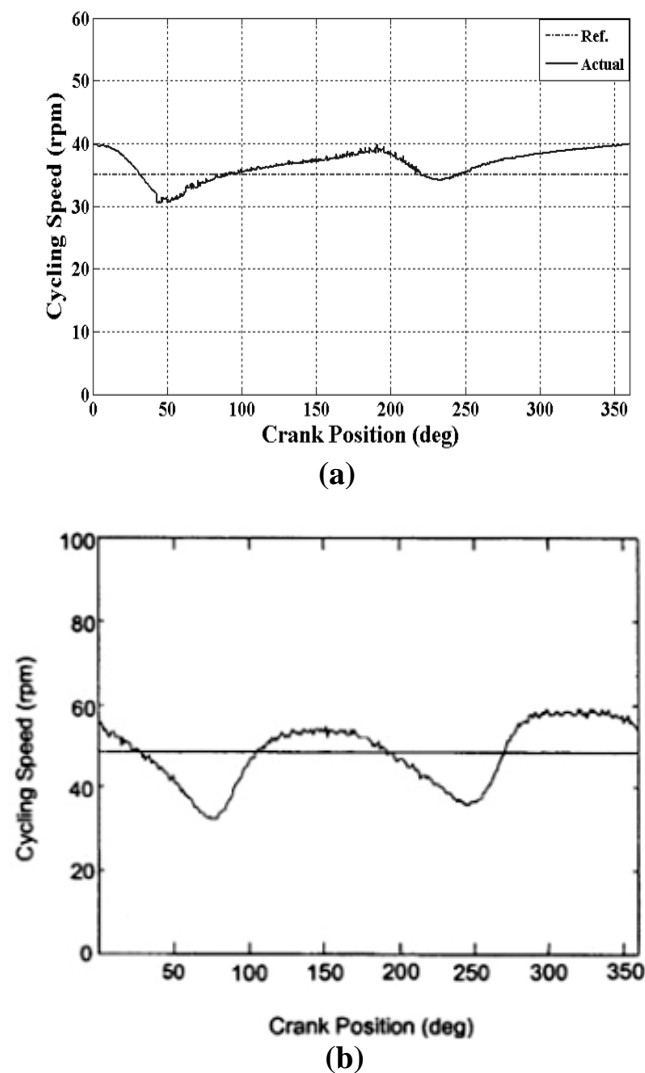
Figure 6.18: Cycling cadence with respect to crank angle, a comparison between (a) using single muscle group, the quadriceps, with flywheel and electrical clutch mechanism using 35 rpm cadence reference recorded for 1200 seconds (this study) (b) using two muscle groups, quadriceps and hamstring, using 50rpm cadence reference (Chen et al., 2004)

The results obtained show that the control design approach, together with the new assist mechanism, has the ability to produce bounded cadence error without suffering from premature termination due to fatigue related problems. Also, the cycling efficiency of the exercise obtained was 8.17% which is acceptable, as the efficiency in FES-cycling ranges 2-14% in SCI individuals (Glaser et al., 1989; Hunt et al., 2007). It can be concluded that the design promotes efficient and prolonged FES cycling exercise, with acceptable cadence error, for disabled individuals by stimulating the quadriceps muscle.

6.4 Summary

Single objective genetic algorithm has been used to optimize five design parameters to obtain minimum cadence error in FES-cycling exercise of 35rpm desired cadence. These parameters are the utilized fuzzy controllers' input/output scaling factors, the reference pulse constant and the flywheel angular velocity scaling factor (FAVSF). After 60 iterations, the optimal parameters obtained by GA have been tested and resulted in cycling with 2.73rpm root mean square error in cadence, 147.56μs average stimulation intensity and 5.5% cycling efficiency. To improve the results further, GA has been used to optimize eleven parameters of the design. These parameters represent the controllers' input/output scaling factors, reference pulse width, the FAVSF, minimum and maximum value of the saturation block applied to the output of the FLC at the pushing phase, the stimulation patterns, weight of the flywheel and the activation time of the flywheel mechanism. After 100 iterations the parameters obtained from the optimization, with minimum cadence error as the objective function, reduced the root mean square error to 2.27rpm and the stimulation intensity to 138.02μs. However, the efficiency of the exercise dropped to 5.02%.

In an attempt to obtain a satisfactory solution to the problem of two conflicting objectives, i.e. minimum cadence error and maximum efficiency, MOGA has been utilized to produce a set of non-dominated solutions. An optimal solution, as a

reasonable compromise between the two objectives, has been selected and tested. Using the optimal solution, the design was tested for 1200 seconds and produced bounded cadence error, ±5 rpm, during the whole duration of the exercise with 136.34μs average stimulation intensity on both legs and 8.17% efficiency without suffering from muscle fatigue related problems. To test the robustness of the design against possible changes in muscle fitness during the exercise, the time fatigue constant T_{fat} of the quadriceps model was dropped from 18 to 4 seconds. The controller was able to keep the cadence error bounded to ±5 rpm during the whole duration of the exercise. Using the optimal solution obtained by MOGA, the introduced design shows better performance in terms of cadence error as compared with results from the literature.

It can be concluded that the proposed control approach together with the new introduced assist mechanism promotes robust, efficient and prolonged FES-cycling exercise by stimulating the quadriceps muscle for disabled individuals.

Chapter 7: Conclusion and future work

7.1 Conclusion

The main aim of the research was to develop an efficient FES-cycling ergometer equipped with an assist mechanism to assist paralyzed legs and reduce the stimulation intensity on the muscle to elongate the exercise. The research has focused on the use of a novel assist mechanism, represented by a flywheel and electrical clutch, to achieve performance enhancement in FES-cycling exercise for people with spinal cord injury (SCI) by stimulating single muscle group, the quadriceps, of each leg. Intelligent control strategies have been used to control the stimulation intensity on the muscle to perform coordinated pedalling movement. Also, intelligent control approaches have been developed to control the assist mechanism and properly assist the legs when required. Further, the research aimed to enhance the performance through optimizing the gear ratio between the flywheel and the crank, seat position, stimulation patterns and controller related parameters.

This chapter evaluates the implications of the research through six issues. First, the development of an appropriate FES-cycling ergometer with a humanoid model was necessary to study, analyze and control the FES-cycling in simulation platform. The use of a dynamic simulation platform was essential to minimize the trials and experiments that might be costly in time and harsh for the disabled. In this research, the humanoid and bicycle model have been developed using vN4D software to simulate the system in a dynamic platform with the ability to measure and adjust several design parameters in real-time. Although vN4D is very slow and computationally exhaustive, it is worth utilizing this software for its ability to produce useful information and results with moderate efforts, which might otherwise be left undiscovered due to the mathematical complexity involved in conventional approaches. Also, the compatibility of vN4D with Simulink/Matlab allows the

integration of a muscle model with the humanoid and the application of intelligent control techniques to imitate real control scenarios. Most of the current muscle models developed either on physiological basis or experimentally are not suitable for simulation of control applications. Those models characterise each muscle feature alone, and sometimes, with no connection between each feature that prevent the implementation of the whole muscle as an integrated model. However, other muscle models, such as the ones introduced by Ferrarin; Riener; Makksoud, have been developed for the purpose of control tests in simulation platforms. In the early stages of this study, the muscle model developed by Ferrarin was utilized. Ferrarin's muscle is a linear, easy-to-implement model but lacks muscle fatigue index. Due to the use of Ferrarin's muscle, the development of a force-drop indicator was necessary to be used for assessment purposes between two control approaches and to evaluate the benefits of the newly proposed assist mechanism.

Second, the use of a proper intelligent control technique is essential to regulate the stimulation intensity on the quadriceps and perform coordinated FES-cycling exercise. The control of functional electrical stimulation to restore functional movement can be achieved by defining desired trajectories or set points of certain variables in the system. In this research, two controllers have been tested, PID and FLC, to regulate the stimulation intensity on the muscle and follow a predefined trajectory. Both of the controllers produced similar tracking performance as they both were activated in predetermined short periods of each cycle; however, the FLC produced smoother stimulation on the muscle. To perform FES-cycling by stimulating the quadriceps only, the muscle should be stimulated twice per cycle to maintain the desired trajectory. Performing FES-cycling by stimulating the quadriceps only, without the use of any assist mechanism, leads to rapid muscle fatigue due to successive stimulation of the muscle.

Third, the use of the flywheel and electrical clutch mechanism is necessary to prevent premature muscle fatigue resulting from successive stimulation on the

quadriceps. The mechanism has been used to produce both assistance and resistance to the motion when necessary. The control of the mechanism has been achieved with two feedback control approaches using FLC and Boolean logic. The first approach depends on the knee joint angular velocity while the second rely on the angular velocity of the crank. The second approach was superior in terms of producing assistance without noticeable jerking in cadence; however, it requires highly sensitive electrical clutch. The use of Boolean logic to build the engagement mechanism has led to high engagement frequency of the flywheel, while building the mechanism using FLC reduced the engagement frequency by approximately 45%, hence cheaper and less sensitive electrical clutch may be sufficient using this method. The use of the flywheel mechanism in FES-cycling by stimulating the quadriceps reduces the number of stimulus to half as the mechanism replaces the resist phase required to follow a predefined trajectory by the quadriceps' effort only. Also, using a predefined trajectory control method, the derived force-drop indicator showed that the use of the flywheel mechanism prolongs the exercise by approximately 14%-17% as compared with exercising without assistance.

Fourth, Using predefined knee joint trajectory of a specific speed in FES-cycling is useful to analyze the system and specify the required stimulation patterns. However, this method requires two position sensors, i.e. goniometer, in practice and is not sensitive to changes in crank speed. By using this method, coordinated pedalling movement can be achieved; however, the desired cadence cannot be guaranteed. For this reason, a control approach to track a predefined cycling speed is necessary to achieve the required pedalling rate. Cadence control approach has been implemented using FLC with and without flywheel assist mechanism. Also, to be able to measure the efficiency of the exercise and obtain results close to reality, i.e. dynamically consider force-length, force-velocity and fatigue properties of the muscle, Ferrarin's muscle model was replaced by a physiological based nonlinear muscle model developed by Riener. This muscle model accounts for the physiological properties of

the muscle including the calcium dynamics and muscle fatigue when activated by FES. Also, it provides information useful for estimating the energy expenditure of the muscle and the efficiency of the exercise.

The control of a desired cadence using the quadriceps, i.e. one-directional actuator, is difficult to achieve due to the effect of the dead spots that cause rapid changes in crank speed. The use of a control approach to track a desired cadence is superior in terms of reducing the error in cadence as compared with that using a predefined knee trajectory. Also, the use of the flywheel assist mechanism is essential to suppress the fluctuation in the cadence and reduce the average stimulation intensity on the muscle from 223µs to 178µs. This implies that the flywheel assist mechanism prolongs the exercise by approximately 20% as compared with that without assistance by stimulating the quadriceps in the introduced cadence control approach.

Fifth, the performance of the flywheel mechanism is influenced by several factors. The effect of the gear ratio between the flywheel and the crank, on the performance of the mechanism has been studied. The gear ratio can be used to obtain mechanical advantage, change the effective flywheel inertia and improve the performance of the mechanism. A gear ratio of less than one, 0.67-0.83, was necessary to increase the damping required during the resist phase of the mechanism and reduce the cadence error. Also the use of the flywheel angular velocity scaling factor (FAVSF) was essential to provide proper engagement of the flywheel during both resist and assist phases when necessary during each cycle. The effect of the crank position with respect to the hip joint has also been studied. The efficiency of the exercise increased with increase of the distance from the hip joint. However, increasing the distance between the hip and the crank made it difficult to control the cadence as the leg was fully extended and the effect of the dead spots became dominant. The best distance between the crank and the hip was horizontally 0.7m and vertically 0.0m for the bicycle dimensions used.

Sixth, the optimal design parameters have been obtained using evolutionary algorithms to further enhance the FES-cycling performance. Genetic algorithm was used to optimize the design parameters including fuzzy controllers' input/output scaling factors, the reference pulse constant, FAVSF and stimulation patterns. The GA was successful in optimizing the parameters with the objective of minimizing the cadence error. However, the efficiency of the exercise was not optimized since GA was only capable of dealing with a single objective. To obtain the optimal solution in terms of minimum cadence error and maximum efficiency, MOGA was used to obtain non-dominated solutions that meet the desired two conflicting objectives.

The optimal solution provided by MOGA was tested for 1200 seconds without suffering from muscle fatigue related problems. Also, tests with exaggerated fatigue index showed the robustness of the design to possible changes in muscle fitness during the exercise. Finally, it can be concluded that the design provides efficient and prolonged FES cycling exercise, with bounded cadence error, for disabled individuals by stimulating the quadriceps muscle.

7.2 Future work

This study has covered the most important aspects in FES-cycling using a novel assist mechanism, represented by a flywheel and electrical clutch, by stimulating the quadriceps muscle only. However, recommendations for further investigations can be summarised as follows for possible future work and improvement.

- The use of a more developed simulation software that allows on-line changes to all of the design so as to optimize the design parameters, such as the flywheel inertia; gear ratio; crank position and crank arm length, simultaneously using evolutionary algorithms such as GA and MOGA.

- The optimal stimulation periods and the required assistance vary with each pedalling speed; therefore, it is necessary to optimize the stimulation patterns and the gear ratio between the flywheel and the crank to obtain optimal performance with different desired cycling speeds.

- Enhance the performance through the use of GA and/or MOGA to optimize other parameters, such as the FL's rule base and MFs.

- The use of an adaptive approach to dynamically alter the stimulation patterns and tune the gear ratio for each desired speed and/or in case of drop in muscle power.

- The use of an adaptive approach to automatically tune the stimulation intensity on the muscle and allow trainees of different physical characteristics, such as legs length; muscle strength and fatigue resistance, to exercise using the same ergometer.

- For the importance of exercising with a specific cadence and power output at the same time in some FES-cycling training programs, intelligent control techniques can be utilized to control both the desired cadence and the power output simultaneously.

- This study has introduced the benefits of the newly proposed assist mechanism in FES-cycling exercise by stimulating the quadriceps only. It is worth studying and testing the mechanism in FES-cycling exercise by stimulating more than one muscle to figure out whether the mechanism will provide the same mentioned benefits or not.

- Building a design prototype to investigate and validate the findings of the proposed assist mechanism and intelligent control strategies in experimental and practical settings.

Appendix A: Miscellaneous

This appendix provides basic information about different concepts related to this project. These include an introduction to PID control, Fuzzy logic principles, flywheel energy storage, electrical clutch and the mechanical gears between a motor and its load.

A.1 PID control

The PID controller attempts to correct the error between the desired set point and the measured process variable by computing a corrective that adjusts the process accordingly. It comprises of three parts: Proportional (P), Integral (I) and Derivative (D). With the proportional part, the control output is proportional to the error multiplied by a constant (K_p) called proportional gain and is expressed as:

$$P = K_p . e(t)$$

(A.1)

The proportional term determines the reaction based on the current error. With the proportional controller an offset (deviation from the set-point) is presented and increasing the proportional gain may lead to unstable output.

The integral action of the controller is used to eliminate this offset. With the integral action, the output of the controller is changed at a rate proportional to the error by the integral gain ($K_i = \dfrac{K_p}{T_i}$), as:

$$I = K_i \int e(t) \, dt$$

(A.2)

The integral term determines the reaction based on the sum of past errors. Although the integral part of the controller is used to eliminate the steady-state error, it may make the transient response worse, i.e. increase the overshoot and the settling time.

To improve the transient response and decrease the overshoot, the derivative action is added. The derivative term determines the reaction based on future error. With the derivative action, the controller output is proportional to the rate of change of the error signal multiplied by a constant ($Kd = K_p.T_d$), as:

$$D = K_d \cdot \left(\frac{de}{dt} \right) \tag{A.3}$$

The PID controller has the advantages of the three mentioned control actions. The PID controller is a combination of these three terms and is expressed as:

$$u(t) = K_p\, e(t) + K_i \int e(t)dt + K_d \left(\frac{de}{dt} \right) \tag{A.4}$$

A.2   Fuzzy logic control

Fuzzy logic is an approach in computer science that mimics the way a human brain thinks and solves problems. The idea of fuzzy logic is to approximate human decision making using natural language terms instead of quantitative terms. The concept of fuzzy logic was introduced in 1965 by Lotfi Zadeh, a professor at the University of California at Berkley, as a way of processing data by allowing partial set membership rather than crisp set membership or non-membership. This approach to set theory was not applied to control systems until the 1970's due to insufficient and small-computer capability prior to that time. After the implementation of FLC by Mamdani on system

engine in 1974 (Mamdani, 1974), FLC was implemented in many practical applications such as the subway Sendai Transportation control system in Japan, automated aircraft vehicle landing and the first fuzzy TV set by Sony in 1990.

Fuzzy logic control is very robust and forgiving of operator and data input and often works when first implemented with little or no tuning. Nowadays, FLC is widely used to control consumer products such as rice cooker, washing machines and video cameras. It is also used as a powerful tool to control different systems in many areas such as underground trains, robots and cement kilns.

A typical fuzzy system comprises of fuzzy rules, membership functions and an inference system. Figure A.1 shows the basic configuration of a fuzzy logic system.
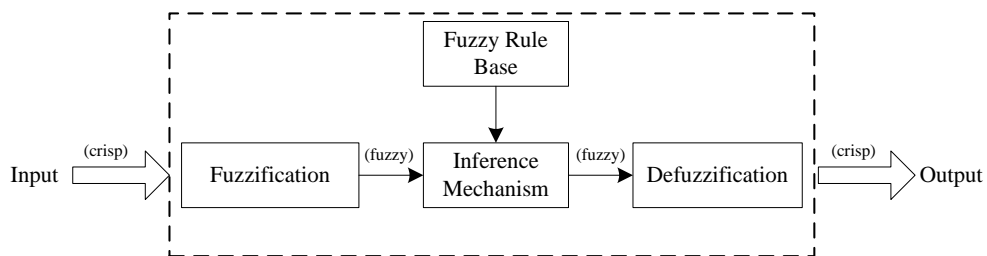
Figure A.1: Basic configuration of a fuzzy logic system

A.2.1 Fuzzy sets

An ordinary set can be defined as a collection of objects of any kind such as books, bags, cars. Once all the members of a set have been defined, the set is fully determined. If an individual object (u) is a member of a set (S), this can be expressed as $u \in S$, while if the object (u) is not a member of the set (S), this can be written as $u \notin S$.

Any set is a subset of a universal set (U) that contains all the possible elements having the nature and property being investigated. For example, in the set "Racing Cars" the universal set will be "All Cars". The mapping from the universal set into a defined set is known as membership function (Mahfouf, 2011).

The membership function (μ) of a fuzzy set (S) is a continuous function in the range [0, 1]. The membership function quantifies the certainty of an element that belongs to a fuzzy set. Each membership function has a boundary that starts from one point and ends at another. This boundary might fall into a triangle, Gaussian or trapezium shape. The elements that are mapped by the membership functions are said to be its members. Figure A.2 shows a triangular membership function.
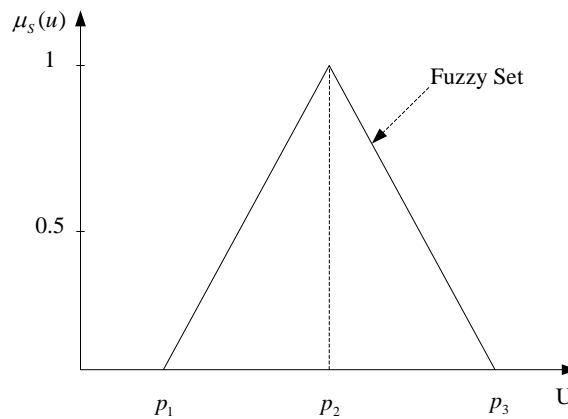
Figure A.2: An illustration of a triangular membership function

A fuzzy set (S) in the universe (U) is a set of ordered pairs of an element (u) and its membership degree $\mu_S(u)$ such that:

$$S = \{(u, \mu_S(u)) \mid u \in U\} \qquad \textbf{(A.5)}$$

A.2.2 Fuzzification

The process of converting a numeric input into a fuzzy input is known as "fuzzification". Fuzzification maps a crisp input $u_i \in U$ into fuzzy set (S_{ui}) in U in two ways; singleton and non-singleton. The fuzzy set (S_{ui}) is a fuzzy singleton such that the membership function ($\mu_{S_{u_i}}$):

$$\mu_{S_{u_i}}(u) = \begin{cases} 1 & if \ \ u = u_i \\ 0 & otherwise \end{cases} \quad \textbf{(A.6)}$$

The fuzzy set (S_{ui}) is a fuzzy non-singleton such that the membership function ($\mu_{S_{u_i}}$):

$$\mu_{S_{u_i}}(u) = \begin{cases} 1 & if \ \ u = u_i \\ decreases \ from \ 1 \ as \ u \ moves \ from \ u_i \end{cases} \quad \textbf{(A.7)}$$

The singleton fuzzification is generally used in implementations where there is no noise (Mahfouf, 2011).

A.2.3 Fuzzy inference mechanism

A fuzzy inference is a mechanism that uses fuzzy set theory to map input to output based on user defined rules. The fuzzy inference process involves the membership functions, fuzzy logic operators and user defined if-then rules base. There are two types of fuzzy rules processing widely employed in various control applications. These are the Mamdani-type and Sugeno-type fuzzy rules processing.

Mamdani's fuzzy inference method is the most commonly employed. Mamdani method considers the output membership functions as fuzzy set. After aggregation process there is a fuzzy set for each output variable that needs defuzzification. The Sugeno-type method replaces the consequent part of the fuzzy rules by a function.

A.2.3.1 Fuzzy rule base

A set of linguistic statements based on expert knowledge forms the fuzzy rule base. Each rule is usually expressed in the form of if-then format. The rules may use several

variables for both the condition and the conclusion part of the rule. Fuzzy systems are divided into two categories depending on the type of their fuzzy rules:

- Standard fuzzy systems: This fuzzy system uses linguistic fuzzy rules (Mamdani-type fuzzy rules) which are solely formed from linguistic variables and values. The general form of Mamdani rules is

  IF <premise> **OPERATION** <premise> **THEN** <consequent>

- Functional fuzzy systems: This is known as Takagi-Sugeno-Kang (TSK) fuzzy system, proposed as an alternative to the standard fuzzy systems. The TSK rules can be described as:

  IF x_1 is A_1 and x_2 is A_2 and…and x_n is A_n **THEN** $y = f(x_1, x_2,…,x_n)$

The IF part of the rules are the same as the standard fuzzy; however, the consequent part in the standard fuzzy is replaced by a function (*f*). This function can be linear, non-linear, static or dynamic function (Mahfouf, 2011).

A.2.4 Defuzzification

The fuzzy output, resulting from the fired fuzzy rules, needs to be translated to crisp values. This translation is achieved by a defuzzification process. Defuzzification is the process of producing single crisp value that best represents the inferred fuzzy value of the output. There are several widely used defuzzification methods such as centroid of

gravity (COG), maximum membership and weighted average. In this study, centroid of gravity (COG) and weighted average methods are used as described below:

- Centroid of gravity (COG): This is also known as Centroid of Area (COA) method that computes the centroid of the composite representing the output fuzzy term. Figure A.3 shows an illustration of the COG defuzzification method, where u_c is chosen to represent the centre of gravity of the shaded area.
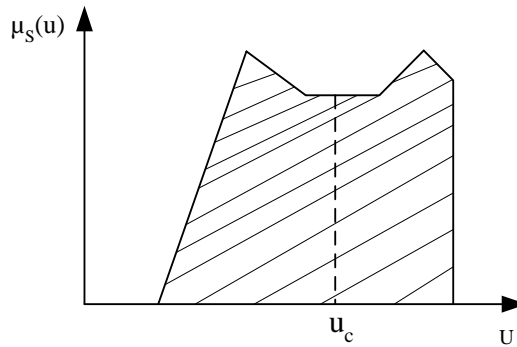
Figure A.3: The COG defuzzification method

$$u_c = \begin{cases} \dfrac{\int \mu_A(u).u.du}{\int \mu_A(u).du} & \text{in the continuous case} \\[4mm] \dfrac{\sum \mu_A(u).u}{\sum \mu_A(u)} & \text{in the discrete case} \end{cases} \qquad \text{(A.8)}$$

- Weighted average: In this method each membership function of the output is weighted by the membership's maximum value. The weighted average defuzzification method can be expressed as:

$$D = \frac{\sum\limits_{i=1}^{n} w_i z_i}{\sum\limits_{i=1}^{n} w_i} \qquad \text{(A.9)}$$

where D is the defuzzified output, z_i is the output value of each rule, w_i is the weight, of each rule. Although this method is usually restricted to symmetrical output membership functions, it is easy to implement, computationally fast and produces fairly accurate results (Ross, 2010).

A.3 Flywheel and electrical clutch mechanism

A.3.1 Flywheel energy storage

A flywheel is a rotating mechanical device that stores energy in the form of kinetic energy. The faster the flywheel rotates the more kinetic energy it stores. The flywheel spins with the aid of a shaft at which energy transfer, to/from the flywheel, takes place. The flywheel is mainly beneficial in systems where the main power source is unsteady, i.e. provides unsteady bursts. In such systems, the flywheel absorbs the energy as it is released from the main source in a burst, and releases it when the energy in the main source decreases. Hence, by the use of the flywheel, such systems receive steady and uninterruptable source of energy.

The flywheel has been used in different applications for a long time. One of the earliest uses of the flywheel is the potter's wheel. The potter's wheel is a mechanical device equipped with a rotating turntable used to shape the clay. The turntable is connected with a rotating flywheel through a shaft. As the potter rotates the wheel, the flywheel keeps the speed of the turntable stable. Due to the kinetic energy stored in the flywheel, the turntable keeps rotating even if the operator stopped pedaling. Hence, the use of the flywheel enables the potter to form the clay without suffering from problems due to unsteady rate of speed. Nowadays, the flywheel is used in electrical systems to rectify power surges and in cars to smoothen the vibration, due to rapid explosions, in the engine.

The inertia of a ring ($\frac{r_0}{r_1} \to 1$, where r_0 is the outer radius and r_1 is the inner radius) flywheel around axis of rotation can be expressed as:

$$I = r^2 m \tag{A.10}$$

where r is the radius of the flywheel [m] and m is the mass [kg]. The kinetic energy of the flywheel is calculated as:

$$E_k = \frac{1}{2} I\omega^2 \tag{A.11}$$

where E_k is the kinetic energy [J], I is the moment of inertia around its center of mass [$kg.m^2$], and ω is the angular velocity [rad/s].

It is clear from equations (A.10) and (A.11) that the energy of the flywheel depends on the inertia and the angular velocity of the flywheel. The inertia of the flywheel depends on the mass, radius and the shape of the flywheel. The angular velocity of the flywheel has greater impact on the amount of energy stored by the flywheel than the inertia. If the angular velocity of the flywheel doubles, the amount of the energy the flywheel stores will quadruple. However, a flywheel cannot rotate at a speed faster than its material's density and strength can support. The flywheel breaks apart if the stresses in the flywheel exceed the tensile strength of the material (Östergård, 2011). The maximum tensile strength of a thin rim flywheel can be expressed as:

$$\sigma_{max} = \rho r^2 \omega^2 \tag{A.12}$$

where σ_{max} is the maximum tensile stress [N/m^2] and ρ is the density of the material [kg/m^3].

From equations (A.11) and (A.12) a general expression of the maximum specific energy ($e_{k,m}$) [J/kg] and energy density ($e_{k,v}$) [J/m^3] for a certain material used to make the flywheel can be expressed as:

$$e_{k,m} = K\frac{\sigma_{max}}{\rho} \tag{A.13}$$

$$e_{k,v} = K\sigma_{max} \tag{A.14}$$

where K is a shape factor of the flywheel.

Figure A.4 shows the most common flywheel geometries with their shape factors. It is obvious from equation (A.14) that to obtain high energy density, materials of high tensile strength are required. However, the overall weight of the system is crucial for most applications. This is taken in consideration from the specific energy of the flywheel, equation (A.13). Hence, the optimal material for flywheels is that of high tensile strength and low density. Table A.1 shows the properties of different flywheel materials.
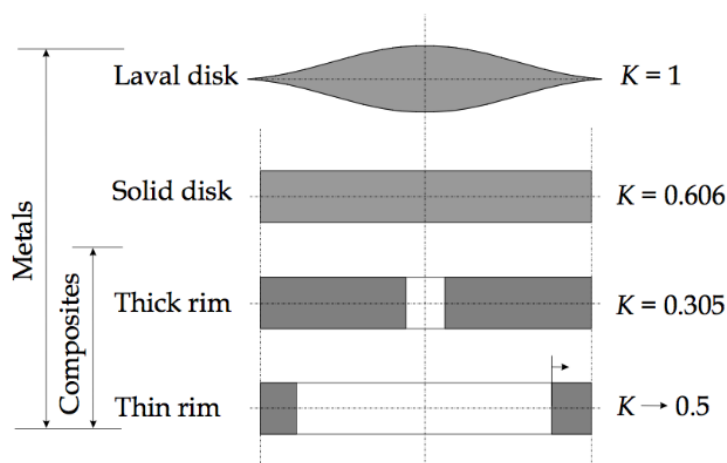
Figure A.4: Different shapes of flywheel with associated shape factor values (Östergård, 2011)

Table A.1: Properties of different flywheel materials (Östergård, 2011)

Material	Density [kg/m^3]	Tensile strength [GPa]	Specific energy [Wh/kg]
Steel			
4320 Steel	7700	1.52	50
AISI 4340	7800	1.80	64
Alloy			
AlMnMg	2700	0.60	62
Titanium			
TiAl6Zr	4500	1.20	74
Composites			
E-glass	200	0.10	14
S-Glass	1920	1.4	210
Carbon T-1000	1520	1.95	350
Projected composites	1780	10	780

Using modern materials, the flywheels become smaller, lighter, faster and can store more energy. One of the most promising fields where the flywheel has been used is the automotive industry. It has been used for Formula 1 racing cars to reduce fuel consumption (Cross and Brockbank, 2009). In flywheel hybrid car system, the flywheel stores energy from the car as it breaks and reuses this energy to accelerate the car, after slowing down or stopping, instead of consuming the fuel. The flywheels would never lose their ability to charge and discharge, unlike batteries, so they would be more efficient, cheaper and friendly to the environment.

A.3.2 Electrical clutches

Electrical clutches are equipment drive assemblies that use electrically actuated components to connect two shafts so that they can either lock and rotate together at same speed or decouple and rotate separately at different speeds.

Clutch engagement leads to transfer power from an engine to devices such as drive wheels and transmission. Clutch disengagement stops power transfer but allows the engine to continue running. Electrical clutches are faster than pneumatic or hydraulic clutches, however they do not provide the same range of torque.

Electrical clutches are useful for automatic machinery, such as printers, conveyors and textile machinery, that use electrical control signals to activate the clutch rather than a lever or a pedal. Also, they are beneficial in applications where the

clutch is far from the control point that the mechanical connection of a pneumatic or hydraulic piping would be extremely difficult and expensive.

Electrical clutches are electrically activated but transmit torque mechanically. For this reason, they are also known as electro-mechanical or electromagnetic clutches. Several types of electrical clutches are available nowadays to suit different applications. The most popular type is friction-plate electromagnetic clutch. However, the basic operation of all electrical clutches remains the same (Thomson, 2014). Figure A.5 shows an example of an electromagnetic clutch. When the clutch is activated by electrical signal, a magnetic field will be generated in the coil. The magnetic field overcomes the air gap between the rotor and the armature. The magnetic attraction pulls the armature to contact with the rotor. The frictional contact between the armature and the rotor causes the rotational motion to start. The resultant torque is the outcome of the magnetic attraction and the friction between the steel of the rotor and the steel of the armature. When the coil is de-energized, the armature and the rotor are no longer attracted and separated by a spring within the armature assembly. The motor shaft and the load are no longer connected, the motor continues running while the load is idle.
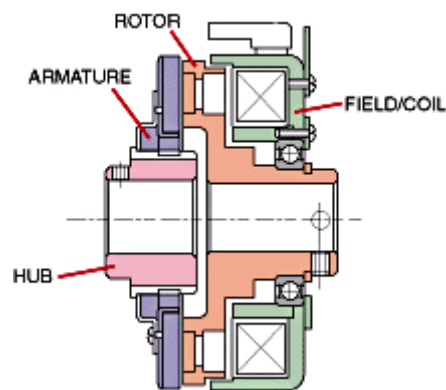
Figure A.5: An example of electromagnetic clutches
(Electromagnetic clutch, 2014)

A.4 Mechanical gears

A gear is a mechanical rotating part with teeth, combines and meshes with another similar part, in most cases of different size, to obtain mechanical advantages through a gear ratio. A gearbox, between a device and its load, is generally designed to provide transmission and change in speed and torque, known as mechanical advantage, between the output of the device and the load (Tooley and Dingle, 2013). Devices equipped with gears are able to change the speed, direction of motion, torque and the power of the source. Gears are often used in transmission systems due to being rigid, non slippery and efficient transmission devices. Several types of gears, such as spur, bevel, helical, non-circular, can be designed according to the application. Regardless of their different shapes, they all work under the same basic principle. For example, the transmission system in automotive is commonly helical to provide smooth and efficient meshing which consequently leads to quieter action. On the other hand, bevel gears can be used to provide transmission in application with right angles such as hand drills.

In a simple gear train that consists of two gears, the input gear, also known as the driver gear, which is connected to the power source, such as motor or engine, transmits the power of the input source to the load through the output gear or the driven gear. The velocity of the pitch circle at the contact point of the two gears is the same and given by:

$$v = r_A \omega_A = r_B \omega_B \qquad \text{(A.15)}$$

where r_A and r_B are the radii [m] of the pitch circles, ω_A and ω_B are the angular velocities [*rad/s*] of gear A and gear B. Figure A.6 shows an illustration of a spur gear between a motor and its load.
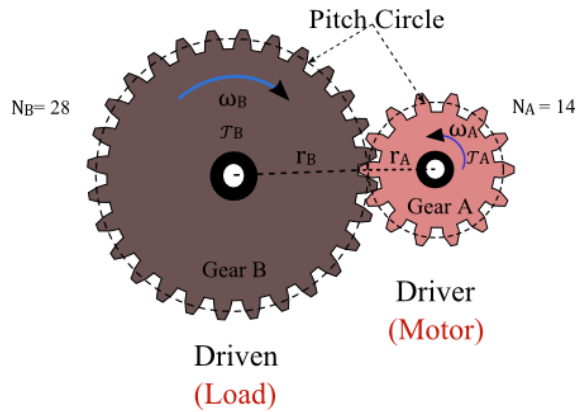
Figure A.6: Shows spur gears between a motor and its load

The number of teeth in a gear is proportional to the radius of its pitch circle; hence the ratio of the number of teeth, radii and the angular velocities are the same and the gear ratio between a simple pair of gears can be expressed as:

$$R = \frac{\omega_A}{\omega_B} = \frac{r_B}{r_A} = \frac{N_B}{N_A} \tag{A.16}$$

where R is the gear ratio, N_A and N_B are the number of teeth of gear A and gear B respectively.

Equation (A.16) implies that if the number of teeth of the output gear, gear B, is larger than the number of teeth of the input gear, gear A, the input gear will rotate faster than the output gear. Also, it implies that the gear ratio, or the speed ratio, is inversely proportional to the number of teeth and the radius of the pitch circle of the gears. Further, the torque (T_A) applied to the input gear and the torque (T_B) at the output gear are also proportional as:

$$R = \frac{T_B}{hT_A} = MA \tag{A.17}$$

The torque ratio, which is equal to the gear ratio R, is also known as the mechanical advantage (MA) of the gear, where h is the efficiency factor of the gearbox.

The gear ratio between a motor and its load is used to alter the effective inertia of the load with respect to the input. Figure A.7 shows an illustration of a gear ratio (R) between a motor and a flywheel. The effective inertia of the flywheel can be derived as follows:
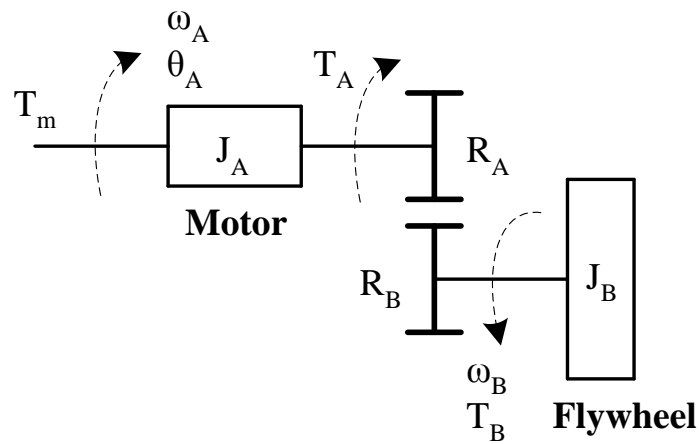
Figure A.7: An illustration of a simple gearbox between a motor and a flywheel. Where T_m is the motor torque [N.m], T_A and T_B are the input and ouput torque of the gearbox [N.m], θ_A is the rotation angle [rad], ω_A and ω_B are the angular velocities in the input and output respectively [rad/s], J_A and J_B are the mass moment of inertia of the motor and the flywheel respectively [kg.m2]

The input power ($P_{A=}T_A.\omega_A$) [W] is equal to the output power ($P_{B=}T_B.\omega_B$) [W] in case of an ideal gearbox, i.e. frictionless with efficiency factor (h) equal to 1.

$$hT_A\omega_A = T_B\omega_B \quad \Rightarrow \quad T_B = hT_A\frac{\omega_A}{\omega_B} \qquad \textbf{(A.18)}$$

The inertia torque of the flywheel is calculated as:

$$J_B \alpha_B = T_B \qquad\qquad\qquad\qquad \text{(A.19)}$$

The inertia torque of the motor can be expressed as:

$$J_A \alpha_A = T_m - T_A \qquad\qquad\qquad\qquad \text{(A.20)}$$

From (A.18) and (A.19), we obtain:

$$J_B \alpha_B = h T_A \frac{\omega_A}{\omega_B} \quad \Rightarrow \quad T_A = (J_B \alpha_B) \frac{\omega_B}{h\omega_A} \qquad\qquad \text{(A.21)}$$

From (A.20) and (A.21):

$$J_A \alpha_A = T_m - \frac{\omega_B}{h\omega_A} J_B \alpha_B \quad \Rightarrow \quad T_m = J_A \alpha_A + \frac{\omega_B}{h\omega_A} J_B \alpha_B \qquad \text{(A.22)}$$

Since the gear ratio can be expressed as:

$$R = \frac{R_B}{R_A} = \frac{\omega_A}{\omega_B} = \frac{\alpha_A}{\alpha_B} \qquad\qquad\qquad \text{(A.23)}$$

From (A.22) and (A.23), we obtain the motor torque as the acceleration in the input multiplied by the inertia of the motor (J_A) and the effective inertia of the flywheel, as:

$$T_m = J_A \alpha_A + J_B \frac{\alpha_A}{hR^2} = (J_A + \frac{J_B}{hR^2})\alpha_A \qquad \textbf{(A.24)}$$

The effective/referred inertia of the flywheel with respect to the input can be expressed as:

$$J_{flywheel\,effective} = \frac{J_B}{hR^2} \qquad \textbf{(A.25)}$$

It is clear from equation (A.25) that a gear ratio greater than one will significantly reduce the effective inertia of the flywheel on the motor.

Appendix B: Inertia of the humanoid and bicycle model

This appendix provides information about the calculated inertia of the humanoid and bicycle model for 20 different crank positions. To calculate the inertia, the velocity of each segment was set to zero. Also, a resistive torque (T_R) of 0.04 [N.m] was applied to the crank. The inertia was calculated according to:

$$I = \frac{T_R}{\ddot{\theta}}$$

(B.1)

where I is the inertia [Kg.m^2], $\ddot{\theta}$ is the acceleration of the crank [rad/s^2].

For each crank angle, at the beginning of the movement, the velocity of the model is set to zero and the inertia is calculated. This process is repeated at each crank angle for 20 crank positions. Tables B.1-B.4 show the calculated inertia values at each position. The position of the crank is represented by (x,y) value where x denotes the horizontal distance of the crank from the hip joint, while y denotes the vertical position of the crank with respect to the hip joint. Further information about the different crank positions can be found in chapter five.

Table B.1: The inertia of the model at crank position 0.6m from the hip joint

Position(m) (X,Y) / Angle (deg)	Inertia [Kg.m^2]				
	(0.6, 0.1)	(0.6, 0.05)	(0.6, 0.0)	(0.6, -0.05)	(0.6, -1.0)
1	0.1266	0.1451	0.1559	0.1790	0.1910
2	0.1239	0.1415	0.1592	0.1749	0.1894
3	0.1206	0.1381	0.1549	0.1723	0.1863
4	0.1169	0.1348	0.1518	0.1685	0.1819
5	0.1146	0.1310	0.1488	0.1649	0.1790
6	0.1107	0.1273	0.1451	0.1649	0.1763
7	0.1081	0.1239	0.1415	0.1581	0.1723
8	0.1051	0.1206	0.1372	0.1538	0.1698
9	0.1019	0.1169	0.1340	0.1508	0.1661
10	0.0996	0.1146	0.1310	0.1469	0.1614
11	0.0967	0.1113	0.1273	0.1441	0.1581

Position(m) (X,Y) Angle (deg)	Inertia [Kg.m²]				
	(0.6, 0.1)	(0.6, 0.05)	(0.6, 0.0)	(0.6, -0.05)	(0.6, -1.0)
12	0.0939	0.1081	0.1239	0.1397	0.1549
13	0.0917	0.1051	0.1206	0.1364	0.1518
14	0.0892	0.1019	0.1169	0.1325	0.1479
15	0.0875	0.1001	0.1146	0.1295	0.1441
16	0.0849	0.0967	0.1107	0.1259	0.1406
17	0.0830	0.0943	0.1076	0.1226	0.1372
18	0.0816	0.0917	0.1051	0.1194	0.1340
19	0.0790	0.0895	0.1019	0.1157	0.1302
20	0.0780	0.0868	0.0996	0.1129	0.1273
21	0.0764	0.0849	0.0963	0.1102	0.1239
22	0.0751	0.0833	0.0939	0.1061	0.1206
23	0.0737	0.0810	0.0917	0.1042	0.1169
24	0.0728	0.0793	0.0888	0.1014	0.1140
25	0.0716	0.0777	0.0871	0.0979	0.1107
26	0.0710	0.0764	0.0846	0.0955	0.1076
27	0.0703	0.0751	0.0827	0.0932	0.1046
28	0.0697	0.0737	0.0810	0.0906	0.1023
29	0.0692	0.0728	0.0793	0.0881	0.0992
30	0.0690	0.0716	0.0777	0.0865	0.0971
31	0.0690	0.0710	0.0764	0.0839	0.0939
32	0.0686	0.0703	0.0747	0.0821	0.0913
33	0.0690	0.0697	0.0739	0.0804	0.0895
34	0.0690	0.0692	0.0725	0.0788	0.0871
35	0.0694	0.0690	0.0718	0.0772	0.0846
36	0.0699	0.0688	0.0710	0.0759	0.0827
37	0.0703	0.0688	0.0703	0.0742	0.0810
38	0.0712	0.0690	0.0697	0.0735	0.0793
39	0.0721	0.0690	0.0692	0.0721	0.0780
40	0.0728	0.0697	0.0690	0.0714	0.0764
41	0.0737	0.0699	0.0688	0.0707	0.0749
42	0.0749	0.0703	0.0688	0.0701	0.0739
43	0.0761	0.0712	0.0690	0.0694	0.0725
44	0.0774	0.0721	0.0692	0.0692	0.0718
45	0.0788	0.0728	0.0694	0.0690	0.0710
46	0.0799	0.0739	0.0701	0.0688	0.0703
47	0.0819	0.0749	0.0705	0.0688	0.0699
48	0.0830	0.0761	0.0714	0.0690	0.0692

Position(m) (X,Y) Angle (deg)	Inertia [Kg.m²]				
	(0.6, 0.1)	(0.6, 0.05)	(0.6, 0.0)	(0.6, -0.05)	(0.6, -1.0)
49	0.0849	0.0774	0.0721	0.0694	0.0690
50	0.0868	0.0788	0.0730	0.0697	0.0688
51	0.0885	0.0804	0.0742	0.0701	0.0688
52	0.0906	0.0819	0.0754	0.0707	0.0690
53	0.0920	0.0836	0.0764	0.0718	0.0692
54	0.0947	0.0852	0.0777	0.0723	0.0694
55	0.0963	0.0868	0.0790	0.0735	0.0701
56	0.0984	0.0888	0.0804	0.0747	0.0705
57	0.1010	0.0902	0.0821	0.0754	0.0714
58	0.1028	0.0928	0.0843	0.0769	0.0718
59	0.1046	0.0943	0.0855	0.0782	0.0728
60	0.1076	0.0967	0.0871	0.0796	0.0742
61	0.1097	0.0988	0.0888	0.0807	0.0749
62	0.1118	0.1010	0.0906	0.0827	0.0761
63	0.1146	0.1032	0.0932	0.0839	0.0772
64	0.1169	0.1056	0.0959	0.0858	0.0790
65	0.1187	0.1076	0.0971	0.0878	0.0804
66	0.1219	0.1102	0.0992	0.0895	0.0816
67	0.1239	0.1123	0.1014	0.0913	0.0833
68	0.1266	0.1146	0.1037	0.0935	0.0852
69	0.1295	0.1175	0.1051	0.0955	0.0871
70	0.1317	0.1194	0.1081	0.0975	0.0881
71	0.1340	0.1219	0.1102	0.0996	0.0906
72	0.1372	0.1246	0.1129	0.1019	0.0928
73	0.1397	0.1273	0.1146	0.1042	0.0943
74	0.1423	0.1295	0.1181	0.1061	0.0963
75	0.1441	0.1317	0.1194	0.1086	0.0988
76	0.1479	0.1348	0.1169	0.1107	0.1005
77	0.1498	0.1364	0.1246	0.1135	0.1032
78	0.1518	0.1397	0.1273	0.1157	0.1051
79	0.1549	0.1423	0.1295	0.1181	0.1081
80	0.1570	0.1441	0.1325	0.1206	0.1097
81	0.1592	0.1469	0.1348	0.1232	0.1123
82	0.1625	0.1498	0.1381	0.1252	0.1146
83	0.1649	0.1528	0.1397	0.1280	0.1169
84	0.1673	0.1549	0.1423	0.1310	0.1194
85	0.1698	0.1570	0.1451	0.1332	0.1219
86	0.1723	0.1603	0.1479	0.1356	0.1246

Position(m) (X,Y) Angle (deg)	Inertia [Kg.m²]				
	(0.6, 0.1)	(0.6, 0.05)	(0.6, 0.0)	(0.6, -0.05)	(0.6, -1.0)
87	0.1749	0.1625	0.1488	0.1381	0.1266
88	0.1763	0.1649	0.1528	0.1406	0.1295
89	0.1790	0.1673	0.1549	0.1432	0.1317
90	0.1819	0.1698	0.1581	0.1460	0.1348
91	0.1833	0.1723	0.1603	0.1479	0.1364
92	0.1863	0.1736	0.1625	0.1508	0.1397
93	0.1879	0.1763	0.1649	0.1538	0.1423
94	0.1910	0.1790	0.1673	0.1559	0.1451
95	0.1926	0.1819	0.1698	0.1581	0.1469
96	0.1959	0.1833	0.1723	0.1614	0.1498
97	0.1976	0.1863	0.1749	0.1637	0.1518
98	0.1993	0.1879	0.1777	0.1661	0.1549
99	0.2010	0.1910	0.1790	0.1685	0.1570
100	0.2028	0.1926	0.1819	0.1710	0.1603
101	0.2065	0.1942	0.1848	0.1736	0.1625
102	0.2083	0.1976	0.1863	0.1749	0.1649
103	0.2083	0.1993	0.1879	0.1777	0.1673
104	0.2103	0.2010	0.1910	0.1805	0.1698
105	0.2142	0.2028	0.1926	0.1833	0.1723
106	0.2142	0.2046	0.1959	0.1848	0.1749
107	0.2162	0.2083	0.1976	0.1879	0.1763
108	0.2183	0.2083	0.1993	0.1894	0.1790
109	0.2204	0.2122	0.2010	0.1910	0.1816
110	0.2225	0.2122	0.2028	0.1942	0.1839
111	0.2225	0.2142	0.2046	0.1959	0.1863
112	0.2247	0.2162	0.2083	0.1976	0.1894
113	0.2269	0.2183	0.2103	0.2010	0.1910
114	0.2269	0.2204	0.2122	0.2028	0.1926
115	0.2292	0.2225	0.2122	0.2046	0.1959
116	0.2301	0.2225	0.2142	0.2065	0.1976
117	0.2310	0.2247	0.2162	0.2083	0.1993
118	0.2324	0.2269	0.2183	0.2103	0.2010
119	0.2334	0.2269	0.2204	0.2122	0.2028
120	0.2343	0.2292	0.2225	0.2142	0.2055
121	0.2353	0.2301	0.2225	0.2162	0.2083
122	0.2360	0.2315	0.2247	0.2183	0.2093
123	0.2368	0.2324	0.2269	0.2183	0.2112
124	0.2375	0.2336	0.2269	0.2204	0.2142

Position(m) (X,Y) Angle (deg)	Inertia [Kg.m²]				
	(0.6, 0.1)	(0.6, 0.05)	(0.6, 0.0)	(0.6, -0.05)	(0.6, -1.0)
125	0.2382	0.2346	0.2292	0.2225	0.2142
126	0.2387	0.2355	0.2303	0.2247	0.2162
127	0.2392	0.2365	0.2315	0.2247	0.2183
128	0.2395	0.2372	0.2329	0.2269	0.2204
129	0.2397	0.2380	0.2339	0.2292	0.2225
130	0.2400	0.2387	0.2348	0.2296	0.2225
131	0.2400	0.2392	0.2358	0.2306	0.2247
132	0.2400	0.2397	0.2365	0.2320	0.2269
133	0.2397	0.2400	0.2375	0.2329	0.2269
134	0.2395	0.2402	0.2382	0.2341	0.2292
135	0.2397	0.2405	0.2387	0.2351	0.2301
136	0.2385	0.2407	0.2395	0.2360	0.2310
137	0.2380	0.2407	0.2400	0.2368	0.2324
138	0.2375	0.2407	0.2402	0.2375	0.2334
139	0.2365	0.2405	0.2405	0.2382	0.2343
140	0.2358	0.2402	0.2407	0.2390	0.2353
141	0.2346	0.2400	0.2410	0.2395	0.2360
142	0.2336	0.2395	0.2407	0.2397	0.2370
143	0.2322	0.2390	0.2410	0.2402	0.2375
144	0.2310	0.2380	0.2407	0.2405	0.2382
145	0.2294	0.2375	0.2405	0.2407	0.2387
146	0.2269	0.2365	0.2400	0.2407	0.2392
147	0.2269	0.2355	0.2402	0.2407	0.2395
148	0.2247	0.2346	0.2390	0.2407	0.2400
149	0.2225	0.2331	0.2385	0.2405	0.2400
150	0.2204	0.2320	0.2377	0.2402	0.2402
151	0.2183	0.2303	0.2365	0.2397	0.2402
152	0.2162	0.2292	0.2355	0.2392	0.2400
153	0.2142	0.2269	0.2346	0.2387	0.2400
154	0.2103	0.2247	0.2336	0.2377	0.2395
155	0.2083	0.2225	0.2320	0.2370	0.2392
156	0.2065	0.2225	0.2306	0.2360	0.2387
157	0.2028	0.2183	0.2292	0.2351	0.2380
158	0.2010	0.2162	0.2269	0.2341	0.2375
159	0.1976	0.2142	0.2247	0.2324	0.2368
160	0.1942	0.2122	0.2225	0.2310	0.2355
161	0.1910	0.2103	0.2204	0.2296	0.2348
162	0.1959	0.2065	0.2183	0.2292	0.2334

Position(m) (X,Y) / Angle (deg)	Inertia [Kg.m²]				
	(0.6, 0.1)	(0.6, 0.05)	(0.6, 0.0)	(0.6, -0.05)	(0.6, -1.0)
163	0.1894	0.2046	0.2183	0.2269	0.2324
164	0.1819	0.2010	0.2142	0.2247	0.2308
165	0.1777	0.1993	0.2122	0.2225	0.2294
166	0.1749	0.1959	0.1993	0.2204	0.2292
167	0.1710	0.1926	0.2065	0.2183	0.2269
168	0.1673	0.1894	0.2046	0.2162	0.2247
169	0.1649	0.1848	0.2010	0.2142	0.2225
170	0.1614	0.1833	0.1976	0.2103	0.2204
171	0.1581	0.1790	0.1959	0.2083	0.2183
172	0.1538	0.1763	0.1926	0.2065	0.2162
173	0.1508	0.1723	0.1894	0.2028	0.2142
174	0.1469	0.1685	0.1863	0.1993	0.2122
175	0.1432	0.1649	0.1819	0.1976	0.2065
176	0.1415	0.1592	0.1790	0.1942	0.2046
177	0.1397	0.1549	0.1749	0.1910	0.2028
178	0.1364	0.1508	0.1723	0.1879	0.1993
179	0.1332	0.1479	0.1685	0.1848	0.1976
180	0.1288	0.1432	0.1661	0.1805	0.1942
181	0.1259	0.1406	0.1614	0.1777	0.1910
182	0.1226	0.1372	0.1581	0.1736	0.1879
183	0.1194	0.1332	0.1538	0.1710	0.1848
184	0.1157	0.1295	0.1508	0.1673	0.1819
185	0.1135	0.1266	0.1479	0.1637	0.1790
186	0.1097	0.1226	0.1432	0.1603	0.1749
187	0.1066	0.1200	0.1397	0.1570	0.1710
188	0.1037	0.1163	0.1364	0.1528	0.1685
189	0.1014	0.1129	0.1332	0.1498	0.1649
190	0.0984	0.1102	0.1288	0.1460	0.1614
191	0.0959	0.1071	0.1259	0.1423	0.1570
192	0.0932	0.1042	0.1226	0.1389	0.1538
193	0.0909	0.1010	0.1194	0.1348	0.1508
194	0.0885	0.0988	0.1163	0.1317	0.1469
195	0.0862	0.0955	0.1123	0.1280	0.1432
196	0.0843	0.0932	0.1097	0.1246	0.1406
197	0.0830	0.0909	0.1066	0.1219	0.1356
198	0.0804	0.0881	0.1037	0.1181	0.1332
199	0.0788	0.0865	0.1005	0.1146	0.1288
200	0.0772	0.0843	0.0979	0.1123	0.1266

Position(m) (X,Y) Angle (deg)	Inertia [Kg.m²]				
	(0.6, 0.1)	(0.6, 0.05)	(0.6, 0.0)	(0.6, -0.05)	(0.6, -1.0)
201	0. 0761	0.0824	0.0955	0.1086	0.1226
202	0.0747	0.0807	0.0932	0.1056	0.1187
203	0.0735	0.0790	0.0909	0.1023	0.1163
204	0.0725	0.0774	0.0885	0.1001	0.1123
205	0.0716	0.0759	0.0858	0.0971	0.1097
206	0.0710	0.0744	0.0839	0.0947	0.1066
207	0.0703	0.0737	0.0824	0.0920	0.1042
208	0.0699	0.0725	0.0801	0.0895	0.1005
209	0.0694	0.0716	0.0785	0.0878	0.0988
210	0.0692	0.0710	0.0774	0.0852	0.0955
211	0.0692	0.0703	0.0759	0.0836	0.0932
212	0.0692	0.0699	0.0744	0.0813	0.0902
213	0.0692	0.0694	0.0735	0.0799	0.0888
214	0.0694	0.0692	0.0723	0.0780	0.0862
215	0.0701	0.0692	0.0716	0.0769	0.0846
216	0.0703	0.0692	0.0705	0.0754	0.0821
217	0.0712	0.0694	0.0703	0.0739	0.0804
218	0.0716	0.0697	0.0699	0.0732	0.0774
219	0.0725	0.0699	0.0694	0.0721	0.0788
220	0.0737	0.0613	0.0692	0.0714	0.0774
221	0.0744	0.0712	0.0692	0.0705	0.0756
222	0.0756	0.0718	0.0692	0.0701	0.0749
223	0.0769	0.0730	0.0694	0.0697	0.0735
224	0.0777	0.0737	0.0697	0.0694	0.0728
225	0.0796	0.0747	0.0701	0.0692	0.0716
226	0.0810	0.0759	0.0707	0.0692	0.0710
227	0.0827	0.0772	0.0712	0.0692	0.0703
228	0.0839	0.0785	0.0721	0.0694	0.0699
229	0.0858	0.0796	0.0730	0.0697	0.0694
230	0.0878	0.0813	0.0737	0.0703	0.0692
231	0.0895	0.0827	0.0749	0.0707	0.0692
232	0.0913	0.0843	0.0759	0.0716	0.0692
233	0.0935	0.0862	0.0772	0.0723	0.0697
234	0.0951	0.0878	0.0782	0.0732	0.0699
235	0.0975	0.0899	0.0801	0.0742	0.0705
236	0.0996	0.0917	0.0813	0.0754	0.0710
237	0.1019	0.0932	0.0833	0.0764	0.0718
238	0.1042	0.0955	0.0846	0.0777	0.0725

Position(m) (X,Y) Angle (deg)	Inertia [Kg.m²]				
	(0.6, 0.1)	(0.6, 0.05)	(0.6, 0.0)	(0.6, -0.05)	(0.6, -1.0)
239	0.1061	0.0975	0.0865	0.0790	0.0735
240	0.1086	0.0996	0.0881	0.0801	0.0747
241	0.1107	0.1019	0.0902	0.0821	0.0759
242	0.1129	0.1042	0.0917	0.0833	0.0769
243	0.1152	0.1061	0.0939	0.0852	0.0782
244	0.1175	0.1086	0.0963	0.0868	0.0796
245	0.1200	0.1107	0.0979	0.0888	0.0813
246	0.1226	0.1129	0.1001	0.0906	0.0824
247	0.1252	0.1157	0.1023	0.0924	0.0846
248	0.1273	0.1175	0.1042	0.0947	0.0858
249	0.1302	0.1206	0.1066	0.0963	0.0878
250	0.1317	0.1206	0.1091	0.0984	0.0892
251	0.1348	0.1252	0.1113	0.1010	0.0917
252	0.1372	0.1280	0.1135	0.1028	0.0932
253	0.1406	0.1295	0.1163	0.1046	0.0959
254	0.1423	0.1325	0.1187	0.1076	0.0975
255	0.1451	0.1356	0.1194	0.1097	0.0996
256	0.1479	0.1372	0.1181	0.1118	0.1019
257	0.1498	0.1397	0.1252	0.1146	0.1037
258	0.1528	0.1432	0.1280	0.1169	0.1066
259	0.1549	0.1451	0.1310	0.1187	0.1081
260	0.1570	0.1469	0.1317	0.1219	0.1107
261	0.1603	0.1498	0.1356	0.1239	0.1135
262	0.1625	0.1528	0.1381	0.1266	0.1157
263	0.1649	0.1549	0.1415	0.1288	0.1181
264	0.1673	0.1570	0.1432	0.1317	0.1206
265	0.1698	0.1603	0.1451	0.1340	0.1226
266	0.1723	0.1625	0.1488	0.1356	0.1252
267	0.1736	0.1649	0.1508	0.1389	0.1273
268	0.1763	0.1673	0.1528	0.1406	0.1302
269	0.1790	0.1698	0.1549	0.1432	0.1325
270	0.1819	0.1723	0.1581	0.1460	0.1348
271	0.1833	0.1736	0.1603	0.1488	0.1381
272	0.1863	0.1763	0.1625	0.1518	0.1397
273	0.1879	0.1790	0.1625	0.1538	0.1423
274	0.1910	0.1819	0.1673	0.1559	0.1451
275	0.1926	0.1833	0.1698	0.1581	0.1479
276	0.1942	0.1863	0.1723	0.1614	0.1498

Position(m) (X,Y)	Inertia [Kg.m²]				
Angle (deg)	(0.6, 0.1)	(0.6, 0.05)	(0.6, 0.0)	(0.6, -0.05)	(0.6, -1.0)
277	0.1959	0.1879	0.1749	0.1637	0.1518
278	0.1993	0.1910	0.1777	0.1661	0.1549
279	0.2010	0.1926	0.1790	0.1685	0.1581
280	0.2028	0.1942	0.1819	0.1710	0.1603
281	0.2046	0.1959	0.1833	0.1723	0.1625
282	0.2065	0.1993	0.1863	0.1749	0.1649
283	0.2083	0.2010	0.1879	0.1777	0.1673
284	0.2103	0.2028	0.1910	0.1805	0.1698
285	0.2122	0.2046	0.1926	0.1819	0.1723
286	0.2142	0.2065	0.1942	0.1848	0.1749
287	0.2162	0.2083	0.1976	0.1863	0.1777
288	0.2162	0.2103	0.1993	0.1894	0.1790
289	0.2183	0.2122	0.2010	0.1910	0.1819
290	0.2204	0.2142	0.2028	0.1926	0.1833
291	0.2225	0.2162	0.2046	0.1959	0.1863
292	0.2225	0.2162	0.2065	0.1976	0.1879
293	0.2247	0.2183	0.2083	0.1993	0.1894
294	0.2269	0.2183	0.2103	0.2010	0.1926
295	0.2269	0.2225	0.2122	0.2028	0.1942
296	0.2292	0.2225	0.2142	0.2046	0.1959
297	0.2296	0.2247	0.2162	0.2083	0.1993
298	0.2308	0.2269	0.2183	0.2083	0.2010
299	0.2317	0.2269	0.2183	0.2103	0.2028
300	0.2329	0.2292	0.2204	0.2122	0.2046
301	0.2336	0.2299	0.2225	0.2142	0.2065
302	0.2346	0.2310	0.2247	0.2162	0.2083
303	0.2353	0.2322	0.2247	0.2183	0.2103
304	0.2360	0.2329	0.2269	0.2204	0.2122
305	0.2365	0.2339	0.2269	0.2204	0.2142
306	0.2372	0.2348	0.2292	0.2225	0.2162
307	0.2377	0.2355	0.2299	0.2247	0.2162
308	0.2380	0.2363	0.2313	0.2247	0.2183
309	0.2382	0.2370	0.2322	0.2269	0.2204
310	0.2385	0.2375	0.2334	0.2269	0.2225
311	0.2385	0.2380	0.2343	0.2292	0.2225
312	0.2387	0.2385	0.2351	0.2315	0.2247
313	0.2385	0.2387	0.2360	0.2299	0.2269
314	0.2385	0.2390	0.2368	0.2303	0.2269

Position(m) (X,Y) Angle (deg)	Inertia [Kg.m²]				
	(0.6, 0.1)	(0.6, 0.05)	(0.6, 0.0)	(0.6, -0.05)	(0.6, -1.0)
315	0.2382	0.2392	0.2372	0.2315	0.2292
316	0.2377	0.2392	0.2377	0.2324	0.2299
317	0.2375	0.2392	0.2382	0.2336	0.2308
318	0.2368	0.2390	0.2387	0.2343	0.2317
319	0.2360	0.2387	0.2390	0.2353	0.2329
320	0.2355	0.2385	0.2392	0.2360	0.2336
321	0.2346	0.2382	0.2395	0.2368	0.2346
322	0.2334	0.2377	0.2395	0.2372	0.2353
323	0.2324	0.2370	0.2395	0.2377	0.2360
324	0.2315	0.2363	0.2395	0.2382	0.2368
325	0.2299	0.2355	0.2392	0.2387	0.2372
326	0.2292	0.2343	0.2387	0.2390	0.2377
327	0.2269	0.2334	0.2385	0.2392	0.2380
328	0.2247	0.2322	0.2380	0.2392	0.2382
329	0.2247	0.2310	0.2372	0.2392	0.2385
330	0.2225	0.2296	0.2365	0.2390	0.2387
331	0.2204	0.2269	0.2358	0.2387	0.2387
332	0.2183	0.2269	0.2346	0.2385	0.2387
333	0.2162	0.2247	0.2339	0.2380	0.2385
334	0.2142	0.2225	0.2329	0.2375	0.2382
335	0.2122	0.2204	0.2313	0.2368	0.2377
336	0.2083	0.2183	0.2296	0.2360	0.2375
337	0.2065	0.2162	0.2292	0.2351	0.2368
338	0.2028	0.2142	0.2269	0.2341	0.2360
339	0.2010	0.2122	0.2225	0.2329	0.2355
340	0.1976	0.2103	0.2204	0.2317	0.2346
341	0.1942	0.2065	0.2183	0.2303	0.2336
342	0.1926	0.2046	0.2183	0.2292	0.2324
343	0.1894	0.2010	0.2122	0.2269	0.2315
344	0.1863	0.1993	0.2103	0.2247	0.2299
345	0.1819	0.1959	0.2122	0.2247	0.2292
346	0.1777	0.1926	0.2083	0.2225	0.2269
347	0.1763	0.1894	0.2046	0.2204	0.2247
348	0.1723	0.1863	0.2028	0.2183	0.2247
349	0.1698	0.1833	0.1993	0.2162	0.2225
350	0.1661	0.1805	0.1976	0.2122	0.2204
351	0.1614	0.1777	0.1926	0.2122	0.2183
352	0.1592	0.1736	0.1894	0.2083	0.2162

Position(m) (X,Y) / Angle (deg)	Inertia [Kg.m²]				
	(0.6, 0.1)	(0.6, 0.05)	(0.6, 0.0)	(0.6, -0.05)	(0.6, -1.0)
353	0.1549	0.1698	0.1863	0.2065	0.2142
354	0.1508	0.1661	0.1833	0.2028	0.2103
355	0.1488	0.1637	0.1819	0.2010	0.2083
356	0.1441	0.1592	0.1010	0.1976	0.2065
357	0.1415	0.1559	0.1736	0.1942	0.2028
358	0.1372	0.1528	0.1698	0.1910	0.2010
359	0.1340	0.1488	0.1661	0.1879	0.1942
360	0.1310	0.1423	0.1625	0.1848	0.1976

Table B.2: The inertia of the model at crank position 0.65m from the hip joint

Position(m) (X,Y) / Angle(deg)	Inertia [Kg.m²]				
	(0.65, 0.1)	(0.65, 0.05)	(0.65, 0.0)	(0.65, -0.05)	(0.65, -1.0)
1	0.1200	0.1317	0.1508	0.1649	0.1777
2	0.1356	0.1280	0.1469	0.1614	0.1749
3	0.1135	0.1259	0.1441	0.1581	0.1710
4	0.1107	0.1226	0.1397	0.1549	0.1685
5	0.1076	0.1187	0.1364	0.1508	0.1649
6	0.1051	0.1157	0.1332	0.1479	0.1614
7	0.1023	0.1123	0.1302	0.1441	0.1581
8	0.0992	0.1097	0.1266	0.1415	0.1549
9	0.0967	0.1066	0.1239	0.1372	0.1518
10	0.0943	0.1042	0.1206	0.1348	0.1479
11	0.0920	0.1010	0.1175	0.1317	0.1451
12	0.0899	0.0963	0.1140	0.1273	0.1406
13	0.0875	0.0988	0.1113	0.1246	0.1381
14	0.0852	0.0959	0.1086	0.1213	0.1348
15	0.0833	0.0935	0.1056	0.1181	0.1310
16	0.0816	0.0909	0.1028	0.1146	0.1280
17	0.0799	0.0892	0.0996	0.1123	0.1246
18	0.0785	0.0865	0.0975	0.1091	0.1213
19	0.0769	0.0871	0.0947	0.1061	0.1181
20	0.0754	0.0827	0.0920	0.1028	0.1157
21	0.0754	0.0810	0.0902	0.1010	0.1118
22	0.0730	0.0793	0.0881	0.0979	0.1091

Position(m) (X,Y) Angle (deg)	Inertia [Kg.m²]				
	(0.65, 0.1)	(0.65, 0.05)	(0.65, 0.0)	(0.65, -0.05)	(0.65, -1.0)
23	0.0721	0.0780	0.0855	0.0955	0.1066
24	0.0714	0.0764	0.0836	0.0932	0.1037
25	0.0705	0.0749	0.0821	0.0909	0.1005
26	0.0699	0.0739	0.0801	0.0881	0.0984
27	0.0694	0.0725	0.0782	0.0868	0.0955
28	0.0690	0.0718	0.0772	0.0843	0.0932
29	0.0688	0.0710	0.0756	0.0824	0.0906
30	0.0686	0.0703	0.0742	0.0807	0.0888
31	0.0686	0.0699	0.0735	0.0790	0.0865
32	0.0688	0.0692	0.0721	0.0777	0.0849
33	0.0692	0.0690	0.0714	0.0761	0.0824
34	0.0694	0.0688	0.0705	0.0747	0.0807
35	0.0701	0.0688	0.0699	0.0737	0.0790
36	0.0705	0.0684	0.0694	0.0725	0.0777
37	0.0714	0.0688	0.0690	0.0718	0.0759
38	0.0721	0.0692	0.0688	0.0707	0.0749
39	0.0730	0.0697	0.0688	0.0701	0.0737
40	0.0739	0.0703	0.0686	0.0697	0.0725
41	0.0751	0.0707	0.0688	0.0692	0.0716
42	0.0764	0.0716	0.0690	0.0688	0.0710
43	0.0777	0.0723	0.0694	0.0659	0.0701
44	0.0790	0.0735	0.0701	0.0686	0.0697
45	0.0804	0.0744	0.0705	0.0688	0.0692
46	0.0821	0.0756	0.0712	0.0690	0.0688
47	0.0836	0.0769	0.0718	0.0692	0.0688
48	0.0855	0.0782	0.0730	0.0699	0.0686
49	0.0871	0.0796	0.0737	0.0703	0.0688
50	0.0892	0.0810	0.0749	0.0712	0.0690
51	0.0909	0.0827	0.0761	0.0716	0.0692
52	0.0932	0.0846	0.0772	0.0728	0.0697
53	0.0951	0.0865	0.0790	0.0735	0.0703
54	0.0971	0.0878	0.0804	0.0747	0.0707
55	0.0996	0.0895	0.0816	0.0759	0.0718
56	0.1010	0.0920	0.0833	0.0772	0.0723
57	0.1042	0.0935	0.0852	0.0782	0.0735
58	0.1061	0.0963	0.0871	0.0801	0.0747
59	0.1081	0.0979	0.0892	0.0813	0.0756
60	0.1107	0.1001	0.0909	0.0833	0.0769

Position(m) (X,Y) Angle (deg)	Inertia [Kg.m²]				
	(0.65, 0.1)	(0.65, 0.05)	(0.65, 0.0)	(0.65, -0.05)	(0.65, -1.0)
61	0.1135	0.1019	0.0928	0.0846	0.0782
62	0.1157	0.1046	0.0947	0.0865	0.0796
63	0.1181	0.1071	0.0967	0.0881	0.0816
64	0.1206	0.1091	0.0992	0.0902	0.0827
65	0.1232	0.1118	0.1014	0.0917	0.0846
66	0.1259	0.1140	0.1037	0.0939	0.0865
67	0.1288	0.1163	0.1056	0.0967	0.0881
68	0.1310	0.1187	0.1086	0.0988	0.0902
69	0.1340	0.1219	0.1102	0.1005	0.0920
70	0.1364	0.1239	0.1129	0.1028	0.0939
71	0.1389	0.1266	0.1152	0.1028	0.0959
72	0.1415	0.1295	0.1175	0.1076	0.0984
73	0.1441	0.1317	0.1200	0.1097	0.1005
74	0.1469	0.1340	0.1226	0.1118	0.1023
75	0.1488	0.1372	0.1259	0.1123	0.1051
76	0.1508	0.1397	0.1273	0.1175	0.1071
77	0.1549	0.1423	0.1302	0.1194	0.1097
78	0.1581	0.1451	0.1325	0.1219	0.1118
79	0.1603	0.1479	0.1356	0.1246	0.1146
80	0.1625	0.1498	0.1381	0.1273	0.1163
81	0.1649	0.1528	0.1406	0.1295	0.1194
82	0.1673	0.1559	0.1432	0.1325	0.1219
83	0.1698	0.1581	0.1460	0.1348	0.1246
84	0.1723	0.1603	0.1488	0.1381	0.1266
85	0.1749	0.1625	0.1518	0.1397	0.1295
86	0.1777	0.1649	0.1538	0.1423	0.1317
87	0.1805	0.1685	0.1559	0.1451	0.1348
88	0.1833	0.1710	0.1592	0.1479	0.1372
89	0.1848	0.1736	0.1614	0.1508	0.1406
90	0.1879	0.1749	0.1649	0.1528	0.1423
91	0.1894	0.1777	0.1673	0.1559	0.1451
92	0.1926	0.1805	0.6548	0.1592	0.1479
93	0.1942	0.1833	0.1723	0.1614	0.1508
94	0.1959	0.1848	0.1749	0.1637	0.1538
95	0.1993	0.1879	0.1763	0.1661	0.1559
96	0.2010	0.1894	0.1790	0.1685	0.1581
97	0.2028	0.1926	0.1819	0.1710	0.1614
98	0.2046	0.1942	0.1833	0.1736	0.1637

Position(m) (X,Y) Angle (deg)	Inertia [Kg.m²]				
	(0.65, 0.1)	(0.65, 0.05)	(0.65, 0.0)	(0.65, -0.05)	(0.65, -1.0)
99	0.2065	0.1976	0.1863	0.1763	0.1661
100	0.2083	0.1993	0.1894	0.1790	0.1685
101	0.2103	0.2010	0.1910	0.1805	0.1710
102	0.2122	0.2028	0.1926	0.1833	0.1736
103	0.2142	0.2046	0.1959	0.1863	0.1763
104	0.2162	0.2083	0.1976	0.1879	0.1790
105	0.2183	0.2083	0.1993	0.1910	0.1819
106	0.2204	0.2122	0.2028	0.1926	0.1833
107	0.2225	0.2122	0.2046	0.1959	0.1863
108	0.2225	0.2142	0.2065	0.1976	0.1879
109	0.2247	0.2162	0.2083	0.1993	0.1910
110	0.2269	0.2183	0.2103	0.2010	0.1926
111	0.2269	0.2204	0.2122	0.2046	0.1959
112	0.2292	0.2225	0.2142	0.2065	0.1976
113	0.2301	0.2225	0.2162	0.2083	0.1993
114	0.2313	0.2247	0.2183	0.2103	0.2010
115	0.2324	0.2269	0.2183	0.2122	0.2046
116	0.2336	0.2269	0.2204	0.2142	0.2065
117	0.2343	0.2292	0.2225	0.2162	0.2083
118	0.2353	0.2299	0.2247	0.2162	0.2103
119	0.2363	0.2313	0.2247	0.2183	0.2122
120	0.2368	0.2322	0.2269	0.2204	0.2142
121	0.2375	0.2331	0.2292	0.2225	0.2162
122	0.2380	0.2343	0.2292	0.2225	0.2183
123	0.2385	0.2351	0.2306	0.2247	0.2183
124	0.2390	0.2358	0.2315	0.2269	0.2204
125	0.2392	0.2368	0.2327	0.2269	0.2225
126	0.2395	0.2372	0.2336	0.2292	0.2247
127	0.2395	0.2377	0.2346	0.2301	0.2247
128	0.2397	0.2382	0.2351	0.2315	0.2269
129	0.2395	0.2385	0.2353	0.2324	0.2269
130	0.2395	0.2390	0.2360	0.2334	0.2294
131	0.2392	0.2390	0.2368	0.2343	0.2306
132	0.2387	0.2392	0.2372	0.2353	0.2320
133	0.2385	0.2392	0.2380	0.2360	0.2329
134	0.2377	0.2392	0.2382	0.2368	0.2339
135	0.2370	0.2390	0.2387	0.2372	0.2348
136	0.2365	0.2387	0.2390	0.2377	0.2355

Position(m) (X,Y) Angle (deg)	Inertia [Kg.m²]				
	(0.65, 0.1)	(0.65, 0.05)	(0.65, 0.0)	(0.65, -0.05)	(0.65, -1.0)
137	0.2355	0.2385	0.2392	0.2382	0.2363
138	0.2346	0.2380	0.2392	0.2387	0.2372
139	0.2334	0.2372	0.2390	0.2390	0.2377
140	0.2324	0.2365	0.2387	0.2392	0.2382
141	0.2310	0.2360	0.2385	0.2392	0.2387
142	0.2296	0.2351	0.2380	0.2392	0.2390
143	0.2292	0.2341	0.2375	0.2392	0.2392
144	0.2269	0.2329	0.2370	0.2390	0.2395
145	0.2247	0.2320	0.2363	0.2385	0.2395
146	0.2225	0.2303	0.2355	0.2382	0.2395
147	0.2204	0.2292	0.2346	0.2377	0.2395
148	0.2204	0.2269	0.2334	0.2372	0.2392
149	0.2183	0.2269	0.2324	0.2365	0.2390
150	0.2142	0.2247	0.2310	0.2358	0.2385
151	0.2122	0.2225	0.2299	0.2348	0.2380
152	0.2103	0.2204	0.2292	0.2339	0.2375
153	0.2083	0.2183	0.2269	0.2327	0.2360
154	0.2046	0.2162	0.2247	0.2317	0.2351
155	0.2028	0.2142	0.2247	0.2301	0.2341
156	0.2010	0.2122	0.2204	0.2292	0.2331
157	0.1976	0.2103	0.2183	0.2269	0.2317
158	0.1942	0.2065	0.2162	0.2247	0.2303
159	0.1910	0.2046	0.2122	0.2247	0.2292
160	0.1879	0.2028	0.2122	0.2225	0.2269
161	0.1848	0.1993	0.2083	0.2204	0.2269
162	0.1819	0.1959	0.2065	0.2183	0.2247
163	0.1790	0.1926	0.2028	0.2162	0.2225
164	0.1763	0.1910	0.2010	0.2142	0.2204
165	0.1723	0.1879	0.1976	0.2122	0.2183
166	0.1698	0.1833	0.1942	0.2083	0.2162
167	0.1661	0.1805	0.1926	0.2065	0.2142
168	0.1625	0.1790	0.1894	0.2046	0.2122
169	0.1592	0.1749	0.1863	0.2010	0.2083
170	0.1559	0.1710	0.1833	0.1993	0.2065
171	0.1518	0.1685	0.1790	0.1959	0.2046
172	0.1488	0.1649	0.1763	0.1926	0.2010
173	0.1451	0.1614	0.1736	0.1894	0.1993
174	0.1423	0.1581	0.1698	0.1863	0.1959

Position(m) (X,Y) Angle (deg)	Inertia [Kg.m²]				
	(0.65, 0.1)	(0.65, 0.05)	(0.65, 0.0)	(0.65, -0.05)	(0.65, -1.0)
175	0.1381	0.1549	0.1661	0.1833	0.1942
176	0.1356	0.1518	0.1637	0.1805	0.1926
177	0.1317	0.1479	0.1559	0.1777	0.1894
178	0.1288	0.1441	0.1592	0.1736	0.1863
179	0.1252	0.1406	0.1559	0.1710	0.1833
180	0.1219	0.1372	0.1528	0.1673	0.1805
181	0.1187	0.1340	0.1498	0.1637	0.1777
182	0.1152	0.1302	0.1460	0.1614	0.1749
183	0.1135	0.1280	0.1432	0.1570	0.1710
184	0.1097	0.1239	0.1389	0.1538	0.1673
185	0.1066	0.1213	0.1356	0.1508	0.1649
186	0.1037	0.1175	0.1317	0.1469	0.1603
187	0.1019	0.1152	0.1295	0.1432	0.1570
188	0.0984	0.1113	0.1259	0.1406	0.1538
189	0.0959	0.1086	0.1226	0.1364	0.1508
190	0.0935	0.1061	0.1194	0.1340	0.1479
191	0.0913	0.1032	0.1157	0.1302	0.1432
192	0.0892	0.1001	0.1129	0.1266	0.1406
193	0.0865	0.0975	0.1107	0.1239	0.1372
194	0.0849	0.0951	0.1071	0.1206	0.1332
195	0.0827	0.0928	0.1042	0.1169	0.1310
196	0.0810	0.0906	0.1019	0.1146	0.1266
197	0.0793	0.0881	0.0988	0.1107	0.1239
198	0.0777	0.0858	0.0963	0.1081	0.1206
199	0.0761	0.0839	0.0939	0.1056	0.1175
200	0.0751	0.0824	0.0917	0.1023	0.1140
201	0.0737	0.0801	0.0895	0.1001	0.1113
202	0.0730	0.0785	0.0868	0.0971	0.1086
203	0.0718	0.0774	0.0855	0.0947	0.1056
204	0.0712	0.0759	0.0830	0.0924	0.1028
205	0.0703	0.0744	0.0813	0.0902	0.0996
206	0.0699	0.0737	0.0796	0.0875	0.0975
207	0.0694	0.0723	0.0780	0.0858	0.0955
208	0.0690	0.0716	0.0766	0.0836	0.0920
209	0.0688	0.0707	0.0751	0.0819	0.0902
210	0.0688	0.0701	0.0742	0.0801	0.0881
211	0.0688	0.0697	0.0728	0.0785	0.0855
212	0.0690	0.0692	0.0721	0.0772	0.0836

Position(m) (X,Y) Angle (deg)	Inertia [Kg.m²]				
	(0.65, 0.1)	(0.65, 0.05)	(0.65, 0.0)	(0.65, -0.05)	(0.65, -1.0)
213	0.0694	0.0690	0.0712	0.0754	0.0824
214	0.0697	0.0688	0.0705	0.0747	0.0801
215	0.0703	0.0688	0.0699	0.0735	0.0782
216	0.0710	0.0690	0.0694	0.0721	0.0772
217	0.0718	0.0692	0.0690	0.0714	0.0759
218	0.0725	0.0694	0.0690	0.0707	0.0744
219	0.0735	0.0701	0.0688	0.0701	0.0735
220	0.0747	0.0705	0.0690	0.0697	0.0723
221	0.0756	0.0714	0.0690	0.0692	0.0716
222	0.0769	0.0718	0.0692	0.0690	0.0707
223	0.0782	0.0730	0.0699	0.0688	0.0701
224	0.0796	0.0739	0.0703	0.0688	0.0697
225	0.0813	0.0751	0.0710	0.0690	0.0692
226	0.0827	0.0764	0.0716	0.0692	0.0690
227	0.0846	0.0777	0.0725	0.0697	0.0688
228	0.0862	0.0790	0.0732	0.0701	0.0688
229	0.0881	0.0801	0.0744	0.0707	0.0690
230	0.0899	0.0821	0.0756	0.0714	0.0692
231	0.0920	0.0833	0.0769	0.0721	0.0694
232	0.0935	0.0852	0.0780	0.0732	0.0701
233	0.0959	0.0868	0.0799	0.0739	0.0705
234	0.0984	0.0888	0.0813	0.0751	0.0714
235	0.0996	0.0906	0.0824	0.0764	0.0721
236	0.1028	0.0924	0.0843	0.0774	0.0730
237	0.1046	0.0947	0.0862	0.0793	0.0739
238	0.1066	0.0967	0.0878	0.0807	0.0754
239	0.1097	0.0988	0.0899	0.0819	0.0759
240	0.1118	0.1010	0.0913	0.0836	0.0777
241	0.1140	0.1028	0.0939	0.0855	0.0790
242	0.1163	0.1056	0.0955	0.0875	0.0801
243	0.1194	0.1076	0.0979	0.0892	0.0821
244	0.1213	0.1107	0.1001	0.0909	0.0833
245	0.1246	0.1123	0.1023	0.0928	0.0852
246	0.1266	0.1152	0.1046	0.0951	0.0871
247	0.1288	0.1169	0.1066	0.0971	0.0888
248	0.1317	0.1200	0.1091	0.0992	0.0909
249	0.1340	0.1219	0.1113	0.1014	0.0924
250	0.1348	0.1246	0.1135	0.1032	0.0951

Position(m) (X,Y) Angle (deg)	Inertia [Kg.m²]				
	(0.65, 0.1)	(0.65, 0.05)	(0.65, 0.0)	(0.65, -0.05)	(0.65, -1.0)
251	0.1397	0.1280	0.1157	0.1061	0.0967
252	0.1423	0.1295	0.1187	0.1081	0.0988
253	0.1451	0.1325	0.1213	0.1107	0.1014
254	0.1479	0.1356	0.1232	0.1129	0.1032
255	0.1498	0.1372	0.1259	0.1152	0.1061
256	0.1518	0.1397	0.1288	0.1181	0.1081
257	0.1549	0.1432	0.1310	0.1206	0.1107
258	0.1570	0.1451	0.1332	0.1226	0.1135
259	0.1603	0.1479	0.1364	0.1252	0.1146
260	0.1625	0.1508	0.1389	0.1280	0.1181
261	0.1649	0.1528	0.1415	0.1302	0.1206
262	0.1673	0.1559	0.1441	0.1332	0.1226
263	0.1710	0.1581	0.1469	0.1356	0.1252
264	0.1723	0.1603	0.1498	0.1381	0.1280
265	0.1749	0.1637	0.1518	0.1406	0.1302
266	0.1777	0.1661	0.1538	0.1432	0.1332
267	0.1805	0.1685	0.1570	0.1460	0.1348
268	0.1833	0.1710	0.1592	0.1488	0.1381
269	0.1848	0.1736	0.1625	0.1508	0.1406
270	0.1879	0.1763	0.1649	0.1538	0.1432
271	0.1894	0.1777	0.1673	0.1559	0.1460
272	0.1910	0.1805	0.1698	0.1592	0.1488
273	0.1942	0.1833	0.1723	0.1614	0.1508
274	0.1959	0.1848	0.1749	0.1637	0.1538
275	0.1976	0.1879	0.1763	0.1661	0.1559
276	0.2010	0.1894	0.1790	0.1685	0.1592
277	0.2028	0.1926	0.1819	0.1710	0.1614
278	0.2046	0.1942	0.1833	0.1736	0.1637
279	0.2065	0.1959	0.1863	0.1763	0.1661
280	0.2083	0.1993	0.1894	0.1790	0.1685
281	0.2103	0.2010	0.1910	0.1805	0.1710
282	0.2122	0.2028	0.1926	0.1833	0.1736
283	0.2142	0.2046	0.1959	0.1863	0.1763
284	0.2162	0.2065	0.1976	0.1879	0.1790
285	0.2183	0.2083	0.1993	0.1910	0.1819
286	0.2183	0.2103	0.2010	0.1926	0.1833
287	0.2204	0.2122	0.2028	0.1942	0.1863
288	0.2225	0.2142	0.2065	0.1976	0.1879

Position(m) (X,Y) Angle (deg)	Inertia [Kg.m²]				
	(0.65, 0.1)	(0.65, 0.05)	(0.65, 0.0)	(0.65, -0.05)	(0.65, -1.0)
289	0.2247	0.2162	0.2083	0.1993	0.1910
290	0.2247	0.2183	0.2103	0.2010	0.1926
291	0.2269	0.2183	0.2122	0.2028	0.1942
292	0.2269	0.2204	0.2122	0.2046	0.1976
293	0.2292	0.2225	0.2142	0.2065	0.1993
294	0.2301	0.2247	0.2162	0.2046	0.2010
295	0.2313	0.2247	0.2183	0.2103	0.2028
296	0.2322	0.2269	0.2204	0.2122	0.2046
297	0.2331	0.2269	0.2204	0.2142	0.2083
298	0.2341	0.2292	0.2225	0.2162	0.2103
299	0.2348	0.2301	0.2247	0.2183	0.2122
300	0.2355	0.2310	0.2247	0.2204	0.2122
301	0.2363	0.2322	0.2269	0.2204	0.2142
302	0.2368	0.2329	0.2292	0.2225	0.2162
303	0.2372	0.2339	0.2292	0.2247	0.2183
304	0.2377	0.2346	0.2306	0.2247	0.2204
305	0.2380	0.2353	0.2313	0.2269	0.2225
306	0.2382	0.2358	0.2324	0.2269	0.2225
307	0.2382	0.2365	0.2331	0.2292	0.2247
308	0.2382	0.2368	0.2341	0.2301	0.2247
309	0.2382	0.2372	0.2348	0.2313	0.2269
310	0.2380	0.2375	0.2355	0.2322	0.2292
311	0.2380	0.2377	0.2360	0.2331	0.2306
312	0.2375	0.2380	0.2365	0.2339	0.2294
313	0.2370	0.2380	0.2370	0.2348	0.2308
314	0.2365	0.2377	0.2372	0.2355	0.2317
315	0.2360	0.2377	0.2375	0.2360	0.2327
316	0.2351	0.2375	0.2377	0.2365	0.2336
317	0.2343	0.2370	0.2377	0.2370	0.2343
318	0.2334	0.2368	0.2377	0.2372	0.2353
319	0.2324	0.2360	0.2377	0.2375	0.2358
320	0.2313	0.2355	0.2375	0.2377	0.2365
321	0.2301	0.2346	0.2372	0.2380	0.2370
322	0.2292	0.2339	0.2368	0.2380	0.2375
323	0.2269	0.2329	0.2363	0.2377	0.2377
324	0.2247	0.2320	0.2358	0.2377	0.2380
325	0.2247	0.2308	0.2351	0.2372	0.2382
326	0.2225	0.2292	0.2341	0.2370	0.2382

Position(m) (X,Y) Angle (deg)	Inertia [Kg.m²]				
	(0.65, 0.1)	(0.65, 0.05)	(0.65, 0.0)	(0.65, -0.05)	(0.65, -1.0)
327	0.2204	0.2269	0.2334	0.2365	0.2382
328	0.2183	0.2247	0.2324	0.2360	0.2382
329	0.2162	0.2225	0.2315	0.2353	0.2380
330	0.2142	0.2225	0.2301	0.2346	0.2377
331	0.2122	0.2204	0.2292	0.2336	0.2372
332	0.2103	0.2183	0.2269	0.2329	0.2368
333	0.2083	0.2162	0.2269	0.2317	0.2363
334	0.2046	0.2142	0.2247	0.2306	0.2355
335	0.2028	0.2122	0.2225	0.2294	0.2348
336	0.2010	0.2083	0.2204	0.2269	0.2339
337	0.1976	0.2065	0.2183	0.2269	0.2331
338	0.1942	0.2046	0.2162	0.2247	0.2317
339	0.1942	0.2010	0.2142	0.2225	0.2308
340	0.1910	0.1993	0.2122	0.2225	0.2296
341	0.1879	0.1959	0.2103	0.2204	0.2269
342	0.1848	0.1926	0.2083	0.2183	0.2269
343	0.1819	0.1910	0.2065	0.2162	0.2247
344	0.1790	0.1879	0.2028	0.2142	0.2225
345	0.1763	0.1848	0.2010	0.2103	0.2225
346	0.1723	0.1819	0.1959	0.2083	0.2204
347	0.1698	0.1790	0.1959	0.2065	0.2183
348	0.1661	0.1749	0.1926	0.2046	0.2162
349	0.1625	0.1723	0.1894	0.2010	0.2142
350	0.1603	0.1685	0.1863	0.1976	0.2103
351	0.1559	0.1661	0.1833	0.1959	0.2083
352	0.1528	0.1614	0.1805	0.1926	0.2065
353	0.1488	0.1592	0.1763	0.1894	0.2046
354	0.1469	0.1559	0.1736	0.1879	0.2010
355	0.1423	0.1518	0.1710	0.1833	0.1976
356	0.1397	0.1488	0.1673	0.1805	0.1959
357	0.1364	0.1451	0.1637	0.1777	0.1926
358	0.1332	0.1423	0.1603	0.1749	0.1894
359	0.1295	0.1381	0.1570	0.1710	0.1879
360	0.1232	0.1348	0.1538	0.1673	0.1848

Table B.3: The inertia of the model at crank position 0.7m from the hip joint

Position(m) (X,Y) Angle (deg)	Inertia [Kg.m²]				
	(0.7, 0.1)	(0.7, 0.05)	(0.7, 0.0)	(0.7, -0.05)	(0.7, -1.0)
1	0.1102	0.1239	0.1372	0.1518	0.1685
2	0.1076	0.1206	0.1340	0.1479	0.1649
3	0.1046	0.1169	0.1310	0.1451	0.1614
4	0.1019	0.1146	0.1273	0.1406	0.1581
5	0.0988	0.1113	0.1246	0.1381	0.1549
6	0.0963	0.1081	0.1213	0.1340	0.1508
7	0.0939	0.1056	0.1181	0.1302	0.1469
8	0.0917	0.1028	0.1146	0.1273	0.1441
9	0.0895	0.0996	0.1123	0.1252	0.1406
10	0.0868	0.0971	0.1086	0.1206	0.1372
11	0.0852	0.0947	0.1056	0.1181	0.1332
12	0.0830	0.0924	0.1032	0.1152	0.1302
13	0.0796	0.0902	0.1005	0.1113	0.1266
14	0.0807	0.0881	0.0975	0.1086	0.1239
15	0.0796	0.0855	0.0951	0.1061	0.1206
16	0.0780	0.0836	0.0928	0.1028	0.1169
17	0.0764	0.0821	0.0906	0.1010	0.1146
18	0.0754	0.0804	0.0881	0.0975	0.1107
19	0.0742	0.0788	0.0865	0.0955	0.1081
20	0.0728	0.0772	0.0839	0.0928	0.1051
21	0.0721	0.0759	0.0821	0.0906	0.1023
22	0.0712	0.0744	0.0807	0.0885	0.1001
23	0.0705	0.0735	0.0790	0.0858	0.0967
24	0.0699	0.0723	0.0774	0.0843	0.0947
25	0.0694	0.0716	0.0761	0.0824	0.0924
26	0.0690	0.0707	0.0744	0.0807	0.0899
27	0.0688	0.0701	0.0737	0.0790	0.0875
28	0.0688	0.0697	0.0725	0.0774	0.0858
29	0.0688	0.0694	0.0716	0.0761	0.0836
30	0.0690	0.0690	0.0710	0.0747	0.0819
31	0.0697	0.0688	0.0701	0.0737	0.0801
32	0.0697	0.0688	0.0697	0.0725	0.0785
33	0.0703	0.0688	0.0692	0.0718	0.0769
34	0.0707	0.0690	0.0690	0.0707	0.0754
35	0.0716	0.0697	0.0688	0.0701	0.0744
36	0.0725	0.0699	0.0688	0.0697	0.0730

Position(m) (X,Y) Angle (deg)	Inertia [Kg.m²]				
	(0.7, 0.1)	(0.7, 0.05)	(0.7, 0.0)	(0.7, -0.05)	(0.7, -1.0)
37	0.0732	0.0707	0.0688	0.0692	0.0725
38	0.0744	0.0712	0.0690	0.0690	0.0714
39	0.0756	0.0721	0.0694	0.0690	0.0707
40	0.0769	0.0728	0.0697	0.0688	0.0701
41	0.0782	0.0739	0.0705	0.0688	0.0694
42	0.0793	0.0751	0.0710	0.0690	0.0692
43	0.0813	0.0764	0.0718	0.0694	0.0690
44	0.0827	0.0777	0.0730	0.0699	0.0688
45	0.0846	0.0788	0.0737	0.0703	0.0688
46	0.0862	0.0807	0.0747	0.0712	0.0690
47	0.0881	0.0819	0.0759	0.0718	0.0692
48	0.0902	0.0839	0.0772	0.0728	0.0697
49	0.0917	0.0852	0.0785	0.0739	0.0701
50	0.0943	0.0871	0.0804	0.0747	0.0707
51	0.0959	0.0892	0.0816	0.0759	0.0714
52	0.0984	0.0906	0.0836	0.0769	0.0723
53	0.1005	0.0932	0.0849	0.0788	0.0730
54	0.1028	0.0951	0.0868	0.0801	0.0742
55	0.1051	0.0971	0.0888	0.0816	0.0751
56	0.1081	0.0996	0.0902	0.0833	0.0764
57	0.1102	0.1019	0.0928	0.0852	0.0777
58	0.1123	0.1042	0.0947	0.0871	0.0790
59	0.1152	0.1061	0.0967	0.0888	0.0807
60	0.1175	0.1086	0.0992	0.0909	0.0821
61	0.1200	0.1118	0.1014	0.0924	0.0839
62	0.1226	0.1135	0.1037	0.0951	0.0858
63	0.1259	0.1169	0.1056	0.0967	0.0875
64	0.1288	0.1194	0.1086	0.0992	0.0895
65	0.1302	0.1213	0.1107	0.1014	0.0917
66	0.1340	0.1239	0.1135	0.1037	0.0932
67	0.1364	0.1273	0.1157	0.1056	0.0955
68	0.1389	0.1288	0.1181	0.1081	0.0979
69	0.1415	0.1325	0.1213	0.1107	0.0996
70	0.1451	0.1348	0.1232	0.1135	0.1019
71	0.1479	0.1372	0.1259	0.1163	0.1046
72	0.1498	0.1406	0.1288	0.1187	0.1066
73	0.1528	0.1432	0.1317	0.1206	0.1097
74	0.1559	0.1460	0.1340	0.1232	0.1118

Position(m) (X,Y) / Angle (deg)	Inertia [Kg.m²]				
	(0.7, 0.1)	(0.7, 0.05)	(0.7, 0.0)	(0.7, -0.05)	(0.7, -1.0)
75	0.1581	0.1488	0.1364	0.1259	0.1140
76	0.1614	0.1518	0.1397	0.1295	0.1163
77	0.1637	0.1538	0.1423	0.1317	0.1200
78	0.1673	0.1570	0.1451	0.1310	0.1219
79	0.1698	0.1603	0.1479	0.1348	0.1252
80	0.1723	0.1625	0.1508	0.1372	0.1273
81	0.1749	0.1649	0.1528	0.1397	0.1302
82	0.1777	0.1685	0.1559	0.1423	0.1325
83	0.1805	0.1710	0.1592	0.1451	0.1356
84	0.1833	0.1736	0.1614	0.1479	0.1381
85	0.1863	0.1763	0.1649	0.1518	0.1406
86	0.1879	0.1790	0.1673	0.1538	0.1441
87	0.1910	0.1819	0.1685	0.1570	0.1469
88	0.1926	0.1848	0.1723	0.1592	0.1498
89	0.1959	0.1863	0.1749	0.1614	0.1518
90	0.1993	0.1894	0.1777	0.1649	0.1549
91	0.2010	0.1910	0.1805	0.1673	0.1581
92	0.2028	0.1942	0.1833	0.1698	0.1603
93	0.2065	0.1959	0.1848	0.1723	0.1637
94	0.2083	0.1993	0.1879	0.1777	0.1661
95	0.2103	0.2010	0.1910	0.1805	0.1685
96	0.2122	0.2028	0.1926	0.1833	0.1710
97	0.2142	0.2065	0.1959	0.1863	0.1749
98	0.2162	0.2083	0.1976	0.1894	0.1763
99	0.2183	0.2122	0.1993	0.1910	0.1790
100	0.2204	0.2122	0.2010	0.1942	0.1819
101	0.2225	0.2162	0.2028	0.1959	0.1848
102	0.2247	0.2162	0.2046	0.1993	0.1879
103	0.2269	0.2204	0.2065	0.2010	0.1894
104	0.2292	0.2204	0.2103	0.2028	0.1926
105	0.2299	0.2225	0.2122	0.2065	0.1942
106	0.2320	0.2247	0.2142	0.2083	0.1976
107	0.2334	0.2269	0.2162	0.2103	0.1993
108	0.2346	0.2292	0.2183	0.2122	0.2028
109	0.2363	0.2296	0.2204	0.2142	0.2046
110	0.2377	0.2315	0.2225	0.2162	0.2065
111	0.2390	0.2329	0.2247	0.2183	0.2083
112	0.2402	0.2343	0.2247	0.2204	0.2122

Position(m) (X,Y) Angle (deg)	Inertia [Kg.m²]				
	(0.7, 0.1)	(0.7, 0.05)	(0.7, 0.0)	(0.7, -0.05)	(0.7, -1.0)
113	0.2412	0.2358	0.2269	0.2225	0.2142
114	0.2425	0.2370	0.2292	0.2247	0.2162
115	0.2433	0.2382	0.2306	0.2269	0.2183
116	0.2443	0.2395	0.2322	0.2269	0.2204
117	0.2451	0.2405	0.2339	0.2296	0.2225
118	0.2459	0.2415	0.2351	0.2310	0.2247
119	0.2464	0.2425	0.2365	0.2327	0.2269
120	0.2470	0.2433	0.2377	0.2341	0.2269
121	0.2475	0.2441	0.2387	0.2353	0.2292
122	0.2478	0.2446	0.2400	0.2368	0.2310
123	0.2480	0.2451	0.2410	0.2380	0.2329
124	0.2483	0.2459	0.2418	0.2392	0.2341
125	0.2491	0.2456	0.2428	0.2405	0.2358
126	0.2483	0.2464	0.2436	0.2412	0.2372
127	0.2480	0.2405	0.2441	0.2423	0.2385
128	0.2478	0.2467	0.2446	0.2430	0.2397
129	0.2475	0.2247	0.2451	0.2438	0.2407
130	0.2470	0.2467	0.2456	0.2446	0.2420
131	0.2464	0.2464	0.2459	0.2451	0.2428
132	0.2459	0.2462	0.2462	0.2456	0.2438
133	0.2451	0.2456	0.2462	0.2459	0.2449
134	0.2443	0.2451	0.2462	0.2462	0.2454
135	0.2430	0.2446	0.2462	0.2464	0.2462
136	0.2420	0.2438	0.2459	0.2467	0.2467
137	0.2407	0.2430	0.2456	0.2467	0.2472
138	0.2392	0.2420	0.2454	0.2464	0.2475
139	0.2380	0.2410	0.2449	0.2464	0.2478
140	0.2365	0.2397	0.2443	0.2462	0.2480
141	0.2348	0.2385	0.2433	0.2456	0.2480
142	0.2331	0.2372	0.2428	0.2451	0.2480
143	0.2315	0.2358	0.2418	0.2446	0.2480
144	0.2292	0.2339	0.2407	0.2438	0.2478
145	0.2269	0.2322	0.2395	0.2430	0.2475
146	0.2247	0.2308	0.2382	0.2420	0.2470
147	0.2225	0.2292	0.2368	0.2410	0.2464
148	0.2204	0.2269	0.2355	0.2397	0.2459
149	0.2183	0.2247	0.2339	0.2387	0.2451
150	0.2142	0.2225	0.2322	0.2372	0.2443

Position(m) (X,Y) Angle (deg)	Inertia [Kg.m²]				
	(0.7, 0.1)	(0.7, 0.05)	(0.7, 0.0)	(0.7, -0.05)	(0.7, -1.0)
151	0.2122	0.2204	0.2306	0.2358	0.2433
152	0.2103	0.2183	0.2292	0.2341	0.2423
153	0.2065	0.2142	0.2269	0.2363	0.2410
154	0.2046	0.2122	0.2247	0.2310	0.2395
155	0.2010	0.2103	0.2225	0.2292	0.2385
156	0.1976	0.2065	0.2204	0.2269	0.2368
157	0.1942	0.2028	0.2183	0.2247	0.2351
158	0.1910	0.2010	0.2142	0.2225	0.2336
159	0.1879	0.1976	0.2122	0.2204	0.2315
160	0.1848	0.1942	0.2103	0.2183	0.2296
161	0.1819	0.1910	0.2065	0.2142	0.2269
162	0.1790	0.1879	0.2046	0.2122	0.2247
163	0.1749	0.1848	0.2010	0.2103	0.2225
164	0.1710	0.1819	0.1993	0.2065	0.2204
165	0.1673	0.1790	0.1942	0.2046	0.2183
166	0.1637	0.1749	0.1926	0.2010	0.2162
167	0.1603	0.1723	0.1894	0.1993	0.2122
168	0.1570	0.1685	0.1863	0.1959	0.2103
169	0.1528	0.1649	0.1819	0.1926	0.2083
170	0.1469	0.1614	0.1790	0.1894	0.2046
171	0.1423	0.1581	0.1749	0.1863	0.2010
172	0.1389	0.1538	0.1723	0.1833	0.1976
173	0.1356	0.1508	0.1685	0.1790	0.1959
174	0.1325	0.1469	0.1649	0.1763	0.1926
175	0.1317	0.1441	0.1614	0.1723	0.1894
176	0.1295	0.1397	0.1581	0.1661	0.1863
177	0.1252	0.1332	0.1549	0.1649	0.1819
178	0.1219	0.1364	0.1518	0.1614	0.1790
179	0.1187	0.1332	0.1479	0.1581	0.1749
180	0.1152	0.1302	0.1441	0.1549	0.1723
181	0.1123	0.1266	0.1406	0.1518	0.1685
182	0.1102	0.1232	0.1372	0.1479	0.1649
183	0.1061	0.1200	0.1340	0.1441	0.1614
184	0.1042	0.1169	0.1302	0.1406	0.1581
185	0.1014	0.1135	0.1273	0.1372	0.1549
186	0.0979	0.1107	0.1232	0.1340	0.1508
187	0.0959	0.1076	0.1200	0.1302	0.1479
188	0.0932	0.1051	0.1175	0.1273	0.1432

Position(m) (X,Y) Angle (deg)	Inertia [Kg.m²]				
	(0.7, 0.1)	(0.7, 0.05)	(0.7, 0.0)	(0.7, -0.05)	(0.7, -1.0)
189	0.0909	0.1019	0.1140	0.1239	0.1397
190	0.0885	0.0996	0.1118	0.1200	0.1364
191	0.0868	0.0967	0.1081	0.1175	0.1332
192	0.0843	0.0943	0.1046	0.1140	0.1295
193	0.0824	0.0917	0.1028	0.1118	0.1266
194	0.0807	0.0895	0.0996	0.1081	0.1232
195	0.0793	0.0871	0.0975	0.1046	0.1200
196	0.0777	0.0852	0.0947	0.1028	0.1169
197	0.0761	0.0836	0.0920	0.0996	0.1135
198	0.0747	0.0813	0.0895	0.0975	0.1102
199	0.0737	0.0796	0.0878	0.0943	0.1076
200	0.0725	0.0780	0.0855	0.0920	0.1046
201	0.0718	0.0764	0.0839	0.0895	0.1014
202	0.0707	0.0754	0.0816	0.0878	0.0996
203	0.0701	0.0739	0.0799	0.0855	0.0963
204	0.0697	0.0730	0.0782	0.0839	0.0939
205	0.0692	0.0718	0.0772	0.0816	0.0917
206	0.0690	0.0712	0.0756	0.0799	0.0895
207	0.0688	0.0703	0.0742	0.0782	0.0868
208	0.0686	0.0699	0.0732	0.0769	0.0849
209	0.0688	0.0694	0.0721	0.0756	0.0833
210	0.0690	0.0690	0.0714	0.0742	0.0810
211	0.0692	0.0688	0.0705	0.0732	0.0796
212	0.0699	0.0686	0.0699	0.0721	0.0777
213	0.0703	0.0688	0.0694	0.0714	0.0766
214	0.0712	0.0690	0.0690	0.0705	0.0751
215	0.0716	0.0692	0.0688	0.0699	0.0737
216	0.0728	0.0694	0.0686	0.0694	0.0730
217	0.0739	0.0701	0.0686	0.0690	0.0718
218	0.0747	0.0707	0.0688	0.0688	0.0712
219	0.0759	0.0716	0.0692	0.0688	0.0703
220	0.0769	0.0723	0.0694	0.0688	0.0697
221	0.0788	0.0732	0.0701	0.0688	0.0692
222	0.0801	0.0744	0.0705	0.0692	0.0690
223	0.0816	0.0754	0.0714	0.0694	0.0688
224	0.0833	0.0766	0.0721	0.0694	0.0688
225	0.0852	0.0782	0.0730	0.0701	0.0688
226	0.0868	0.0796	0.0742	0.0705	0.0688

Position(m) (X,Y) Angle (deg)	Inertia [Kg.m²]				
	(0.7, 0.1)	(0.7, 0.05)	(0.7, 0.0)	(0.7, -0.05)	(0.7, -1.0)
227	0.0885	0.0807	0.0751	0.0714	0.0692
228	0.0909	0.0824	0.0761	0.0721	0.0697
229	0.0928	0.0846	0.0780	0.0730	0.0701
230	0.0947	0.0858	0.0793	0.0742	0.0710
231	0.0967	0.0878	0.0804	0.0751	0.0714
232	0.0992	0.0895	0.0824	0.0764	0.0723
233	0.1014	0.0920	0.0836	0.0777	0.0735
234	0.1037	0.0935	0.0855	0.0793	0.0744
235	0.1056	0.0963	0.0875	0.0804	0.0756
236	0.1086	0.0979	0.0895	0.0821	0.0769
237	0.1107	0.1001	0.0909	0.0843	0.0782
238	0.1135	0.1023	0.0935	0.0855	0.0796
239	0.1163	0.1051	0.0955	0.0875	0.0810
240	0.1181	0.1071	0.0975	0.0895	0.0827
241	0.1213	0.1102	0.1001	0.0909	0.0849
242	0.1232	0.1118	0.1023	0.0935	0.0862
243	0.1259	0.1146	0.1046	0.0955	0.0881
244	0.1288	0.1169	0.1066	0.0975	0.0895
245	0.1317	0.1200	0.1097	0.1001	0.0920
246	0.1340	0.1226	0.1113	0.1028	0.0939
247	0.1372	0.1252	0.1140	0.1046	0.0963
248	0.1397	0.1273	0.1163	0.1066	0.0988
249	0.1423	0.1302	0.1194	0.1091	0.1001
250	0.1451	0.1332	0.1213	0.1123	0.1032
251	0.1479	0.1356	0.1246	0.1140	0.1056
252	0.1508	0.1381	0.1266	0.1169	0.1076
253	0.1538	0.1415	0.1295	0.1194	0.1102
254	0.1559	0.1441	0.1317	0.1219	0.1129
255	0.1592	0.1469	0.1356	0.1246	0.1152
256	0.1625	0.1498	0.1372	0.1280	0.1181
257	0.1649	0.1518	0.1406	0.1295	0.1200
258	0.1673	0.1549	0.1432	0.1325	0.1232
259	0.1710	0.1570	0.1451	0.1356	0.1252
260	0.1723	0.1603	0.1488	0.1381	0.1280
261	0.1749	0.1625	0.1518	0.1406	0.1310
262	0.1790	0.1649	0.1538	0.1432	0.1332
263	0.1805	0.1685	0.1570	0.1460	0.1364
264	0.1833	0.1710	0.1592	0.1488	0.1389

Position(m) (X,Y) Angle (deg)	Inertia [Kg.m²]				
	(0.7, 0.1)	(0.7, 0.05)	(0.7, 0.0)	(0.7, -0.05)	(0.7, -1.0)
265	0.1863	0.1736	0.1625	0.1518	0.1415
266	0.1879	0.1763	0.1649	0.1549	0.1451
267	0.1910	0.1790	0.1673	0.1570	0.1479
268	0.1942	0.1819	0.1698	0.1603	0.1498
269	0.1959	0.1833	0.1736	0.1625	0.1528
270	0.1993	0.1863	0.1749	0.1649	0.1559
271	0.2010	0.1894	0.1777	0.1673	0.1592
272	0.2028	0.1926	0.1805	0.1710	0.1614
273	0.2046	0.1942	0.1833	0.1736	0.1637
274	0.2083	0.1959	0.1863	0.1763	0.1661
275	0.2103	0.1993	0.1894	0.1790	0.1698
276	0.2122	0.2010	0.1910	0.1819	0.1723
277	0.2142	0.2046	0.1942	0.1833	0.1749
278	0.2162	0.2065	0.1959	0.1863	0.1777
279	0.2183	0.2083	0.1976	0.1879	0.1805
280	0.2204	0.2103	0.2010	0.1910	0.1833
281	0.2225	0.2122	0.2028	0.1942	0.1848
282	0.2247	0.2142	0.2046	0.1959	0.1879
283	0.2269	0.2162	0.2065	0.1993	0.1910
284	0.2269	0.2183	0.2103	0.2010	0.1926
285	0.2299	0.2204	0.2122	0.2028	0.1959
286	0.2313	0.2225	0.2142	0.2065	0.1976
287	0.2329	0.2247	0.2162	0.2083	0.2010
288	0.2341	0.2269	0.2183	0.2103	0.2028
289	0.2355	0.2269	0.2204	0.2122	0.2046
290	0.2370	0.2292	0.2225	0.2142	0.2065
291	0.2382	0.2308	0.2225	0.2162	0.2103
292	0.2397	0.2324	0.2247	0.2183	0.2122
293	0.2438	0.2336	0.2269	0.2204	0.2142
294	0.2415	0.2351	0.2292	0.2225	0.2162
295	0.2425	0.2365	0.2301	0.2247	0.2183
296	0.2436	0.2375	0.2317	0.2247	0.2204
297	0.2443	0.2387	0.2329	0.2269	0.2225
298	0.2449	0.2397	0.2343	0.2292	0.2247
299	0.2456	0.2407	0.2358	0.2306	0.2247
300	0.2462	0.2415	0.2368	0.2320	0.2269
301	0.2464	0.2425	0.2380	0.2334	0.2292
302	0.2467	0.2430	0.2390	0.2348	0.2306

Position(m) (X,Y) / Angle (deg)	Inertia [Kg.m²]				
	(0.7, 0.1)	(0.7, 0.05)	(0.7, 0.0)	(0.7, -0.05)	(0.7, -1.0)
303	0.2470	0.2438	0.2400	0.2360	0.2322
304	0.2472	0.2443	0.2410	0.2372	0.2336
305	0.2472	0.2449	0.2418	0.2385	0.2351
306	0.2472	0.2451	0.2425	0.2395	0.2365
307	0.2470	0.2454	0.2430	0.2405	0.2377
308	0.2467	0.2456	0.2438	0.2415	0.2390
309	0.2464	0.2456	0.2441	0.2423	0.2402
310	0.2459	0.2456	0.2446	0.2430	0.2412
311	0.2454	0.2456	0.2449	0.2436	0.2420
312	0.2449	0.2454	0.2451	0.2441	0.2430
313	0.2438	0.2451	0.2451	0.2446	0.2438
314	0.2430	0.2446	0.2451	0.2451	0.2446
315	0.2420	0.2441	0.2451	0.2454	0.2456
316	0.2410	0.2433	0.2449	0.2454	0.2451
317	0.2397	0.2428	0.2446	0.2456	0.2456
318	0.2382	0.2418	0.2441	0.2456	0.2462
319	0.2370	0.2410	0.2436	0.2454	0.2464
320	0.2353	0.2400	0.2430	0.2454	0.2470
321	0.2339	0.2387	0.2423	0.2451	0.2470
322	0.2320	0.2372	0.2415	0.2446	0.2470
323	0.2301	0.2363	0.2407	0.2441	0.2470
324	0.2292	0.2346	0.2395	0.2436	0.2467
325	0.2269	0.2331	0.2385	0.2428	0.2464
326	0.2247	0.2313	0.2372	0.2420	0.2459
327	0.2225	0.2294	0.2358	0.2410	0.2454
328	0.2204	0.2269	0.2346	0.2400	0.2449
329	0.2162	0.2247	0.2327	0.2390	0.2441
330	0.2142	0.2247	0.2313	0.2375	0.2433
331	0.2122	0.2225	0.2294	0.2363	0.2423
332	0.2083	0.2183	0.2269	0.2348	0.2412
333	0.2065	0.2162	0.2247	0.2334	0.2400
334	0.2028	0.2142	0.2225	0.2315	0.2385
335	0.2010	0.2122	0.2204	0.2299	0.2372
336	0.1976	0.2083	0.2183	0.2269	0.2355
337	0.1942	0.2065	0.2162	0.2269	0.2343
338	0.1910	0.2028	0.2142	0.2247	0.2324
339	0.1879	0.2010	0.2122	0.2225	0.2308
340	0.1848	0.1976	0.2083	0.2204	0.2292

Position(m) (X,Y) Angle (deg)	Inertia [Kg.m²]				
	(0.7, 0.1)	(0.7, 0.05)	(0.7, 0.0)	(0.7, -0.05)	(0.7, -1.0)
341	0.1819	0.1942	0.2065	0.2162	0.2269
342	0.1777	0.1910	0.2046	0.2142	0.2247
343	0.1749	0.1879	0.2010	0.2122	0.2225
344	0.1710	0.1848	0.1976	0.2103	0.2204
345	0.1637	0.1819	0.1959	0.2065	0.2183
346	0.1603	0.1777	0.1910	0.2028	0.2142
347	0.1570	0.1749	0.1879	0.2010	0.2122
348	0.1538	0.1723	0.1848	0.1976	0.2103
349	0.1498	0.1685	0.1819	0.1942	0.2065
350	0.1460	0.1649	0.1790	0.1926	0.2046
351	0.1432	0.1614	0.1749	0.1894	0.2010
352	0.1397	0.1581	0.1723	0.1848	0.1976
353	0.1356	0.1549	0.1685	0.1819	0.1959
354	0.1332	0.1508	0.1649	0.1790	0.1910
355	0.1288	0.1479	0.1625	0.1763	0.1879
356	0.1266	0.1432	0.1549	0.1723	0.1848
357	0.1226	0.1406	0.1538	0.1685	0.1819
358	0.1187	0.1372	0.1549	0.1649	0.1790
359	0.1163	0.1340	0.1498	0.1625	0.1749
360	0.1129	0.1302	0.1460	0.1549	0.1723

Table B.4: The inertia of the model at crank position 0.75m from the hip joint

Position(m) (X,Y) Angle (deg)	Inertia [Kg.m²]				
	(0.75, 0.1)	(0.75, 0.05)	(0.75, 0.0)	(0.75, -0.05)	(0.75, -1.0)
1	0.1649	0.1451	0.1340	0.1451	0.1649
2	0.1614	0.1415	0.1310	0.1415	0.1614
3	0.1581	0.1372	0.1266	0.1372	0.1581
4	0.1518	0.1332	0.1226	0.1332	0.1518
5	0.1488	0.1288	0.1194	0.1288	0.1488
6	0.1441	0.1252	0.1152	0.1252	0.1441
7	0.1397	0.1219	0.1123	0.1219	0.1397
8	0.1356	0.1187	0.1091	0.1187	0.1356
9	0.1317	0.1146	0.1061	0.1146	0.1317
10	0.1288	0.1113	0.1032	0.1113	0.1288

Position(m) (X,Y) Angle (deg)	Inertia [Kg.m²]				
	(0.75, 0.1)	(0.75, 0.05)	(0.75, 0.0)	(0.75, -0.05)	(0.75, -1.0)
11	0.1239	0.1086	0.1001	0.1086	0.1239
12	0.1200	0.1051	0.0979	0.1051	0.1200
13	0.1163	0.1023	0.0943	0.1023	0.1163
14	0.1135	0.0988	0.0917	0.0988	0.1135
15	0.1097	0.0963	0.0899	0.0963	0.1097
16	0.1066	0.0939	0.0878	0.0939	0.1066
17	0.1037	0.0917	0.0852	0.0917	0.1037
18	0.1001	0.0892	0.0833	0.0892	0.1001
19	0.0979	0.0865	0.0816	0.0865	0.0979
20	0.0947	0.0846	0.0799	0.0846	0.0947
21	0.0924	0.0830	0.0785	0.0830	0.0924
22	0.0895	0.0810	0.0769	0.0810	0.0895
23	0.0878	0.0793	0.0756	0.0793	0.0878
24	0.0852	0.0774	0.0742	0.0774	0.0852
25	0.0833	0.0764	0.0735	0.0764	0.0833
26	0.0819	0.0754	0.0723	0.0754	0.0819
27	0.0799	0.0739	0.0718	0.0739	0.0799
28	0.0782	0.0732	0.0710	0.0732	0.0782
29	0.0772	0.0723	0.0705	0.0723	0.0772
30	0.0759	0.0716	0.0703	0.0716	0.0759
31	0.0744	0.0710	0.0701	0.0710	0.0744
32	0.0737	0.0705	0.0699	0.0705	0.0737
33	0.0728	0.0703	0.0699	0.0703	0.0728
34	0.0721	0.0701	0.0701	0.0701	0.0721
35	0.0714	0.0701	0.0703	0.0701	0.0714
36	0.0710	0.0701	0.0707	0.0701	0.0710
37	0.0705	0.0703	0.0712	0.0703	0.0705
38	0.0705	0.0705	0.0718	0.0705	0.0705
39	0.0705	0.0710	0.0725	0.0710	0.0705
40	0.0705	0.0714	0.0732	0.0714	0.0705
41	0.0705	0.0721	0.0744	0.0721	0.0705
42	0.0710	0.0730	0.0754	0.0730	0.0710
43	0.0712	0.0732	0.0766	0.0732	0.0712
44	0.0718	0.0737	0.0777	0.0737	0.0718
45	0.0721	0.0747	0.0790	0.0747	0.0721
46	0.0725	0.0759	0.0801	0.0759	0.0725
47	0.0739	0.0769	0.0821	0.0769	0.0739
48	0.0759	0.0782	0.0833	0.0782	0.0759

Position(m) (X,Y) Angle (deg)	Inertia [Kg.m²]				
	(0.75, 0.1)	(0.75, 0.05)	(0.75, 0.0)	(0.75, -0.05)	(0.75, -1.0)
49	0.0761	0.0793	0.0852	0.0793	0.0761
50	0.0772	0.0813	0.0871	0.0813	0.0772
51	0.0790	0.0824	0.0888	0.0824	0.0790
52	0.0705	0.0843	0.0906	0.0843	0.0705
53	0.0935	0.0862	0.0932	0.0862	0.0935
54	0.0821	0.0878	0.0947	0.0878	0.0821
55	0.0852	0.0899	0.0971	0.0899	0.0852
56	0.0852	0.0917	0.0996	0.0917	0.0852
57	0.0888	0.0932	0.1010	0.0932	0.0888
58	0.0899	0.0955	0.1037	0.0955	0.0899
59	0.0963	0.0979	0.1061	0.0979	0.0963
60	0.0655	0.1001	0.1081	0.1001	0.0655
61	0.0793	0.1023	0.1107	0.1023	0.0793
62	0.0672	0.1046	0.1135	0.1046	0.0672
63	0.1432	0.1066	0.1163	0.1066	0.1432
64	0.1441	0.1097	0.1187	0.1097	0.1441
65	0.1451	0.1123	0.1219	0.1123	0.1451
66	0.1559	0.1146	0.1239	0.1146	0.1559
67	0.1518	0.1175	0.1266	0.1175	0.1518
68	0.1581	0.1200	0.1295	0.1200	0.1581
69	0.1129	0.1219	0.1325	0.1219	0.1129
70	0.1169	0.1252	0.1348	0.1252	0.1169
71	0.1194	0.1280	0.1381	0.1280	0.1194
72	0.1226	0.1310	0.1406	0.1310	0.1226
73	0.1232	0.1332	0.1441	0.1332	0.1232
74	0.1273	0.1364	0.1469	0.1364	0.1273
75	0.1302	0.1389	0.1488	0.1389	0.1302
76	0.1302	0.1423	0.1528	0.1423	0.1302
77	0.1364	0.1451	0.1549	0.1451	0.1364
78	0.1389	0.1479	0.1581	0.1479	0.1389
79	0.1423	0.1508	0.1614	0.1508	0.1423
80	0.1451	0.1538	0.1649	0.1538	0.1451
81	0.1479	0.1570	0.1673	0.1570	0.1479
82	0.1508	0.1603	0.1710	0.1603	0.1508
83	0.1538	0.1625	0.1736	0.1625	0.1538
84	0.1570	0.1661	0.1763	0.1661	0.1570
85	0.1592	0.1685	0.1790	0.1685	0.1592
86	0.1625	0.1723	0.1790	0.1723	0.1625

Position(m) (X,Y) Angle (deg)	Inertia [Kg.m²]				
	(0.75, 0.1)	(0.75, 0.05)	(0.75, 0.0)	(0.75, -0.05)	(0.75, -1.0)
47	0.0739	0.0769	0.0821	0.0769	0.0739
48	0.0759	0.0782	0.0833	0.0782	0.0759
49	0.0761	0.0793	0.0852	0.0793	0.0761
50	0.0772	0.0813	0.0871	0.0813	0.0772
51	0.0790	0.0824	0.0888	0.0824	0.0790
52	0.0705	0.0843	0.0906	0.0843	0.0705
53	0.0935	0.0862	0.0932	0.0862	0.0935
54	0.0821	0.0878	0.0947	0.0878	0.0821
55	0.0852	0.0899	0.0971	0.0899	0.0852
56	0.0852	0.0917	0.0996	0.0917	0.0852
57	0.0888	0.0932	0.1010	0.0932	0.0888
58	0.0899	0.0955	0.1037	0.0955	0.0899
59	0.0963	0.0979	0.1061	0.0979	0.0963
60	0.0655	0.1001	0.1081	0.1001	0.0655
61	0.0793	0.1023	0.1107	0.1023	0.0793
62	0.0672	0.1046	0.1135	0.1046	0.0672
63	0.1432	0.1066	0.1163	0.1066	0.1432
64	0.1441	0.1097	0.1187	0.1097	0.1441
65	0.1451	0.1123	0.1219	0.1123	0.1451
66	0.1559	0.1146	0.1239	0.1146	0.1559
67	0.1518	0.1175	0.1266	0.1175	0.1518
68	0.1581	0.1200	0.1295	0.1200	0.1581
69	0.1129	0.1219	0.1325	0.1219	0.1129
70	0.1169	0.1252	0.1348	0.1252	0.1169
71	0.1194	0.1280	0.1381	0.1280	0.1194
72	0.1226	0.1310	0.1406	0.1310	0.1226
73	0.1232	0.1332	0.1441	0.1332	0.1232
74	0.1273	0.1364	0.1469	0.1364	0.1273
75	0.1302	0.1389	0.1488	0.1389	0.1302
76	0.1302	0.1423	0.1528	0.1423	0.1302
77	0.1364	0.1451	0.1549	0.1451	0.1364
78	0.1389	0.1479	0.1581	0.1479	0.1389
79	0.1423	0.1508	0.1614	0.1508	0.1423
80	0.1451	0.1538	0.1649	0.1538	0.1451
81	0.1479	0.1570	0.1673	0.1570	0.1479
82	0.1508	0.1603	0.1710	0.1603	0.1508
83	0.1538	0.1625	0.1736	0.1625	0.1538
84	0.1570	0.1661	0.1763	0.1661	0.1570

Position(m) (X,Y) / Angle (deg)	Inertia [Kg.m²]				
	(0.75, 0.1)	(0.75, 0.05)	(0.75, 0.0)	(0.75, -0.05)	(0.75, -1.0)
85	0.1592	0.1685	0.1790	0.1685	0.1592
86	0.1625	0.1723	0.1790	0.1723	0.1625
87	0.1661	0.1749	0.1819	0.1749	0.1661
88	0.1685	0.1777	0.1848	0.1777	0.1685
89	0.1723	0.1805	0.1879	0.1805	0.1723
90	0.1749	0.1777	0.1910	0.1777	0.1749
91	0.1777	0.1863	0.1942	0.1863	0.1777
92	0.1805	0.1894	0.1959	0.1894	0.1805
93	0.1833	0.1926	0.1993	0.1926	0.1833
94	0.1863	0.1942	0.2046	0.1942	0.1863
95	0.1894	0.1976	0.2083	0.1976	0.1894
96	0.1926	0.2010	0.2103	0.2010	0.1926
97	0.1959	0.2028	0.2122	0.2028	0.1959
98	0.1976	0.2065	0.2162	0.2065	0.1976
99	0.2010	0.2083	0.2183	0.2083	0.2010
100	0.2028	0.2122	0.2204	0.2122	0.2028
101	0.2065	0.2142	0.2225	0.2142	0.2065
102	0.2103	0.2162	0.2247	0.2162	0.2103
103	0.2122	0.2204	0.2292	0.2204	0.2122
104	0.2142	0.2225	0.2306	0.2225	0.2142
105	0.2183	0.2247	0.2331	0.2247	0.2183
106	0.2204	0.2269	0.2353	0.2269	0.2204
107	0.2225	0.2296	0.2375	0.2296	0.2225
108	0.2247	0.2322	0.2397	0.2322	0.2247
109	0.2269	0.2343	0.2418	0.2343	0.2269
110	0.2308	0.2365	0.2438	0.2365	0.2308
111	0.2329	0.2390	0.2459	0.2390	0.2329
112	0.2353	0.2410	0.2478	0.2410	0.2353
113	0.2377	0.2433	0.2497	0.2433	0.2377
114	0.2400	0.2451	0.2516	0.2451	0.2400
115	0.2423	0.2472	0.2530	0.2472	0.2423
116	0.2443	0.2491	0.2546	0.2491	0.2443
117	0.2467	0.2507	0.2564	0.2507	0.2467
118	0.2488	0.2530	0.2578	0.2530	0.2488
119	0.2505	0.2544	0.2593	0.2544	0.2505
120	0.2527	0.2561	0.2604	0.2561	0.2527
121	0.2546	0.2575	0.2616	0.2575	0.2546
122	0.2564	0.2590	0.2628	0.2590	0.2564

Position(m) (X,Y) Angle (deg)	Inertia [Kg.m²]				
	(0.75, 0.1)	(0.75, 0.05)	(0.75, 0.0)	(0.75, -0.05)	(0.75, -1.0)
123	0.2581	0.2604	0.2640	0.2604	0.2581
124	0.2598	0.2616	0.2650	0.2616	0.2598
125	0.2613	0.2631	0.2656	0.2631	0.2613
126	0.2628	0.2643	0.2665	0.2643	0.2628
127	0.2643	0.2653	0.2671	0.2653	0.2643
128	0.2656	0.2662	0.2677	0.2662	0.2656
129	0.2668	0.2668	0.2681	0.2668	0.2668
130	0.2677	0.2677	0.2684	0.2677	0.2677
131	0.2690	0.2684	0.2687	0.2684	0.2690
132	0.2699	0.2687	0.2687	0.2687	0.2699
133	0.2706	0.2693	0.2687	0.2693	0.2706
134	0.2715	0.2696	0.2684	0.2696	0.2715
135	0.2722	0.2696	0.2684	0.2696	0.2722
136	0.2725	0.2699	0.2677	0.2699	0.2725
137	0.2732	0.2696	0.2674	0.2696	0.2732
138	0.2735	0.2696	0.2668	0.2696	0.2735
139	0.2735	0.2693	0.2659	0.2693	0.2735
140	0.2735	0.2690	0.2650	0.2690	0.2735
141	0.2735	0.2684	0.2640	0.2684	0.2735
142	0.2735	0.2677	0.2628	0.2677	0.2735
143	0.2732	0.2668	0.2616	0.2668	0.2732
144	0.2728	0.2659	0.2601	0.2659	0.2728
145	0.2722	0.2650	0.2584	0.2650	0.2722
146	0.2715	0.2637	0.2569	0.2637	0.2715
147	0.2709	0.2622	0.2549	0.2622	0.2709
148	0.2696	0.2610	0.2530	0.2610	0.2696
149	0.2687	0.2596	0.2513	0.2596	0.2687
150	0.2674	0.2575	0.2486	0.2575	0.2674
151	0.2662	0.2558	0.2462	0.2558	0.2662
152	0.2646	0.2535	0.2438	0.2535	0.2646
153	0.2628	0.2516	0.2410	0.2516	0.2628
154	0.2610	0.2497	0.2387	0.2497	0.2610
155	0.2593	0.2467	0.2353	0.2467	0.2593
156	0.2572	0.2441	0.2324	0.2441	0.2572
157	0.2549	0.2418	0.2299	0.2418	0.2549
158	0.2521	0.2390	0.2247	0.2390	0.2521
159	0.2499	0.2358	0.2225	0.2358	0.2499
160	0.2475	0.2329	0.2204	0.2329	0.2475

Position(m) (X,Y) Angle (deg)	Inertia [Kg.m²]				
	(0.75, 0.1)	(0.75, 0.05)	(0.75, 0.0)	(0.75, -0.05)	(0.75, -1.0)
161	0.2446	0.2296	0.2162	0.2296	0.2446
162	0.2418	0.2269	0.2122	0.2269	0.2418
163	0.2385	0.2225	0.2083	0.2225	0.2385
164	0.2358	0.2204	0.2046	0.2204	0.2358
165	0.2320	0.2162	0.2010	0.2162	0.2320
166	0.2313	0.2122	0.1959	0.2122	0.2313
167	0.2247	0.2083	0.1926	0.2083	0.2247
168	0.2204	0.2046	0.1879	0.2046	0.2204
169	0.2183	0.2010	0.1848	0.2010	0.2183
170	0.2142	0.1959	0.1805	0.1959	0.2142
171	0.2103	0.1926	0.1763	0.1926	0.2103
172	0.2065	0.1879	0.1723	0.1879	0.2065
173	0.2010	0.1833	0.1673	0.1833	0.2010
174	0.1976	0.1805	0.1625	0.1805	0.1976
175	0.1926	0.1749	0.1592	0.1749	0.1926
176	0.1894	0.1710	0.1549	0.1710	0.1894
177	0.1848	0.1661	0.1498	0.1661	0.1848
178	0.1790	0.1625	0.1469	0.1625	0.1790
179	0.1763	0.1581	0.1423	0.1581	0.1763
180	0.1710	0.1538	0.1381	0.1538	0.1710
181	0.1673	0.1498	0.1348	0.1498	0.1673
182	0.1625	0.1451	0.1302	0.1451	0.1625
183	0.1581	0.1415	0.1266	0.1415	0.1581
184	0.1528	0.1381	0.1232	0.1381	0.1528
185	0.1498	0.1340	0.1194	0.1340	0.1498
186	0.1441	0.1295	0.1157	0.1295	0.1441
187	0.1406	0.1259	0.1129	0.1259	0.1406
188	0.1364	0.1219	0.1086	0.1219	0.1364
189	0.1325	0.1187	0.1051	0.1187	0.1325
190	0.1280	0.1146	0.1032	0.1146	0.1280
191	0.1239	0.1113	0.0996	0.1113	0.1239
192	0.1206	0.1081	0.0975	0.1081	0.1206
193	0.1163	0.1051	0.0939	0.1051	0.1163
194	0.1135	0.1019	0.0913	0.1019	0.1135
195	0.1097	0.0988	0.0895	0.0988	0.1097
196	0.1056	0.0959	0.0871	0.0959	0.1056
197	0.1037	0.0935	0.0846	0.0935	0.1037
198	0.1005	0.0909	0.0827	0.0909	0.1005

Position(m) (X,Y) Angle (deg)	Inertia [Kg.m²]				
	(0.75, 0.1)	(0.75, 0.05)	(0.75, 0.0)	(0.75, -0.05)	(0.75, -1.0)
199	0.0975	0.0881	0.0810	0.0881	0.0975
200	0.0943	0.0865	0.0793	0.0865	0.0943
201	0.0913	0.0839	0.0777	0.0839	0.0913
202	0.0895	0.0821	0.0761	0.0821	0.0895
203	0.0871	0.0804	0.0747	0.0804	0.0871
204	0.0846	0.0788	0.0739	0.0788	0.0846
205	0.0827	0.0772	0.0725	0.0772	0.0827
206	0.0810	0.0759	0.0718	0.0759	0.0810
207	0.0793	0.0744	0.0710	0.0744	0.0793
208	0.0777	0.0735	0.0705	0.0735	0.0777
209	0.0764	0.0723	0.0701	0.0723	0.0764
210	0.0749	0.0716	0.0697	0.0716	0.0749
211	0.0739	0.0710	0.0694	0.0710	0.0739
212	0.0728	0.0703	0.0694	0.0703	0.0728
213	0.0721	0.0701	0.0694	0.0701	0.0721
214	0.0712	0.0697	0.0699	0.0697	0.0712
215	0.0707	0.0694	0.0699	0.0694	0.0707
216	0.0703	0.0694	0.0710	0.0694	0.0703
217	0.0699	0.0697	0.0710	0.0697	0.0699
218	0.0694	0.0699	0.0716	0.0699	0.0694
219	0.0699	0.0701	0.0723	0.0701	0.0699
220	0.0699	0.0707	0.0732	0.0707	0.0699
221	0.0701	0.0712	0.0742	0.0712	0.0701
222	0.0705	0.0718	0.0754	0.0718	0.0705
223	0.0707	0.0730	0.0764	0.0730	0.0707
224	0.0716	0.0735	0.0777	0.0735	0.0716
225	0.0721	0.0747	0.0790	0.0747	0.0721
226	0.0728	0.0759	0.0804	0.0759	0.0728
227	0.0739	0.0769	0.0824	0.0769	0.0739
228	0.0747	0.0782	0.0836	0.0782	0.0747
229	0.0759	0.0799	0.0855	0.0799	0.0759
230	0.0769	0.0813	0.0871	0.0813	0.0769
231	0.0785	0.0827	0.0892	0.0827	0.0785
232	0.0799	0.0843	0.0909	0.0843	0.0799
233	0.0810	0.0862	0.0935	0.0862	0.0810
234	0.0830	0.0881	0.0951	0.0881	0.0830
235	0.0843	0.0899	0.0975	0.0899	0.0843
236	0.0862	0.0917	0.0996	0.0917	0.0862

Position(m) (X,Y) Angle (deg)	Inertia [Kg.m²]				
	(0.75, 0.1)	(0.75, 0.05)	(0.75, 0.0)	(0.75, -0.05)	(0.75, -1.0)
237	0.0881	0.0943	0.1023	0.0943	0.0881
238	0.0895	0.0959	0.1046	0.0959	0.0895
239	0.0920	0.0984	0.1066	0.0984	0.0920
240	0.0939	0.1005	0.1091	0.1005	0.0939
241	0.0963	0.1028	0.1118	0.1028	0.0963
242	0.0979	0.1051	0.1146	0.1051	0.0979
243	0.1005	0.1081	0.1169	0.1081	0.1005
244	0.1023	0.1102	0.1194	0.1102	0.1023
245	0.1056	0.1129	0.1219	0.1129	0.1056
246	0.1076	0.1152	0.1246	0.1152	0.1076
247	0.1102	0.1175	0.1273	0.1175	0.1102
248	0.1123	0.1206	0.1302	0.1206	0.1123
249	0.1152	0.1232	0.1332	0.1232	0.1152
250	0.1175	0.1259	0.1356	0.1259	0.1175
251	0.1206	0.1288	0.1389	0.1288	0.1206
252	0.1226	0.1317	0.1423	0.1317	0.1226
253	0.1259	0.1348	0.1441	0.1348	0.1259
254	0.1288	0.1372	0.1469	0.1372	0.1288
255	0.1317	0.1397	0.1508	0.1397	0.1317
256	0.1340	0.1432	0.1538	0.1432	0.1340
257	0.1372	0.1460	0.1570	0.1460	0.1372
258	0.1397	0.1488	0.1592	0.1488	0.1397
259	0.1423	0.1518	0.1625	0.1518	0.1423
260	0.1460	0.1549	0.1649	0.1549	0.1460
261	0.1488	0.1570	0.1685	0.1570	0.1488
262	0.1518	0.1603	0.1710	0.1603	0.1518
263	0.1549	0.1637	0.1736	0.1637	0.1549
264	0.1570	0.1661	0.1777	0.1661	0.1570
265	0.1603	0.1698	0.1790	0.1698	0.1603
266	0.1637	0.1723	0.1833	0.1723	0.1637
267	0.1661	0.1749	0.1863	0.1749	0.1661
268	0.1698	0.1790	0.1879	0.1790	0.1698
269	0.1723	0.1819	0.1926	0.1819	0.1723
270	0.1749	0.1848	0.1942	0.1848	0.1749
271	0.1790	0.1863	0.1976	0.1863	0.1790
272	0.1819	0.1910	0.1993	0.1910	0.1819
273	0.1848	0.1926	0.2028	0.1926	0.1848
274	0.1863	0.1959	0.2065	0.1959	0.1863

Position(m) (X,Y) / Angle (deg)	Inertia [Kg.m²]				
	(0.75, 0.1)	(0.75, 0.05)	(0.75, 0.0)	(0.75, -0.05)	(0.75, -1.0)
275	0.1910	0.1993	0.2083	0.1993	0.1910
276	0.1926	0.2010	0.2122	0.2010	0.1926
277	0.1959	0.2046	0.2142	0.2046	0.1959
278	0.1993	0.2065	0.2162	0.2065	0.1993
279	0.2010	0.2103	0.2183	0.2103	0.2010
280	0.2046	0.2122	0.2204	0.2122	0.2046
281	0.2083	0.2142	0.2247	0.2142	0.2083
282	0.2103	0.2183	0.2269	0.2183	0.2103
283	0.2122	0.2204	0.2292	0.2204	0.2122
284	0.2162	0.2225	0.2310	0.2225	0.2162
285	0.2183	0.2247	0.2334	0.2247	0.2183
286	0.2204	0.2269	0.2355	0.2269	0.2204
287	0.2247	0.2299	0.2380	0.2299	0.2247
288	0.2269	0.2324	0.2400	0.2324	0.2269
289	0.2292	0.2348	0.2420	0.2348	0.2292
290	0.2310	0.2368	0.2486	0.2368	0.2310
291	0.2339	0.2390	0.2462	0.2390	0.2339
292	0.2358	0.2412	0.2478	0.2412	0.2358
293	0.2382	0.2430	0.2499	0.2430	0.2382
294	0.2402	0.2454	0.2513	0.2454	0.2402
295	0.2428	0.2475	0.2532	0.2475	0.2428
296	0.2443	0.2491	0.2546	0.2491	0.2443
297	0.2472	0.2510	0.2561	0.2510	0.2472
298	0.2491	0.2527	0.2578	0.2527	0.2491
299	0.2507	0.2544	0.2593	0.2544	0.2507
300	0.2527	0.2561	0.2601	0.2561	0.2527
301	0.2549	0.2575	0.2613	0.2575	0.2549
302	0.2564	0.2590	0.2625	0.2590	0.2564
303	0.2578	0.2604	0.2634	0.2604	0.2578
304	0.2598	0.2616	0.2643	0.2616	0.2598
305	0.2613	0.2628	0.2653	0.2628	0.2613
306	0.2628	0.2637	0.2659	0.2637	0.2628
307	0.2640	0.2650	0.2665	0.2650	0.2640
308	0.2653	0.2659	0.2671	0.2659	0.2653
309	0.2665	0.2665	0.2674	0.2665	0.2665
310	0.2677	0.2671	0.2677	0.2671	0.2677
311	0.2687	0.2677	0.2681	0.2677	0.2687
312	0.2696	0.2684	0.2681	0.2684	0.2696

Position(m) (X,Y) Angle (deg)	Inertia [Kg.m²]				
	(0.75, 0.1)	(0.75, 0.05)	(0.75, 0.0)	(0.75, -0.05)	(0.75, -1.0)
313	0.2706	0.2687	0.2681	0.2687	0.2706
314	0.2712	0.2690	0.2677	0.2690	0.2712
315	0.2719	0.2693	0.2674	0.2693	0.2719
316	0.2722	0.2690	0.2671	0.2690	0.2722
317	0.2728	0.2690	0.2665	0.2690	0.2728
318	0.2725	0.2687	0.2659	0.2687	0.2725
319	0.2728	0.2684	0.2653	0.2684	0.2728
320	0.2732	0.2674	0.2643	0.2674	0.2732
321	0.2732	0.2668	0.2631	0.2668	0.2732
322	0.2728	0.2662	0.2619	0.2662	0.2728
323	0.2728	0.2653	0.2604	0.2653	0.2728
324	0.2725	0.2640	0.2329	0.2640	0.2725
325	0.2722	0.2628	0.2578	0.2628	0.2722
326	0.2715	0.2616	0.2558	0.2616	0.2715
327	0.2706	0.2601	0.2541	0.2601	0.2706
328	0.2699	0.2584	0.2518	0.2584	0.2699
329	0.2690	0.2566	0.2499	0.2566	0.2690
330	0.2677	0.2546	0.2475	0.2546	0.2677
331	0.2665	0.2530	0.2454	0.2530	0.2665
332	0.2653	0.2505	0.2428	0.2505	0.2653
333	0.2637	0.2480	0.2397	0.2480	0.2637
334	0.2619	0.2456	0.2375	0.2456	0.2619
335	0.2601	0.2433	0.2341	0.2433	0.2601
336	0.2578	0.2402	0.2315	0.2402	0.2578
337	0.2561	0.2380	0.2292	0.2380	0.2561
338	0.2535	0.2346	0.2247	0.2346	0.2535
339	0.2521	0.2317	0.2225	0.2317	0.2521
340	0.2488	0.2292	0.2183	0.2292	0.2488
341	0.2464	0.2247	0.2142	0.2247	0.2464
342	0.2436	0.2225	0.2103	0.2225	0.2436
343	0.2405	0.2183	0.2065	0.2183	0.2405
344	0.2372	0.2142	0.2028	0.2142	0.2372
345	0.2343	0.2103	0.1993	0.2103	0.2343
346	0.2317	0.2065	0.1959	0.2065	0.2317
347	0.2225	0.2028	0.1910	0.2028	0.2225
348	0.2247	0.1993	0.1879	0.1993	0.2247
349	0.2204	0.1959	0.1833	0.1959	0.2204
350	0.2162	0.1910	0.1790	0.1910	0.2162

Position(m) (X,Y) Angle (deg)	Inertia [Kg.m^2]				
	(0.75, 0.1)	(0.75, 0.05)	(0.75, 0.0)	(0.75, -0.05)	(0.75, -1.0)
351	0.2122	0.1879	0.1749	0.1879	0.2122
352	0.2083	0.1833	0.1710	0.1833	0.2083
353	0.2046	0.1790	0.1673	0.1790	0.2046
354	0.2010	0.1749	0.1625	0.1749	0.2010
355	0.1959	0.1710	0.1592	0.1710	0.1959
356	0.1926	0.1661	0.1538	0.1661	0.1926
357	0.1879	0.1614	0.1508	0.1614	0.1879
358	0.1819	0.1581	0.1460	0.1581	0.1819
359	0.1790	0.1538	0.1423	0.1538	0.1790
360	0.1698	0.1498	0.1381	0.1498	0.1698

References

Abbas, J. & Chizeck, H. (1991). Feedback control of coronal plane hip angle in paraplegic subjects using functional neuromuscular stimulation. *IEEE Transactions on Biomedical Engineering*, **38**, pp.687-698.

Abbas, J. J. & Chizeck, H. J. (1995). Neural network control of functional neuromuscular stimulation systems: computer simulation studies. *IEEE Transactions on Biomedical Engineering*, **42**, pp.1117-1127.

Abbas, J. J. & Triolo, R. J. (1997). Experimental evaluation of an adaptive feedforward controller for use in functional neuromuscular stimulation systems. *IEEE Transactions on Rehabilitation Engineering*, **5**, pp.12-22.

Angeli, T., Gföhler, M., Eberharter, T., & Rinder, L. (1999). Tricycle for paraplegics using functional electrostimulation. *In Proc. of the European Medical and Biological Engineering Conference (EMBEC'99)*, Vienna, Austria, November 1999, pp. 326-327.

Ann, B.-T., Chen, J. & Ju, M.-S (1997). Implementation of an adaptive fuzzy controller for FES-cycling system. *The 19th IEEE Annual International Conference on Engineering in Medicine and Biology Society*, Chicago, USA, pp.1119-1120.

Apparelyzed, (2013). Spinal cord injury statistics[online]. Apparelyzed Spinal Cord Injury Peer Support. Available from: *http://www.apparelyzed.com/statistics.html* [Accessed January 2014].

Bajzek, T. & Jaeger, R. (1987). Characterization and control of muscle response to electrical stimulation. *Annals of biomedical engineering*, **15**, pp.485-501.

Berkelmans, R. (2008). FES cycling. *Journal of Automatic Control*, **18**, pp.73-76.

Bhanu, B., Lee, S. & Ming, J. (1995). Adaptive image segmentation using a genetic algorithm. *IEEE Transactions on Systems, Man and Cybernetics*, **25**, pp.1543-1567.

Chen, J., Yu, N. Y., Huang, D. G., Ann, B. T. & Chang, G. C. (1997). Applying fuzzy logic to control cycling movement induced by functional electrical stimulation. *IEEE Transactions on Rehabilitation Engineering*, **5**, pp.158-169.

Chen, K., Chen, S. C., Tsai, K. H., Chen, J. J. J., Yu, N. Y. & Huang, M. H. (2004). An improved design of home cycling system via functional electrical stimulation for paraplegics. *International Journal of Industrial Ergonomics*, **34**, pp.223-235.

Chipperfield, A. & Fleming, P. (1995). The MATLAB genetic algorithm toolbox. *IEE Colloquium on Applied Control Techniques Using MATLAB*. The Institute of Electrical Engineering, pp.10/1-10/4.

Chipperfield, A., Purshouse, R., Fleming, P., J., Thompson, H. and Griffin, I. (2002). Multi-objective optimisation in control system design: an evolutionary computing approach. *IFAC World Congress*, Barcelona, 20 July 2002.

Chizek, H., Kobetic, R., Marsolais, E., Abbas, J., Donner, I. & Simon, E. (1988). Control of functional neuromuscular stimulation systems for standing and locomotion in paraplegics. *Proceedings of the IEEE*, **76**, pp.1155-1165.

Coley, D. A. (1999). *An introduction to genetic algorithms for scientists and engineers*, World Scientific, Singapore.

Comolli, L., Ferrante, S., Pedrocchi, A., Bocciolone, M., Ferrigno, G. & Molteni, F. (2010). Metrological characterization of a cycle-ergometer to optimize the cycling induced by functional electrical stimulation on patients with stroke. *Medical Engineering & Physics*, **32**, pp.339-348.

Cross, D. & Brockbank, C. (2009). Mechanical hybrid system comprising a flywheel and CVT for motorsport and mainstream automotive applications. *SAE Technical Paper*, 2009-01-1312.

Cyclingpower, 2014. Cycling power lab: Power Essentials [online]. Available from: http://www.cyclingpowerlab.com/Introduction.aspx. [Accessed April 2014].

Davis, G. M., Hamzaid, N. A. & Fornusek, C. (2008). Cardiorespiratory, metabolic, and biomechanical responses during functional electrical stimulation leg exercise: health and fitness benefits. *Artificial Organs*, **32**, pp.625-629.

Davoodi, R. & Andrews, B. J. (1999). Optimal control of FES-assisted standing up in paraplegia using genetic algorithms. *Medical Engineering & Physics*, **21**, pp.609-617.

Ding, J., Wexler, A. S. & Binder-Macleod, S. A. (2000). A predictive model of fatigue in human skeletal muscles. *Journal of Applied Physiology*, **89**, pp.1322-1332.

Drillis, R., Contini, R. & Bluestein, M. (1964). Body segment parameters. *Artificial limbs*, **8**, pp.44-66.

Duffell, L. D., De N Donaldson, N. & Newham, D. J. (2009). Why is the metabolic efficiency of FES cycling low?. *IEEE Transactions on Neural Systems and Rehabilitation Engineering*, **17**, pp.263-269.

Edrich, T., Riener, R. & Quintern, J. (2000). Analysis of passive elastic joint moment in paraplegics. *IEEE Transactions on Biomedical Engineering*, **47**, pp.1058-1065.

Electromagnetic clutch, (2014). Electromagnetic clutches [online]. How it works. Available from: *http://en.wikipedia.org/wiki/Electromagnetic_clutch* [Accessed November 2013].

Everyeighthours, (2014). Spinal Cord Injuries Day [online]. Some Statistics About Spinal Cord Injury. Available from: *http://www.everyeighthours.com/about-spinal-cord-injury* [Accessed May 2013].

Exercise Physiology, (2014). Basic Skeletal Muscle Physiology–The Motor Unit [online]. Available from: *http://www.time-to-run.com/physiology/skeletal-muscle/motor.htm* [Accessed February 2014].

Fachgebiet Regelungssysteme, (2009). Controlled Functional Electric Stimulation (FES) in the Rehabilitation of Spinal Cord Injured Persons and Stroke Patients [online]. Available from: *http://www.control.tu-berlin.de /Controlled_Functional _Electric_Stimulation_(FES)_in_the_Rehabilitation_of_Spinal_Cord_Injured_P ersons_and_Stroke_Patients* [Accessed January 2014].

Farhoud, A. & Erfanian, A. (2010). Higher-Order Sliding Mode Control of Leg Power in Paraplegic FES-Cycling. *The Annual International Conference of the IEEE Engineering in Medicine and Biology Society*. Buenos Aires, Argentina, August 2010. pp.5891-5894.

Farhoud, A. & Erfanian, A. (2014). Fully Automatic Control of Paraplegic FES PedalingUsing Higher-Order Sliding Mode and Fuzzy Logic Control. *IEEE Transactions on Neural Systems and Rehabilitation Engineering*, **22**, pp.533-542.

Ferrarin, M. & Pedotti, A. (2000). The relationship between electrical stimulus and joint torque: a dynamic model. *IEEE Transactions on Rehabilitation Engineering*, **8**, pp.342-352.

Ferrario, C. (2006). Functional electrical stimulation (FES) leg cycling exercise in paraplegia: a pilot study for the definition and assessment of exercise testing protocols and efficacy of exercise. *Ph.D. dissertation*, submitted to the Department of Mechanical Engineering, University of Glasgow, United Kingdom.

Fonseca, C. M. & Fleming, P. J. (1993). Genetic Algorithms for Multiobjective Optimization: FormulationDiscussion and Generalization. *In Genetic Algorithms: Proceedings of the Fifth International Conference*, San Mateo, CA: Morgan Kaufmann, July 1993. pp.416-423.

Fornusek, C., Davis, G. M., Sinclair, P. J. & Milthorpe, B. (2004). Development of an isokinetic functional electrical stimulation cycle ergometer. *Neuromodulation: Technology at the Neural Interface*, **7**, pp.56-64.

Fregly, B. J., Zajac, F. E. & Dairaghi, C. A. (2000). Bicycle drive system dynamics: theory and experimental validation. *Journal of biomechanical engineering*, **122**, pp.446-452.

Gaesser, G. A. & Brooks, G. A. (1975). Muscular efficiency during steady-rate exercise: effects of speed and work rate. *Journal of Applied Physiology*, **38**, pp.1132-1139.

Gföhler, M., Loicht, M. & Lugner, P. (1998). Exercise tricycle for paraplegics. *Medical and Biological Engineering and Computing*, **36**, pp.118-121.

Gföhler, M. & Lugner, P. (2000). Cycling by means of functional electrical stimulation. *IEEE Transactions on Rehabilitation Engineering*, **8**, pp.233-243.

Gföhler, M. & Lugner, P. (2004). Dynamic simulation of FES-cycling: influence of individual parameters. *IEEE Transactions on Neural Systems and Rehabilitation Engineering*, **12**, pp.398-405.

Gharooni, S., Sareh, S., & Tokhi, M. (2007). Development of FES-rowing machine with quadriceps stimulation and energy storing device. *The 12th Annual Conference of the International FES Society*, November 2007, Philadelphia, USA.

Giambattista, A., Richardson, B. M. & Richardson, R. C. (2004). Torque and Angular Momentum [online]. *College physics*. Chapter eight. Student edition, McGraw-Hill.

Giat, Y., Mizrahi, J. & Levy, M. (1993). A musculotendon model of the fatigue profiles of paralyzed quadriceps muscle under FES. *IEEE Transactions on Biomedical Engineering*, **40**, pp.664-674.

Giat, Y., Mizrahi, J. & Levy, M. (1996). A model of fatigue and recovery in paraplegic's quadriceps muscle subjected to intermittent FES. *Journal of biomechanical engineering*, **118**, pp.357-366.

Glaser, R. M., Figoni, S. F., Hooker, S. P., Rodgers, M. M., Ezenwa, B. N., Suryaprasad, A. G., Gupta, S. C. & Mathews, T. (1989). Efficiency of FNS leg cycle ergometry. *Proceedings of the Annual International Conference of the IEEE Engineering in Medicine and Biology Society*. November 1989, Seattle, USA, pp.961-963.

Glaser, R. M., Couch, W. P., Janssen, T., Almeyda, J. W., Pringle, D. D., Collins, S. R., & Mathews, T. (1996). A development system to enhance FES leg cycle ergometer technology. *Paper presented at the Proceedings of the RESNA Conference*, June 1996, pp. 279-281.

Griffin, L., Decker, M., Hwang, J., Wang, B., Kitchen, K., Ding, Z. & Ivy, J. (2009). Functional electrical stimulation cycling improves body composition, metabolic

and neural factors in persons with spinal cord injury. *Journal of Electromyography and Kinesiology,* **19**, pp.614-622.

Gross Anatomy, (2010). Gross Anatomy of Skeletal Muscle [online]. Available from: *http://apbrwww5.apsu.edu/thompsonj/Anatomy%20&%20Physiology/2010/2010%20Exam%20Reviews/Exam%203%20Review/CH%2009%20Gross%20Anatomy%20of%20Skeletal%20Muscle.htm* [Accessed December 2013].

Hakansson, N. A. & Hull, M. L. (2009). Muscle stimulation waveform timing patterns for upper and lower leg muscle groups to increase muscular endurance in functional electrical stimulation pedaling using a forward dynamic model. *IEEE Transactions on Biomedical Engineering*, **56**, pp.2263-2270.

Hansen, E. A., Jørgensen, L. V., Jensen, K., Fregly, B. J. & Sjøgaard, G. (2002). Crank inertial load affects freely chosen pedal rate during cycling. *Journal of biomechanics*, **35**, pp.277-285.

Hibi, N., Fujinaga, H. & Ishii, K. (1996). Work and power outputs determined from pedalling and flywheel friction forces during brief maximal exertion on a cycle ergometer. *European journal of applied physiology and occupational physiology*, **74**, pp.435-442.

Hill, A. (1938). The heat of shortening and the dynamic constants of muscle. *Proceedings of the Royal Society of London. Series B, Biological Sciences*, **126**, pp.136-195.

Holland, J. H. (1975). *Adaptation in natural and artificial systems: An introductory analysis with applications to biology, control, and artificial intelligence*, University of Michigan Press, Ann Arbour.

Hong, Y. & Bartlett, R. (2008). *Routledge handbook of biomechanics and human movement science*, Routledge, USA.

Hongyuan, J., Changbo, M., Nianli, L. & Hongrui, A. (2008). Study on automatic power control in FES cycling. *IEEE 2nd International Symposium on Systems and Control in Aerospace and Astronautics (ISSCAA)*, December 2008, Shenzhen, China, pp.1-4.

Hooker, S. P., Scremin, A. E., Mutton, D. L., Kunkel, C. F. & Cagle, G. (1995). Peak and submaximal physiologic responses following electrical stimulation leg cycle ergometer training. *Journal of rehabilitation research and development,* **32**, pp.361-366.

Hunt, K., Fang, J., Saengsuwan, J., Grob, M. & Laubacher, M. (2012). On the efficiency of FES cycling: A framework and systematic review. *Technology and Health Care*, **20**, pp.395-422.

Hunt, K., Rothe, M., Schauer, T., Ronchi, A. & Negård, N. (2001). Automatic speed control in FES cycling. *Proceedings of the 6th Annual Conference of the International Functional Electrical Stimulation Society*, 16-20 June 2001, Cleveland, Ohio. pp.300-302.

Hunt, K., Saunders, B., Perret, C., Berry, H., Allan, D., Donaldson, N. & Kakebeeke, T. (2007). Energetics of paraplegic cycling: a new theoretical framework and efficiency characterisation for untrained subjects. *European journal of applied physiology*, **101**, pp.277-285.

Hunt, K., Stone, B., Negard, N.-O., Schauer, T., Fraser, M. H., Cathcart, A. J., Ferrario, C., Ward, S. A. & Grant, S. (2004). Control strategies for integration of electric motor assist and functional electrical stimulation in paraplegic cycling: utility for exercise testing and mobile cycling. *IEEE Transactions on Neural Systems and Rehabilitation Engineering*, **12**, pp.89-101.

Huq, M., Alam, M., Gharooni, S. & Tokhi, M. (2005). Genetic Optimization of Spring Brake Orthosis Parameters: Spring Properties. *The 10th Annual Conference of International Functional Electrical Stimulation Society (IFESS)*, July 2005, Montreal, Canada, pp.279-281.

Hussain, Z. (2009). Intelligent Control Techniques for FES-Assisted Paraplegic Indoor Rowing Exercise. *Ph.D. dissertation*, submitted to the Department of Automatic Control and System Engineering, The University of Sheffield, United Kingdom.

Huxley, A. F. (1957). Muscle structure and theories of contraction. *Progress in biophysics and biophysical chemistry*, **7**, pp.255-318.

Idsø, E., Johansen, T. & Hunt, K. (2004). Finding the metabolically optimal stimulation pattern for FES-cycling. *The 9th Annual Conference of the International FES Society*, September 2004, Bournemouth, UK, pp.239-241.

Iwami, T., Aizawa, T., Miyawaki, K., Matsunaga, T., Shimada, Y. & Obinata, G. (2009). Model simulation of FES for the treatment of shoulder subluxation. *IEEE International Symposium on Micro-NanoMechatronics and Human Science*, Nagoya, Japan, November 2009, pp.68-73.

Jailani, R., Tokhi, M., Gharooni, S. & Hussain, Z. (2010). Development of dynamic muscle model with functional electrical stimulation. *Complexity in Engineering*, Rome, February 2010, pp.132-134.

Karu, Z. Z., Durfee, W. K. & Barzilai, A. M. (1995). Reducing muscle fatigue in FES applications by stimulating with N-let pulse trains. *IEEE Transactions on Biomedical Engineering*, **42**, pp.809-817.

Kim, C.-S., Eom, G.-M., Hase, K., Khang, G., Tack, G.-R., Yi, J.-H. & Jun, J.-H. (2008). Stimulation pattern-free control of FES cycling: simulation study. *IEEE*

Transactions on Systems, Man, and Cybernetics, Part C: Applications and Reviews, **38**, pp.125-134.

Kjær, M., Perko, G., Secher, N. H., Boushel, R., Beyer, N., Pollack, S., Horn, A., Fernandes, A., Mohr, T. & Lewis, S. (1994). Cardiovascular and ventilatory responses to electrically induced cycling with complete epidural anaesthesia in humans. *Acta physiologica scandinavica*, **151**, pp.199-207.

Konak, A., Coit, D. W. & Smith, A. E. (2006). Multi-objective optimization using genetic algorithms: A tutorial. *Reliability Engineering & System Safety*, **91**, pp.992-1007.

Lan, N., Crago, P. E. & Chizeck, H. J. (1991). Feedback control methods for task regulation by electrical stimulation of muscles. *IEEE Transactions on Biomedical Engineering*, **38**, pp.1213-1223.

Li, P.-F., Hou, Z.-G., Zhang, F., Chen, Y.-X., Xie, X.-L., Tan, M. & Wang, H.-B (2010). Adaptive Neural Network Control of FES Cycling. *The 4th International Conference on Bioinformatics and Biomedical Engineering*, July 2010,pp.1-4.

Lin, C.-H. & Wu, J.-L. (1999). Automatic facial feature extraction by genetic algorithms. *IEEE Transactions on Image Processing*, **8**, pp.834-845.

Mahfouf, M. (2011). *Intelligent Systems–ACS6117, A Course in Fuzzy Systems*, Department of Automatic Control and systems Engineering, the University of Sheffield, MSc Course Notes.

Makssoud, H., Guiraud, D. & Poignet, P. (2004). Mathematical muscle model for functional electrical stimulation control strategies. *IEEE International Conference on Robotics and Automation*, New Orleans, LA., pp.1282-1287.

Marieb, E., N. and Hoehn, K. (2006). *Human anatomy and physiology*. Seventh edition, Pearson Education Inc., publishing as Benjamin Cummings, USA.

Massoud, R. (2007). Intelligent control techniques for spring-assisted FES-cycling. *Ph.D. dissertation*, submitted to the Department of Automatic Control and System Engineering, The University of Sheffield, United Kingdom.

Massoud, R. (2012). Energy Storage Devices to Support Functional Movements' Restoration. *Energy Procedia*, **19**, pp.63-70.

Matsunaga, T., Shimada, Y. & Sato, K. (1999). Muscle fatigue from intermittent stimulation with low and high frequency electrical pulses. *Archives of physical medicine and rehabilitation*, **80**, pp.48-53.

Mamdani, E. H. (1974). Application of fuzzy algorithms for control of simple dynamic plant. *Proceedings of the Institution of Electrical Engineers*, **121**, pp.1585-1588.

McNeal, D. R., Nakai, R., Meadows, P. & Tu, W. (1989). Open-loop control of the freely-swinging paralyzed leg. *IEEE Transactions on Biomedical Engineering*, **36**, pp.895-905.

Medrtonic, (2013). About Spinal Cord Injury and Disease [online]. Available from: *http://www.medtronic.com/patients/severe-spasticity/about/spinal-cord-injury* [Accessed February 2012].

Melanie, M. (1999). *An introduction to genetic algorithms*. The MIT press, Cambridge, Massachusetts, London, England, Fifth printing, **3**.

Mutton, D. L., Erika Scremin, A., Barstow, T. J., Scott, M. D., Kunkel, C. F. & Cagle, T. G. (1997). Physiologic responses during functional electrical stimulation leg cycling and hybrid exercise in spinal cord injured subjects* 1,* 2. *Archives of physical medicine and rehabilitation*, **78**, pp.712-718.

Nagano, A., Komura, T., Fukashiro, S. & Himeno, R. (2005). Force, work and power output of lower limb muscles during human maximal-effort countermovement jumping. *Journal of Electromyography and Kinesiology*, **15**, pp.367-376.

Nagano, A., & Gerritsen, K. G. (2001). Effects of neuromuscular strength training on vertical jumping performance-a computer simulation study. *Journal of Applied Biomechanics*, **17(2)**, pp.113-128.

Nguyen, R., Masani, K., Micera, S., Morari, M. & Popovic, M. R. (2011). Spatially distributed sequential stimulation reduces fatigue in paralyzed triceps surae muscles: a case study. *Artificial Organs*, **35**, pp.1174-1180.

NSCIA, (2012). Understanding Spinal Cord Injury [online]. The National Spinal Cord Injury Association, a program of United Spinal Association. Available from: *http://www.spinalcord.org/resource-enter/askus/index.php?pg=kb.page&id= 1383* [Accessed February 2014].

NSCISC, (2013).Spinal Cord Injury facts and figures at a glance 2013[online]. Birmingham, Alabama, National Spinal Cord Injury Statistical Centre. Available from:*https://www.nscisc.uab.edu/PublicDocuments/fact_figures_docs/Facts%20 2013.pdf* [Accessed December 2013].

Ogata, K. (2002). *Modern Control Engineering.* Prentice-Hall, Inc., USA.

Ombuki, B., Ross, B. J. & Hanshar, F. (2006). Multi-objective genetic algorithms for vehicle routing problem with time windows. *Applied Intelligence*, **24**, pp.17-30.

Östergård, R. (2011). *Flywheel energy storage: a conceptucal study*, Uppsala Universitet.

Peng, C. W., Chen, S. C., Lai, C. H., Chen, C. J., Chen, C. C., Mizrahi, J. & Handa, Y. (2011). Review: Clinical Benefits of Functional Electrical Stimulation Cycling

Exercise for Subjects with Central Neurological Impairments. *Journal of Medical and Biological Engineering*, **31**, pp.1-11.

Pennestri, E., Stefanelli, R., Valentini, P. & Vita, L. (2007). Virtual musculo-skeletal model for the biomechanical analysis of the upper limb. *Journal of biomechanics*, **40**, pp.1350-1361.

Perkins, T. A., Donaldson, N., Hatcher, N. A., Swain, I. D. & Wood, D. E. (2002). Control of leg-powered paraplegic cycling using stimulation of the lumbo-sacral anterior spinal nerve roots. *IEEE Transactions on Neural Systems and Rehabilitation Engineering*, **10**, pp.158-164.

Perumal, R., Wexler, A. S., Ding, J. & Binder-Macleod, S. A. (2002). Modeling the length dependence of isometric force in human quadriceps muscles. *Journal of biomechanics*, **35**, pp.919-930.

Petrofsky, J. S., Heaton, H. & Phillips, C. A. (1983). Outdoor bicycle for exercise in paraplegics and quadriplegics. *Journal of biomedical engineering*, **5**, pp.292-296.

Petrofsky, J. S., Phillips, C. A., Heaton, H. H., Glaser, R. M. (1984). Bicycle ergometer for paralyzed muscle. *Journal of Clinical Engineering* **9(1),** pp.13-20.

Petrofsky, J. & Smith, J. (1988). Computer aided rehabilitation. *Aviation, space, and environmental medicine*, **59**, pp.670-678.

Petrofsky, J. & Smith, J. (1992). Three-wheel cycle ergometer for use by men and women with paralysis. *Medical and Biological Engineering and Computing*, **30**, pp.364-369.

Pons, D., Vaughan, C. & Jaros, G. (1989). Cycling device powered by the electrically stimulated muscles of paraplegics. *Medical and Biological Engineering and Computing*, **27**, pp.1-7.

Rabischong, E. & Chavet, P. (1997). Regression-based indices of fatigue in paraplegics' electrically stimulated quadriceps. *Medical engineering & physics*, **19**, pp.749-754.

Radu, D. & Besanger, Y. A multi-objective genetic algorithm approach to optimal allocation of multi-type FACTS devices for power systems security (2006). *IEEE Power Engineering Society General Meeting*, 2006, Montreal, Canada.

Rasmussen, J., Christensen, S. T., Gföhler, M., Damsgaard, M. & Angeli, T. (2004). Design optimization of a pedaling mechanism for paraplegics. *Structural and Multidisciplinary Optimization*, **26**, pp.132-138.

Raymond, J., Davis, G. M. & Van Der Plas, M. (2002). Cardiovascular responses during submaximal electrical stimulation-induced leg cycling in individuals with paraplegia. *Clinical physiology and functional imaging*, **22**, pp.92-98.

Ribeiro Filho, J. L., Treleaven, P. C. & Alippi, C. (1994). Genetic-algorithm programming environments. *Computer*, **27**, pp.28-43.

Riener, R. & Fuhr, T. (1998). Patient-driven control of FES-supported standing up: a simulation study. *IEEE Transactions on Rehabilitation Engineering*, **6**, pp.113-124.

Riener, R. & Quintern, J. (1997). A physiologically based model of muscle activation verified by electrical stimulation. *Bioelectrochemistry and bioenergetics*, **43**, pp.257-264.

Riener, R., Quintern, J. & Schmidt, G. (1996). Biomechanical model of the human knee evaluated by neuromuscular stimulation. *Journal of biomechanics*, **29**, pp.1157-1167.

Riess, J. & Abbas, J. J. (2000). Adaptive neural network control of cyclic movements using functional neuromuscular stimulation. *IEEE Transactions on Rehabilitation Engineering*, **8**, pp.42-52.

Ritchison, G. (2001). Lecture notes 3- Muscle [online]. Human Physiology. Available from: *http://people.eku.edu/ritchisong/301notes3.htm* [Accessed January 2012].

Ross, T. J. (2010). *Fuzzy logic with engineering applications*, 3rd edition, John Wiley & Sons, UK.

Semat, H. & Katz, R. (1958). Physics, Chapter 11: Rotational Motion (The Dynamics of a Rigid Body). *Research Papers in Physics and Astronomy*. Robert Katz Publications. **141**. pp.198-224.

Schutte, L. M., Rodgers, M. M., Zajac, F. & Glaser, R. M. (1993). Improving the efficacy of electrical stimulation-induced leg cycle ergometry: an analysis based on a dynamic musculoskeletal model. *IEEE Transactions on Rehabilitation Engineering*, **1**, pp.109-125.

SCI-therapies, (2009). Functional electrical stimulation [online]. Human Spinal Cord Injury: New and Emerging Therapies. Available from: *http://www.sci-therapies.info/FES.htm* [Accessed September 2012].

Sinacore, D. R., Jacobson, R. B. & Delitto, A. (1994). Quadriceps femoris muscle resistance to fatigue using an electrically elicited fatigue test following intense endurance exercise training. *Physical Therapy*, **74**, pp.930-939.

Stainbsy, W. N., Gladden, L. B., Barclay, J. K. & Wilson, B. A. (1980). Exercise efficiency: validity of base-line subtractions. *Journal of Applied Physiology*, **48**, pp.518-522.

Stone, B. A. (2005). Control strategies for functional electrical stimulation induced cycling. *Ph.D. dissertation*, University of Glasgow, United Kingdom.

Takahashi, T., Takazawa, M., Nishiyama, Y., Nakano, E. & Handa, Y. (2004). FES cycling chair for the lower limbs disabled people with electric motor power assist. *The 9th Annual Conference of the International FES Society,* Bournemouth, UK, September 2004.

Tapia, M. C. & Coello, C. A. C. (2007). Applications of multi-objective evolutionary algorithms in economics and finance: A survey. *IEEE Congress on Evolutionary Computation*, 2007, pp.532-539.

Theisen, D., Fornusek, C., Raymond, J. & Davis, G. (2002). External power output changes during prolonged cycling with electrical stimulation. *Journal of rehabilitation medicine*, **34**, pp.171-175.

Thomson, (2014). Thomson Linear Motion. Oprimized, Literature: Clutches & Brakes[online]. Available from: http://www.thomsonlinear.com/website/com/ eng/products/clutches_and_brakes.php [Accessed January 2014].

Tooley, M. & Dingle, L. (2013). *Engineering Science: For Foundation Degree and Higher National*, Routledge, USA.

Umberger, B. R., Gerritsen, K. G. & Martin, P. E. (2003). A model of human muscle energy expenditure. *Computer methods in biomechanics and biomedical engineering*, **6**, pp.99-112.

Van Der Woude, L., De Groot, S. & Janssen, T. (2006). Manual wheelchairs: research and innovation in sports and daily life. *Science & sports*, **21**, pp.226-235.

Veltink, P. H., Chizeck, H. J., Crago, P. E. & El-bialy, A. (1992). Nonlinear joint angle control for artificially stimulated muscle. *IEEE Transactions on Biomedical Engineering*, **39**, pp.368-380.

Verbitsky, O., Mizrahi, J., Levin, M. & Isakov, E. (1997). Effect of ingested sodium bicarbonate on muscle force, fatigue, and recovery. *Journal of Applied Physiology*, **83**, pp.333-337.

Vukic, Z. & Kuljaca, O. (2002). *Lectures on PID Controllers*. Faculty of Electrical Engineering and Computing University of Zagreb.

Wang, S.-L. (2001). Motion Simulation With Working Model 2D and MSC. visualNastran 4D. *Journal of Computing and Information Science in Engineering*, **1**, pp.193-196.

Wang, W., Crompton, R. H., Carey, T. S., Günther, M. M., Li, Y., Savage, R. & Sellers, W. I. (2004). Comparison of inverse-dynamics musculo-skeletal models of AL 288-1< i> Australopithecus afarensis</i> and KNM-WT 15000< i> Homo ergaster</i> to modern humans, with implications for the evolution of bipedalism. *Journal of human evolution*, **47**, pp.453-478.

Winter, D. A. (1990). *Biomechanics and motor control of human movement*, John Wiley & Sons Inc, USA.

Whipp, B. J. & Wasserman, K. (1969). Efficiency of muscular work. *Journal of Applied Physiology*, **26**, pp.644-648.

Zajac, F., Topp, E. & Stevenson, P. (1986). A dimensionless musculotendon model. *Proceedings of the 8th Annual Conference of the IEEE Engineering in Medicine and Biology Society*, Dallas-Ft Worth, Texas, USA, 7-10 November 1986, pp.601-604.

Zajac, F. E. (1989). Muscle and tendon: properties, models, scaling, and application to biomechanics and motor control. *Critical reviews in biomedical engineering*, **17**, pp.359-411.